Chemistry of Antiviral Cyclam Complexes

A Thesis Submitted for the Degree of

Doctor of Philosophy

by

Xiangyang Liang, *M.Sc.*

Department of Chemistry
University of Edinburgh
King's Buildings, West Mains Road
Edinburgh, EH9 3JJ

May 2002

Abstract

Bicyclams which bind the target co-receptor CXCR4, represent a new class of highly potent and selective HIV inhibitors. The most active bicyclam is AMD3100 (1,1'-(1,4-phenylenebismethylene)-bis-1,4,8,11-tetraazacyclotetradecane octahydrochloride dihydrate). In order to elucidate the mechanism of action of AMD3100 and aid the design of more effective drugs, AMD3100 and 15N-labelled cyclam, and their Zn(II), Cd(II) (NMR-active ^{111}Cd) complexes have been synthesised.

1D and 2D ^{1}H, ^{13}C and ^{15}N NMR studies revealed that Zn cyclam complexes exist in three configurations in aqueous solution: *trans*-I, *trans*-III and *cis*-V. Crystal structures of $[Zn(cyclam)(H_2O)_2](OAc)_2$ and $[Zn(cyclam)(phthalate)]_n(CH_3OH)_{2n}$ were obtained and indicate that in the solid state the Zn cyclam complexes adopt the *trans*-III conformation in which six membered-rings are in the chair conformation and five membered-rings are in the gauche conformation. However, the *trans*-III configuration, which is the most stable conformation for small metal ions, is no longer stable for large metals, e.g., Cd(II), and only the configurations *trans*-I and *cis*-V were detected using ^{1}H, ^{13}C, ^{15}N and ^{111}Cd NMR spectroscopy for chloride and perchlorate Cd cyclam complexes in solution. The Cd cyclam perchlorate complex was shown to fix atmospheric CO_2 and $[Cd_3(cyclam)_3(CO_3)](ClO_4)_4 \cdot 3H_2O$ was crystallised. This complex shows bidentate CO_3^{2-} coordination to three Cd cyclam units and adopts a *cis*-I configuration in the solid state, the first example for unsubstituted cyclam complexes. The ^{3}J(H,H) and $^{3}J(^{1}H,^{111}Cd)$ coupling constants

were determined and used to derive structural information using a Karplus relationship. The six-membered rings adopt the chair conformation in solution as in the solid state, and the five-membered rings adopt eclipsed conformations in solution for the *trans*-I configuration.

1D and 2D ^{1}H, ^{13}C and ^{15}N NMR studies also revealed that the cyclam rings of Zn bicyclam AMD3100 adopt three configurations, *trans*-I, *trans*-III and *cis*-V, in aqueous solution. The mixture of *trans*-I/*trans*-I, *trans*-I/*trans*-III, *trans*-I/*cis*-V, *trans*-III/*trans*-III, *trans*-III/*cis*-V and *cis*-V/*cis*-V configurations was shown to exist in water. Only two types of the cyclam ring (*trans*-I and *cis*-V) predominate for the Zn acetate complex, while *trans*-I and *trans*-III predominate for the Zn perchlorate complex. X-ray crystallographic studies showed that both cyclam rings in the Zn bicyclam acetate complex, $[Zn_2(bicyclam)(OAc)_2](OAc)_2 \cdot 2CH_3OH$, adopt the *cis*-V configuration in the solid state.

Anions affect the distribution of the three configurations in solution. The *cis*-V configuration predominates for Zn (bi)cyclam complexes in the presence of water. Titrations of Zn (bi)cyclam complexes with acetate also confirmed that carboxylates readily increase the proportion of the *cis*-V configuration.

The interaction between the model target protein lysozyme and Zn_2bicyclam^{4+} was confirmed by ESI-MS and attempts were made to cocrystallise lysozyme with Zn_2bicyclam^{4+}.

Declaration

I hereby declare that this thesis was composed by myself and has never been presented or accepted in any previous application for a degree. All work presented in this thesis was, unless acknowledged, carried out by myself. All sources of information have been acknowledged by reference.

Xiangyang Liang

2002

Dedicated to

my wife

mum and dad

Acknowledgements

I would like to thank Professor Peter J. Sadler for his support and advice throughout the course of my study. A huge amount of NMR knowledge acquired in his research group greatly helps me with my research. I will not forget forever he taught me NMR theories and discussed my project very often. All words are insufficient to express my gratitude to him.

I am very grateful to Dr. John A. Parkinson for his teaching and help on NMR experiments and result analysis, molecular modelling, and NMR simulation, Dr. Michael Weishäupl for his help and advice on syntheses and NMR analysis, and Dr. Simon Parsons, Dr. Robert O. Gould and Pamela A. McGregor for the determination of all the crystal structures for me.

I would like to thank all other members of PJS group, past and present, for their friendship and help. Among them, thanks especially go to Dr. Fuyi Wang for his help on UV and ESI-MS experiments, Dr. Claudia Blindauer for protein sequence alignment and protein modelling and all cyclam people in PJS group, Dr. Hye-seo Park, Dr. Stephen J. Paisey and Tina M. Hunter for their help and contributions to my work.

I also thank the Committee of Vice-Chancellors and Principals (CVCP) for an ORS Award and University of Edinburgh for a Faculty Scholarship.

Finally, my sincere thanks go to my wife and parents for their constant support, understanding, encouragement, and patience in these years.

Contents

List of Figures

List of Tables

List of Schemes

Abbreviations

AIDS	Acquired immune deficiency syndrome
Asp	Aspartic acid
acq	Acquision
AZT	Zidovudine
Bz-cyclam	1-Benzyl-1,4,8,11-tetraazacyclotetradecane
COSY	Correlated spectroscopy
CXCR4	CXCR4 protein
Cp	Cyclopentadienyl
CD4	CD4 protein
CCR5	CCR5 protein
DDI	Didanosine
DQF	Double-quantum filtered
d1	Delay
ES-MS	Electrospray mass spectrometry
EC_{50}	50% Effective concentration
ECL	Extral cellular loop
FID	Free induction decay
Glu	Glutamic acid
gp	Glycoprotein
HSQC	Heteronuclear single quantum correlation
HIV	Human immunodeficiency virus
HEWL	Hen egg white lysozyme

IC_{50}	50% Inhibitory concentration
MRI	Magnetic resonance imaging
Mabs	Monoclonal antibodies
Nt	Amino-terminal
NOE	Nuclear Overhauser effect
NOESY	Nuclear overhauser enhancement spectroscopy
PDB	Protein database
RF	Radio frequency
SOD	Superoxide dimutase
CSD	Cambridge structural database
SDF-1	Stromal cell-derived factor-1 chemokine
SIV	Simian immunodeficiency virus
SEM-EDX	Scanning electron microscope with energy dispersive X-ray detector
TM	Trans-membrane
TBTU	o-(benzotriazol-1-yl)-N,N,N',N'-tetramethyluronium tetrafluoroborate
THF	Tetrahydrofuran
TSP	Sodium trimethylsilylpropionate
TMS	Tetramethylsilane
TOCSY	Total correlation spectroscopy

Chapter 1

Introduction – Zinc, Cyclams and the CXCR4 Co-receptor

1.1 Zinc

Zinc, atomic number 30 and atomic weight of 65.38, is the last element in the first transition series, in group 12 together with cadmium and mercury.[1] While only the 25th element in order of abundance, zinc is very widely distributed over the earth's surface. The abundance of zinc varies from 0.02 to 0.0005% (w/w) in the crust, and from 0.001 to 0.0001% (w/w) in vegetable and animal matter. Some organisms accumulate zinc: thus oysters gathered from the Atlantic are reported to contain an average of 0.04% Zn. Zinc has two valence electrons $3d^{10}4s^2$ and its common oxidation state is +2. The Pauling ionic radius for Zn(II) is 0.74 Å. Its coordination number can vary from 4, 5, to 6.[2] Zinc has an extensive coordination chemistry, though less so than that of some of the preceding 3d elements. Zinc does not form stable, discrete fluoro complexes, although it is octahedrally six-coordinated in ZnF_2, which has the rutile structure, and in $KZnF_3$ (perovskite structure), but discrete complex anions of the other halides are readily obtained and may be isolated as solids using the standard technique of precipitation using a large cation such as $[Ph_4As]^+$ or $[Co(NH_3)_6]^{3+}$.[3] Tetrahedral complexes are particularly readily formed with a variety of O-donors, such as $[Zn(OMe)_4]^{2-}$ and more stable ones are formed with N-donors such as NH_3, amines, and N-heterocycles; complexation to phosphines is limited. Complexes with S-donors are common and

several have unusual structural features.[3] There are relatively few five-coordinate complexes; typically zinc complexes have a (distorted) trigonal bipyramidal shape.[4] For example, $ZnCl_2$(terpyridyl) has the tridentate ligand occupying one equatorial and the two axial positions of the trigonal bipyramid.[4]

1.2 Metallodrugs

Medical inorganic chemistry developed greatly, since the discovery of the anticancer activity of cisplatin, *cis*-$[Pt(NH_3)_2Cl_2]$ in the 1960s by Rosenberg.[5] Today, cisplatin is still one of the three most widely clinically-used anticancer drugs.[6] Since the introduction of cisplatin, thousands of Pt compounds have been synthesised and evaluated as potential anticancer agents. Three injectable Pt(II) compounds have been approved and several other *cis* diam(m)ine complexes are on clinical trials, including an oral Pt(IV) complex.[7] The established structure-activity rules are being broken: active Pt complexes without coordinated NH groups and active *trans* complexes are emerging. With appropriate choice of ligands, it is possible to change the mode of Pt binding to DNA and to circumvent acquired resistance of cancer cells to cisplatin; a trinuclear Pt complex with two monofunctional Pt centres has recently been found to exhibit an intriguing new mode of DNA binding and has entered clinical trials.[8]

Metallocenes are another important class of agents with promising anticancer activity. While these compounds were initially tested as possible analogues of cisplatin, the effectiveness of Cp_2TiCl_2 against platinum-resistant cell lines indicates a different mechanism of action that may lead to new therapeutic options against

ovarian cancer.[9] Two Ti(IV) complexes are on clinical trial, an acetylacetonate derivative (budotitane)[10] and titanocene dichloride[11].

Injectable Au(I) thiolates and an oral Au(I) phosphine complex are widely used for the treatment of rheumatoid arthritis. Au(I) has a high affinity for sulfur and selenium ligands, which suggests that proteins, including enzymes and transport proteins, will be critical in vivo targets.[12] In addition, extracellular gold in the blood is primarily protein bound, suggesting protein-mediated transport of gold during therapy. The recent discovery that oxidation of administered Au(I) compounds to Au(III) may be responsible for some of the side-effects of gold therapy[13] has highlighted interests in the biological redox chemistry of gold, including possible stabilisation of Au(III) by peptides and proteins.

Many complexes of manganese have been reported to be capable of functioning as superoxide dismutase (SOD) enzyme. The native enzymes catalyse the dismutation of superoxide to oxygen and hydrogen peroxide. Therefore, it is critical that SOD mimics must act as a true catalyst. Three general classes of vanadium-containing compounds are of interest for their utility as insulin-mimetic agents in the treatment of human diabetes mellitus.[14]

The injection of gram quantities of Gd(III) complexes to provide contrast in magnetic resonance images (MRI) of the body illustrates how the toxicity of metal ions and their targeting can be finely controlled by the appropriate choice of the ligands.[7] Four Gd(III) complexes and a Mn(II) complex are currently in clinical use. Relaxation and contrast can be optimised *via* control of the number of metal-bound H_2O molecules, their exchange rate with bulk water, and the tumbling time of the complex. Radioactive metal ions can be used in diagnosis and therapy, or for both

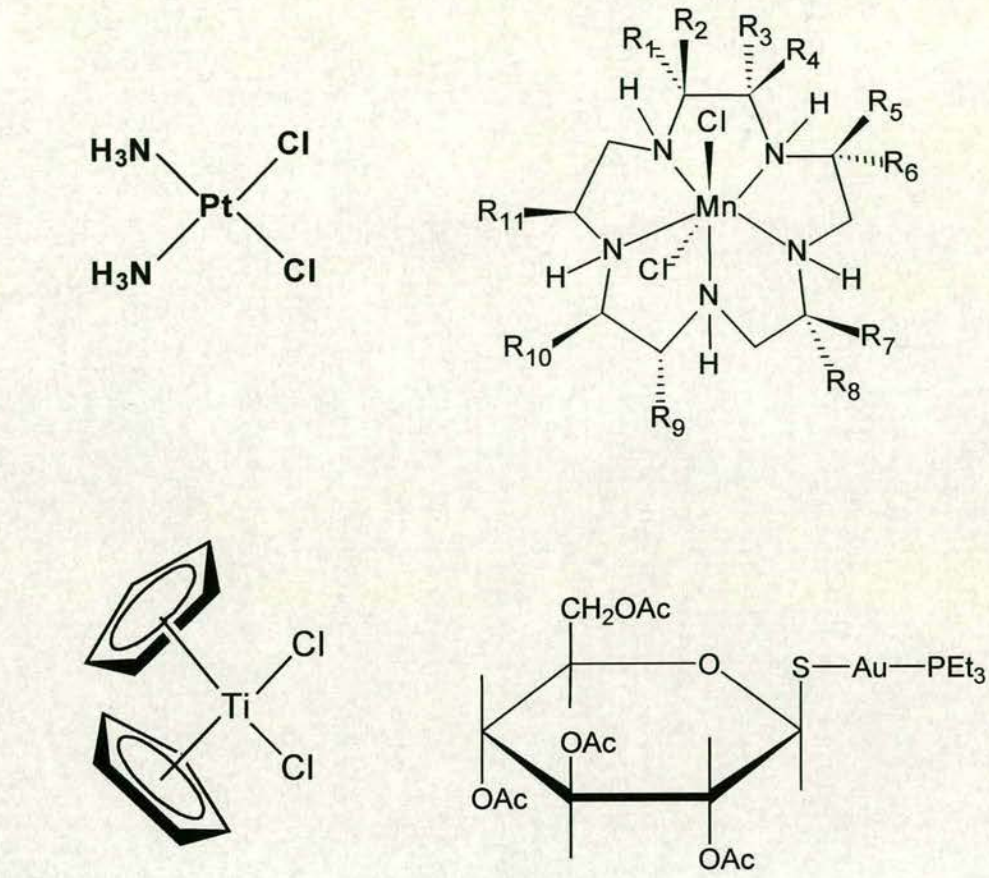

Figure 1.1 Some examples of metallodrugs

(e.g. ^{67}Cu). ^{99m}Tc has optimum radioemission and half-life properties for diagnosis and with the appropriate choice of oxidation state and ligands can be targeted to many different organs; its chemistry is rich with oxidation states ranging from -1 to +7 and coordination numbers from 4 to 7. More than twenty ^{99m}Tc complexes are currently in clinical use. Metal-tagged antibodies offer promise for specific targeting to tumour cells. Exciting is the potential use of activatable radioactive or paramagnetic complexes to probe biological functions, for example specific diastereomers of Tc complexes can be trapped in the brain via biotransformation mechanisms, and the ability of certain Gd(III) complexes to produce MRI contrast can be switched on by enzymes.

The strong relationship between metals and some organic drugs is becoming apparent.[7] Some are activated or biotransformed by metal ions. The organic anticancer drug, Batimastat, for example, is a chelating agent targeted to a zinc metalloenzyme, bleomycin requires iron for activation, and complexation of anthracyclines with Ca(II) can inhibit their oral adsorption. Metalloenzyme inhibitors in particular will provide new generations of novel drugs.

1.3 Cyclam and bicyclam

Saturated macrocyclic polyamines have been known for a long time.[15] Until the early 1970's, macrocyclic polyamines had been used mostly as chelating agents for transition metal ions for the study of basic coordination chemistry. As the study has developed, these macrocyclic polyamines were discovered to possess some

biofunctional properties. Accordingly, macrocyclic polyamines are highly protonated and bind transition metal ions and some other metal ions strongly. Moreover, upon cyclisation, polyamines gain new properties beyond those anticipated from mere assemblies of amines or linear polyamines. This is best illustrated by their behaviour towards protons and metal ions. For macrocyclic polyamines, due to their restricted conformation, the nitrogen lone pairs may overlap to bring about higher electron densities in the macrocyclic cavities. Thus, the proton affinities at the initial stage are unusually high, *i.e.* pK_a values are higher than *ca* 10, a value common for ordinary, isolated secondary amines. Once protons are incorporated into the macrocyclic cavities, the already protonated amines are so close (due to the macrocyclic conformational restraint) that the proton affinities for the last two steps are extremely weak. This is apparent from the protonation constants (pK) for cyclam (Figure 1.2).[15]

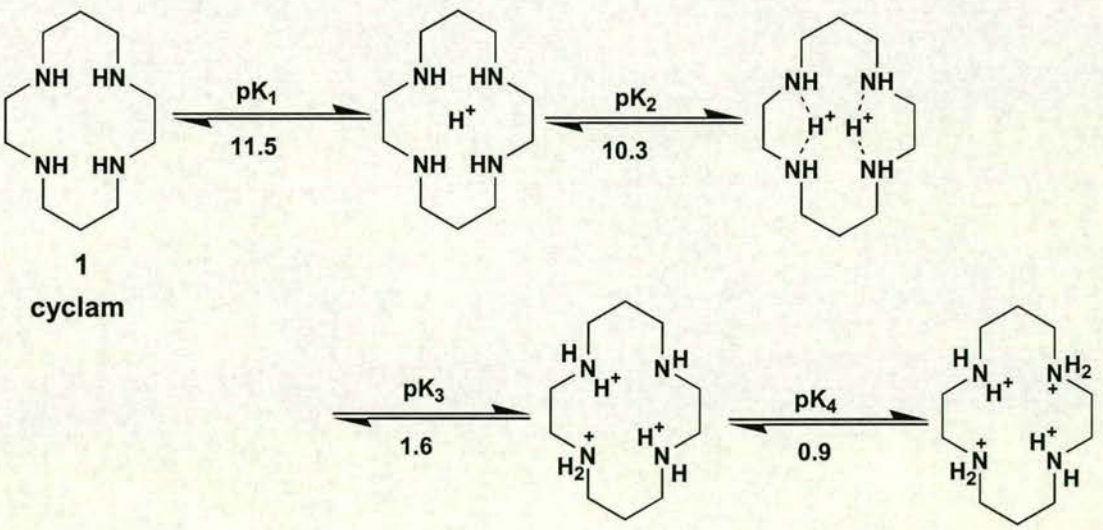

Figure 1.2 Protonation constants pK for cyclam (**1**) (ref. 15)

Macrocyclic structures are also extremely favourable for metal complexation. In terms of the entropy factor, this may be viewed as an extension of the "chelate effect" that is a major contribution to an increase in complex stability as the number of chelate rings increases.

While macrocyclic polyamines thus act as host molecules for protons and metal cations, upon protonation (at neutral pH) polyamines can form complexes with anions (Figure 1.3).[16]

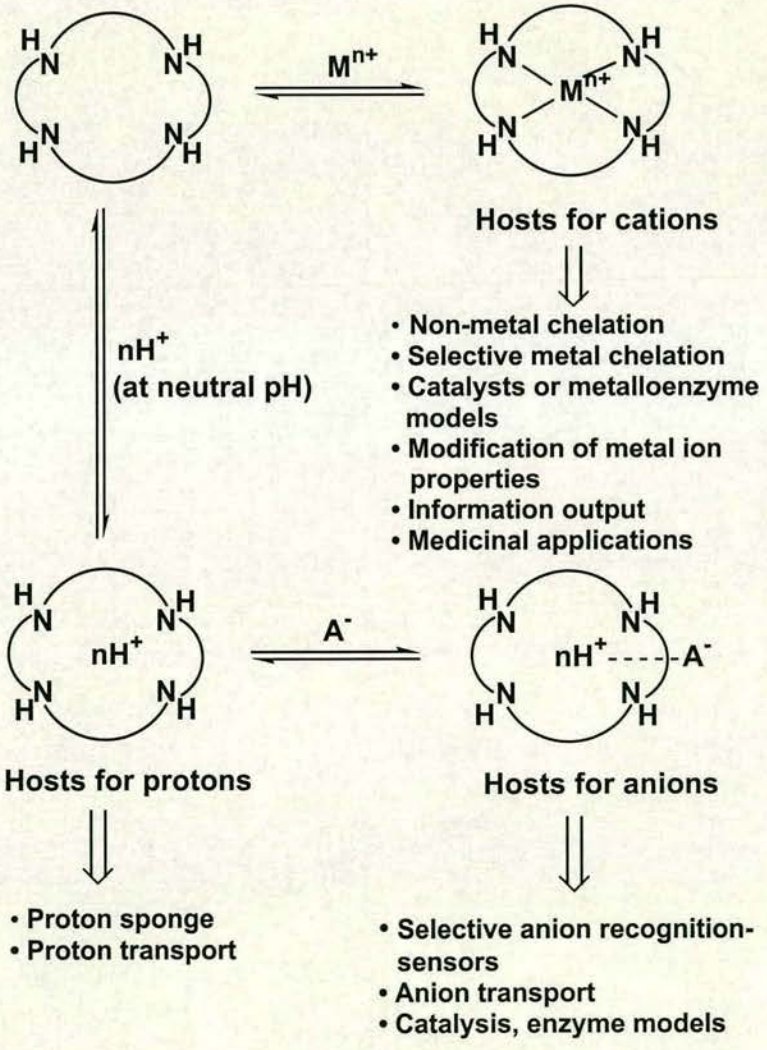

Figure 1.3 Characteristic properties of macrocyclic polyamines and their applications

The polyamine host-guest interaction can develop into more highly advanced chemical functions for (1) design of more sophisticated hosts for more selective and efficient uptake of wider ranges of guest molecules and ions, (2) selective separation, dissolution and membrane transport of guests, (3) information input or output upon host-guest interaction, (4) new functions as complex assemblies, (5) new chemical reactants or catalysis due to host-guest interactions, and (6) recognition of external stimulus and/or messages to initiate above functions (*i.e.* attachment of robotic functions).

The 14-membered macrocycle 1,4,8,11-tetraazacyclotetradecane (cyclam, [14]aneN_4) is one of the most commonly studied and used macrocycles.[17] Cyclam was first synthesised in 1937,[18] and new uses for this macrocycle and its derivatives continue to be found. They have applications in a variety of areas, including catalysis, bioinorganic, biomimetic, and coordination chemistry.

Macrocyclic polyamines can complex with virtually all kinds of transition metal ions and some other metal ions.[15] However, these complexes are generally so stable (logK > 15) that they are of no practical use as selective metal chelating agents. Comparing the values of logK for Cu(II), Ni(II), Zn(II), and Cd(II) complexes with cyclam shows, that the stability of the cyclam complexes depends on the sizes of the metal ions (Table 1.1) but also on the configuration of the cyclam complexes.

The importance of nitrogen configurational isomers in the chemistry of metal complexes of tetraaza macrocyclic ligands is becoming more and more apparent.[19] Depending on the spatial alignment of the NH protons there are five possible configurational isomers of planar complexes of the macrocyclic ligand cyclam (1,4,8,11-tetraazacyclotetradecane): *RSRS* (*trans*-I), *RSRR* (*trans*-II), *RRSS* (*trans*-III), *RSSR* (*trans*-IV), and *RRRR* (*trans*-V) (Figure 1.4).[20]

Table 1.1 Stability constants for cyclam complexes and ionic radii

M^{2+}	r (Å)	log K	Ref.
Cu^{2+}	0.72	27.2[a]	21
Ni^{2+}	0.69	22.2[b]	22
Zn^{2+}	0.74	15.0[c] or 15.5[d]	23 and 24
Co^{2+}	0.75	12.7[e]	25
Cd^{2+}	0.97	11.7[f]	26

[a] I = 0.2 M at 298 K; [b] μ = 0.1 M at 298 K; [c] I = 0.2 M at 298 K by pH-metric method. [d] I = 0.2 M at 298 K by polarographic method; [e] I = 0.2 M at 298 K; [f] conditions not available.

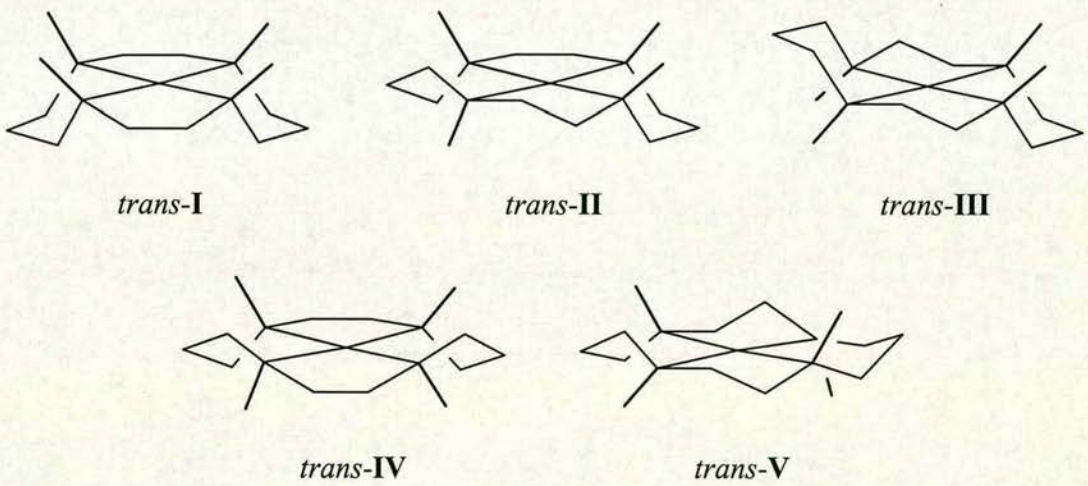

Figure 1.4 Schematic picture of the five possible configurational isomers of planar *trans* coordinated cyclam complexes

For the more labile metal ions, extensive ligand N– or C–substitution makes isomerization more sluggish and has permitted the isolation of thermodynamically unstable configurational isomers.[19] Semiquantitative estimates of the relative strain energies of the five isomers of cyclam by Bosnich *et al*[27] and later by Whimp *et al*[28] have indicated that the *trans*-III form is the most stable in octahedral coordination and is the lowest energy configuration available for Ni(II) cyclam. After analysis of all the nickel complexes containing the cyclam backbone in the Cambridge Structural Database (CSD), Donnelly and Zimmer reported that the most commonly found configuration is the *trans*-III configuration.[17] The same result was obtained in this project for Cu(II) complexes with a cyclam backbone (Table 1.2).

Table 1.2 Configurational distribution[a] of cyclam complexes in the CSD (amide-containing macrocycles not included; data for Ni(II) complexes from ref. 17)

	overall		Oct		Spl		Spy		Tbp	
			%		%		%		%	
	Ni	Cu	Ni	Cu	Ni	Cu	Ni	Cu	Ni	Cu
no of structs	138	64	75	42	58	12	4	5	1	5
trans-I	20.3	9.4	9.3	2.4	29.3	8.3	75.0	80.0	100	0.0
trans-III	57.2	87.5	52.0	97.6	67.2	91.7	25.0	20.0	0.0	60.0
trans-V	1.5	3.1	0.0	0.0	3.5	0.0	0.0	0.0	0.0	40.0
cis-V	21.0	0.0	38.7	0.0	0.0	0.0	0.0	0.0	0.0	0.0

[a] Oct =octahedral; Spl = square-planar; Spy = square-pyramidal; Tbp = trigonal bipyramidal

Molecular mechanics calculations have shown that the *trans*-I configuration becomes more stable relative to the *trans*-III configuration in going from octahedral Ni(II) cyclam complexes to a square-planar analogue.[29] The occurrence of *trans*-I macrocycles was higher for square-planar complexes than for octahedral complexes. This is due to the non-bonded interactions between the atoms/substituents at positions 1,4,8,11 and the nonmacrocyclic coordinating ligands (Figure 1.5).[17]

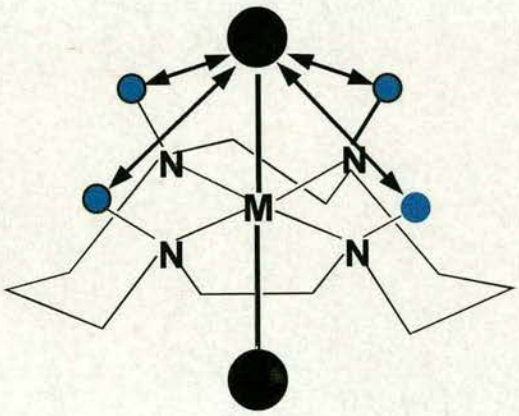

Figure 1.5 The *trans*-I configuration becomes less stable relative to *trans*-III in octahedral geometry since there is repulsion by an axial ligand to four NH protons on the same side (Ref. 17).

This effect is enhanced for nitrogen-substituted macrocycles. Wagner and Barefield have isolated complexes of Ni(II) with cyclam in both the *trans*-III (*RRSS*) and the *trans*-I (*RSRS*) geometries.[30] Moore and co-workers have shown that the two isomers equilibrate readily in donor solvents, presumably via an intermediate *trans*-II (*RSRR*) isomer.[31] The *RSRR* isomer has been detected by NMR.[31,32] The most common conformation reported for Zn complexes with cyclam is *trans*-III, in which two N-H bonds are oriented up and two down as shown in Figure 1.4. The *trans*-III conformation was found in the octahedral complex $[Zn(cyclam)(ClO_4)_2]$,[33] and

$[Zn(cyclam)(NCS)_2]$.[34] Alcock and co-workers reported that the product of the reaction of $ZnCl_2$ and cyclam comprises infinite $-Cl-[Zn(cyclam)]^{2+}-Cl-$ chains interspersed with $[ZnCl_4]^{2-}$ ions.[35] However, the cyclam molecule shows the same *trans*-III conformation in this complex. ^{13}C NMR spectra show that the complex undergoes a slow isomerisation in aqueous solution. $[ZnCl(cyclam)]^+$ in nitromethane solution is probably derived from the break up of the chloride chain, *i.e.* with the *trans*-III conformation and with an axially coordinated chloride ligand. In aqueous solution, an analogous *trans*-III structure is likely upon first dissolution of the complex, probably with water replacing the axial chloride, but a minor isomer forms after 24 hours. This isomer has the same number of resonances as the original species, and only the *trans*-I isomer satisfies this requirement. It is likely that in the *trans*-I complex, Zn(II) is five coordinate, with the axial position occupied by a water molecule or chloride ion. In water, the *trans*-III form is most probably six-coordinate with two axially bonded water molecules.

Kato and Ito reported that the Zn(II)-cyclam complex **2** yielded a carbonate monoester-bound product **4** in a CH_3OH solution through which CO_2 had been bubbled.[36] CO_2 was evidently fixed between Zn(II) and CH_3O^- bonding at the axial position as a possible intermediate **3** (Figure 1.6).

Kimura and co-workers gained insight into the acidic properties of Zn(II) cyclam.[37] They determined the pK_a value for the H_2O that is in the fifth (axial) site in complex **5**. The pK_a value of 9.8 (298 K and I = 0.1 M) for Zn(II)-cyclam was determined by potentiometry.[38] For the Ni(II) and Cu(II) complexes, proton dissociation did not occur until pH 11. Zn(II) can be a stronger acid than Cu(II) under certain circumstances. Zn(II) in the square-planar cyclam N_4 cavity exerts the most acidic effect towards an axial direction. The deprotonation is shown in Figure 1.7.

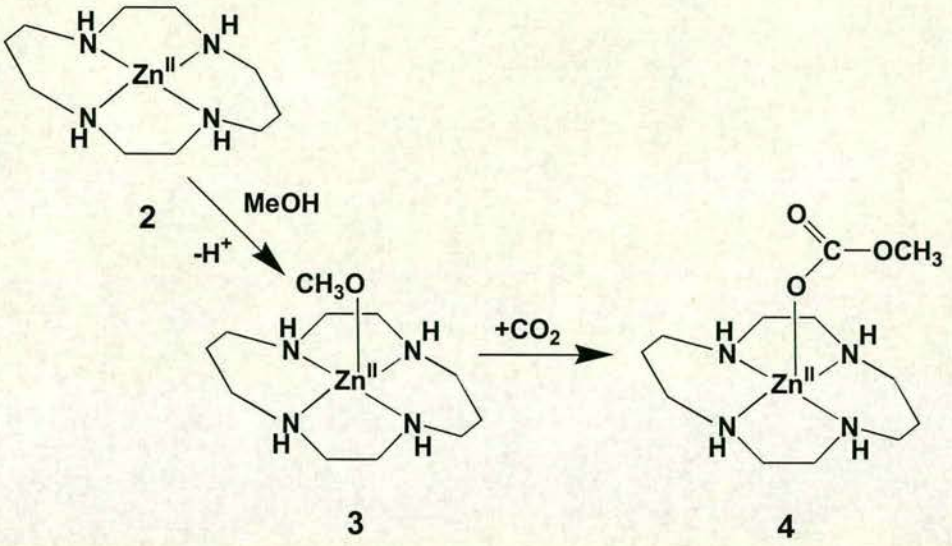

Figure 1.6 Carbon dioxide fixation by Zn(II)-cyclam in MeOH (Ref. 36)

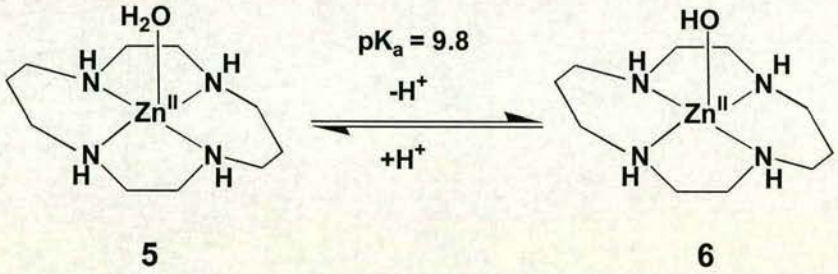

Figure 1.7 Deprotonation equilibrium for Zn(II)-cyclam

The Zn(II) ion coordinated to cyclam in MeOH is acidic enough to permit proton dissociation from MeOH to form the axial MeO^- on the Zn(II) ion that is presumably the reaction intermediate for CO_2 fixation.

Kimura and co-workers used $[Zn(cyclam)](TfO)_2$ ($TfO = CF_3SO_3^-$) as a model for catalytically active Zn(II) in liver alcohol dehydrogenase.[39] Shelton and Morrow

have studied catalytic transesterification and hydrolysis of RNA by a cyclam complex with $Zn(NO_3)_2$.[40] Compared with Zn(II) complexes with other cyclic polyamines, Zn(II) complexes with cyclam are inactive in these reactions.

Bicyclams in which two monocyclam rings are connected by a bridging unit can be divided into two classes. First, two monocyclam units can be linked together by bridging the carbon atoms of the cyclam backbone. An early example of this

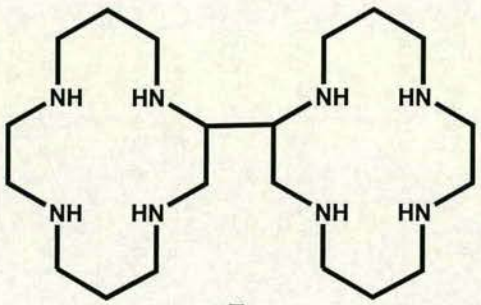

7

class, complex **7**, was obtained as a side product during the template synthesis of cyclam.[41] Two cyclam units are linked through a C-C covalent bond. The dimeric structure of the product as a Ni(II) salt was confirmed by an X-ray diffraction study. The ligand has not been isolated free of its Ni^{2+} ion. The *eq-eq* (equatorial-equatorial) and *ax-ax* (axial-axial) linkage modes were found for the Co(III) complex with **8**, although three

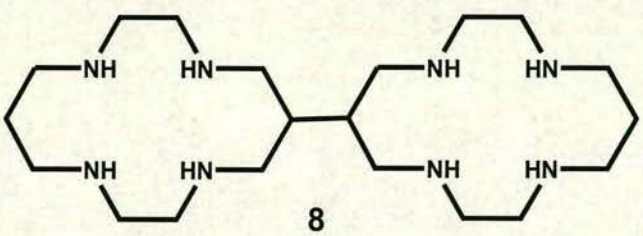

8

complexes with *eq-eq*, *ax-eq* (axial-equatorial) and *ax-ax* C-C linkage modes between two monocyclam units were proposed.[42] Two complex cations, $[Co_2(eq\text{-}eq)Cl_4]^{2+}$ and $[Co_2(ax\text{-}ax)Cl_4]^{2+}$, are isomers due to the difference in the C-C linkage mode between the two monocyclam units. Each monocyclam adopts the *trans*-III configuration and all the Co(III) ions are six-coordinate with chloride ions in both complexes. In bicyclam

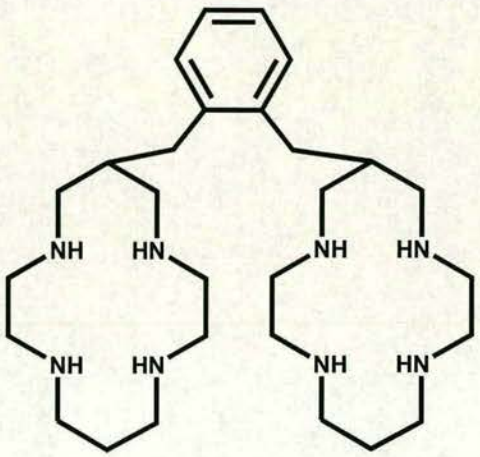

9

ligand **9** comprises two cyclam units bridged by a xylyl group.[43] Both Ni^{2+} and Zn^{2+} complexes of **9** adopt the most stable conformation, *trans*-III. In both crystal structures, the two cyclam rings are arranged in a face-to-face manner, and the two metallic sites are connected by a bridging ligand, Br^- in the Ni^{2+} complex, and CO_3^{2-} in the Zn^{2+} complex.

Secondly, two monocyclam units can be linked together by bridging the amine nitrogen atoms of the cyclam backbone. The redox chemistry of some of these dinickel(II) and dicopper(II) complexes has been investigated with regard to

oxidation of M(II) to M(III).[44] However, no crystals or NMR studies have been reported.

1.4 Current Clinical Drugs for the treatment of HIV

Pandemic HIV-1 infection has led to an intensive search for antiviral agents to control this disease. Theoretically, any stage in the viral replication cycle could be a target for anti-viral therapy (see Figure 1.9).[45] In reality, only a few virus-specific events could function as targets for chemotherapeutic intervention. Limited classes of drugs have already been demonstrated to be effective in the treatment of HIV-1 disease. The current clinical drugs act either at the substrate binding site of the reverse transcriptase (Zidovudine, Didanosine, Zalcitabine, Stavudine, Lamivudine) or a non-substrate binding site of the reverse transcriptase (Nevirapine, Delavirdine), or the viral protease (Saquinavir, Ritonavir, Indinavir, Nelfinavir).[46]

1.4.1 Nucleoside reverse transcriptase Inhibitors

The majority of available antiviral agents are nucleoside analogues.[47] They inhibit the replication of HIV by blocking the synthesis of proviral DNA. They are first activated in the cell via several phosphorylation steps by cell enzymes to form the corresponding triphosphate nucleotide. The phosphorylated metabolite is the active compound that inhibits the reverse transcriptase enzyme and viral DNA synthesis. In addition, some analogues can be incorporated into the nucleic acid and block further synthesis or alter its function. The clinical use of such compounds depends on a high therapeutic ratio, so that the benefit of viral inhibition outweighs

the inherent toxicity. Zidovudine (AZT) was the first antiretrovirus drug approved for the treatment of HIV infection (1987).

1.4.2 Non-nucleoside reverse transcriptase inhibitors

Unlike the nucleoside analogues, these inhibitors are not DNA chain-terminators.[48] Instead, these structurally diverse compounds cripple the reverse-transcriptase enzyme by binding near to and changing the conformation of its catalytic site. Resistant virus mutants arise rapidly, so these drugs are recommended for use in combination therapies. Nevirapine is the first member of this class of nonnucleoside reverse transcriptase inhibitors. It was approved in 1996.

1.4.3 Protease inhibitors

Saquinavir was the first protease inhibitor to be approved (1995) for treatment of HIV infection.[49] It was designed by computer modelling as a molecule that would fit into the active site of the HIV protease enzyme. It inhibits the viral protease that is required during the late stage of the replicative cycle. This protease cleaves the viral structural proteins to form the mature virion core and activate the reverse transcriptase that will be used in the next round of infection. Inhibition of the protease yields noninfectious virus particles. Protease inhibitors are often used in combination with other classes of antiretrovirus drugs.

1.5 Antiviral activity of cyclams

1.5.1 HIV life cycle

Viral spikes (as seen in Figure 1.8) are formed by the two major viral envelope proteins, gp120 and gp41.[50] The HIV-1 lipid bilayer is also studded with a number of host proteins, including class I and class II histocompatibility antigens,

acquired during virion budding. The core of HIV-1 contains four nucleocapsid proteins, p24, p17, p9, and p7, each of which is proteolytically cleaved from a precursor by the HIV-1 protease. The phosphorylated p24 polypeptide forms the chief component of the inner shell of the nucleocapsid, whereas the myristylated p17 protein is associated with the inner surface of the lipid bilayer and probably stabilises the exterior and interior components of the virion. The p7 protein binds directly to the genomic RNA through a zinc-finger structural motif and, together with p9, forms the nucleoid core. Importantly, this retroviral core also contains two copies of the single-stranded HIV-1 genomic RNA that are associated with the various viral enzymes, including the reverse transcriptase, integrase, and protease.

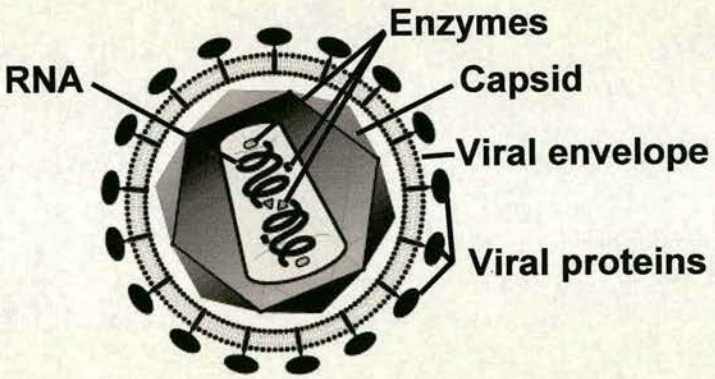

Figure 1.8 Icosahedral structure of the HIV-1 virion containing 72 external spikes

As shown in Figure 1.9, the replicative cycle of HIV includes the following steps. The initial phase of the cycle involves binding of specific epitopes of the CD4 molecule on the surface of the target cell to defined regions of $gp120^{51}$ and fusion of the virus envelope with the cell membrane. Virus-cell fusion requires interaction of the envelope protein with a second cell surface molecule, or

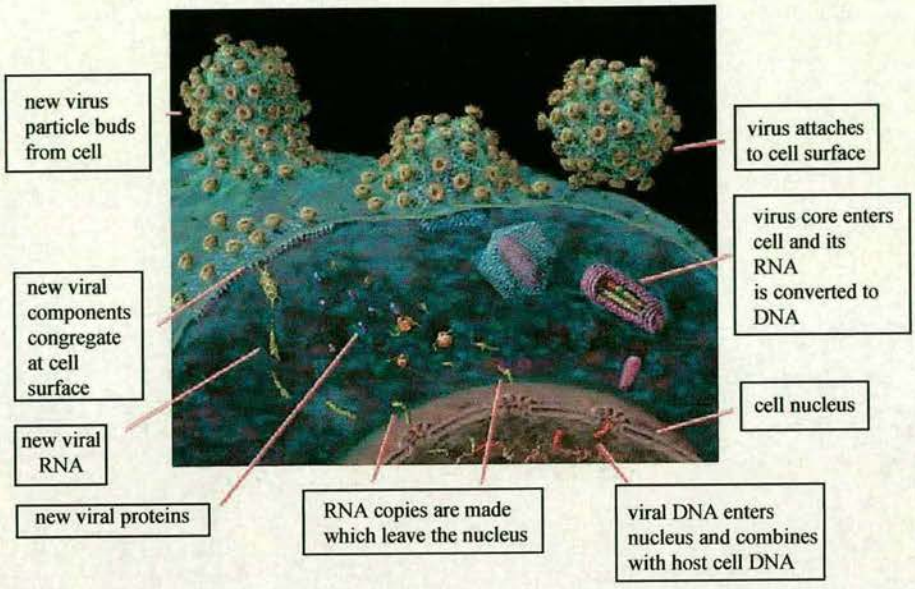

Figure 1.9 The replicative cycle of HIV virus (ref. 52)

co-receptor.[53] As a result, the virion loses its integrity and characteristic morphology. Genomic RNA is released into the cytoplasm within the virus core, which includes molecules of reverse transcriptase. Viral RNA is then used as a template by reverse transcriptase to make a minus-strand DNA copy, thus forming an RNA-DNA hybrid. Soon thereafter, the RNA strand is degraded by the ribonuclease H activity of reverse transcriptase. A positive DNA strand is synthesized, and the linear double-stranded DNA molecule changes conformation to become circular. Some of this DNA migrates to the nucleus and subsequently becomes integrated into the cellular DNA to form the HIV provirus, through the interaction of the viral integrase. In the "productive phase", viral DNA is transcribed into messenger RNA by host cell RNA polymerase. After transcription, some of these viral RNA molecules are used as messengers for the synthesis of viral proteins. Others become incorporated as genomes into progeny viral particles. The replication cycle continues with the translation of viral genomic RNA and viral

proteins from unspliced, single spliced, and multiply spliced *m*RNA species. These proteins undergo post-translational protein cleavage and glycosylation. Within the cytoplasm the final stage of assembly of viral proteins occurs and is followed by the budding of the mature virion through the cell membrane, with simultaneous acquisition of envelope.

As illustrated in Figure 1.10, the HIV envelope contains two glycoproteins, surface gp120 and transmembrane gp41 to which it is noncovalently attached.[54] The initial step in infection is the binding of the viral envelope glycoprotein gp120 to CD4 molecules on the target cell membrane. This binding leads to an important conformational change that results in the formation of a new recognition site on gp120 for the co-receptors CCR5 or CXCR4.

HIV strains can be classified into two groups on the basis of their ability to infect macrophages and CD4+T Cells. Macrophage-tropic (M-tropic) strains, their name notwithstanding, can infect both monocytes/macrophages and freshly isolated peripheral blood T cells (but not in *vitro* propagated T-cell lines). The T-cell tropic

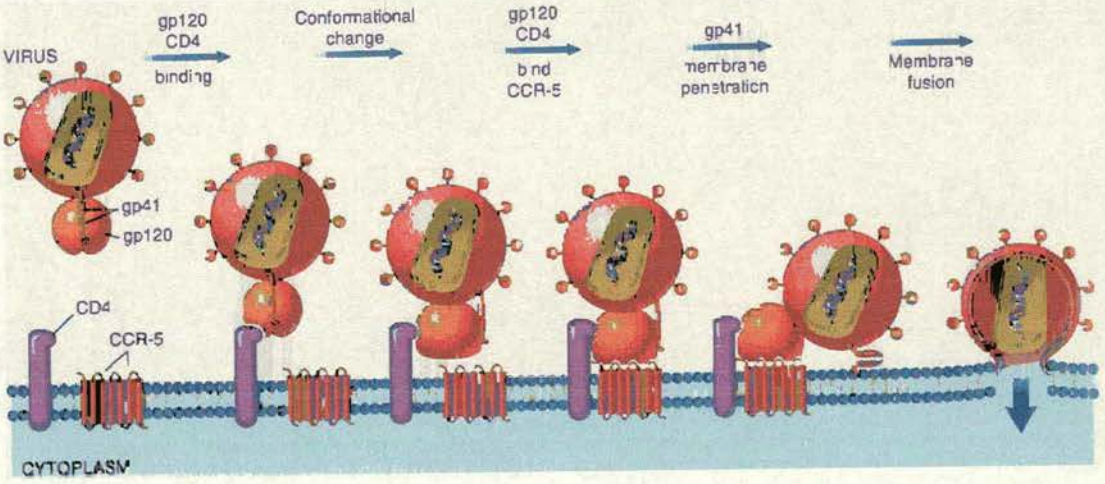

Figure 1.10 HIV entry into host cell (ref. 54)

strains can infect only T cells, both freshly isolated and retained in culture. M-tropic strains use CCR5, whereas T-tropic strains bind to the CXCR4 receptor. Because CCR5 is expressed on both monocytes and T cells, they succumb to infection by M-tropic strains; CXCR4 is expressed on T cells but not on monocytes/macrophages, and hence T cells but not macrophages are susceptible to infection with T-tropic strains. Primary T cells (freshly isolated) express both CCR5 and CXCR4 and hence can be infected by either of the two viral types.

The next step involves conformational changes in the gp41 protein; these changes result in the insertion of a fusion peptide at the tip of gp41 into the cell membrane of the target T cells or macrophages. After fusion, the virus core containing the HIV genome enters the cytoplasm of the cell. Molecular details of this fatal binding between HIV glycoproteins and their cell surface receptors are important because they may provide the basis of anti-HIV therapy.

1.5.2 CXCR4 co-receptor

The migration of leukocytes can be activated and directed by chemokines through G-protein-coupled seven-transmembrane receptors. CXCR4 is a G-protein-coupled, 7-transmembrane domain receptor whose physiological ligand is the stromal cell-derived factor-1 (SDF-1) chemokine, which is also used by distinct strains of HIV-1 as cofactors for viral entry (Figure 1.11).[55,56]

Crump and co-workers have determined the three-dimensional structure of SDF-1 by NMR spectroscopy.[57] As for other chemokines, the N-terminal amino acids KPVSLSYR before the first two cysteines form an essential part of the binding site. The residues RFFESH (12-17) immediately downstream to the second Cys are also an important part of the binding site. A model for SDF-1 and CXCR4

interaction in which the RFFESH motif is the initial docking site with CXCR4 and the N-terminal residues are responsible for signalling has been proposed.

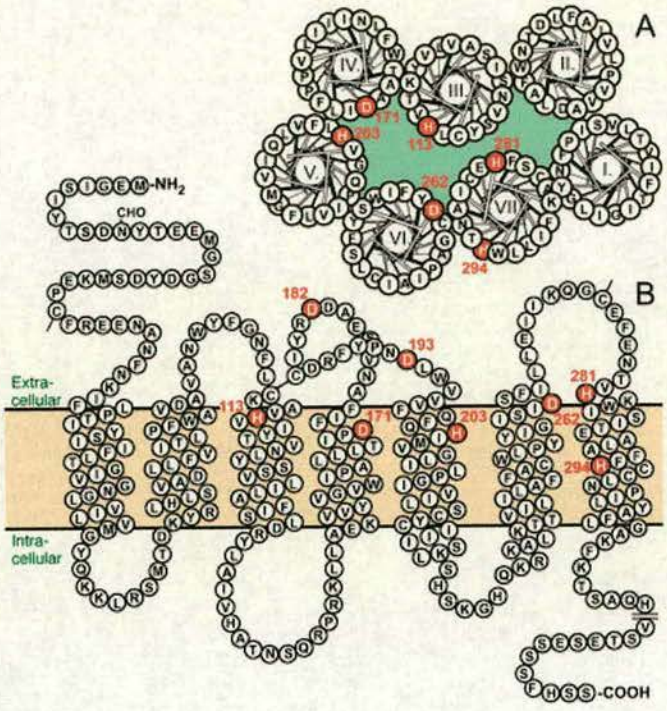

Figure 1.11 Helical wheel (A) and serpentine diagram (B) of the CXCR4 receptor. White letters in red circles represent residues substituted with Ala or Asn probing the binding site of AMD3100 (ref. 58)

The general conclusion from studies on the determinants of the CXCR4 co-receptor function is that the CXCR4 amino-terminal domain (Nt) and the second extracellular (ECL2) are essential for its co-receptor activity.[59] Studies of CXCR4 point mutants have delineated more precisely a region of CXCR4 that plays a pivotal role in virus fusion and entry. Several mutations enable CXCR4 to mediate weak

fusion and entry of R5 strains, including conversion of Asp187 to a neutral residue,[60] alanine substitutions of Arg30 and Asp193,[61] and removal of an N-linked glycosylation site in the CXCR4 Nt.[62] Charged residues Asp193, Arg183 and Arg188 in ECL2 were shown to affect differently the entry of various HIV-1 strains; for example, only HIV-1NDK was sensitive to substitutions of Asp193, whereas all other test strains are sensitive to changes in Arg183 and Arg188.[63] In a recent report, Glu15 and Glu32 in the Nt, Asp97 in ECL1 and Arg188 in ECL2 were found to be involved in CXCR4-mediated entry of X4 and R5X4 isolates.[61] Another study found that multiple substitutions of Tyr7, Asp10, Tyr12, Asp20, Tyr21, Asp22, Ser23 and Glu26 in the Nt and Asp182, Tyr184, Asp187, Tyr190 and Asp193 in ECL2 influence HIV-1 entry, albeit in an isolate-dependent manner.[64] No clear patterns of CXCR4 amino acid usage by X4 and R5X4 isolates, taken as phenotypic groups, were observed.[64] A study by Brelot *et al* confirms the role of Tyr7, Tyr12 and Tyr21 in the Nt, as well as Asp193 in ECL2 and Asp262 in ECL3, in CXCR4 co-receptor function. Presumably, Tyr, Asp and Glu residues important for CXCR4-mediated virus entry are implicated in gp120 binding.[65] It should be noted here that the CXCR4 Nt is sulfated, presumably due to the presence of sulfotyrosines. Inhibition of cellular sulfation pathways, including tyrosine sulfation, blocks CXCR4-mediated HIV-1 entry. It is therefore probable that, like gp120 binding to CCR5, gp120 binding to CXCR4 requires the presence of sulfotyrosines.

The use of Mabs (monoclonal antibodies), chemokines and their derivatives, peptides and small molecules (<1 kDa) that inhibit CXCR4-mediated HIV-1 entry has provided further insight into the structure–function relationships of this co-receptor. Little is known, however, about the mechanisms of action of these agents.

Lack of a practical and reproducible binding assay has made it difficult to determine whether inhibitors of CXCR4-mediated entry block gp120 binding to the co-receptor. Also, surprisingly few anti-CXCR4 Mabs have been generated and only one has been extensively characterized. Mab 12G5 recognises an epitope in ECL2 and inhibits HIV-1 fusion and entry both in an isolate- and a cell type-specific manner.[66] Differences in gp120 affinities for CXCR4 and post-translational modifications of CXCR4 in different cell types could account for these discrepancies. Other anti-CXCR4 Mabs, whose epitopes remain to be determined, also variably inhibit the entry of the HIV-1NL-43 isolate.[67]

1.5.3 Anti-HIV activity of bicyclams

1. Bicyclam

The co-receptor has been identified as a cell surface protein which is called fusin due to its pivotal role in helping HIV fuse with CD4 cells. The discovery of fusin is considered a breakthrough because it reveals a new target for anti-HIV drugs. Bicyclams are a new class of highly potent and selective HIV inhibitors which interact with the receptor CXCR4, the main co-receptor used by T-cell tropic strains of HIV.[68]

Bicyclam activity originated from the serendipitous discovery of anti-HIV activity in a monocyclam preparation that contained bicyclam as a contaminant.[69] Starting from this lead compound, several bicyclam derivatives were prepared that showed increased anti-HIV activity. Unlike the non-nucleoside type of HIV-1-specific reverse transcriptase inhibitors, which are inhibitory to HIV-1 but not HIV-2. The bicyclams are active against both HIV-1 and HIV-2.[68]

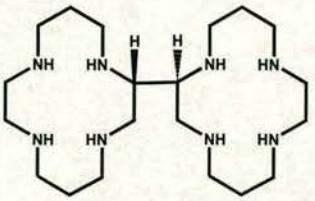

AMD1657

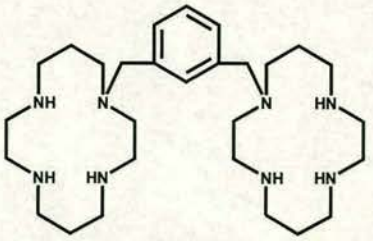

AMD2986

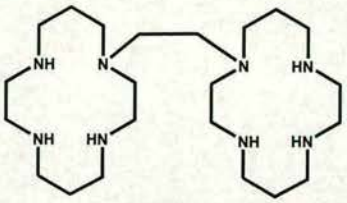

AMD2762

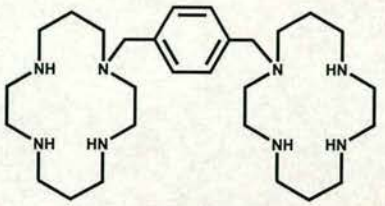

AMD3100

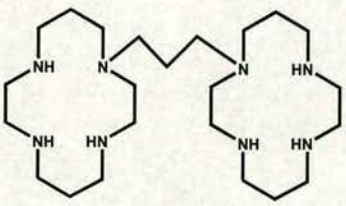

AMD2763

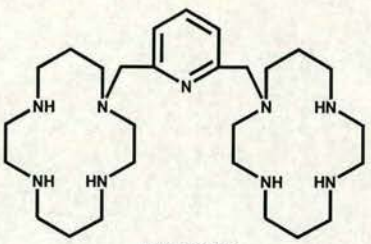

AMD3106

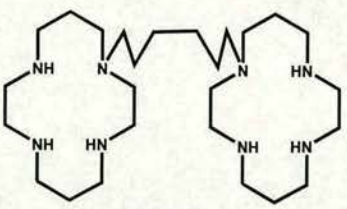

AMD2849

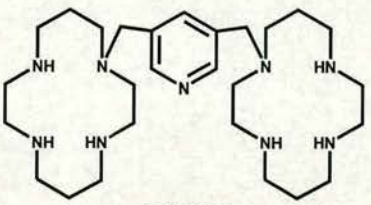

AMD3109

The most active of this series is AMD3100[70], being on clinical trial[71], which has been found to inhibit HIV-induced cytopathicity at a concentration of a few nanograms per ml, while not being toxic to the host cells at concentrations up to 500 μg/ml, thus achieving a selectivity index of 100,000 or higher (Table 1.3). It is active against both laboratory strains and clinical isolates of HIV in T4 lymphocytes and monocytes. Finally, it acts additively when combined with dideoxynucleoside analogues such as AZT or DDI.

Table 1.3 Anti-HIV activity of bicyclam AMD3100 (data from ref. 75)

Virus	Strain	Cell line	EC_{50}(μg/ml)	CC_{50}(μg/ml)	Selectivity index CC_{50}/EC_{50}
HIV-1	III_b	MT-4	0.005	>500	>100000
HIV-1	RF	MT-4	0.001	>500	>500000
HIV-1	HE	MT-4	0.003	>500	>16700
HIV-2	ROD	MT-4	0.007	>500	>71400
HIV-2	EHO	MT-4	0.004	>500	>125000
SIV	MAC251	MT-4	>100	>100	...
SIV	AGM3	MOLT-4	>100	>100	...
SIV	MNDGB1	MOLT-4	>100	>100	...

The compound AMD3100 did not lead to development of resistance (as measured by viral cytopathicity) following at least 14 to 30 passages (49 to 105 days) of HIV-1(III_B) in CEM cells in the presence of various drug concentrations. However, full resistance to the bicyclams AMD2763 and AMD2987 was observed.[68]

The anti-HIV activity exhibited by bicyclams is particularly intriguing due to the possibility that binding to the molecular target at the HIV-inhibitory step is transition metal-mediated.[63] For example, Mallick and co-workers[72] have proposed that bis-transition metal complexes of AMD3100 can provide complementary coordinating sites for the chelating amino acid residues on a protein surface. This type of mechanism is plausible since AMD3100 will almost certainly complex free transition metals in vitro, and a variety of preformed transition metal complexes of

AMD3100 and several other bicyclams exhibit antiviral activity.[73] In this manner, AMD3100 could be viewed as a prodrug for a transition metal complex in a similar manner to the antitumour agent bleomycin.[74]

A series of bicyclam analogues connected through a heteroaromatic linker have been synthesized and evaluated for their inhibitory effects on HIV-1 (IIIB) and HIV-2 (ROD) replication in MT-4 cells.[63] The activity of pyridine- and pyrazine-linked bicyclams was found to be highly dependent upon the substitution of the heteroaromatic linker connecting the cyclam rings. For example, 2,6- and 3,5-pyridine-linked bicyclams were potent inhibitors of HIV-1 and HIV-2 replication, whereas the 2,5- and 2,4-substituted pyridine-linked compounds exhibited substantially reduced activity and, in addition, were found to be highly toxic to MT-4 cells. Subsequent discovery also showed that amino-substituted linkers also have the potential to deactivate phenylenebis(methylene)-linked bicyclams. A model has been proposed to explain the deactivating effects of the pyridine group in certain substitution patterns based on the ability of the pyridine nitrogen to participate in pendant conformations (complexation) with the adjacent azamacrocyclic ring, which may involve hydrogen bonding or coordination to a transition metal. The introduction of a sterically hindering group such as phenyl at the 6-position of the 2,4-substituted pyridine-linked bicyclam appears to prevent pendant conformations, providing an analogue with comparable anti-HIV-1 and anti-HIV-2 activities to the parent m-phenylenebis(methylene)-linked bicyclam. The results of this study have been used to develop a quantitative structure-activity relationship model with improved predictive capability in order to aid the design of antiviral bis-azamacrocyclic analogues.[70]

2. Bicyclam complexes

The initial events (virus adsorption and fusion with the cells) in the replicative cycle of human immunodificiency virus (HIV) can serve as targets for the antiviral action of metal-binding compounds such as polyanionic compounds, bicyclams and G-octet-forming oligonucleotides.[75]

Table 1.4 Inhibitory effects of different bicyclam-metal complexes on HIV-induced cytopathicity and syncytium formation (see p24 for the structures of compounds AMD3100 etc; data from ref. 75)

Compound	Complexing metal	EC_{50} (μg/ml)			
		Viral cytopathicity		Syncytium formation	
		HIV-1(III_B)	HIV-2(ROD)	HIV-1(III_B)	HIV-2(ROD)
AMD3100		0.009	0.021	0.1	1.8
AMD3479	Zn	0.008	0.025	0.1	0.2
AMD3462	Ni	0.017	0.028	0.3	0.3
AMD3469	Cu	0.048	0.21	1.5	2.4
AMD3461	Co	0.74	18.21	62.5	125
AMD3158	Pd	68.62	>250	>250	>250

Zn may play a key role in the anti-HIV activity of the bicyclams, as is evident from Table 1.4. Only the zinc complex with the bicyclam AMD3100 (i.e. AMD3479) is equipotent to AMD3100. The other metal bicyclam complexes (AMD3462, AMD3469, AMD3461, and AMD3158) containing Ni, Cu, Co, and Pd, showed gradual loss in activity, the Pd complex being inactive as an anti-HIV compound. Furthermore, the early events in HIV infection are known, i.e. virus adsorption to the cells and virus cell fusion, and have been shown to be the points of attack for zinc complexes of bicyclam.

A recent study also reached a similar conclusion.[76] The Zn(II) complex (AMD3479) was slightly more active (10-fold) than AMD3100; the Ni(II) complex (AMD3462) was as active as AMD3100 in its capacity to inhibit 12G5 binding (Table 1.5). The Cu^{2+} (AMD3469) and Co^{3+} (AMD3461) complexes were 5-fold and 2220-fold less active, respectively, than AMD3100. The Pd^{2+} complex (AMD3158) was virtually inactive. Similar differential inhibitory effects were noted for the metal complexes on the binding of the Mab with CXCR4; the IC_{50} for 12G5 binding to SUP-T1 cells closely paralleled the EC_{50} for anti-HIV activity. Similarly, the EC_{50} for anti-viral activity of metal complexes correlated with the IC_{50} for inhibition of the Ca^{2+} flux induced by SDF-1α indicating the dependence on the interaction of metal-complexed bicyclams with CXCR4 for their respective anti-HIV activity.

Table 1.5 Anti-HIV activity, inhibition of 12G5 Mab binding and inhibition of $[Ca^{2+}]_i$ flux of AMD3100 and its different transition metal complexes (data from ref. 76)

Compound (bound metal)	EC_{50}[a] for HIV-1 (IIIb)	IC_{50}[b] 12G5 Binding ($\mu g/ml$)	IC_{50} $[Ca^{2+}]_i$[c]
AMD3100	0.009	0.01	0.005
AMD3479 (Zn)	0.008	0.001	0.003
AMD3462 (Ni)	0.008	0.016	0.002
AMD3469 (Cu)	0.048	0.2	0.05
AMD3461(Co)	0.74	0.5	0.6
AMD3158 (Pd)	68.62	12.5	70

[a] EC_{50} as measured by the MTT assay.

[b] IC_{50}: 50% inhibitory concentration, or concentration of the compound required to inhibit by 50% the binding of 12G5 Mab to CXCR4+ SUP-T1 cells.

[c] IC_{50} $[Ca^{2+}]_i$ by SDF-1α in SUP-T1 cells. (NB: Cells were first stimulated with dilution buffer (control) or test compound at different concentrations. SDF-1α was used as a second stimulus to induce $[Ca^{2+}]_i$ increase; it was added 100 s after the first stimulus. The compound concentration required to inhibit the $[Ca^{2+}]_i$ increase by 50% ($IC_{50\ [Ca2+]i}$) was calculated.

1.5.4 Mechanism of action of bicyclams

Bicyclam derivatives exhibit a mode of anti-HIV action that is clearly different from those of any of the other anti-HIV agents that are presently used or considered for use in the treatment of HIV infections.[68] They are not inhibitory to either HIV reverse transcriptase or HIV protease,[68] and they do not inhibit virus binding to cells.[77]

The bicyclams inhibit a specific event that is involved in viral uncoating and represent the first compounds that have been postulated to affect the uncoating of the retrovirus.[68] Time-of-addition experiments have revealed that the bicyclams interact at a stage following virus adsorption but preceding reverse transcription. The possibility that this stage may be associated with the uncoating process was then assessed by experiments in which the sensitivity of the viral RNA to degradation by ribonuclease A was determined. It was reasoned that as long as uncoating had not taken place, the viral RNA would be protected by the capsid proteins against degradation by RNase A. These experiments revealed that the bicyclams, i.e., AMD2763 and AMD3100, but not any of the reverse transcriptase inhibitors or protease inhibitors, protected the viral RNA against degradation. Because of the intervention of the bicyclams, the capsid proteins remained associated with and thus could not be uncoated from the viral RNA.

Inhibitors of the uncoating (disassembly) process might also be expected to interfere with the opposite process, namely, assembly. In support of such an assumption, the bicyclam AMD3100 was found to inhibit (at an EC_{50} of 0.02 μg/ml) the production of infectious HIV particles from the chronically infected Jurkat/III_B cell line, whereas p24 antigen production by this cell line was not affected by AMD3100 at concentrations up to 1 μg/ml. The mechanism of this late effect of the bicyclams may well be associated with an interference with virus assembly, and therefore bear resemblance to the mechanism of their inhibitory action on virus uncoating.

It was demonstrated recently that AMD3100 inhibits HIV entry through the co-receptor CXCR4 but not through the co-receptor CCR5.[78] AMD3100 completely

blocked HIV-1 infection mediated by a mutant CXCR4 bearing a deletion of most of the amino-terminal extracellular domain. Relative resistance to AMD3100 was conferred by different single amino acid substitutions in the second extracellular loop (ECL2), or in the adjacent membrane-spanning domain, TM4. Only substitutions of a neutral residue for aspartic acid and of a non-aromatic residue for phenylalanine (Phe) were associated with drug resistance.[78] This suggests a direct interaction of AMD3100 with these amino acids rather than indirect effects of their mutation on CXCR4 structure. Bicyclams are strongly basic due to the presence of four secondary amines in each cyclam unit and might interact with a negatively-charged domain of CXCR4, in particular ECL2 (5 acidic residues; net charge, -3), which might block HIV-1 entry by preventing electrostatic interactions between CXCR4 and the HIV-1 envelope protein gp120. Other features of AMD3100 must account for its high antiviral activity, in particular the presence of an aromatic linker between the cyclam units. This aromatic group might engage in hydrophobic interactions with the Phe-X-Phe motifs of ECL2 or TM4.

When the supposedly main binding site for the free cyclam moiety was eliminated in the D171N mutation, the affinity of the monocyclam was determined to be *ca* 400 μM. This could possibly represent the affinity of the cyclam at the Asp262 site, which could have been confirmed by the D171N/D262N double mutation.[58] However, the low expression level of this construct unfortunately prohibited this. Another possibility is that although cyclam binds to Asp262, this binding could be silent with respect to the effect on SDF-1 binding. Nevertheless, the fact that the binding of bicyclam AMD3100 clearly is dependent on both Asp171 and Asp262 and the fact that cyclam has a strong propensity to interact with carboxylate indicate

that each of the cyclam moieties of the bicyclam binds to each of these two Asp residues located in TM-IV and TM-VI, respectively.

1.6 Aims of this thesis

As described above, the CXCR4 co-receptor antagonist bicyclam AMD3100 has recently been on phase II clinical trial against AIDS and may be active in vivo as a Zn(II) complex. The aim of this thesis was therefore to investigate structural and dynamic properties of metal cyclam and bicyclam complexes as a potential aid to the design of more active anti-HIV agents. Specific aims were as follows:

1. To synthesise and characterise Zn(II) and Cd(II) cyclam and xylylbicyclam complexes both in the solid state and in solution, particularly using X-ray crystallography and multinuclear and multidimensional NMR spectroscopy.

2. To investigate synthetic routes to ^{15}N-labelled cyclam and (xylylbicyclam) which might allow detailed ^{15}N NMR studies to be undertaken in order to probe the interaction of cyclam complexes with biomolecules.

3. To investigate the factors which control the configurations of metal (bi)cyclam complexes in solution and relate them to the interaction of metal (bi)cyclam complexes and its receptor protein CXCR4.

4. To investigate the interaction of Zn(II) xylylbicyclam with lysozyme as a model protein for the co-receptor CXCR4.

1.7 References

(1) Moeller, T. In *Inorganic Chemistry*; John Wiley & Sons: New York, 1952, Chap. 19, p 847.

(2) Cotton, F. A.; Wilkinson, G. In *Advanced Inorganic Chemistry*, 4th ed.; John Wiley & Sons: New York, 1980, Chap. 19, p 590.

(3) Luchinat, C.; Sola, M. In *Encyclopaedia of Inorganic Chemistry*; King, R. B., Ed-in-Chief; John Wiley & Sons: Chichester, 1994; Vol. 8, p 4410.

(4) Massey, A. G. In *Main Group Chemistry*, Ellis Horwood Ltd.: Chichester, 1990, Chap. 5, p171.

(5) (a) Rosenberg, B.; Van Camp, L.; Trosko, J. E.; Mansour, H. V. *Nature* **1969**, *222*, 385. (b) Rosenberg, B.; Van Camp, L. *Cancer Res.* **1970**, *30*, 1799. (c) Kociba, R. J.; Sleight, S. D.; Rosenberg, B. *Cancer Chemother. Rep.* **1970**, (Part I 54), 325.

(6) (a) Weiss, R. B.; Christian, M. C. *Drugs* **1993**, *46*, 360. (b) Gordon, M.; Hollander, S. *J. Med.* **1993**, 209.

(7) Guo, Z.; Sadler, P. J. *Adv. Inorg. Chem.* **2000**, *49*, 183.

(8) Di Blasi, P.; Bernareggi, A.; Beggiolin, G.; Piazzoni, L.; Menta, E.; Formento, M. L. *Anticancer Res.* **1998**, *18*, 3113.

(9) (a) Christodoulou, C. V.; Eliopoulos, A. G.; Young, L. S.; Hodgkins, L.; Ferry, D. R.; Kerr, D. J. *Br. J. Cancer* **1998**, *77*, 2088. (b) Villena-Heinsen, C.; Friedrich, M.; Ertan, A. K.; Farnhammer, C.; Schmidt, W. *Anticancer Drugs* **1998**, *9*, 557. (c) Friedrich, M.; Villena-Heinsen, C.; Farnhammer, C.; Schmidt, W. *Eur. J. Gynaecol. Oncol.* **1998**, *19*, 333.

(10) Keppler, B. K.; Schmähl, D. *Arzneim.-Forsch / Drug Res.* **1986**, *36*, 1822.

(11) Christodoulou, C.; Ferry, D.; Fyfe, D.; Young, A.; Doran, J.; Sass, G.; Eliopoulos, A.; Sheehan, T.; Kerr, D. J. "Proc. 88th Annual Meeting American Association for Cancer Research," April 12-16, 1997, San Diego, CA, Vol. 38, No. 1495, pp. 222.

(12) Shaw, C. F., III *Chem. Rev.* **1999**, *99*, 2589.

(13) Griem, P.; Gleichmann, E. *Zeitsch. Rheumatol.* **1996**, *55*, 348.

(14) Thompson, K. H.; McNeill, J. H.; Orvig, C. *Chem. Rev.* **1999**, *99*, 2561.

(15) Kimura, E. *Tetrahedron* **1992**, *48*, 6175.

(16) Kimura, E., In *Biomimetic and Bioinorganic Chemistry*, Topics in Current Chemistry; Springer Verlag: Heideberg, 1985, Vol. 128, p 1131.

(17) Donnelly, M. A.; Zimmer, M. *Inorg. Chem.* **1999**, *38*, 1650.

(18) Van Alphen, J. *Recl. Trav. Chim. Pays-Bas* **1937**, *56*, 343.

(19) Barefield, E. K.; Bianchi, A.; Billo, E. J.; Connolly, P. J.; Paoletti, P.; Summers, J. S.; Derveer, D. G. V. *Inorg. Chem.* **1986**, *25*, 4197.

(20) Pierce, D. T.; Hatfield, T. L.; Billo, E. J.; Ping, Y. *Inorg. Chem.* **1997**, *36*, 2950.

(21) Kodama, M.; Kimura, E. *J. Chem. Soc., Dalton Trans.* **1977**, 1473.

(22) Hinz, F. P.; Margerum, D. W. *Inorg. Chem.* **1974**, *13*, 2941.

(23) Kodama, M.; Kimura, E. *J. Chem. Soc., Dalton Trans.* **1978**, 1081.

(24) Kodama, M.; Kimura, E. *J. Chem. Soc., Dalton Trans.* **1977**, 2269.

(25) Kodama, M.; Kimura, E., *J. Chem. Soc., Dalton Trans.* **1980**, 327.

(26) Kimura, E., *Prog. Inorg. Chem.* **1994**, *41*, 443.

(27) Bosnich, B.; Poon, C. K.; Tobe, M. L. *Inorg. Chem.* **1965**, *4*, 1102.

(28) Whimp, P. O.; Bailey, M. F.; Curtis, N. F. *J. Chem. Soc. A* **1970**, 1956.

(29) Connolly, P. J.; Billo, E. J. *Inorg. Chem.* **1987**, *26*, 3224.

(30) (a) Wagner, F.; Barefield, E. K. *Inorg. Chem.* **1976**, *15*, 408; (b) Alcock, N. W.; Curzon, E. H.; Moore, P.; Pierpoint, C.; *J. Chem. Soc., Dalton Trans.* **1984**, 605.

(31) Moore, P.; Sachinidis, J.; Willey, G. R. *J. Chem. Soc., Chem. Commun.* **1983**, 522.

(32) Lincoln, S. F.; Pisaniello, D. L.; Coates, J. H.; Hadi, D. A. *Inorg. Chim. Acta Lett.* **1984**, *81*, 9.

(33) Tyson, T. A.; Hodgson, K. O. *Acta Cryst.* **1990**, *C46*, 1638.

(34) Ito, T.; Kato, M.; Ito, H. *Bull. Chem. Soc. Jpn.* **1984**, *57*, 2634.

(35) Alcock, N. W.; Berry, A.; Moore, P. *Acta Cryst.* **1992**, *C48*, 16.

(36) Kato, M.; Ito, T. *Inorg. Chem.* **1985**, *24*, 505.

(37) Kimura, E.; Kurosaki, H.; Koike, T.; Toriumi, K. *J. Inclusion Phenomena Mol. Recog. Chem.*, **1992**, *12*, 377.

(38) Kimura, E.; Shiota, T.; Koike, T.; Shiro, M.; Kodama, M. *J. Am. Chem. Soc.* **1990**, *112*, 5805.

(39) Kimura, E.; Shionoya, M.; Hoshino, A.; Ikeda, T.; Yamada, Y. *J. Am. Chem. Soc.*, **1992**, *114*, 10134.

(40) Shelton, V. M.; Morrow, J. R. *Inorg. Chem.*, **1991**, *30*, 4295.

(41) Barefield, E. K.; Chueng, D.; Van Derveer, D. G.; Wagner, F. *Chem. Commun.* **1981**, 302.

(42) Mochizuki, K. *Chem. Lett.*, **2000**, 26.

(43) Kajiwara, T.; Yamaguchi, T.; Kawabata, H. S.; Kuroda, R.; Ito, T. *Inorg. Chem.* **1993**, *32*, 4990.

(44) Ciampolini, M.; Fabbrizzi, L.; Perotti, A.; Poggi, A.; Seghi, B.; Zanobini, F. *Inorg. Chem.*, **1987**, *26*, 3527.

(45) Brooks, G. F.; Butel, J. S.; Morse, S. A. In *Medical Microbiology*, 21st ed.; Appleton & Lange: London, 1998, p 345.

(46) De Clercq, E., *Pure Appl. Chem.*, **1998**, *70*, 567.

(47) Winter, H.; Maeda, Y.; Uchida, H.; Mitsuya, H.; Zemlicka, J. *J. Med. Chem.*, **1997**, *40*, 2191.

(48) Murphy, R., *The PRN Notebook*, 1998, 3(1), article3 (http://www.prn.org/prn_nb_cntnt/vol3/num1/article3_frm_set.htm)

(49) James, J. S. *AIDs Treatment News*, Issue 237 (http://www.immunet.org/immunet/atn.nsf/page/ZQX23701.html

(50) Greene, W. C. In *The Medical Management of AIDS*, 5th ed.; Sande, M. A., Volberding, P. A.; Saunders: London, 1997, p17.

(51) Growe, S.; Mills, J. In *Basic and Clinical Immunology*, 8th ed.; Stites, D. P., Terr, A. I., Parslow, T. G., Eds.; Appleton & Lange: East Norwalk, 1994, p 689.

(52) The illustration of the life cycle of virus was downloaded from the website: http://www.rkm.com.au/AIDSeducation.html.

(53) Meissner, C.; Coffin, J. M. In *Mechanisms of Microbial Disease*, 3rd ed.; Schaechter, M., Engleberg, N. C., Eisenstein, B. I., Medoff, G., Eds.; Williams & Wilkins: London, **1998**, p 350.

(54) Robbins, S. L. In *Robbins Pathologic Basis of Disease*, 6th ed.; Cotran, R. S., Kumar, V., Collins, T., Eds.; Saunders: London, 1999, p 188.

(55) Bleul, C. C.; Farzan, M.; Choe, H.; Parolin, C.; Clark-Lewis, I.; Sodroski, J.; Springer, T. A. *Nature*, **1996**, *382*, 829.

(56) Oberlin, E.; Amara, A.; Bachelerie, F.; Bessia, C.; Virelizier, J.-L.; Arenzana-Seisdedos, F.; Schwartz, O.; Heard, J.-M.; Clark-Lewis, I.; Legler, D. F.; Loetscher, M.; Baggiolini, M.; Moser, B. *Nature*, **1996**, *382*, 833.

(57) Crump, M. P.; Gong, J.-H.; Loetscher, P.; Rajarathnam, K; Amara, A.; Arenzana-Seisdedos, F.; Virelizier, J.-L.; Baggiolini, M.; Sykes, B. D.; Clark-Lewis, I. *EMBO J.* **1997**, *16*, 6996.

(58) Gerlach, L. O., Skerlj, R., Bridgers, G. J. & Schwartz, T. W. *J. Biol. Chem.*, **2001**, *276*, 14153.

(59) (a) Brelot, A.; Heveker, N.; Pleskoff, O.; Sol, N; Alizon, M. *J. Virol.* **1997**, *71*, 4744. (b) Doranz, B.; Orsini, M.; Turner, J.; Hoffman, T.; Berson, J.; Hoxie, J.; Peiper, S.; Brass, L.; Doms, R. *J. Virol.* **1999**, *73*, 2757. (c) Lu, Z.; Berson, J. F.; Chen, Y.; Turner, J. D.; Zhang, T.; Sharron, M.; Jenks, M. H.; Wang, Z.; Kim, J.; Rucker, J.; Hoxie, J. A.; Peiper, S. C.; Doms, R. W. *Proc. Natl. Acad. Sci. USA* **1997**, *94*, 6426. (d) Reeves, J. D.; Heveker, N.; Brelot, A.; Alizon, M.; Clapham, P. R.; Picard, L. *J. Gen. Virol.* **1998**, *79*, 1793. (e) Willett, B. J.; Adema, K.; Heveker, N.; Brelot, A.; Picard, L.; Alizon, M.; Turner, J. D.; Hoxie, J. A.; Peiper, S.; Neil, J. C.; Hosie, M. J. *J. Virol.* **1998**, *72*, 6475. erratum 8460.

(60) (a). Chabot, D. J.; Broder, C. C. *J. Biol. Chem.* **2000**, *275*, 23774. (b) Wang, Z. X.; Berson, J. F.; Zhang, T. Y.; Cen, Y. H.; Sun, Y.; Sharron, M.; Lu, Z. H.; Peiper, S. C. *J. Biol. Chem.* **1998**, *273*, 15007.

(61) Chabot, D. J.; Zhang, P. F.; Quinnan, G. V.; Broder, C. C. *J. Virol.* **1999**, *73*, 6598.

(62) Chabot, D. J.; Chen, H.; Dimitrov, D. S.; Broder, C. C. *J. Virol.* **2000**, *74*, 4404.

(63) Brelot, A.; Heveker, N.; Adema, K.; Hosie, M. J.; Willett, B.; Alizon, M. *J. Virol.* **1999**, *73*, 2576.

(64) Kajumo, F.; Thompson, D. A. D.; Guo, Y.; Dragic, T. *Virol.* **2000**, *271*, 240.

(65) Brelot, A.; Heveker, N.; Montes, M.; Alizon, M. *J. Biol. Chem.* **2000**, *275*, 23736.

(66) (a) McKnight, A.; Wilkinson, D.; Simmons, G.; Talbot, S.; Picard, L.; Ahuja, M.; Marsh, M.; Hoxie, J. A.; Clapham, P. R. *J. Virol.* **1997**, *71*, 1692. (b) Strizki, J. M.; Turner, J. D.; Collman, R. G.; Hoxie, J.; Gonzalez-Scarano, F. *J. Virol.* **1997**, *71*, 5678.

(67) Hori, T.; Sakaida, H.; Sato, A.; Nakajima, T.; Shida, H.; Yoshie, O.; Uchiyama, T. *J. Immunol.* **1998**, *160*, 180.

(68) (a) De Clercq, E.; Yamamoto, N.; Pauwels, R.; Baba, M.; Schols, D.; Nakashima, H.; Balzarini, J.; Debyser, Z.; Murrer, B. A.; Schwartz, D.; Thornton, D.; Bridger, G.; Fricker, S.; Henson, G.; Abrams, M.; Picker, D. *Proc. Natl. Acad. Sci. U.S.A.* **1992**, *89*, 5286. (b) De Clercq, E.; Yamamoto, N.; Pauwels, R.; Balzarini, J.; Witvrouw, M.; De Vreese, K.; Debyser, Z.; Rosenwirth, B.; Peichl, P.; Datema, R.; Thornton, D.; Skerlj, R.; Gaul, F.; Padamanabhan, S.; Bridger, G.; Henson, G.; Abrams, M. *Antimicrob. Agents Chemother.* **1994**, *38*, 668.

(69) (a)De Clercq, E. *Mol. Pharmacol.* **2000**, *57*, 833. (b) De Clercq, E.; Yamamoto, N.; Pauwels, R.; Baba, M.; Schols, D.; Nakashima, H.; Balzarini, J.; Debyser, Z.;

Murrer, B. A.; Schwartz, D.; Thornton, D.; Bridger, G.; Fricker, S.; Henson, G.; Abrams, M.; Picker, D. *Proc. Natl. Acad. Sci. U.S.A.* **1992**, *89*, 5286.

(70) (a) Bridger, G. J.; Skerlj, R. T.; Thornton, D.; Padmanabhan, S.; Martellucci, S. A.; Henson, G. W.; Abrams, M. J.; Yamamoto, N.; De Vreese, K.; Pauwels, R.; De Clercq, E. *J. Med. Chem.* **1995**, *38*, 366. (b) Bridger, G. J.; Skerlj, R. T.; Padmanabhan, S.; Martellucci, S. A.; Henson, G. W.; Abrams, M. J.; Joao, H.; Witvrouw, M.; De Vreese, K.; Pauwels, R.; De Clercq, E. *J. Med. Chem.* **1996**, *39*, 109. (c) Joao, H. C.; De Vreese, K.; Pauwels, R.; De Clercq, E.; Henson, G. W.; Bridger, G. J. *J. Med. Chem.* **1995**, *38*, 3865. (e) De Vreese, K.; Reymen, D.; Griffin, P.; Steinkasserer, A.; Werner, G.; Bridger, G. J.; Este, J.; James, W.; Henson, G. W.; Desmyter, J.; Anne, J.; De Clercq, E. *Antiviral Res.* **1996**, *29*, 209.

(71) Wallace, O. *Chem. Brit.* **2000**, *36*, 38.

(72) (a) Mallick, S.; Johnson, R. D.; Arnold, F. H. *J. Am. Chem. Soc.* **1993**, *115*, 2518. (b) Mallick, S.; Johnson, R. D.; Arnold, F. H. *J. Am. Chem. Soc.* **1994**, *116*, 8902.

(73) (a) Bridger, G.; Skerlj, R.; Thornton, D.; Padmanabhan, S.; Martellucci, S.; Henson, G.; Abrams, M.; Yamamoto, N.; De Vreese, K.; Pauwels, R.; De Clercq, E. *J. Med. Chem.* **1995**, *38*, 366. (b) Inouye, Y.; Kanamori, T.; Yoshida, T.; Bu, X.; Shionoya, M.; Koike, T.; Kimura, E. *Biol. Pharm. Bull.* **1994**, *17*, 243.

(74) Hecht, S. M. *Bioconjug. Chem.* **1994**, *5*, 513.

(75) DeClercq, E., *Metal-Based Drugs*, **1997**, *4*, 173.

(76) Este, J. A.; Cabrera, C.; De Clercq, E.; Struyf, S.; Van Damme, J.; Bridger, G.; Skerlj, R. T.; Abrams, M. J.; Henson, G.; Gutierrez, A.; Clotet, B.; Schols, D. *Mol. Pharmacol.* **1999**, *55*, 67.

(77) De Clercq, E., Int. *J. Immunother.* **1992**, *8*, 115.

(78) (a) Labrosse, B., Brelot, A., Heveker, N., Sol, N., Schols, D., Declercq, E., Alizon, M., *J. Virol.* **1998**, *72*, 6381. (b) Donzella, G. A., Schols, D., Lin, S. W., Este, J. A., Nagashima, K. A., Maddon, P. J., Allaway, G. P., Sakmar, T. P., Henson, G., De Clercq, E. & Moore, J. P. *Nature Medicine*, **1998**, *4*, 72.

(61) Chabot, D. J.; Zhang, P. F.; Quinnan, G. V.; Broder, C. C. *J. Virol.* **1999**, *73*, 6598.

(62) Chabot, D. J.; Chen, H.; Dimitrov, D. S.; Broder, C. C. *J. Virol.* **2000**, *74*, 4404.

(63) Brelot, A.; Heveker, N.; Adema, K.; Hosie, M. J.; Willett, B.; Alizon, M. *J. Virol.* **1999**, *73*, 2576.

(64) Kajumo, F.; Thompson, D. A. D.; Guo, Y.; Dragic, T. *Virol.* **2000**, *271*, 240.

(65) Brelot, A.; Heveker, N.; Montes, M.; Alizon, M. *J. Biol. Chem.* **2000**, *275*, 23736.

(66) (a) McKnight, A.; Wilkinson, D.; Simmons, G.; Talbot, S.; Picard, L.; Ahuja, M.; Marsh, M.; Hoxie, J. A.; Clapham, P. R. *J. Virol.* **1997**, *71*, 1692. (b) Strizki, J. M.; Turner, J. D.; Collman, R. G.; Hoxie, J.; Gonzalez-Scarano, F. *J. Virol.* **1997**, *71*, 5678.

(67) Hori, T.; Sakaida, H.; Sato, A.; Nakajima, T.; Shida, H.; Yoshie, O.; Uchiyama, T. *J. Immunol.* **1998**, *160*, 180.

(68) (a) De Clercq, E.; Yamamoto, N.; Pauwels, R.; Baba, M.; Schols, D.; Nakashima, H.; Balzarini, J.; Debyser, Z.; Murrer, B. A.; Schwartz, D.; Thornton, D.; Bridger, G.; Fricker, S.; Henson, G.; Abrams, M.; Picker, D. *Proc. Natl. Acad. Sci. U.S.A.* **1992**, *89*, 5286. (b) De Clercq, E.; Yamamoto, N.; Pauwels, R.; Balzarini, J.; Witvrouw, M.; De Vreese, K.; Debyser, Z.; Rosenwirth, B.; Peichl, P.; Datema, R.; Thornton, D.; Skerlj, R.; Gaul, F.; Padamanabhan, S.; Bridger, G.; Henson, G.; Abrams, M. *Antimicrob. Agents Chemother.* **1994**, *38*, 668.

(69) (a)De Clercq, E. *Mol. Pharmacol.* **2000**, *57*, 833. (b) De Clercq, E.; Yamamoto, N.; Pauwels, R.; Baba, M.; Schols, D.; Nakashima, H.; Balzarini, J.; Debyser, Z.;

Murrer, B. A.; Schwartz, D.; Thornton, D.; Bridger, G.; Fricker, S.; Henson, G.; Abrams, M.; Picker, D. *Proc. Natl. Acad. Sci. U.S.A.* **1992**, *89*, 5286.

(70) (a) Bridger, G. J.; Skerlj, R. T.; Thornton, D.; Padmanabhan, S.; Martellucci, S. A.; Henson, G. W.; Abrams, M. J.; Yamamoto, N.; De Vreese, K.; Pauwels, R.; De Clercq, E. *J. Med. Chem.* **1995**, *38*, 366. (b) Bridger, G. J.; Skerlj, R. T.; Padmanabhan, S.; Martellucci, S. A.; Henson, G. W.; Abrams, M. J.; Joao, H.; Witvrouw, M.; De Vreese, K.; Pauwels, R.; De Clercq, E. *J. Med. Chem.* **1996**, *39*, 109. (c) Joao, H. C.; De Vreese, K.; Pauwels, R.; De Clercq, E.; Henson, G. W.; Bridger, G. J. *J. Med. Chem.* **1995**, *38*, 3865. (e) De Vreese, K.; Reymen, D.; Griffin, P.; Steinkasserer, A.; Werner, G.; Bridger, G. J.; Este, J.; James, W.; Henson, G. W.; Desmyter, J.; Anne, J.; De Clercq, E. *Antiviral Res.* **1996**, *29*, 209.

(71) Wallace, O. *Chem. Brit.* **2000**, *36*, 38.

(72) (a) Mallick, S.; Johnson, R. D.; Arnold, F. H. *J. Am. Chem. Soc.* **1993**, *115*, 2518. (b) Mallick, S.; Johnson, R. D.; Arnold, F. H. *J. Am. Chem. Soc.* **1994**, *116*, 8902.

(73) (a) Bridger, G.; Skerlj, R.; Thornton, D.; Padmanabhan, S.; Martellucci, S.; Henson, G.; Abrams, M.; Yamamoto, N.; De Vreese, K.; Pauwels, R.; De Clercq, E. *J. Med. Chem.* **1995**, *38*, 366. (b) Inouye, Y.; Kanamori, T.; Yoshida, T.; Bu, X.; Shionoya, M.; Koike, T.; Kimura, E. *Biol. Pharm. Bull.* **1994**, *17*, 243.

(74) Hecht, S. M. *Bioconjug. Chem.* **1994**, *5*, 513.

(75) DeClercq, E., *Metal-Based Drugs*, **1997**, *4*, 173.

(76) Este, J. A.; Cabrera, C.; De Clercq, E.; Struyf, S.; Van Damme, J.; Bridger, G.; Skerlj, R. T.; Abrams, M. J.; Henson, G.; Gutierrez, A.; Clotet, B.; Schols, D. *Mol. Pharmacol.* **1999**, *55*, 67.

(77) De Clercq, E., Int. *J. Immunother.* **1992**, *8*, 115.

(78) (a) Labrosse, B., Brelot, A., Heveker, N., Sol, N., Schols, D., Declercq, E., Alizon, M., *J. Virol.* **1998**, *72*, 6381. (b) Donzella, G. A., Schols, D., Lin, S. W., Este, J. A., Nagashima, K. A., Maddon, P. J., Allaway, G. P., Sakmar, T. P., Henson, G., De Clercq, E. & Moore, J. P. *Nature Medicine*, **1998**, *4*, 72.

Chapter 2

Materials and Methods

2.1 Chemicals and Instruments

Chemicals

Cyclam (1,4,8,11-tetraazacyclotetradecane), TBTU (o-(benzotriazol-1-yl)-N,N,N',N'-tetramethyluronium tetrafluoroborate), tritylchloride, BH_3·THF, butanedione, hexamethylphosphoric triamide, 1, 4-bis-bromomethyl-benzene, zinc chloride (Acros Chemical Co.), hen egg white lysozyme (Sigma Chemical Co.), potassium phthalimide-^{15}N (98%), glycine-^{15}N (99%), sodium carbonate-^{13}C (99%), cadmium chloride, cadmium perchlorate hydrate, zinc perchlorate hexahydrate, zinc acetate dihydrate (Aldrich Chemical Co.), 1,3-dibromopropane (Koch-light Laboratories Ltd.), zinc oxide (BDH Ltd.), and phthalic acid (Fisons Scientific Apparatus Ltd.) were used as received. All other chemicals were A.R. grade. Dry solvents were prepared by standard methods. NMR solvents, deuterium oxide (Aldrich, 99.9%), chloroform-*d* (Apollo, 99.8%), acetonitrile-d_3 (Acros, 99%) and methyl-d_3 alcohol-*d* (Acros, 100%) were also used as received.

IR spectroscopy Infrared spectra were recorded as KBr pellets in the range 4000 – 400 cm^{-1} on a Perkin-Elmer Paragon 1000 Fourier-transform spectrometer.

NMR spectroscopy NMR spectra were recorded on either Bruker DMX 500 (^1H, 500.13 MHz; ^{13}C, 125.72 MHz; ^{15}N, 50.66 MHz; ^{111}Cd, 106.03 MHz) or Varian ^{Unity}*INOVA* (^1H, 599.82 MHz; ^{13}C, 150.86 MHz; ^{15}N, 60.80 MHz; ^{111}Cd, 127.23 MHz) NMR spectrometers using TBI [^1H, ^{13}C, X] or triple resonance [^1H,^{13}C,^{15}N]

probeheads, respectively, and equipped for z-field gradients. All spectra were acquired at the probe of 298 K using standard pulse sequences in 5 mm NMR tubes. ^{1}H and ^{13}C shifts were referenced to sodium trimethylsilylpropionate (TSP), and ^{15}N shifts to 1 M $^{15}NH_4Cl$ in 1.5 M HCl (external). NMR data were processed using Xwin-nmr (version 2.0, Bruker U.K. Ltd.).

X-ray crystallography X-ray crystallographic studies were carried out on a Bruker SMART-APEX CCD Stadi-4 diffractometer equipped with Oxford Cryosystems low-temperature devices by Dr. Simon Parsons, Dr. Robert O. Gould, and Pamela A. McGregor.

Electrospray Ionisation-Mass Spectrometry (ESI-MS) Positive-ion electrospray ionisation mass spectra were obtained on a Platform II mass spectrometer (Micromass, Manchester, UK). Data were processed using Masslynx (v3.5) Windows NT PC data system.

Scanning Electron Microscope with Energy Dispersive X-ray Detector (SEM-EDX) Elemental analysis of protein crystals were performed on a scanning-electron-microscope (Philips XL30CP) with an energy dispersive X-ray detector and electron back scatter diffraction systems by Dr. Paula McDade in the Department of Geology.

2.2 Crystallisation

To grow crystals, molecules must be brought into a thermodynamically unstable state known as supersaturation. This is usually achieved by the gradual removal of solvent. Crystallogenesis is affected by a range of factors, such as pH, temperature, and concentration, etc. Protein crystals are rather small, usually < 10

mm^3. They often have a high solvent content of around 20-80% making them rather brittle and fragile and have to be kept in a solvent-saturated environment. In the vapour diffusion methods a droplet of protein solution containing precipitant is equilibrated with a reservoir of precipitant containing a higher concentration of precipitant. The most common method is the hanging drop method. Variants of this include sitting drop and sandwich drop methods.

Equilibration proceeds by diffusion of solvent from the drop to the reservoir until the vapour pressures in the drop and the reservoir are equal, thus achieving supersaturation in the drop. Such methods are very good for screening crystallisation conditions, commonly setting them up in multi-well "Linbro" boxes.

2.3 NMR Simulations Spin system simulations were carried out using the program SpinWorks (version 1.1, Kirk Marat, 1999).[1]

2.4 Molecular Modelling Molecular models were built using the program Sybyl (version 6.3, Tripos Inc.) on a Silicon Graphics computer. WebLab ViewerPro 4 (Molecular Simulations Inc.) and MOLMOL (Version 2K.1)[2] were also used for modelling and graphics.

2.5 NMR spectroscopy

2.5.1 Nuclear spin

Nuclei possess magnetic moments when their spin quantum numbers are greater than 1/2. The spin states of such nuclei are characterised by the magnetic quantum numbers m_I = I, I-1, I-2, ···, -I. Generally, for nuclei with even mass and atomic numbers, the even-even nuclei, I = 0, and for all other nuclei I ≥ 1/2. I is an integral multiple of 1 for even-odd nuclei, and for odd-odd and odd-even nuclei it is an integral multiple of 1/2. The nuclei related to this study are listed in Table 2.1, with their properties that are relevant to nuclear magnetic resonance.

The energy (and thus frequency) of an NMR transition depends on the magnetic-field strength and a proportionality factor for each nucleus called the magnetogyric ratio. The frequency of a transition is given by:

$$\nu = \frac{\gamma}{2\pi} B_o \qquad \text{(Equation 2.1)}$$

where ν is the frequency of the resonant radiation, γ is the magnetogyric ratio and B_0 is the strength of the magnetic field.

Table 2.1 Nuclear properties related to NMR studies in this thesis (data from ref. 3)

Nucleus	I	μ (μ_N)	γ (10^7 rad T^{-1} s^{-1})	Abundance (%)	Sensitivity (relative to ^1H)	ν
^1H	1/2	4.84	26.75	99.99	1.000	500.13
^{13}C	1/2	1.22	6.73	1.10	0.016	125.72
^{15}N	1/2	0.49	-2.71	0.37	0.001	50.66
^{111}Cd	1/2	1.03	-5.70	12.80	0.0095	106.03

2.5.2 Chemical shift and spin-spin coupling

Chemical shift

When an atom is placed in a magnetic field, its electrons circulate about the direction of the applied magnetic field (B_0). This circulation causes a small magnetic field at the nucleus which opposes the externally applied field.[4]

The magnetic field at the nucleus (the effective field, B_e) is therefore generally less than the applied field by a fraction. This effect corresponds to a magnetic shielding of the nucleus that reduces B_0 by an amount equal to σB_0 where σ is known as the shielding of the particular nucleus:

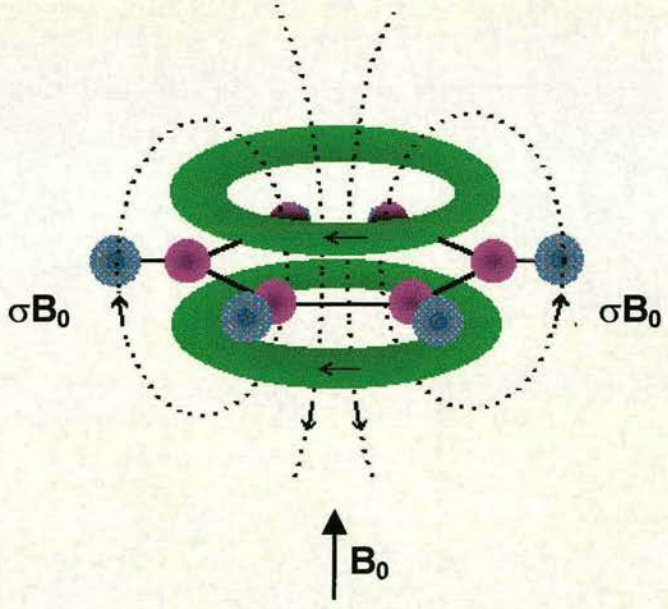

Figure 2.1 The deshielding phenomenon in which the circulation of the electrons in the π orbits of an aromatic ring creates a magnetic field at the hydrogen nuclei which enhances the B_o field.

In some cases, such as the benzene molecule, the circulation of the electrons in the aromatic orbits creates a magnetic field at the hydrogen nuclei which enhances the B_0 field (Figure 2.1). This phenomenon is called deshielding.

$$B_e = B_0 (1-\sigma) \qquad \text{(Equation 2.2)}$$

The electron density around each nucleus in a molecule varies according to the types of nuclei and bonds in the molecule. The opposing field and therefore the effective field at each nucleus will vary. This effect produces a shift of the resonance frequency, or more simply the chemical shift.

The chemical shift of a nucleus is the difference between the resonance frequencies of the nucleus and a standard. This quantity is reported in ppm and given the symbol delta, δ.

$$\delta = (\nu - \nu_{REF}) \times 10^6 / \nu_{REF} \qquad \text{(Equation 2.3)}$$

In ^{1}H NMR spectroscopy, standards are often tetramethylsilane, abbreviated TMS for non aqueous media and sodium trimethylsilylpropionate, abbreviated TSP for aqueous media.

Spin-spin coupling

Nonequivalent nuclei which are close to one another exert an influence on each other's effective magnetic field. If the distance between non-equivalent nuclei is less than or equal to three bond lengths, this effect is observable. This effect is called spin-spin coupling or *J* coupling.

There is a total of four possible configurations for the two nuclei in a magnetic field (Figure 2.2).[4] The vertical lines in this diagram represent the allowed transitions between energy levels. In NMR, an allowed transition is one where the spin of one nucleus changes from spin up to spin down, or spin down to spin up .

Absorptions of energy where two or more nuclei change spin at the same time are not allowed. There are two absorption frequencies for the A nucleus and two for the X nucleus.

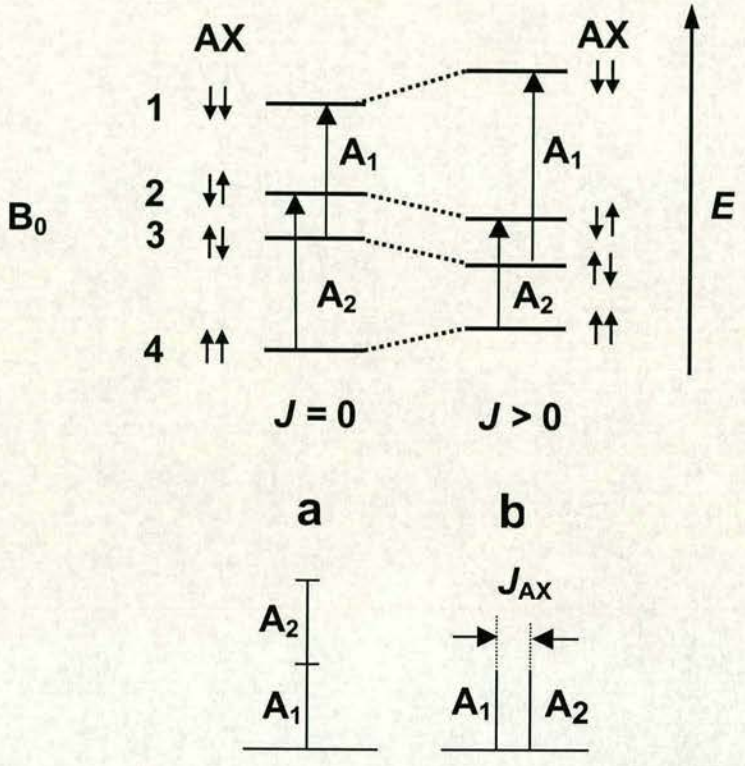

Figure 2.2 Nuclear magnetic energy level diagram for a two-spin system: (a) without spin-spin coupling, (b) with spin –spin coupling

The NMR spectrum for nuclei A and X reflects the splittings observed in the energy level diagram. Both the A absorption line and the X absorption line are split into 2 absorption lines. The distance between the two split absorption lines is called the *J* coupling constant, or the spin-spin splitting constant, and is a measure of the magnetic interaction between two nuclei. Coupling occurs between nuclei because of the spin interaction of the nuclei with bonding electrons. Spin information between two nuclei is "transmitted" by the electrons in the bond(s). Because of this, the better

the orbital overlap between the nuclei (through intervening bonds) the stronger the coupling will be. The bond angle between two interacting nuclei will have a direct affect on the coupling constant.

2.5.3 Karplus relationship

Structural information from NMR experiments comes primarily from through-bond (scalar or *J* coupling) or through-space (the nuclear Overhauser effect, NOE) magnetisation transfer between pairs of protons. The value of a three-bond *J* coupling constant (^3J) contains information about the intervening torsion angle. The relationship between dihedral angle and coupling constant is known as the **Karplus relationship** (Equation 2.4):

$$^3J = A + B\cos\phi + C\cos 2\phi \qquad \text{(Equation 2.4)}$$

where A, B, and C are constants with the values 4.22, -0.5, and 4.5, respectively. **Karplus curve** is shown in Figure 2.3.

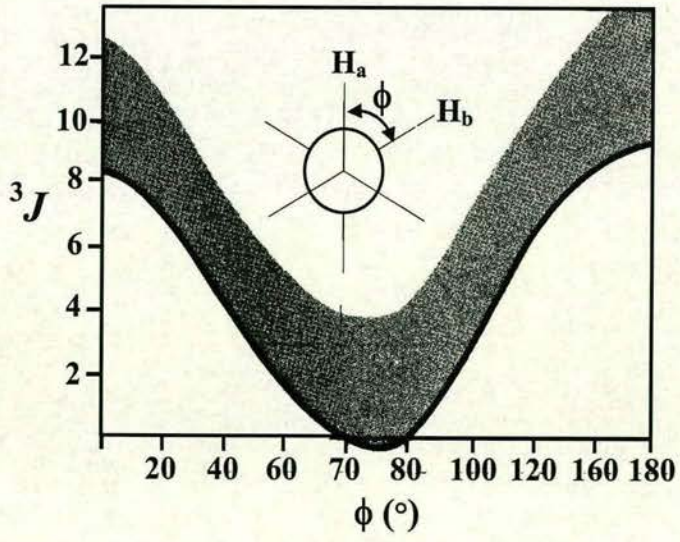

Figure 2.3 Dependence of the magnitude of the vicinal coupling constant on the dihedral angle. Line, theoretical curve; shade area, range of empirical results (ref. 4).

The relationship results from strong coupling when orbits are parallel and can overlap at the synperiplanar (ϕ = 0 - 30°) and antiperiplanar (ϕ = 150 - 180°) geometries, and weak coupling when orbits are staggered or orthogonal (ϕ = 60 - 120°).[4] The Karplus relationship has been shown to be dependent also on a variety of other molecular parameters, such as substitution, bond angles, and bond length.[5] Changes with bond lengths and bond angles, however, appeared to be minor,[5] just as the effect of molecular vibrations is small[6] compared to the effect of electronegativity and relative position of substituents attached to the H-C-C-H fragment. In fact, ample experimental proof demonstrates that the latter effect is the second important factor, next to the dihedral angle dependence, in determining the magnitude of vicinal coupling constants.[7] A great number of modified Karplus relationships were formulated.[8] Haasnoot[9] has set up a generalised and well-accepted Karplus-type relationship. In this case, the generalised Karplus equation takes the form shown in Equation 2.5:

$$^3J(^1H, ^1H) = 13.89\cos^2\phi_{HH} - 0.98\cos\phi_{HH} + \sum\Delta\chi_i\{1.02 - 3.4\cos^2(\zeta_i\phi + 14.9\,|\Delta\chi_i|)\} \qquad \text{(Equation 2.5)}$$

in which ϕ_{HH} (see Newman projection in Figure 2.3) is the Klyne-Prelog defined[10] proton-proton torsion angle and $\Delta\chi_i$ denotes the differences in electronegativity between the substituent S_i and hydrogen on the Huggin's scale[11] corrected for the influence of β substituents[9]; ζ_i takes on a value of +1 or –1 according to the orientation of the substituent S_i with respect to the coupling proton on the same carbon atom.[9]

2.5.4 1D NMR spectroscopy

^{1}H NMR

The basic 1D NMR experiment consists of exciting the nuclei with a single pulse then receiving the free induction decay (FID). The FID is then Fourier transformed to yield the spectrum. This is generally the type of experiment used for proton ^{1}H NMR spectroscopy. The basic pulse sequence for a ^{1}H NMR experiment is shown in Figure 2.4. The pulse sequence consists of the recycle delay followed by an RF pulse. Data are collected following the RF pulse. The pulse angle is, in practice, often chosen to be somewhat less than $\pi/2$. The two pulse sequence parameters shown in the Figure 2.4, $\mathbf{d_1}$ and $\mathbf{p_1}$, correspond to the length of the recycle delay and the length of the RF pulse, respectively, and **acq** is the acquisition time.

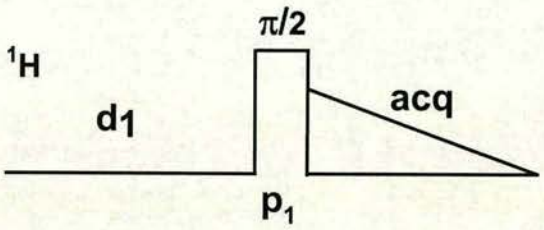

Figure 2.4 ^{1}H One-pulse sequence

^{1}H decoupling in ^{13}C and ^{111}Cd NMR

Extensive X-H coupling (large one-bond coupling $^1J_{XH}$ and many smaller $^2J_{XH}$ and $^3J_{XH}$) *not* only produces complex spectra, but also means that the overall sensitivity is seriously reduced.[3] In order to solve these problems, it is normally necessary to apply proton decoupling. ^{1}H decoupling is typically used to acquire

spectra of any nuclide other than ^{1}H; this is designated by $X\{^{1}H\}$, indicating that protons are being decoupled from nuclide X.

The principles of spin decoupling can be simply illustrated by a consideration of the basic AB spin system. Nucleus A has two transitions due to the two possible orientations (α and β) of nucleus B. In the spin-decoupling experiment, nucleus A is observed with the normal weak RF field (the observe frequency) while simultaneously irradiating nucleus B with a second, much stronger, RF field (the decoupling freqency). The irradiation at B induces transitions between the two spin states of nucleus B ($\alpha \rightarrow \beta$ and $\beta \rightarrow \alpha$) and, if sufficient irradiating power is applied, then B flips backwards and forwards between the α and β states so rapidly that nucleus A can no longer distinguish the separate orientations of B, but 'see' only an average orientation. When this occurs, the coupling J_{AB} between the two nuclei disappears and the doublet A-signal collapses to give a singlet line ν_A.

In the simple heteronuclear decoupling experiment, as described above, a second channel is added and an individual proton signal is selected and irradiated with a strong RF field. Although this simplifies the spectrum by removing all the couplings to that specific proton, the spectrum will still be complicated by the couplings to other protons in the molecule. Though some of these may now be reduced in magnitude. If the decoupler is set to the centre of the proton region and then modulated using a 'noise generator' with a bandwidth wide enough to cover the complete proton region, then this equivalent to simultaneously irradiating every proton frequency and, consequently, results in the effective decoupling of all the protons in the molecule. However, there is an effect called the nuclear Overhauser effect (NOE) which changes the intensity of the ^{13}C or ^{111}Cd line. The NOE results in

the transfer of energy to attached ^{13}C nuclei, resulting in a significant enhancement in the NMR signal. Therefore, integration is almost useless in such a spectrum.

In some cases, decoupling reduces sensitivity such as ^{1}H-decoupled ^{15}N NMR or quantitative results are desired. In such cases the inverse gated pulse sequence minimizes the change in sensitivity while maintaining decoupling (Figure 2.5). The pulse width pw is set to 90° and the decoupler is turned on only during acquisition to prevent buildup of NOE enhancement. In this experiment the proton decoupler is pulsed to produce a spectrum where observed nuclei are decoupled, but the NOE (Nuclear Overhauser Effect) is not able to build up.

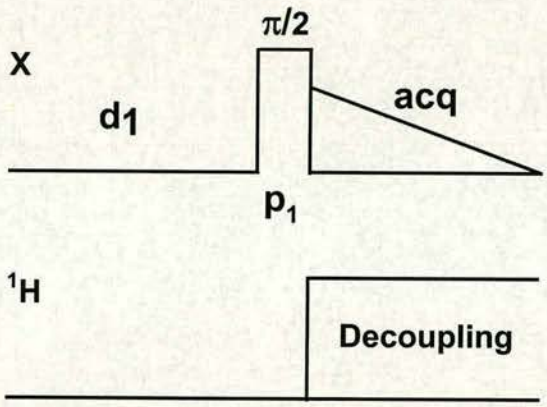

Figure 2.5 Inverse-gated decoupled 1D NMR sequence

2.5.5 2D NMR spectroscopy

Heteronuclear Single Quantum Coherence (HSQC)

The heteronuclear experiments are those which identify the chemical shifts of protons and X-nuclei that are directly coupled. One obvious use of this correlation information is to allow assignments already made for one nuclear species to be

transferred to the other. A more important but less obvious use is in overcoming problems caused by overlap in the proton spectrum: in the heteronuclear 2D spectrum the proton resonances are spread out according to the shifts of the heteronuclei to which they are coupled.

The heteronuclear single quantum coherence (HSQC) technique belongs to the family of indirect (or inverse) detection techniques. An important feature of the experiment is that the proton magnetisation which is detected during t_2 originated as proton magnetisation at the start of the sequence. The main advantage of this technique is the enhanced sensitivity, a theoretical maximum of $[|\gamma_H|/|\gamma_X|]^{5/2}$ (306 for ^{15}N) with respect to direct detection, and relatively short repetition time according to the T_1 of the protons and not of the X-nuclei.[12] By means of selective ^{15}N labelling, this technique can also simplify a complicated spectrum in which only those protons directly attached to ^{15}N atoms are detected. The basic HSQC pulse sequence is shown in Figure 2.6.

Amine protons can be detected selectively by the use of the [^1H, ^{15}N] single quantum coherence (HSQC) pulse sequence. A 1D ^1H spectrum containing only resonances from amine species is obtained by acquiring only the first increment in a two-dimensional experiment; resonances for CH and OH (including water) are eliminated. If ^{15}N decoupling is employed, then each type of amine resonance appears as a singlet. In practice the water resonance is so intense that it is usually necessary to use additional solvent suppression techniques. A large improvement in water suppression is achieved by the use of pulsed field gradients for coherence selection, for example, by use of the HSQC sequences of Stonehouse et al.[13]

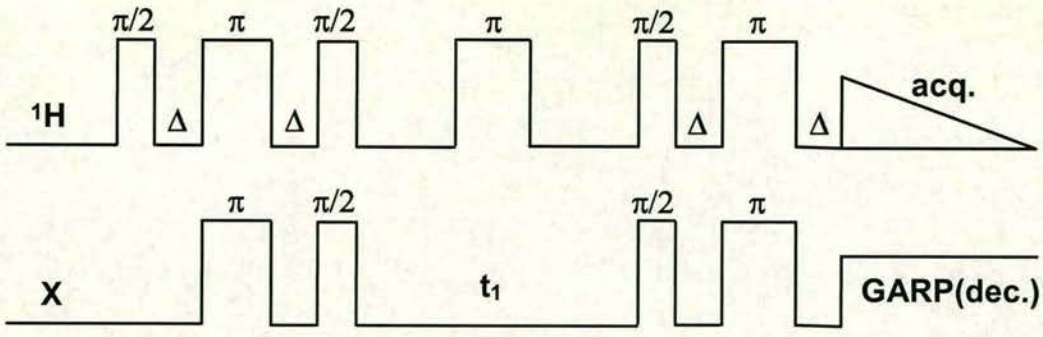

Figure 2.6 Basic HSQC pulse sequence. The delays Δ and τ are ¼J and ½J respectively, where J is the one-bond HX coupling constant.

Correlated Spectroscopy (COSY)

COSY is a two-dimensional homonuclear (^{1}H,^{1}H)-correlated NMR experiment which yields NMR spectra in which ^{1}H chemical shifts along both frequency axes are correlated with each other.[14,15] It is the standard 2D experiment that can be used to identify pairs of protons that have scalar spin-spin coupling connectivities. There are two inherent drawbacks that limit its usefulness with macromolecules: one is that the fine-structure components that make up each cross-peak appear in antiphase; the other is that the diagonal peaks and the cross-peaks are 90° out of phase in both dimensions. These gives poor sensitivity and extremely harsh weighting functions must be used to give spectra with usable lineshapes which in turn gives a further reduction in sensitivity.

More favourable lineshapes can be obtained by using the double-quantum filtered COSY sequence (DQF-COSY),[16] shown in Figure 2.7b. In this experiment the diagonal peaks and the cross-peaks all show the same antiphase absorption mode fine-structure. Although the double-quantum filtering attenuates the signals to some extent, this is more than offset by the gain resulting from not having to use resolution enhancement to impose acceptable lineshapes on the peaks.

Homonuclear Nuclear Overhauser Effect or Enhancement Spectroscopy (NOESY)

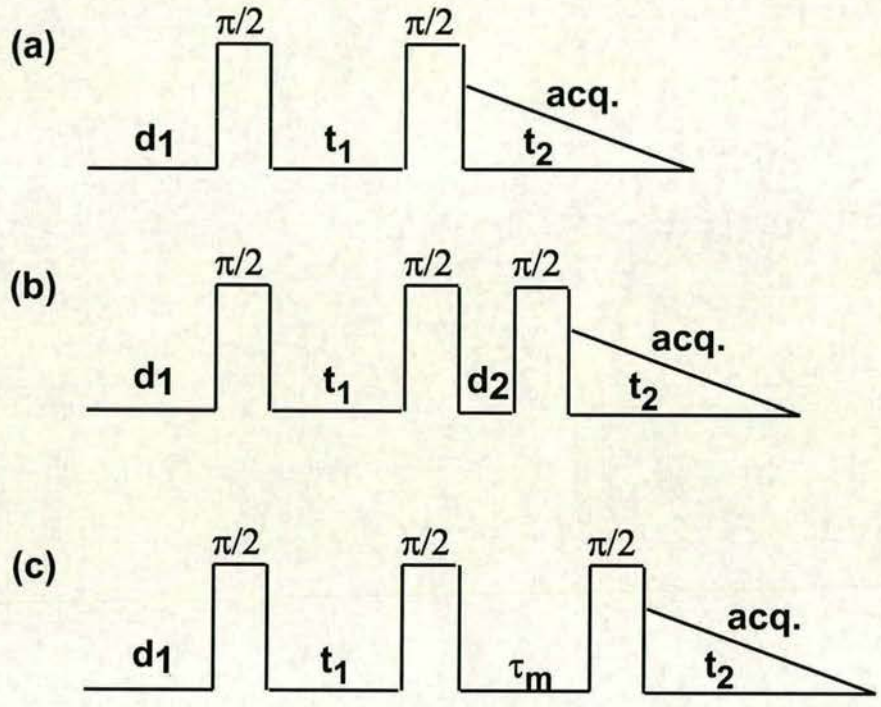

Figure 2.7 Pulse sequences for two-dimensional (a) COSY, (b) DQF-COSY, and (c) NOESY experiments. τ_m is the mixing time.

The NOESY experiment[17,18] is often used to identify pairs of protons that are undergoing cross-relaxation, i.e. protons that would show an NOE in 1D experiments. The characteristic feature of the NOESY pulse sequence (shown in Figure 2.7c) is the mixing time τ. The cross-peaks are generated by magnetisation transfer that takes place during the mixing time so the length of this delay must be chosen according to the rate of the transfer process. In contrast to the COSY experiment, both cross-peaks and diagonal peaks in NOESY spectra can be obtained with absorption-mode lineshapes. The experiments are therefore eminently suitable

for studying macromolecules. If presaturation is used in a NOESY experiment it is usually also necessary to irradiate the solvent during the mixing time. A complicating factor is that the NOESY pulse sequence cannot distinguish between magnetisation transfer caused by cross-relaxation and magnetisation transfer by chemical exchange. In macromolecules, both give cross-peaks of the same sign as the diagonal.

Total Correlation Spectroscopy (TOCSY)

TOCSY provides a different mechanism of coherence transfer from COSY for 2D correlation spectroscopy.[4,19] The cross peaks are generated between all members of a coupled spin network. An advantage is that the "net" coherence transfer produced can be arranged to create pure absorption mode spectra with positive intensity peaks (rather than "differential" coherence transfer which causes spectra with equal positive and negative intensities). In traditional COSY, cross-peaks have zero integrated intensity and coherence transfer is restricted to directly spin-coupled nuclei. In TOCSY, oscillatory exchange is established which proceeds through the entire coupling network so that there can be net magnetisation transfer from one spin to another even without direct coupling. The isotropic mixing which occurs during the spin-lock period of the TOCSY sequence exchanges all in-phase as well as antiphase coherences.

The coherence transfer period of the TOCSY sequence occurs during a multiple-pulse spin-lock period.[4,19] The multiple-pulse spin-lock sequence most commonly used is MLEV-17 which contains a set of 17 90/180° pulses whose duration represents the mixing time t_m. The length of the spin-lock period determines

how "far" the spin coupling network will be probed. The TOCSY spectrum can be phased so that all cross peaks and diagonal peaks have positive intensity.

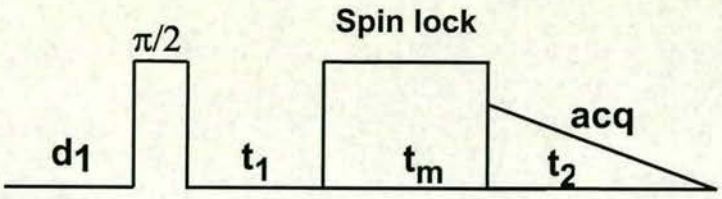

Figure 2.8 2D TOCSY pulse sequence

2.6 IR spectroscopy

There are two kinds of fundamental vibrations for molecules: *stretching*, in which the distance between two atoms increases or decreases, but the atoms remain on the same bond axis, and *bending*, in which the position of the atoms changes relative to the original bond axis.[19,20] The various stretching and bending vibrations of a bond occur at certain quantized frequencies. When infrared light of the same frequency is incident on the molecule, energy is absorbed and the amplitude of that vibration is increased. A molecule can be said to resemble a system of balls of varying masses, corresponding to the atoms of a molecule, and springs of varying strengths, corresponding to the chemical bonds of a molecule. This model can be applied to account for fundamental vibrations occurring between the nonvibrating state and the vibrationally excited state in a simple diatomic molecule A-B.

The vibrational frequency in cm^{-1} is given by

$$\nu = 1/2\pi c\,(k/\mu)^{-2}$$

where k is the force constant of the bond

μ is the reduced mass of the molecule defined by:

$$\mu = m_A m_B/(m_A+m_B)$$

Bending vibrations generally require less energy and occur at longer wavelength than stretching vibrations. Stretching vibrations are found to occur in the order of bond strengths. The triple bond (absorption at 2300 – 2000 cm^{-1}) is stronger than the double bond (absorption at 1900 – 1500 cm^{-1}), which in turn is stronger than the single bond (C – C, C – N, and C – O absorption at 1300 – 800 cm^{-1}). When the single bond involves the very small proton (C – H, O – H, or N – H), stretching vibrations occur at much higher frequency (3700 – 2630 cm^{-1}).

2.7 Electrospray ionisation-mass spectrometry (ESI-MS)

Mass spectrometry is an instrumental approach that allows for the gas phase generation of ions as well as their separation and detection. The five basic parts of any mass spectrometer include: a vacuum system, a sample introduction device, an ionisation source, a mass analyser, and an ion detector. A mass spectrometer determines the molecular weight of chemical compounds by ionising, separating, and measuring molecular ions according to their mass-to-charge ratio (m/z). The ions are generated in the ionisation source by inducing either the loss or the gain of a charge (e.g. electron ejection, protonation, or deprotonation). Once the ions are formed in the gas phase they can be electrostatically directed into a mass analyser, separated according to mass and finally detected. The result of ionisation, ion separation, and

detection is a mass spectrum that can provide molecular weight and even structural information.

Electrospray ionisation is one of the most exciting ionisation techniques recently developed.[21] ESI generates ions directly from solution (usually an aqueous or aqueous/organic solvent system) by creating a fine spray of highly-charged droplets in the presence of a strong electric field (typically 3.5 kV). As the droplet decreases in size, the electric charge density on its surface increases. The mutual repulsion between like charges on this surface becomes so great that it exceeds the forces of surface tension, and ions begin to leave the droplet through what is known as a "Taylor cone". The ions are then electrostatically directed into the mass analyser. Vaporisation of these charged droplets results in the production of singly- or multiply-charged gaseous ions. The number of charges retained by an analyte can depend on such factors as the composition and pH of the electrosprayed solvent as well as the chemical nature of the sample. For small molecules (< 2000 Daltons) ESI typically generates singly or doubly charged ions while for large molecules (> 2000 Daltons) the ESI process typically gives rise to a series of multiply charged species. Because mass spectrometers measure the mass-to-charge (m/z) ratio, the resultant ESI mass spectrum contains multiple peaks corresponding to the different charged states.

ESI is a very sensitive technique and is ideally suited for the analysis of small, large and/or labile molecules including peptides, proteins, organometallics, oligosaccharides, and polymers. Another advantage of ESI-MS is that ions are formed directly from solution (usually an aqueous or aqueous/organic solvent system), a feature that has established the technique as a convenient mass detector

for liquid chromatography (LC) also known as high performance liquid chromatography (HPLC).

2.8 Scanning electron microscope-energy dispersive X-ray detector spectrometer (SEM-EDX)

The SEM microscope consists of a column, detectors, and a viewing console. The column is like the lenses in a light microscope.[22] At the top of the column, a filament tip generates electrons (which are negatively charged). This is called the electron gun. The specimen is at the bottom of the column, in a complete vacuum. Magnets in the column direct and focus the electron beam to travel towards the specimen. Beam deflector coils make the beam of electrons swing across the sample (called rasterisation). Some electrons are reflected from the specimen and some are absorbed. Specialised detectors receive these electrons and process the signal.

There are three types of detectors: secondary electron for topographical imaging, backscattered electrons for phase and chemical compositional imaging, energy dispersive X-ray spectroscopy for chemical elemental analysis.

The scanning electron microscope is used to analyse the surface of specimens over a wide range of magnifications. A focused beam of electrons is either scanned across the surface of a specimen to form an image, or stopped on a fixed location to perform one of a variety of spectrographic or analytical functions. The interaction of the beam with the specimen results in the generation of secondary electrons, backscattered electrons, Auger electrons, characteristic X-rays, and photons of

various energies. Secondary electrons and backscattered electrons are collected by their respective detectors and their signals are amplified.

The secondary electron signal comes from the top 20 - 50 Å. Utilising very low instrument accelerating voltages for very shallow penetration, results in a true surface image. The backscattered electron signal comes from depths in the micron range and provides elemental information arising in the entire volume of specimen involved. The X-ray signal used to form spectra or element maps arises in a volume within the specimen on the order of microns in depth. Both qualitative and quantitative elemental analysis is possible. All elements heavier than B in the periodic table may be detected. The energy-dispersive X-ray spectrometer (EDS) detects X-rays from the sample excited by the highly focused, high-energy primary electron beam penetrating into the sample. When the high-energy electrons interact with the atoms of material in this "interaction volume," typically several microns in diameter, they generate characteristic X-rays which are fingerprints of the individual atoms encountered. These X-rays can penetrate through the material, allowing them to escape and be detected by the X-ray detector. Because the intensity of the individual X-ray is related to the quantity of the "parent atom" in the interaction volume, quantitative elemental analysis can be obtained from the sample with the aid of the computer and software analysis capabilities. "Standardless" quantitative analyses give an accuracy of 1-2%, while ultimate accuracy can be obtained by spectral comparison to known standards. Detection sensitivities are about 0.1 weight percent. Elemental maps of the sample as well as linescans, digitised secondary and backscattered electron images and more sophisticated analyses also can be collected by this method.

2.9 References

(1) SpinWorks: a free NMR processing, analysis and simulation software which was downloaded from ftp://pauli.chem.umanitoba.ca/pub/marat/SpinWorks/.

(2) Koradi, R.; Billeter, M.; Wüthrich, K. *J. Mol. Graphics* **1996**, *14*, 51.

(3) Data from WebElements (http://www.webelements.com/webelements/elements).

(4) Günther, H. In *NMR Spectroscopy*, 2th ed.; John Wiley & Sons Ltd., 1995.

(5) Karplus, M. *J. Am. Chem. Soc.* **1963**, *85*, 2870.

(6) Gutowsky, H. S.; Mochel, V. D.; Sommers, B. G. *J. Chem. Phys.* **1962**, *36*, 1153.

(7) Booth, H. in *Progress in NMR Spectroscopy* Pergamon Press: Oxford, 1969, Vol. 5.

(8) (a) Altona, C.; Sundaralingam, M. *J. Am. Chem. Soc.* **1973**, *95*, 2333. (b) Davies, D. B.; Danyluk, S. S. *Biochemistry* **1974**, *13*, 4417. (c) Kopple, K. D.; Wiley, G. R.; Tauke, T. *Biopolymers* **1973**, *12*, 627. (d) Abraham, R. J.; Pachler, K. G. R. *Mol. Phys.* **1964**, *7*, 165.

(9) Haasnoot, C. A. G. ; de Leeuw, F. A. A. M.; Altona, C. *Tetrahedron* **1980**, *36*, 2783.

(10) Klyne, W.; Prelog, V. *Experientia* **1960**, *16*, 521.

(11) Huggins, M. L. *J. Am. Chem. Soc.* **1953**, *75*, 4123.

(12) (a) Müller, L. *J. Am. Chem. Soc.* **1979**, *101*, 4481. (b) Bax, A.; Griffey, R. G.; Hawkins, B. L. *J. Magn. Reson.* **1983**, *55*, 301. (c) Live, D. H.; Davis, D. G.; Agosta, W. C.; Cowburn, D. *J. Am. Chem. Soc.* **1984**, *106*, 6104.

(13) Stonehouse, J.; Shaw, G. L.; Keeler, J.; Laue, E. D. *J. Magn. Reson.* **1994** A, *107*, 178.

(14) Aue, W. P., Bartholdi, E.; Ernst, R. R. *J. Chem. Phys.* **1976**, *64*, 2229.

(15) Nagayama, K.; Kumar, A.; Wüthrich, K.; Ernst, R. R. *J. Magn. Reson.* **1980**, *40*, 321.

(16) Rance, M.; Sorensen, O. W.; Bodenhausen, G.; Wagner, G.; Ernst, R. R.; Wüthrich, K. *Biochem. Biophys. Res. Commun.* **1983**, *117*, 479.

(17) Jeener, J.; Meier, B. H.; Bachmann, P.; Ernst, R. R. *J. Chem. Phys.* **1979**, *71*, 4546.

(18) Kumar, A.; Ernst, R. R.; Wüthrich, K. *Biochem. Biophys. Res. Commun.* **1980**, *95*, 1.

(19) Lambert, J. B.; Shurvell, H. F.; Lightner, D. A.; Cooks, R. G. in *Organic Structural Spectroscopy* Prentice-Hall Inc.: New Jersey, 1998.

(20) Creswell, C. J.; Runquist, O. A.; Campbell, M. M. in *Spectral Analysis of Organic Compounds* 2nd ed.; Burgess Publishing Company, 1972.

(21) (a) Adlhart, C.; Hinderling, C.; Baumann, H.; Chen, P. *J. Am. Chem. Soc.* **2000**, *122*, 8204. (b) Wan, K. X.; Shibue, T.; Gross, M. L. *J. Am. Chem. Soc.* **2000**, *122*, 300. (c) Nemeth, J. F.; Hochensang, Jr., G. P.; Lawrence, J. M.; Caprioli, R. M. *Biochemistry* **2001**, *40*, 3109. (d) Tomer, K. B *Chem. Rev.* **2001**, *101*, 297. (e) Cole, R. B., ed.; in *Electrospray Ionization Mass Spectrometry: Fundamentals, Instrumentation, and Applications* Wiley: Chichester, 1999.

(22) The World of Scanning Electron Microscopy (http://www.mse.iastate.edu/ microscopy/ home.html).

Chapter 3. Synthesis and Characterisation of ^{15}N-Labelled Cyclam

3.1 Introduction

Examination of less common nuclei has become prominent over recent years and, of these, ^{15}N occupies a unique position because of its importance in biological systems.[1] Although ^{1}H NMR resonances can be detected from NH protons with ^{14}N present in natural abundance (99.6%), they are often broad because of the quadrupolar relaxation of ^{14}N ($I = 1$).[2] The low sensitivity of ^{15}N (3.85×10^{-6} relative to ^{1}H) to some extent limits its usefulness for directly detected ^{15}N NMR studies. However, the sensitivity of detection can be improved by ^{15}N isotopic enrichment (natural abundance ^{15}N: only 0.37%) combined with the inverse (^{1}H-detected) ^{15}N methods. The major advantage of the inverse detection technique is the sensitivity of detection, which is enhanced by a theoretical maximum of 306 ($|\gamma H|/|\gamma N|^{5/2}$) with respect to directly detected ^{15}N.[2] These methods are widely applicable to any compounds which have a ^{15}N atom with a measurable spin-spin coupling to ^{1}H (i.e. ammine, primary and secondary amines, but not tertiary amines). In practice the best results are obtained with large one-bond couplings (about 73 Hz for $^{15}NH_3$). Introduction of ^{15}N by synthetic labelling usually gives rise to a sharp ^{1}H doublet for an amine group. In order to reveal the binding behaviour of bicyclam and the possible conformation of its transition metal complexes in solution by NMR, ^{15}N-labelled cyclam and its Zn cyclam complex were synthesised. Since the commercially available starting materials for syntheses of ^{15}N-labelled compounds

are expensive, effective reactions are required for the synthesis of ^{15}N-labelled compounds. A very convenient and efficient synthesis of (^{15}N)cyclam is presented here. The synthetic route is outlined in the Scheme 3.1.

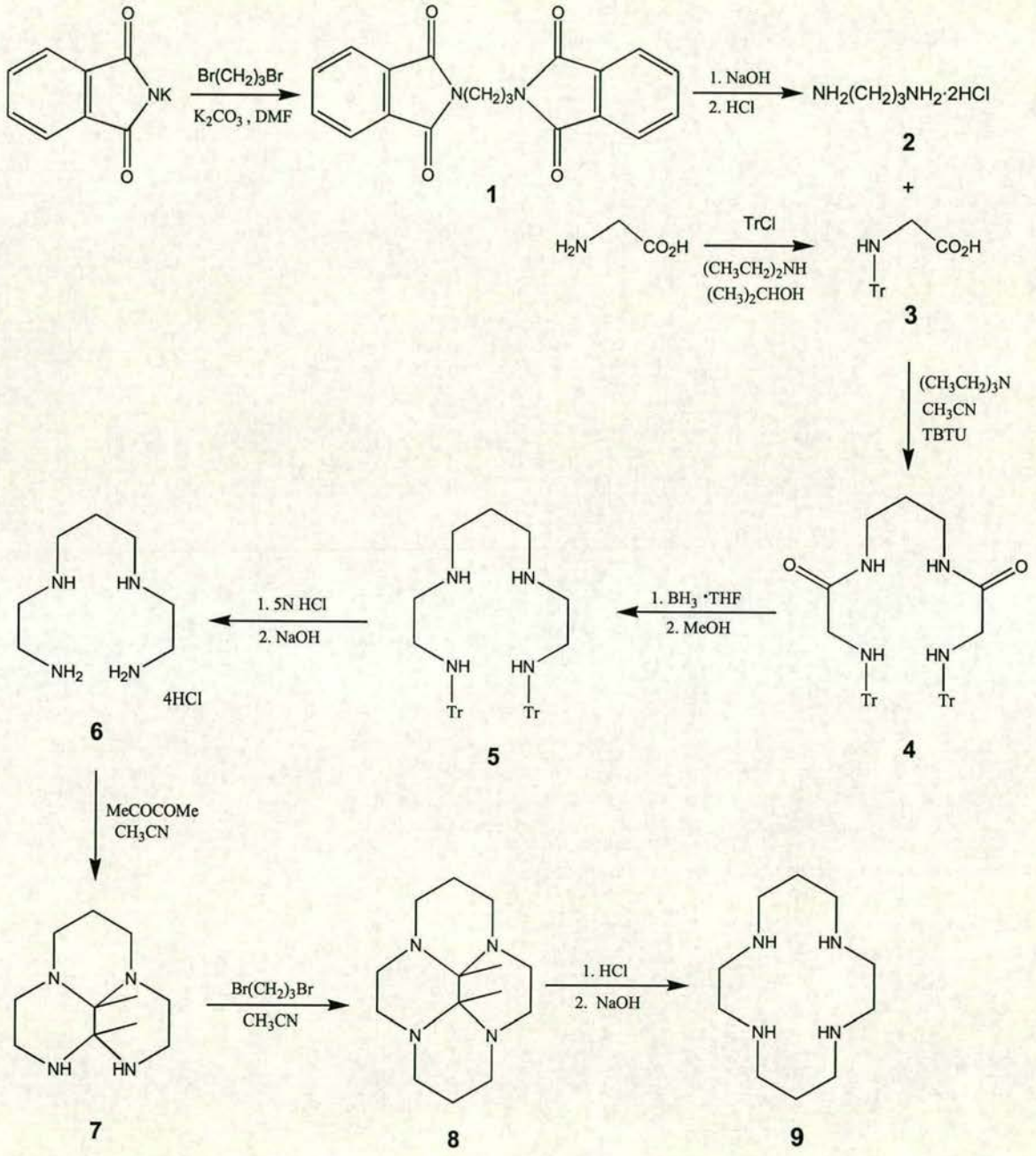

N = ^{15}N; Tr = Trityl group; TBTU = O-(Benzotriazol-1-yl)-N,N,N',N'-tetramethyluronium tetrafluoroborate

Scheme 3.1 Preparation of ^{15}N-cyclam from (^{15}N)potassium phthalimide and ^{15}N-glycine

AMD3100 has been extensively investigated because of its highly potent and selective inhibition of the human immunodeficiency virus (HIV). It is important to study the mechanism of action of bicyclams in order to aid the design of more effective anti-HIV antagonists.

3.2 Experimental

3.2.1 NMR spectroscopy for complexes 1-9 (scheme 3.1)

Typically NMR data were acquired in 10% D_2O / 90% H_2O or $CDCl_3$ in 5 mm tubes at a probe temperature of 298 K on 500 MHz NMR instrument. ^{1}H chemical shifts were externally referenced to the methyl singlet of TSP (3-trimethylsilyl- propionate-d_6) at 0 ppm; ^{13}C chemical shifts were referenced externally also using TSP, and ^{15}N shifts were externally referenced to 1 M $^{15}NH_4Cl$ in 1.5 M HCl.

1D ^{1}H NMR data were acquired typically over a ^{1}H frequency width of 5 kHz into 32 k data points (acquisition time = 3.28 s). The water resonance was suppressed by presaturation or *via* the WATERGATE pulsed-field-gradient sequence.[3]

The ^{13}C-{^{1}H} NMR spectrum of ^{15}N-**6** was acquired at 150 MHz over a ^{13}C frequency width of 27.77 kHz into 16 k data points (acquisition time = 0.29 s).

2D [^{1}H, ^{13}C] HSQC NMR data were acquired for ^{15}N-**6** over a ^{1}H frequency width of 1 kHz and a ^{13}C frequency width of 3.77 kHz (30 ppm) centred at 43 ppm. Data were acquired with 2 transients into 512 complex data points (acquisition time 256 ms) for each of 128 t_1 increments.

2D [^{1}H, ^{13}C] HSQC NMR data were acquired for ^{15}N-**7** over a ^{1}H frequency width of 2.5 kHz and a ^{13}C frequency width of 10 kHz (80 ppm) centred at 43 ppm.

Data were acquired with 32 transients into 1024 complex data points (acquisition time 205 ms) for each of 128 t_1 increments.

2D [^{1}H, ^{15}N] HSQC NMR data for ^{15}N-**6** were acquired over a ^{1}H frequency width of 5 kHz and a ^{15}N frequency width of 4.06 kHz (80 ppm) centred at 10 ppm. Data were acquired with 140 transients into 2 k complex data points for each of 128 t_1 increments.

2D [^{1}H, ^{1}H] DQF-COSY data for ^{15}N-**6** were acquired over a ^{1}H frequency width of 3 kHz. Data were acquired with 8 transients into 1024 complex data points (acquisition time 0.17 s) for each of 128 t_1 increments. 2D [^{1}H, ^{1}H] TOCSY data for ^{15}N-**6** were acquired over a ^{1}H frequency width of 1.9 kHz. Data were acquired with 8 transients into 1024 complex data points (acquisition time 0.14 s) for each of 128 t_1 increments. A spin-lock time of 60 ms was employed.

2D [^{1}H, ^{1}H] TOCSY data for ^{15}N-**7** were acquired over a ^{1}H frequency width of 5 kHz. Data were acquired with 16 transients into 2048 complex data points (acquisition time 0.21 s) for each of 512 t_1 increments. 2D [^{1}H, ^{1}H] TOCSY data for ^{15}N-**7** were acquired over a ^{1}H frequency width of 1.9 kHz. Data were acquired with 32 transients into 512 complex data points (acquisition time 0.14 s) for each of 128 t_1 increments. A spin-lock time of 60 ms was employed.

Spin system simulations were carried out using the program Spinworks (version 1.1, Kirk Marat, University of Manitoba, 1999).

3.2.2 Synthesis of ^{15}N-labelled cyclam

(^{15}N)1,3-Diphthalimidopropane (^{15}N-1). (^{15}N)1,3-Diphthalimidopropane was prepared by modification of the Gabriel synthesis.[4] (^{15}N)Potassium phthalimide (15

mmol, 2.79 g), K_2CO_3 (7.5 mmol, 1.04 g, dried in *vacuo* at 130 °C for 5 h) and 1,3-dibromopropane (7.5 mmol, 0.77 ml) were suspended in dry dimethylformamide (12 ml) and heated under reflux for 4 h at 190 °C. The reaction mixture was further stirred at room temperature for 26.5 h. The volume of the solution was reduced under vacuum to about 2-3 ml. The mixture was stirred for 1.5 h after addition of 50 ml of H_2O into the above solution. A pale yellow precipitate appeared and was collected by filtration and washed with small amounts of methanol and ether to give ^{15}N-1,3-diphthalimidopropane, ^{15}N-**1** (1.79 g, 79.6 %). ^1H NMR ($CDCl_3$): δ = 7.81 - 7.86 (m, 4H, C_6H_4), 7.69 - 7.73 (m, 4H, C_6H_4), 3.71 (dt, 4H, ^2J (^{15}N, ^1H) = 1.22 Hz, NCH_2), 2.04 (m, 2H, $CH_2CH_2CH_2$); IR (KBr): ν = 1712 (s, C=O) cm^{-1}; EI MS 336 *m/e* (M^+).

(^{15}N)1,3-Diaminopropane dihydrochloride (^{15}N-2). (^{15}N)1,3-Diaminopropane was prepared by a synthesis given in the literature.[5] A suspension of ^{15}N-1,3-diphthalimidopropane and potassium hydroxide (2 g, 36 mmol) in H_2O (12 ml) was stirred for 60 h at ambient temperature until a clear solution observed. The solution was distilled into 2 ml of concentrated aqueous solution of HCl under reduced pressure to dryness. After cooling to ambient temperature, 10 ml of water was added to the residue and distilled to dryness again. The procedure was repeated twice. Water was removed to give ^{15}N-**2** (0.89 g, 87.9%). ^1H NMR (10% D_2O/ 90% H_2O, pH 4.6): δ = 7.76 {d, 4H, ^1J(^{15}N, ^1H) = 74.62 Hz, NH_2}, 3.15 (t, 4H, CH_2), 2.10 (m, 2H, CH_2); IR (KBr): ν = 3002 (s, br, ^{15}NH) cm^{-1}; EI MS 149 *m/e* (M^+).

(^{15}N)Tritylglycine (^{15}N-3). (^{15}N)Trityglycine was prepared by a modification of a synthesis given in the literature.[6, 7] To a solution of ^{15}N-glycine (1.53 g , 20.10 mmol) in a mixture of 6 ml of diethylamine, 8 ml of water and 16 ml of isopropanol, tritylchloride (7.29 g, 26.2 mmol) was added every 15 minutes in 13 portions

altogether. After addition, the mixture was stirred for a further 12 h. Then, 50 ml of water was added and the white precipitate was collected and washed with 75 ml of water. The filtrate was acidified with concentrated acetic acid to pH 3 and the formed white precipitate was collected and washed with dilute acetic acid (pH 3). The combined product was dried under vacuum. Yield 4.91 g (77 %). ^{1}H NMR (CD_3OD): δ = 7.27 - 7.40 (m, 15H, C_6H_5), 3.17 (d, 2H, $^{2}J(^{15}N, ^{1}H)$ = 0.46 Hz, CH_2); ^{13}C NMR (CD_3OD): δ = 173.86, 144.74, 129.95, 129.51, 128.76, 73.83 {d, ^{1}J (^{15}N, ^{13}C) = 5.09}, 47.64 (d, ^{1}J (^{15}N, ^{13}C) = 5.51); IR (KBr): ν = 3312 (^{15}NH), 1721 (C=O) cm^{-1}; EI MS 318 *m/e* (M^+).

(^{15}N)1,3-Bis-tritylglycylamnio-propane (^{15}N-4). Triethylamine (4.83 ml, 34.74 mmol), ^{15}N-tritylglycine (3.69 g, 11.58 mmol) and TBTU (3.72 g, 11.58 mmol) were added to a suspension of ^{15}N-diaminopropane dihydrochloride (0.86 mg, 5.79 mmol) in dry acetonitrile (100 ml). The mixture was stirred at ambient temperature for 2 h. Then, water (5 ml) was added and the solution was evaporated to dryness under vacuum. The residue was re-crystallised from ethanol (140 ml) and the white product was collected and dried under vacuum. Yield 2.53 g (65 %). ^{1}H NMR ($CDCl_3$): δ = 7.56 (t, 2H, N*H*), 7.45-7.40 (m, 5H, C_6H_5), 7.31-7.25 (m, 5H, C_6H_5), 7.23-7.18 (m, 5H, C_6H_5), 3.34 (m, 4H, $CH_2CH_2CH_2$), 3.02 (s, 4H, CH_2NH_2), 1.70 (m, 2H, $CH_2CH_2CH_2$); IR (KBr): ν = 3312 (^{15}NH), 1645 (s, C=O) cm^{-1}; EI MS 677 *m/e* (M^+).

(^{15}N)N,N'-Bis(2-tritylaminoethyl)-1,3-propanediamine (^{15}N-5) and **(^{15}N)N,N'-Bis(2-aminoethyl)-1,3-propanediamine·4HCl (^{15}N-6)**. A solution of BH_3·THF (17 ml, 1 M) in dry THF (80 ml) was added to a suspension of ^{15}N-**4** (2.48 g, 3.67 mmol) and stirred for 1.5 h at ambient temperature. Then, the mixture was heated under reflux for 24 h. After cooling to ambient temperature, dry methanol (40 ml) was

added carefully. The insoluble material was filtered off and the filtrate was evaporated to yield the yellowish sticky product ^{15}N-**5**.

Compound ^{15}N-**5** was suspended in 5 N HCl (50 ml) and heated under reflux for 5 h. A white precipitate was produced and filtered off. The volume of solution was reduced to 5 ml and ethanol (30 ml) was added. The white precipitate which formed was collected by filtration and washed with ether. Yield 0.97 g (85 % for steps 5 and 6). ^{1}H NMR (10% D_2O/ 90% H_2O, pH 3.9): δ = 3.44 (m, 4H, NCH_2CH_2N), 3.41 (m, 4H, NCH_2CH_2N), 3.25 (t, 4H, ^{3}J = 7.93 Hz, $CH_2CH_2CH_2$), 2.18 (m, 2H, $CH_2CH_2CH_2$); ^{13}C NMR (10% D_2O/ 90% H_2O, pH 3.9): δ = 47.69 (^{1}J (^{13}C, ^{15}N) = 5.09 Hz, ^{3}J (^{13}C, ^{15}N) = 2.54 Hz), 47.13 (^{1}J (^{13}C, ^{15}N) = 5.51 Hz), 38.27 (^{1}J (^{13}C, ^{15}N) = 5.93 Hz), 25.46; ^{15}N NMR NMR (10% D_2O/ 90% H_2O, pH 3.9) δ = 20.56; IR (KBr): ν = 3425 (br, NH) cm^{-1}; EI MS 165 *m/e* (M^+-4HCl).

(^{15}N)9a,9b-Dimethyl-octahydro-1,3a,6a,9-tetraaza-phenalene (^{15}N-7). The pH of an aqueous solution of ^{15}N-**6** (400 mg, 1.29 mmol) was adjusted with NaOH pellets to pH >13 and distilled until dryness into 15 ml of water under reduced pressure. After cooling to ambient temperature, water (10 ml) was added to the residue and distilled to dryness again. This procedure was repeated twice. Water was removed to give the free tetraamine. The following reactions were carried out according to a literature method.[8] Butanedione (112.08 µl, 1.29 mmol) in a solution of CH_3CN (2 ml) was added dropwise to the cooled and stirred solution of the residue of free tetraamine of ^{15}N-**6** in CH_3CN (5 ml). After completion of the reaction (2 h), the solvent was evaporated under reduced pressure to yield ^{15}N-**7** as a yellow product. The product was used without further purification in the next step. ^{1}H NMR ($CDCl_3$): δ = 3.58 (m, 1H, NCH_2CH_2N), 3.28 (m, 1H, $CH_2CH_2CH_2$), 3.21 (m, 1H,

NC*H*$_2$CH$_2$N), 3.11 (m, 1H, NC*H*$_2$CH$_2$N), 2.90 (m, 1H, ^2J = 12.21, NC*H*$_2$CH$_2$N), 2.70 (m, 1H, *CH*$_2$CH$_2$CH$_2$), 2.59 (m, 1H, *CH*$_2$CH$_2$CH$_2$), 2.58 (m, 1H, NC*H*$_2$CH$_2$N), 2.52 (m, 1H, ^2J = 14.34, *CH*$_2$CH$_2$CH$_2$), 2.44 (m, 1H, NC*H*$_2$CH$_2$N), 2.32 (m, 1H, CH$_2$C*H*$_2$CH$_2$), 2.27 (m, 1H, NC*H*$_2$CH$_2$N), 2.19 (dm, 1H, ^2J = 10.07 Hz, NC*H*$_2$CH$_2$N), 1.37 (s, 3H, CH$_3$), 1.30 (s, 3H, CH$_3$), 1.15 (dm, 1H, ^2J = 13.43 Hz, CH$_2$*CH*$_2$CH$_2$); ^{13}C NMR ($CDCl_3$): δ = 54.08, 51.95, 49.58, 48.42, 44.87, 42.05, 26.23, 21.07, 13.49; IR (KBr, neat): ν = 3289 (^{15}NH), 3232 (^{15}NH) cm^{-1}; EI MS 214 *m/e* (M^+).

(^{15}N)10b,10c-Dimethyl-decahydro-3a,5a,8a,10a-tetraaza-pyrene (^{15}N-8) and **(^{15}N)cyclam (^{15}N-9).** Following the literature method,[8] K_2CO_3 (0.36 g, 2.58 mmol) and 1,3-dibromopropane (130.95 μl, 1.29 mmol) were added to a solution of ^{15}N-**7** in dry CH_3CN (20 ml). The reaction mixture was stirred for 12 h. After the reaction, the insoluble material was filtered off and the solvent evaporated to give ^{15}N-**8** as a brown oil. Purification of the crude product was performed by dissolving the brown oil in dichloromethane (8 ml) and followed by addition of hexane (about 50 ml). A yellow precipitate which formed was filtered off, and the filtrate was evaporated to give ^{15}N-**8**. The product was used without further purification in the next step.

Compound ^{15}N-**8** was dissolved in ethanol (10 ml) and 10% hydrochloric acid (20 ml). The mixture was heated at 60 °C for 2 days. The mixed solvent was evaporated and the residue was recrystallised in EtOH to obtain the cyclam as the tetrahydrochloride salt. The residue was dissolved in a small amount of water (about 1 ml) and the pH of the solution was adjusted by NaOH pellets to pH >13. Then the solution was extracted with $CHCl_3$ (4×10 ml), and the solvent evaporated to give (^{15}N)cyclam (0.14 g, 54% for steps 7, 8 and 9). ^{1}H NMR ($CDCl_3$): δ = 2.81 (t, *J* =

5.49 Hz, 8 H; ^{15}NHCH_2CH$_2$CH_2^{15}NH), 2.77 (s, 8H; ^{15}NHCH_2CH_2^{15}NH), 1.75 (m, 4H; ^{15}NHCH$_2$CH_2CH$_2$^{15}NH); ^{15}N NMR ($CDCl_3$): δ = 4.5; Selected IR (KBr, neat): ν = 3260 (NH), 3178(NH), 2962 (CH_2), 2921(CH_2), 2868(CH_2), 2803(CH_2) cm^{-}; EI MS 204 *m/e* (M^+).

3.3 Results

3.3.1 (^{15}N)N,N'-Bis(2-aminoethyl)-1,3-propanediamine tetra-hydrochloride (^{15}N-6)

The 2D [^{1}H, ^{15}N] HSQC NMR spectrum in 10% D_2O/ 90% H_2O showed four cross-peaks for ^{1}H, ^{15}N correlations (Figure 3.1). Three ^{1}H/^{15}N cross-peaks correlated with the ^{15}N peak at 20.56 ppm and the remaining ^{1}H/^{15}N cross-peak correlated with the ^{15}N peak at 7.74 ppm. The 1D ^{13}C-{^{1}H} NMR spectrum for ^{15}N-**6** in 10% D_2O / 90% H_2O showed four ^{13}C peaks (Figure 3.2). The 2D [^{1}H, ^{13}C] HSQC NMR spectrum 10% D_2O / 90% H_2O also showed cross-peaks which were identified thus: $\mathbf{H_a}$ (δ 2.18/^{13}C 25.46), $\mathbf{H_b}$ (δ 3.25/^{13}C 47.69), $\mathbf{H_c}$ (δ 3.41/^{13}C 38.27) and $\mathbf{H_d}$ (δ 3.44/^{13}C 47.13). Both [^{1}H, ^{1}H] DQF-COSY and TOCSY NMR spectra show that $\mathbf{H_a}$ and $\mathbf{H_b}$ correlate with each other (Figures 3.3 and 3.4).

Further NMR simulation was performed using SpinWorks (Version1.1, Kirk Marat) program (Figure 3.5). All coupling constants acquired from the simulation are listed in Table 3.1.

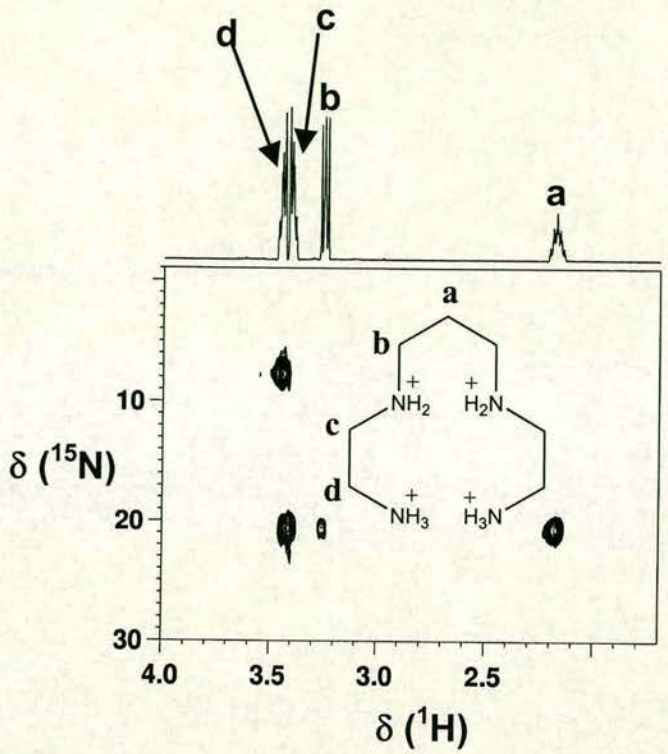

Figure 3.1 ^{1}H and 2D [^{1}H,^{15}N] HSQC NMR spectra of ^{15}N-**6** in 10% D_2O/90% H_2O

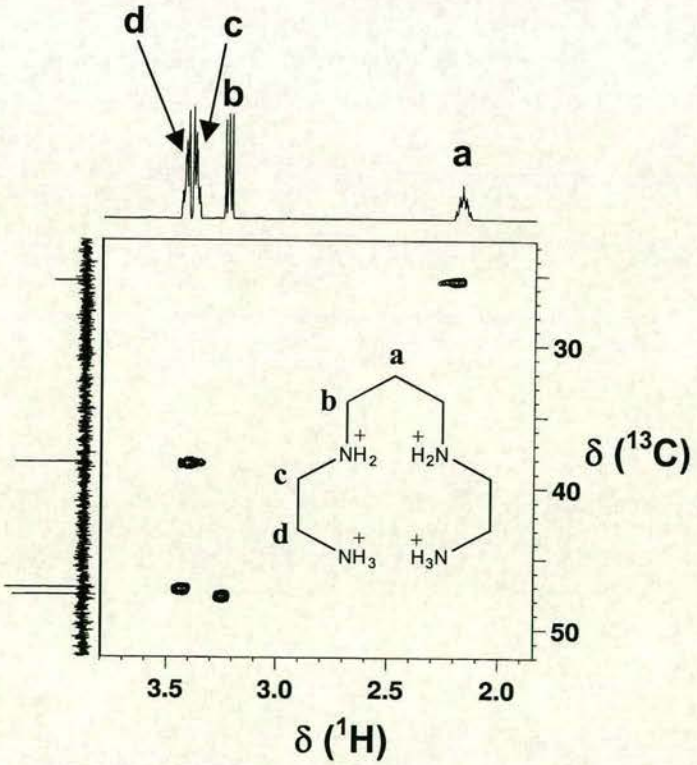

Figure 3.2 2D [^{1}H, ^{13}C] HSQC of ^{15}N-**6** in 10% D_2O / 90% H_2O (N = ^{15}N)

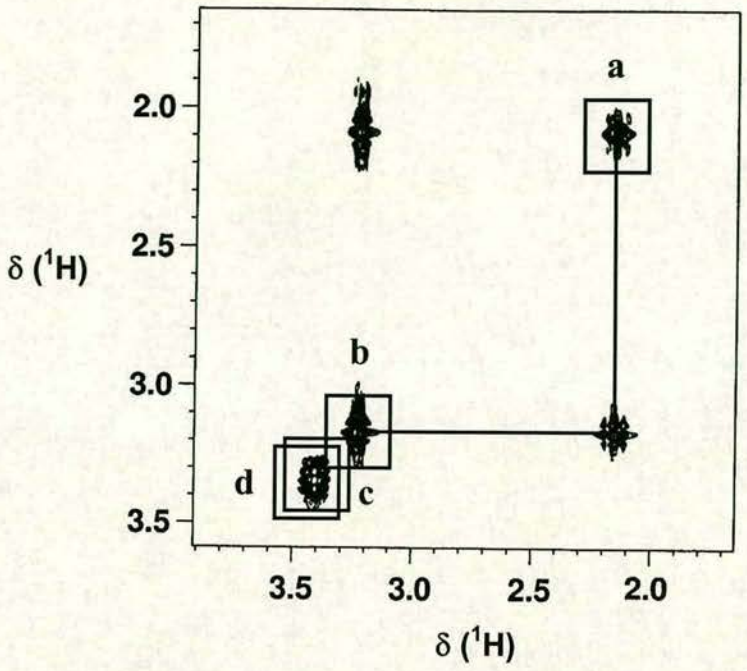

Figure 3.3 2D [^{1}H, ^{1}H] DQF-COSY of ^{15}N-**6** in 10% D_2O / 90% H_2O

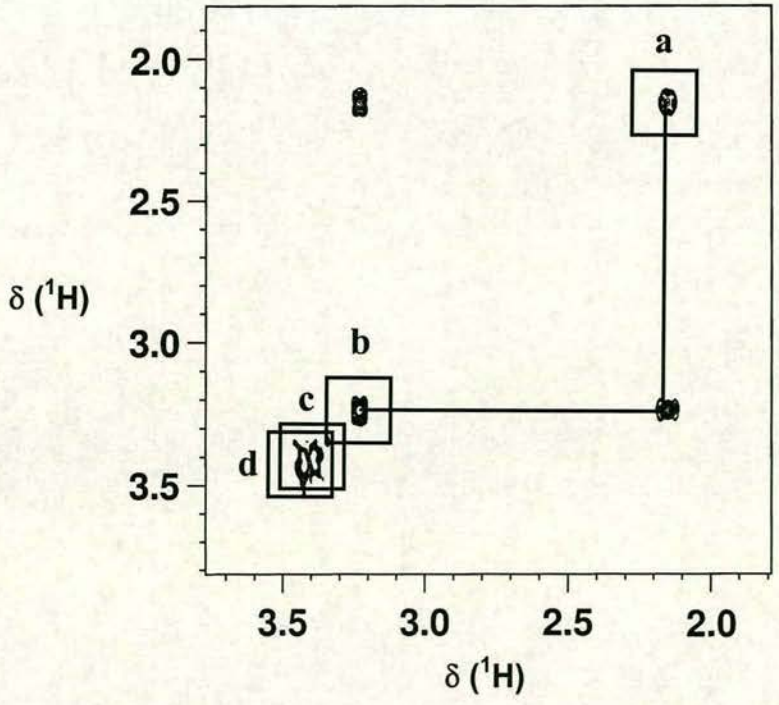

Figure 3.4 2D [^{1}H, ^{1}H] TCOSY of ^{15}N-**6** in 10% D_2O / 90% H_2O

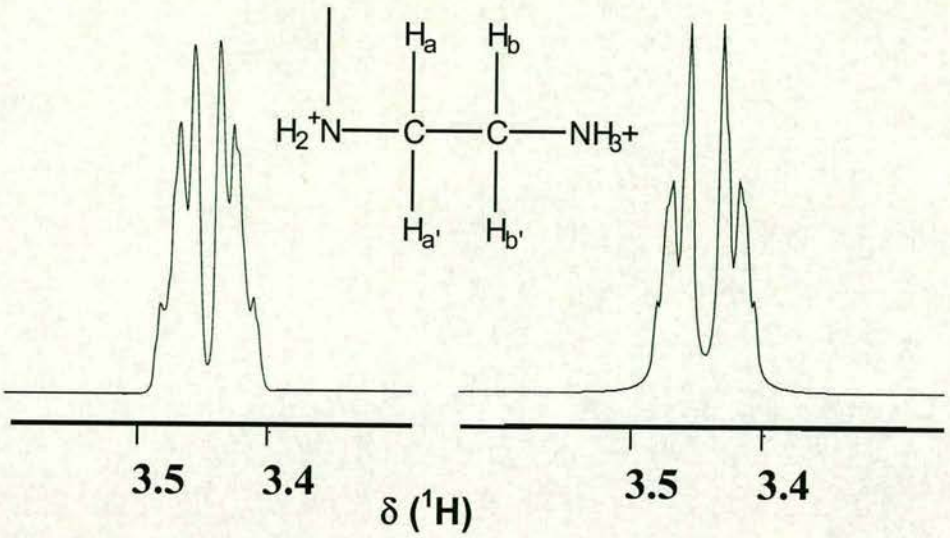

Figure 3.5 Simulated (right) and experimental (left) ^{1}H NMR spectra of ^{15}N-**6** in 10% D_2O / 90% H_2O. The coupling constants obtained from simulation are listed in Table 3.1. A fragment of ^{15}N-**6** is shown.

Table 3.1 ^{1}H, ^{1}H NMR coupling constants (Hz) for ^{15}N-**6** from simulation

	δ (^{1}H, Hz) (500 MHz)	H_a	$H_{a'}$	H_b	$H_{b'}$
H_a	1710.7				
$H_{a'}$	1710.7	^{2}J, 9.0			
H_b	1720.0	^{3}J, 1.2	^{3}J, 3.5		
$H_{b'}$	1720.0	^{3}J, 4.2	^{3}J, 1.2	^{2}J, 9.0	

3.3.2 (^{15}N)9a,9b-Dimethyl-octahydro-1,3a,6a,9-tetraaza-phenalene (^{15}N-7)

The 2D [^{1}H, ^{13}C] HSQC NMR spectrum showed cross-peaks corresponding to sixteen ^{1}H NMR signals and nine ^{13}C NMR signals (Figure 3.6). Geminal pairs of protons were identified thus: **H$_a$** (δ 1.15) / **H$_f$** (δ 2.32) ((δ ^{13}C 21.07), **H$_d$** (δ 2.19) / **H$_p$** (δ 3.58) (δ ^{13}C 48.42), **H$_e$** (δ 2.27) / **H$_g$** (δ 2.44) (δ ^{13}C 54.08), **H$_h$** (δ 2.52) / **H$_o$** (δ 3.28) ((δ ^{13}C 49.58), **H$_i$** (δ 2.58) / **H$_n$** (δ 3.21) (δ ^{13}C 42.05), **H$_j$** (δ 2.59) / **H$_k$** (δ 2.70) (δ ^{13}C 51.95), **H$_l$** (δ 2.90) / **H$_m$** (δ 3.11) ((δ ^{13}C 44.87. The remaining two

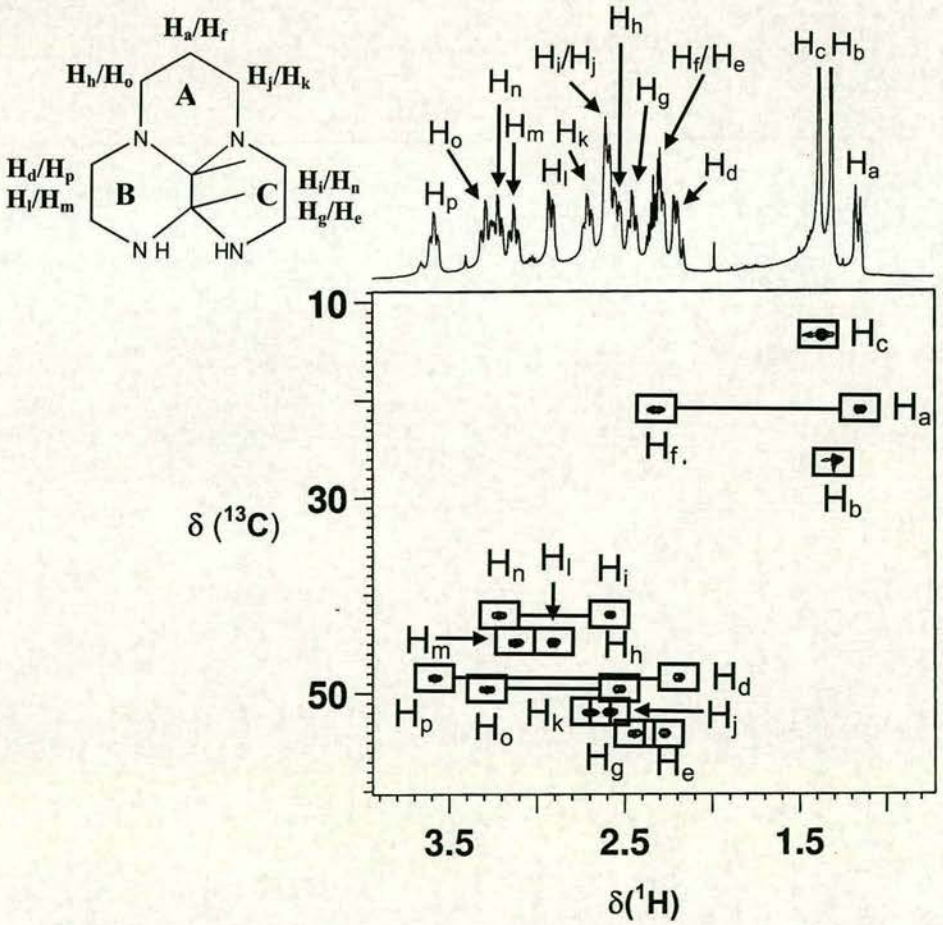

Figure 3.6 1D ^{1}H (top) and 2D [^{1}H, ^{13}C] HSQC (bottom) spectra of ^{15}N-**7** in $CDCl_3$

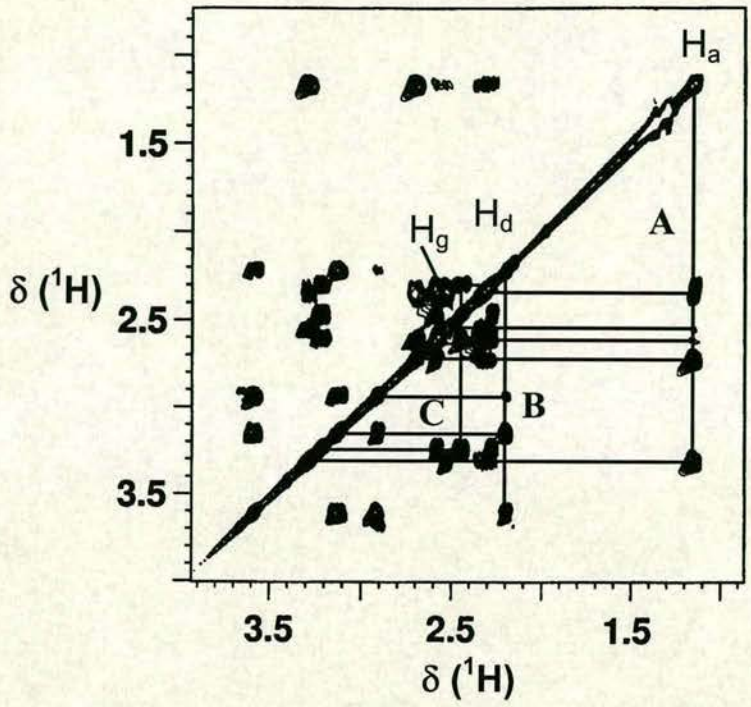

Figure 3.7 2D [^{1}H, ^{1}H] DQF-COSY spectrum of ^{15}N-**7** in $CDCl_3$

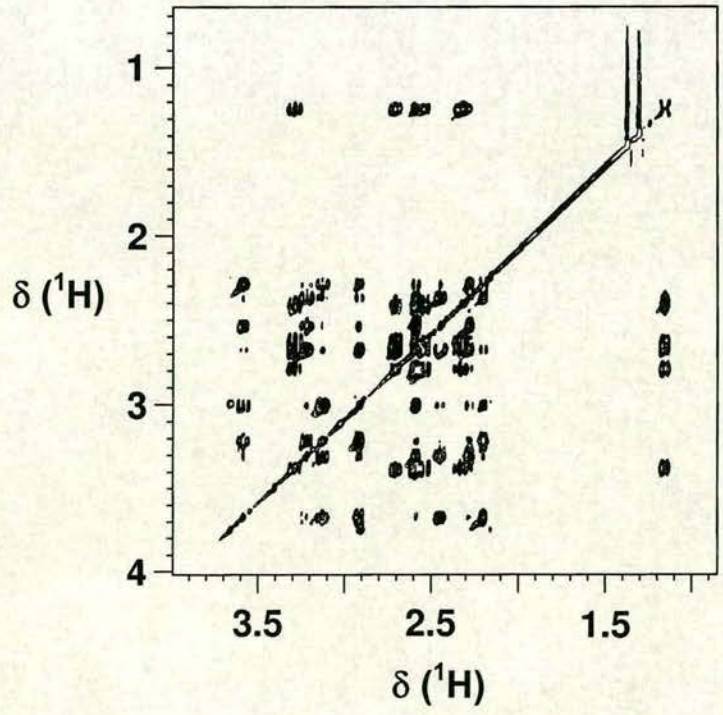

Figure 3.8 2D [^{1}H, ^{1}H] TOCSY spectrum of ^{15}N-**7** in $CDCl_3$

cross-peaks (δ $H_b/^{13}C$ 1.30/26.23) and (δ $H_c/^{13}C$ 1.37/13.49), show that each ^{13}C resonance corresponds to a single ^1H resonance and therefore, they are from two methyl groups. This conclusion was confirmed by 2D [^1H, ^1H] DQF-COSY (Figure 3.7) and TOCSY NMR (Figure 3.8) in which each of them does not correlate with any other resonances.

The two singlets $\mathbf{H_b}$ and $\mathbf{H_c}$ are from two CH_3 methyl groups. There are still three other spin systems besides the two methyl groups in 2D [^1H, ^1H] TOCSY NMR spectrum (Figure 3.8). Within the first spin-system (designated **A**), the main couplings appear to be as follows: $\mathbf{H_a}$ couples to $\mathbf{H_f}$, $\mathbf{H_k}$ and $\mathbf{H_o}$ strongly and to $\mathbf{H_h}$ and $\mathbf{H_j}$ weakly, which also couple to one another. The second spin-system (designated **B**) is composed of 4 signals: $\mathbf{H_d}$ is coupled to $\mathbf{H_l}$ weakly and to $\mathbf{H_m}$ and $\mathbf{H_p}$ strongly, which also couple to one another. The last spin system (designated **C**) also consists of 4 cross-peaks: $\mathbf{H_g}$ couples to $\mathbf{H_e}$, and $\mathbf{H_i}$ and $\mathbf{H_n}$ strongly, which also couple to one another.

In general, introduction of ^{15}N by synthetic labelling gives rise to couplings between ^{15}N and ^1H, or ^{15}N and ^{13}C which were measurable in ^1H NMR and ^{13}C NMR spectra, respectively. The coupling constants are listed in Table 3.2.

Table 3.2 Coupling constants for ^{15}N labelled compounds

compound	solvent	Coupling constant (Hz)			
		J (^{13}C, ^{15}N)		J (^{1}H, ^{15}N)	
		^{1}J	^{3}J	^{1}J	^{2}J
^{15}N-1	$CDCl_3$				1.2
^{15}N-2	D_2O/H_2O			74.6	
^{15}N-3	CD_3OD	5.1; 5.5			0.5
^{15}N-6	D_2O/H_2O	5.5; 5.9	2.5		

3.4 Discussion

3.4.1 (^{15}N)N,N'-Bis(2-aminoethyl)-1,3-propanediamine tetra-hydrochloride (^{15}N-6)

From chemical shifts and/or patterns of resonances in ^{1}H NMR spectrum, $\mathbf{H_a}$ and $\mathbf{H_b}$ can be easily assigned to the middle CH_2 and two side CH_2 groups in the fragment of $NHCH_2CH_2CH_2NH$, respectively. Both [^{1}H, ^{1}H] DQF-COSY and TOCSY NMR spectra show $\mathbf{H_a}$ and $\mathbf{H_b}$ correlate to each other and thus confirm this conclusion (Figures 3.3 and 3.4). The remaining resonances at 3.41 and 3.44 ppm correlating to two separate ^{13}C resonances at 47.13 and 47.69 ppm, respectively, show an AB system for protons in fragment $NHCH_2CH_2NH$. The ^{15}N peak at 20.56 ppm in [^{1}H, ^{15}N] HSQC correlated to $\mathbf{H_a}$, $\mathbf{H_b}$ and $\mathbf{H_c}$. Therefore, $\mathbf{H_c}$ most likely comes from the fragment $^{15}NHCH_2CH_2{}^{15}NH_2$ next to ^{15}NH. The ^{15}N resonance at 20.56 ppm couples to $\mathbf{H_a}$ and $\mathbf{H_b}$ on its neighbour carbons, and $\mathbf{H_c}$ through a 3-bond

coupling. $\mathbf{H_d}$ must come from CH_2 next to $^{15}NH_2$ in the fragment $^{15}NHCH_2CH_2{}^{15}NH_2$.

Unlike in the ethane molecule, the eclipsed conformation in the ethane fragment of ^{15}N-**6** becomes unfavourable because of electrostatic repulsion (see ethane fragment in Figure 3.9). Therefore, most ethane fragments in ^{15}N-**6** exist in the *gauche* and *trans* conformations (Figure 3.9). However, *trans* is the most stable and favourable conformer since NH_3^+ and NH_2^+ are in *trans* positions and, therefore, there is lowest electrostatic repulsion in *trans* conformer. This conclusion can be further confirmed by very low and equal ^3J (H_aH_b) and ^3J ($H_{a'}H_{b'}$) coupling constants (1.2 Hz, see Table 3.1). As shown by the Newman projections, the rapid rotation between *gauche* and *trans* conformers about the C-C bond leads to an average NMR spectrum which appears as an AA'BB' type. The coupling constants in Table 3.1 are from the population-weighted average of those of the different conformers.

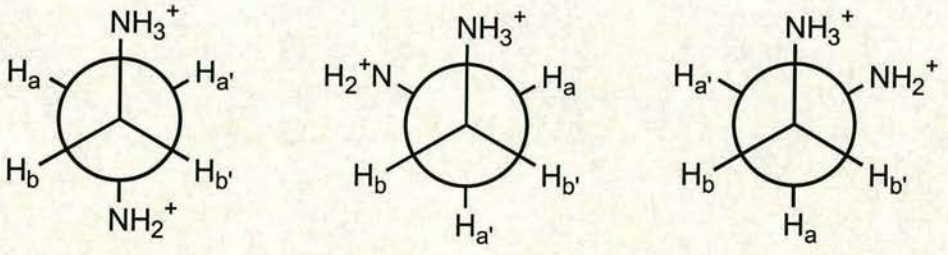

Figure 3.9 Newman projections for the three low-energy conformations around the C-C bond of the ethane fragment in ^{15}N-**6**. (N = ^{15}N)

3.4.2 (^{15}N)9a,9b-Dimethyl-octahydro-1,3a,6a,9-tetraaza-phenalene (^{15}N-7)

There are seven possible configurations for ^{15}N-**7** depending on the alignment of the two CH_3 groups and lone electron pairs of the tetraamine nitrogen atoms (Figure 3.10). The two CH_3 groups are denoted *cis* and *trans* according to the usual conventions. In the crystal structure, the compound **7** adopts configuration **2** (Figures 3.10 and 3.11) in which all three six-membered rings adopt chair conformation.[8] In solution, fourteen NMR resonances as well as two singlets from the two CH_3 groups reveal that all seven geminal pairs of protons from one $CH_2CH_2CH_2$ and two CH_2CH_2 fragments in three six-membered rings in ^{15}N-**7** are nonequivalent. Therefore, it is assumed that the compound adopts the same configuration as in the crystal structure shown in Figure 3.11. Therefore, the compound loses symmetry and all seven geminal pairs of protons are nonequivalent.

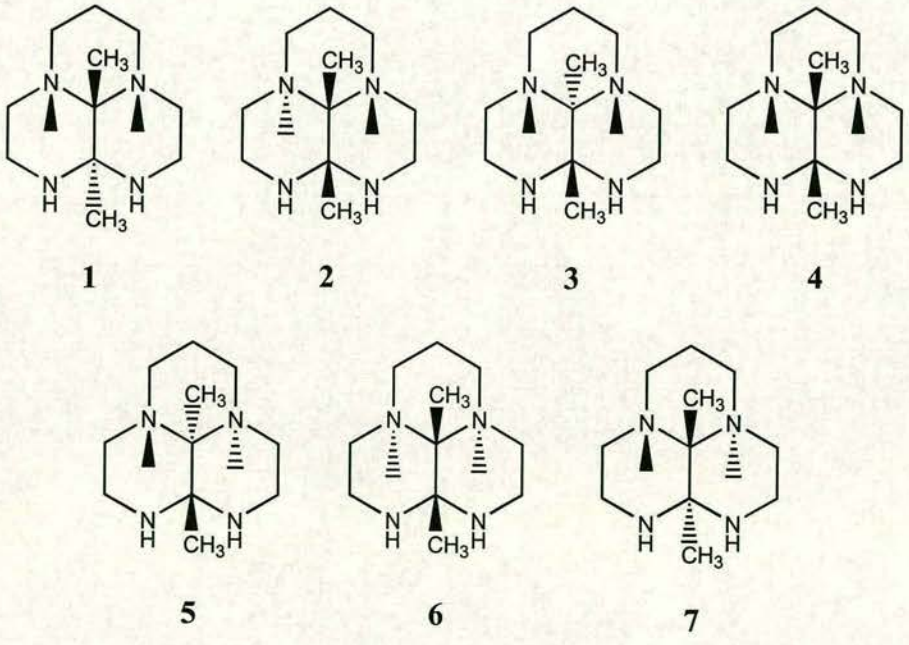

Figure 3.10 Seven possible configurations for compound **7**

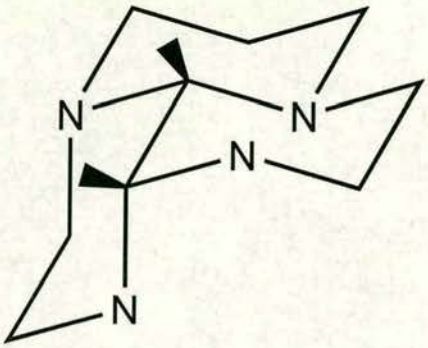

Figure 3.11 Conformation of compound **7** in the crystal structure (ref. 8)

From its chemical shift, $\mathbf{H_a}$ can be easily assigned to the middle CH_2 of $N(CH_2)_3N$ and six [^{1}H,^{1}H] DQF-COSY cross-peaks also confirmed that the spin-system **A** belongs to the six-membered containing $N(CH_2)_3N$ (see Figure 3.7). The other two spin-systems (**B** and **C**), therefore, can be assigned to the other two six-membered rings which contain $NH(CH_2)_2NH$, and the four [^{1}H,^{1}H] DQF-COSY cross-peaks for each of them also confirmed this conclusion (see Figure 3.7).

In 2D [^{1}H, ^{1}H] DQF-COSY NMR spectrum (Figure 3.7), $\mathbf{H_a}$ couples to $\mathbf{H_f}$, $\mathbf{H_k}$ and $\mathbf{H_o}$ strongly and to $\mathbf{H_h}$ and $\mathbf{H_j}$ weakly within the spin-system **A**. 2D [^{1}H,^{13}C] shows that $\mathbf{H_a/H_f}$, $\mathbf{H_j/H_k}$ and $\mathbf{H_h/H_o}$ are geminal pairs of protons. It is more likely that the six-membered ring **A** exists in a twist-boat conformation in solution instead of the chair conformation in the solid state (Figure 3.12).[8] In the twist conformation, the torsion angle between $\mathbf{H_a}$ of the middle CH_2 group and $\mathbf{H_j}$ (or $\mathbf{H_h}$) of the neighbouring CH_2 group is close to 90°. Therefore, there is a weak coupling between $\mathbf{H_a}$ and $\mathbf{H_j}$ (or $\mathbf{H_h}$). This also can be used to explain the weak coupling between $\mathbf{H_f}$ and $\mathbf{H_k}$ (or $\mathbf{H_o}$). In such highly strained system, although the ideal configuration will have as many rings as possible in chair conformation, however, the flexibility will

decrease at the same time. Therefore, although ring **A** with a twist-boat conformation in solution has a higher energy, it will have less strain as well.

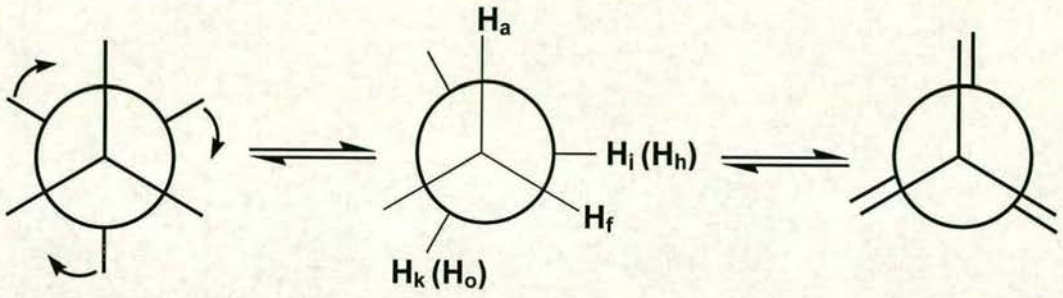

Figure 3.12 Newman projections for the $CH_2CH_2CH_2$ fragment in ^{15}N-**7**

In the 2D [^{1}H, ^{1}H] DQF-COSY NMR spectrum, $\mathbf{H_d}$ is coupled to $\mathbf{H_l}$ weakly and to $\mathbf{H_m}$ and $\mathbf{H_p}$ strongly in spin system **B**. 2D [^{1}H,^{13}C] shows that $\mathbf{H_d/H_p}$ and $\mathbf{H_l/H_m}$ are geminal pairs of protons. It seems that ring **B** has a similar situation as ring **A** and also adopts a twist-boat conformation in solution.

In the 2D [^{1}H, ^{1}H] DQF-COSY NMR spectrum, $\mathbf{H_g}$ couples to $\mathbf{H_e}$, and $\mathbf{H_i}$ and $\mathbf{H_n}$ strongly in spin system **C**. 2D [^{1}H,^{13}C] shows that $\mathbf{H_g/H_e}$ and $\mathbf{H_i/H_n}$ are geminal pairs of protons. Therefore, this shows that ring **C** still adopts chair conformation in solution.

In general, ^{15}N-**7** adopts conformation **2** (Figure 10) the same as in the solid state. However, two rings including ring **A** adopt the twist-boat conformation and third ring remains in the chair conformation.

3.5 Conclusions

^{15}N-cyclam has been successfully synthesised by a very effective synthetic route. ^{15}N isotopic enrichment (natural abundance ^{15}N: only 0.37%) greatly improved the sensitivity of detection combined with the inverse (^{1}H-detected) ^{15}N method.

1D and 2D ^{1}H, ^{13}C, and ^{15}N NMR studies revealed that the ethane fragments in ^{15}N-**6** exist in the *gauche* and *trans* conformations in aqueous solution. The *trans* conformer is the most favourable. The rapid rotation between *gauche* and *trans* conformers about the C-C bond leads to an average NMR spectrum which appears as an AA'BB' type. The coupling constants are also from the population-weighted average of those of the different conformers. 1D and 2D ^{1}H and ^{13}C NMR studies revealed that ^{15}N-**7** adopts conformation **2** (Figure 10) as in the solid state. However, two rings adopt the twist-boat conformations and the third ring remains in the chair conformation.

Successful synthesis of ^{15}N-cyclam allows us to probe the interaction of ^{15}N-cyclam complexes with the target protein by [^{1}H,^{15}N] HSQC.

3.6 References

(1) Della, E. W.; Kasum B.; Kirkbride, K. P. *J. Am. Chem. Soc.* **1987**, *109*, 2746.

(2) Berners-Price, S. J.; Sadler, P. J. *Coordin. Chem. Rev.* **1996**, *151*, 1.

(3) Piotto, M.; Saudek, V.; Sklenar, V. *J. Biomol. NMR* **1992**, *2*, 661.

(4) Gabriel, S.; Weiner, J. *Chem. Ber.* **1888**, *21*, 2669.

(5) Scherer, G.; Limbach, H. H. *J. Am. Chem. Soc.* **1994**, *116*, 1230.

(6) Zang, E.; Sadler, P. J. *Synthesis* **1997**, 410.

(7) Zervas, L.; Theodoropoulos, D. M. *J. Am. Chem. Soc.* **1956**, *78*, 1359.

(8) Hervé, G.; Bernard, H.; Le Bris, N.; Yaouanc, J. J.; Handel, H.; Toupet, L. *Tetrahedron Lett.* **1998**, *39*, 6861.

Chapter 4

Cd Cyclam Complexes

4. 1 Introduction to Cd Chemistry

Cadmium has atomic number 48 and atomic weight 112.40.[1] The main coordination numbers are 4, 5, and 6.[1] Together with zinc and mercury, Cd forms group 12; therefore it has two s-electrons outside filled d shells. Its usual oxidation state is +2, although Cd(I) species have been reported.[2] Cadmium chemistry closely resembles that of zinc, but in some cases remarkable differences can be observed. The nuclear spin of ^{111}Cd and ^{113}Cd is ½ and their natural abundances are 12.75 and 12.26%.[2] Therefore, both ^{111}Cd and ^{113}Cd NMR spectroscopy can be used to study complexes and to examine their binding sites in metalloproteins.[3]

The metal centres of many metalloproteins play an active role in biological function so it is important to obtain as much structural information as we can about such sites. In recent years, ^{111}Cd and ^{113}Cd NMR spectroscopy has been developed and utilised as 'spin spy' to study the Zn(II) sites in metalloproteins.[4] The reason for this strategy is that the nuclear spin of ^{67}Zn is 5/2 and therefore, Zn(II) has prohibitively broad lines in the solution NMR spectrum.[4] Based on parallel chemistry and size considerations, Cd(II) can be employed as a surrogate probe to study these metals in this important class of biological system. NMR studies on ^{113}Cd-substitued metalloproteins and ^{113}Cd-substitued rubredoxin indicate a Karplus-type correlation between the ^{3}J (^{111}Cd, ^{1}H) coupling constants and the H^{β}-C^{β}-S^{γ}-Cd dihedral angle.[5]

Therefore, both vicinal proton-proton and proton-cadmium coupling constants can provide further structural information.

The biological activity of metal (especially zinc) cyclam complexes,[6] is likely to be related to their configurations in solution. However, the determination of cyclam configurations in solution is a difficult problem especially since a mixture of species can be present. I have investigated the possible use of Cd as a substitute for Zn because of its more favourable NMR properties (I=1/2 for ^{111}Cd and ^{113}Cd), although Cd cyclam (log K 11.7)[7] is less stable than Zn cyclam (log K 15.5)[8].

Syntheses and characterisation by X-ray crystallography of two Cd complexes, $[Cd(O_2COCH_3)(Me_4\text{-cyclam})](ClO_4)$ and $[Cd(O_2COH)(Me_4\text{-cyclam})](ClO_4)$ have been reported.[9] In these complexes, each cation has a distorted octahedral geometry of the *cis*-CdO_2N_4 type with the macrocyclic ligand folded and the four methyl groups on the same side as the carbonate ligand. The monomethylcarbonate and hydrogen-carbonate ions chelate the metal unsymmetrically with one short and one long Cd-O bond.[9] The preliminary variable-temperature ^{13}C NMR studies revealed that $[Cd(cyclam)(NO_3)_2]$ exists as a mixture of two isomers in solution.[10]

4. 2 Experimental

4. 2. 1 Synthesis and crystallisation of Cd cyclam complexes

Synthesis of Cd(cyclam)$(ClO_4)_2$ (1). Cyclam (50.1 mg, 0.25 mmol) and $Cd(ClO_4)_2\cdot 6H_2O$ (104.9 mg, 0.25 mmol) were heated under reflux in CO_2-free methanol (10 ml) for 2 h under argon. The volume was reduced (to *ca.* 4 ml) under

reduced pressure until a white precipitate appeared. The precipitate was filtered off and washed with a small amount of methanol under argon to give the product. Yield 83.4 mg (65.2%). Anal. Calcd for $C_{10}H_{24}N_4CdCl_2O_8$: C, 23.48; H, 4.73; N, 10.95%. Found: C, 23.69; H, 4.91; N, 11.07%. Selected IR (KBr, cm^{-1}): 3306 s (NH), 3282 m (NH), 2921 m (CH), 2861 m (CH), 1611 w (NH).

Synthesis of Cd(cyclam)Cl_2 (2). Cyclam (50.1 mg, 0.25 mmol) and $CdCl_2$ (48.3 mg, 0.25 mmol) were heated under reflux in CO_2-free methanol (10 ml) for 2 h under argon. The volume was reduced (to *ca.* 4 ml) under reduced pressure until a white precipitate appeared. The precipitate was filtered off and washed with a small amount of methanol under argon to give the product. Yield 81.7 mg (85.2%). Anal. Calcd for $C_{10}H_{24}N_4CdCl_2$: C, 31.31; H, 6.31; N, 14.60%. Found: C, 31.03; H, 5.96; N, 14.39%. Selected IR (KBr, cm^{-1}): 3179 s (NH), 2906 m (CH), 2838 s (CH), 1623 w (NH).

Synthesis of $[Cd_3(cyclam)_3(CO_3)](ClO_4)_4 \cdot 3H_2O$ (3). Complex **1** (1 g, 2 mmol) was dissolved in water and left standing in air at ambient temperature. After 7 days, colourless crystals of **3** were filtered off and washed with a small amount of methanol. Yield 0.62 g (62%). Anal. Calcd for $C_{31}H_{78}N_{12}Cd_3Cl_4O_{22}$: C, 25.68; H, 5.42; N, 11.59. Found: C, 26.09; H, 4.83; N, 11.45. Selected IR (KBr, cm^{-1}): 3431 s, br (OH), 3303 s (NH), 3175 s (NH), 2909 s (CH), 2852 s (CH), 1451 s (CO).

4. 2. 2 NMR spectroscopy

All data were acquired at a probe temperature of 298 K. ^1H chemical shifts were internally referenced to the methyl singlet of TSP (3-trimethylsilyl- propionate-d_6) at 0 ppm; ^{13}C chemical shifts were referenced externally also using TSP. All NMR experiments were performed in 10% D_2O / 90% H_2O under argon with **1** at a

concentration of 36 mM, pH 7.9, and **2** at a concentration of 47 mM, pH 8.2 unless otherwise stated.

1D ^{1}H NMR data were acquired over a ^{1}H frequency width of 5 kHz into 16 k data points (acquisition time = 1.64 s). The water resonance was suppressed by presaturation or *via* the WATERGATE pulsed-field-gradient sequence.[11]

1D ^{111}Cd-{^{1}H} NMR data were typically acquired (using a broadband probehead) on a sample of **1** prepared with $^{111}Cd(ClO_4)_2$ (generated from ^{111}CdO and $HClO_4$) over a ^{111}Cd frequency width of 15.9 kHz (150 ppm) centred at 246 ppm. ^{111}Cd peaks were referenced to external 1M $^{111}Cd(ClO_4)_2$ in 10% D_2O / 90% H_2O. Data were acquired with 100,000 transients into 4 k complex data points (acquisition time = 0.13 s).

2D [^{1}H, ^{13}C] HSQC NMR data were typically acquired over a ^{1}H frequency width of 5 kHz and a ^{13}C frequency width of 5 kHz (40 ppm) centred at 43 ppm. Data were acquired with 64 transients into 2 k complex data points (acquisition time 205 ms) for each of 128 t_1 increments (acquisition time 12.7 ms).

2D [^{1}H, ^{15}N] HSQC NMR data were acquired over a ^{1}H frequency width of 1 kHz and a ^{15}N frequency width of 250 Hz (5 ppm) centred at 12 ppm. Data were acquired with 240 transients into 2 k complex data points for each of 128 t_1 increments.

2D [^{1}H, ^{111}Cd] HSQC NMR data were acquired for ^{111}Cd labelled **1** over a ^{1}H frequency width of 5 kHz (10 ppm) and a ^{111}Cd frequency width of 2.1 kHz (20 ppm) centred at 244 ppm. 2D [^{1}H, ^{111}Cd] HSQC-TOCSY NMR data were acquired over a ^{111}Cd frequency width of 1 kHz (10 ppm) centred at 246 ppm using a mixing period of 55 ms for the HSQC-TOCSY. Both experiments were adjusted for a $^{2}J(^{1}H_N,^{111}Cd)$

coupling of 30 Hz. Data were acquired with 8 transients (4 for HSQC-TOCSY) for each of 128 (64 for HSQC-TOCSY) t_1 increments into 2 k complex data points (acquisition time 170 ms). For all inverse 2D experiments, the water resonance was eliminated as part of the coherence selection process.

2D [^{1}H, ^{1}H] z-filtered TOCSY data were acquired at 600 MHz for ^{111}Cd labelled **1** and used for the measurement of ^{1}H/^{111}Cd coupling constants: 4096 complex data points were acquired over an F2 frequency width of 3 kHz (acquisition time = 0.683 s); 16 transients were acquired for each of 2 × 512 t_1 increments in F1 (frequency width = 1.5 kHz). A spin-lock time of 70 ms was employed. Solvent suppression was achieved using WET.[12]

All NMR data were processed using Xwin-nmr (version 2.0, Bruker U.K. Ltd.).

4. 2. 3 NMR simulation

Spin system simulations were carried out using the program Spinworks (version 1.1, Kirk Marat, University of Manitoba, 1999).

4. 2. 4 Molecular Modelling

A molecular model for the *trans*-I configuration of Cd-Cyclam was built using the program Sybyl (version 6.3, Tripos Inc.) based on the *cis*-I configuration in the crystal structure of **3**.

4. 2. 5 pH titration

Complex **1** was dissolved in CO_2-free 90% H_2O / 10% D_2O. The pH was adjusted to 12.1 with 0.1 M NaOH in the NMR tube and the back titration was carried out from 12.1 to 5.3 by addition of 0.1 M $HClO_4$. Values of pH were measured with a

Corning 145 pH-meter equipped with a micro-combination electrode calibrated with Aldrich standard buffers (pH 4, 7, and 10). No correction was made for deuterium isotope effects. All experiments were performed on samples saturated with argon.

4. 2. 6 Carbonate binding study

$Na_2{}^{13}CO_3$ was dissolved in 90% H_2O / 10% D_2O to give a 40 mM solution in the presence of TSP. Stepwise addition of a concentrated solution of **1** was made to this solution to give $^{13}CO_3^{2-}$: **1** ratios from 1:0.2 to 1:3.5 in 10 steps. ^{13}C-{^1H} NMR spectra were acquired at 150 MHz (512 transients, 31.44 kHz sweep width, 25216 data points, 0.4 s acquisition time) after each addition of **1**. In a similar experiment Na_2CO_3 was added stepwise to a solution of **1** (16 mM in 90% H_2O / 10% D_2O) to give molar ratios **1**:$^{13}CO_3^{2-}$ of 1:0.5, 1:1, 1:2, 1:4 and ^1H NMR spectra were acquired after each addition.

4. 2. 7 Crystallography

The crystal data and refinement parameters for $[Cd_3(cyclam)_3(CO_3)](ClO_4)_4 \cdot 3H_2O$ (**3**) are summarised in Table 4.1. Colourless needles developed along (001) with other faces along the (110) and (-110) directions. Data were collected with Mo-Kα radiation on a Stoë Stadi-4 diffractometer equipped with an Oxford Cryosystems low-temperature device. An absorption correction was applied by Gaussian integration following refinement of the crystal dimensions against a set of ψ-scan (Stoë X-shape,[13] μ = 1.435 mm^{-1}, T = 0.915 – 0.937). The structure was solved by direct methods (SIR92[14]) and refined by full-matrix least-squares against F^2 (Shelxl97[15]). The perchlorate anions centred on Cl2 and Cl3 are disordered about a –3 special position, that centred on Cl1 is orientationally

disordered in the ratio 70:30 with a common Cl position; equivalent Cl-O and O···O distances were restrained to be similar. H-atoms were placed in calculated positions on C-atoms. The position for H-atoms attached to O1W (water of crystallisation) could not be calculated unambiguously and were therefore not placed at all. All non-H atoms with the exception of the minor-occupancy O-atoms in perchlorate-1 were refined anisotropically.

Table 4.1 Crystal data and refinement parameters for complex **3**

Formula	$C_{31}H_{78}Cd_3Cl_4N_2O_{22}$
M	1309.95
Crystal system	Rhombohedral
Space group	*R*-3
a/ Å	23.142(2)
b/ Å	23.142(2)
c/ Å	17.500(4)
β/ °	90
U/ Å^3	8116.6(19)
Z	6
T/ K	150(2)
D_c/ Mg m^{-3}	1.608
μ/ mm^{-1}	1.435
Unique data	2341
Observed data	3583
R (R')	0.0660 (0.1444)

4.3 Results

Three Cd(II) cyclam complexes were prepared. The perchlorate complex **1**, the chloride complex **2**, and the carbonate complex **3** obtained from **1** via fixation of atmospheric CO_2. The structures of these complexes were studied by IR and NMR spectroscopy and, for **3**, by X-ray crystallography.

4. 3. 1 IR spectroscopy

N-H stretching vibrations occur at 3306 and 3208 cm^{-1} for **1** and 3303 and 3175 cm^{-1} for **3**. A single intense N-H stretching vibration at 3179 cm^{-1} for **2** was observed. Complex **3** exhibits a strong CO stretching band at 1451 cm^{-1}.

4. 3. 2 ^{1}H, ^{13}C, ^{15}N and ^{111}Cd NMR of Cd(cyclam)$(ClO_4)_2$ (1) in aqueous solution

The ^{1}H NMR spectrum of **1**, acquired immediately after dissolving the sample in 10% D_2O / 90% H_2O, is shown in Figure 4.1. No changes were observed over a period of more than 2 weeks at ambient temperature. The 1D ^{1}H NMR spectrum is limited to the 1.5 to 3.5 ppm spectral window and the signals fall into two regions. The first set of 3 multiplets appear between 1.5 and 2.0 ppm, two of which (1.59 and 1.90 ppm) are doublets of triplets. The second region of signals lies between 2.5 and 3.5 ppm. Few signals in this region were cleanly resolved. In order to overcome this problem, and to assign fully the ^{1}H NMR spectrum, 2D homonuclear [^{1}H, ^{1}H] TOCSY and DQF-COSY NMR data sets and natural abundance 2D heteronuclear [^{1}H, ^{13}C] and [^{1}H, ^{15}N] HSQC NMR data were acquired.

2D [^{1}H, ^{1}H] COSY NMR data (Figure 4.2) showed that the doublets of triplets at 1.59 (designated $\mathbf{H_a}$) and 1.90 ppm (designated $\mathbf{H_b}$) are coupled to one another. 2D [^{1}H, ^{1}H] TOCSY NMR data (Figure 4.3) revealed the presence of two spin-systems. Within the first spin-system (labelled **I**), the main couplings appear to be as follows: $\mathbf{H_a}$ couples to $\mathbf{H_b}$ and to $\mathbf{H_c}$ (2.69 ppm); $\mathbf{H_b}$ couples to $\mathbf{H_f}$ (3.23 ppm); $\mathbf{H_c}$ and $\mathbf{H_f}$

couple to one another. $\mathbf{H_e}$ (2.91 ppm) and $\mathbf{H_d}$ (2.75 ppm) couple to one another and also to the broad signal at 3.31 ppm. This signal also correlates strongly with $\mathbf{H_c}$. The

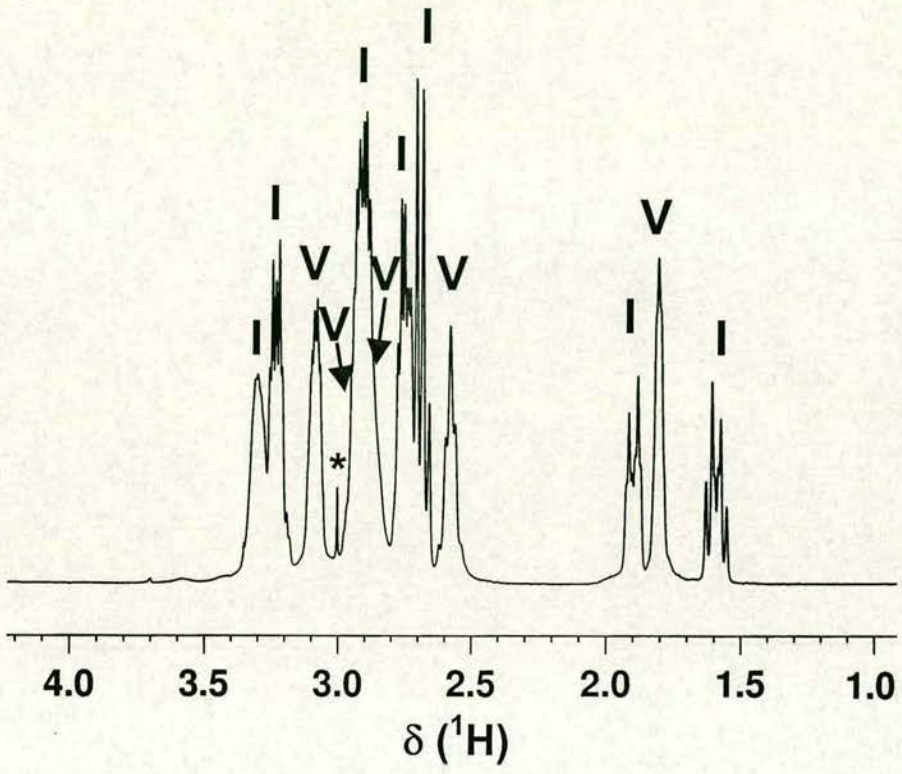

Figure 4.1 ^{1}H NMR spectrum of complex **1** in 10% D_2O / 90% H_2O. Resonances for the *trans*-I configuration are designated **I** and resonances for *cis*-V are designated **V**. * = free ligand.

second spin-system (labelled **V**) is composed of 5 signals: $\mathbf{H_1}$ (1.81 ppm) is coupled to $\mathbf{H_3}$ (2.86 ppm) and $\mathbf{H_5}$ (3.09 ppm), which also couple to one another; $\mathbf{H_2}$ (2.58 ppm) couples to $\mathbf{H_4}$ (2.94 ppm), both of which are also associated with $\mathbf{H_3}$ and $\mathbf{H_5}$ *via* TOCSY correlations.

Only one cross-peak was observed in the 2D [^{1}H, ^{15}N] HSQC NMR spectrum of **1** in 90% H_2O / 10% D_2O (Figure 4.4b), a broad signal at 3.31 ppm. The main cross-peak for the natural abundance ^{15}N signal was centred at 11.91 ppm and was

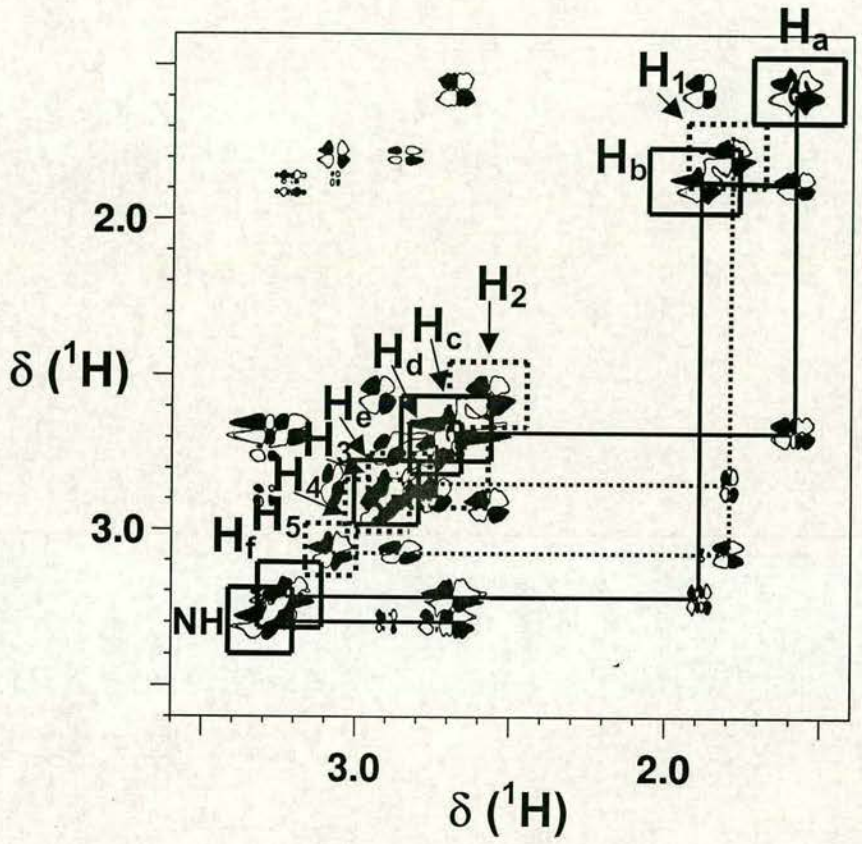

Figure 4.2 2D [^{1}H, ^{1}H] COSY NMR spectrum of **1** in 10% D_2O / 90% H_2O. Resonances for *trans*-I are designated by solid boxes and resonances for *cis*-V are designated by dashed boxes.

accompanied by two satellite cross-peaks, arising from the presence of $^{111/113}$Cd at natural abundance: $^{1}J(^{15}N, ^{111/113}Cd)$ = 118 Hz; $^{2}J(^{1}H_N, ^{111/113}Cd)$ = 27 Hz. Only the spin-system $\mathbf{H_a}$-$\mathbf{H_f}$ showed TOCSY correlations to the **N<u>H</u>** signal; the spin-system

H_1-H_5 did not show any relationship to this **NH** signal or to any of the signals **H_a-H_f** leading to the speculation that the two identified spin-systems arise from two different configurations (**I** and **V**) of Cd(II) cyclam. Supporting evidence for this came from 2D [^{1}H, ^{111}Cd] HSQC, 2D [^{1}H, ^{111}Cd] HSQC-TOCSY and 1D ^{111}Cd-{^{1}H} NMR data.

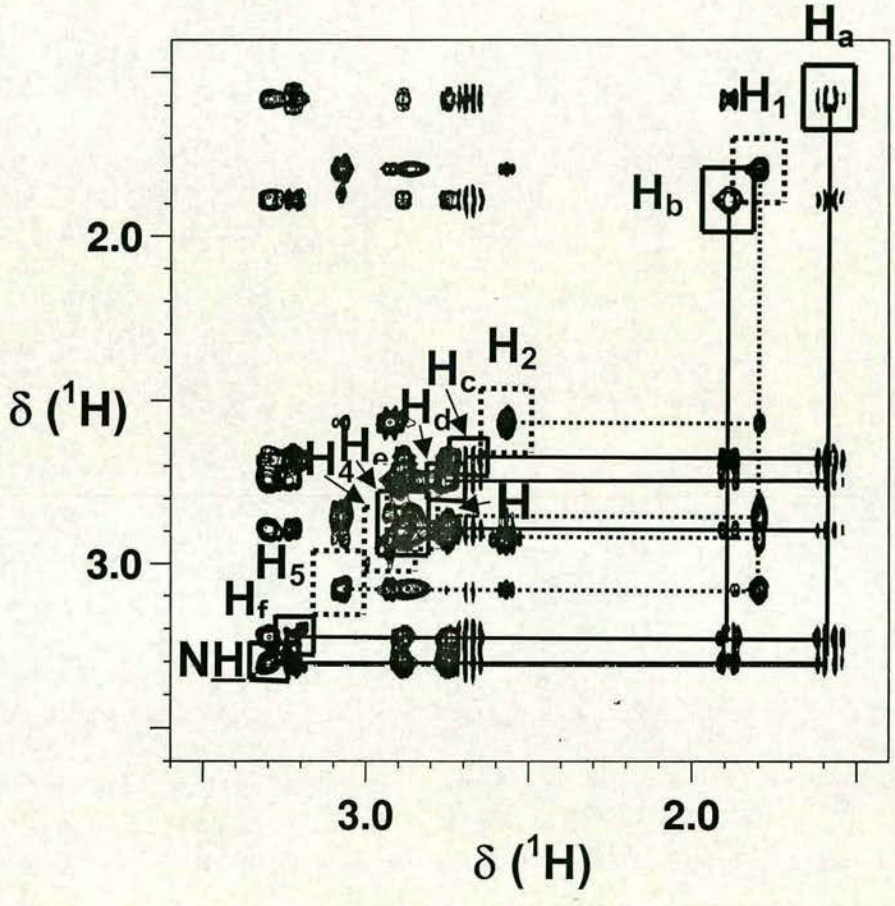

Figure 4.3 2D [^{1}H, ^{1}H] TOCSY NMR spectrum of **1** in 10% D_2O / 90% H_2O. Resonances for the *trans*-I configuration are designated by solid boxes and resonances for the *cis*-V configuration are designated by dashed boxes.

The 1D ^{111}Cd-{^{1}H} NMR spectrum acquired for ^{111}Cd-labelled **1** (Figure 4.5) showed three major ^{111}Cd peaks at 248, 244, and 219 ppm with relative peak areas of

1:0.5:0.1, respectively. The latter minor species was not observed in 1D ^{1}H and 2D NMR spectra. The 2D [^{1}H, ^{111}Cd] HSQC NMR spectrum showed 7 cross-peaks for ^{1}H, ^{111}Cd correlations (Figure 4.6b). Four $^{1}H/^{111}Cd$ cross-peaks correlated with the major ^{111}Cd peak at 248 ppm, and the remaining three $^{1}H/^{111}Cd$ cross-peaks correlated with the ^{111}Cd peak at 244 ppm. The 2D [^{1}H, ^{111}Cd] HSQC-TOCSY NMR data (Figure 4.6a) confirmed the presence of the two spin systems identified from the 2D [^{1}H, ^{1}H] TOCSY NMR data. Thus two major configurations of **1** (**I**: δ ^{111}Cd 248, ^{1}H

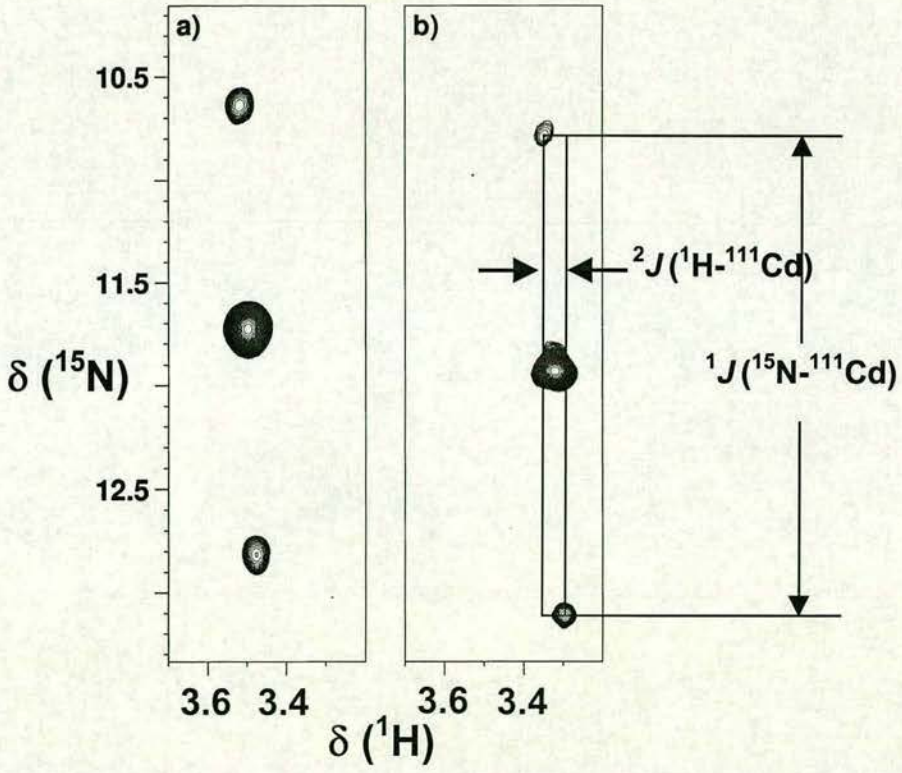

Figure 4.4 (a) 2D [^{1}H, ^{15}N] HSQC NMR spectrum of complex **2** and (b) 2D [^{1}H, ^{15}N] HSQC NMR spectrum of complex **1**, in 10% D_2O / 90% H_2O.

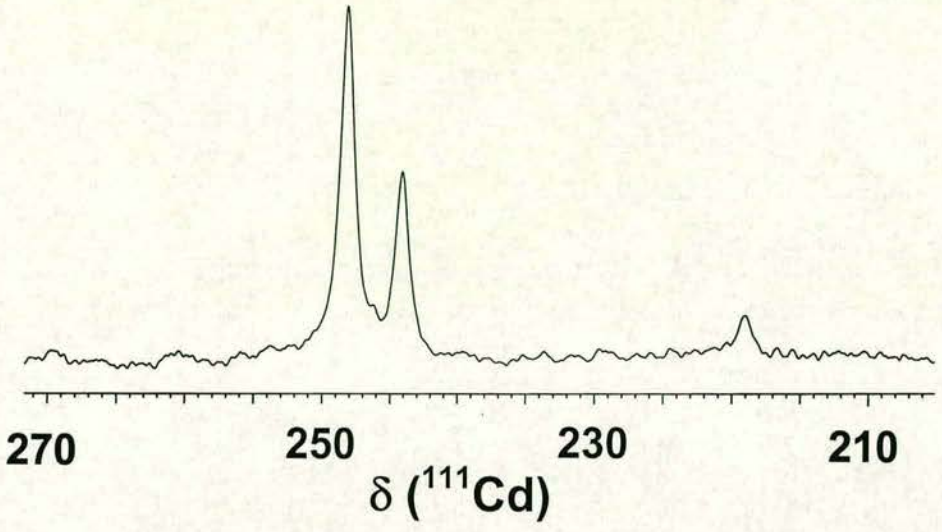

Figure 4.5 1D ^{111}Cd-{^{1}H} NMR spectrum of ^{111}Cd-labelled **1** in 10% D_2O/90% H_2O.

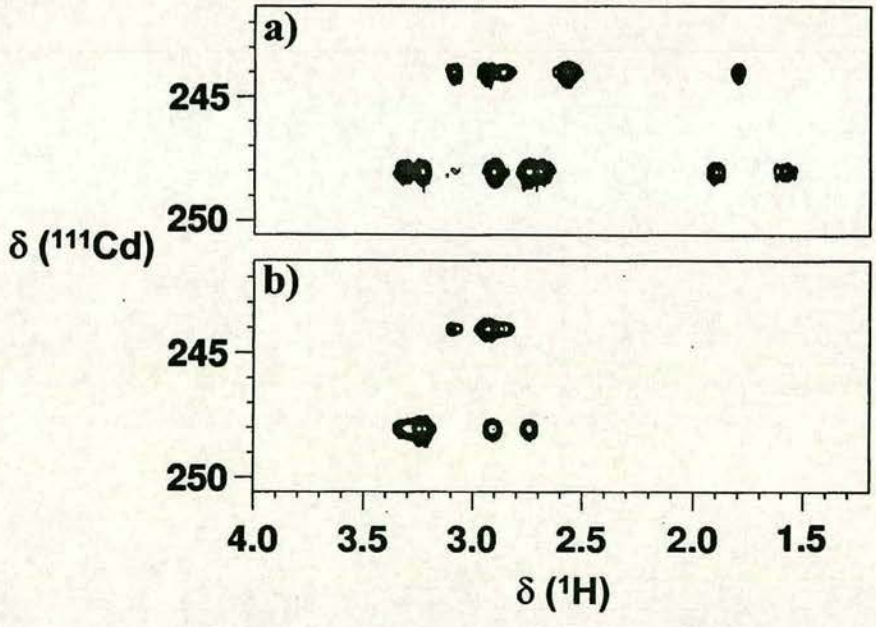

Figure 4.6 (a) 2D [^{1}H, ^{111}Cd] HSQC-TOCSY spectrum of ^{111}Cd-labelled **1**. (b) 2D [^{1}H, ^{111}Cd] HSQC NMR spectrum of ^{111}Cd-labelled **1**. Connectivities to the minor ^{111}Cd resonance at 219 ppm (not shown) are very weak. All samples were dissolved in 10% D_2O / 90% H_2O.

Table 4.2 ^{1}H NMR chemical shifts (δ) for complexes **1**, **2** and **3** in various solvents

complex	solvent	config		δ, assignment						
				NCH_2CH_2N		$NCH_2CH_2CH_2N$		$NCH_2CH_2CH_2N$		NH
1	D_2O/H_2O	*Trans*-I	^{1}H	2.91	2.75	3.23	2.69	1.90	1.59	3.31
			^{13}C	49.73		54.53		31.12		
			^{15}N							11.91
			^{111}Cd			248				
		Cis-V	^{1}H	2.94	2.58	3.09	2.86	1.81		a
			^{13}C	49.08		52.29		27.68		
			^{111}Cd			244				
2	D_2O/H_2O	*Trans*-I	^{1}H	2.91	2.77	3.23	2.72	1.91	1.62	3.48
			^{13}C	49.69		54.43		31.05		
			^{15}N							11.72
		Cis-V	^{1}H	2.93	2.62	3.07	2.86	1.80		a
			^{13}C	49.65		51.95		27.52		
3	CD_3CN	*Trans*-I	^{1}H	3.02	2.84	3.34	2.79	1.96	1.74	2.92

[a] Not observed, presumably broadened by exchange with solvent.

spin system $\mathbf{H_a}$-$\mathbf{H_f}$, and **V**: δ ^{111}Cd 244, ^{1}H spin system $\mathbf{H_1}$-$\mathbf{H_5}$, Figure 4.2; Table 4.2) are present in aqueous solution.

The 2D [^{1}H, ^{13}C] HSQC NMR spectrum also reflects this, showing cross-peaks corresponding to the eleven ^{1}H NMR signals described above and six ^{13}C NMR signals (Figure 4.7; Table 4.2). Geminal pairs of protons were identified thus: for

configuration **I**, $\mathbf{H_a/H_b}$ (δ ^{13}C 31.12), $\mathbf{H_c/H_f}$ (δ ^{13}C 54.53), $\mathbf{H_d/H_e}$ (δ ^{13}C 49.73) and for configuration **V**, $\mathbf{H_2/H_4}$ (δ ^{13}C 49.08), $\mathbf{H_3/H_5}$ (δ ^{13}C 52.29). Since all protons except **NH** belong to geminal pairs in this complex, the remaining cross-peak for configuration **I**, $\mathbf{H_1}$ (δ ^{1}H/^{13}C 1.81/27.68), corresponds to two equivalent protons.

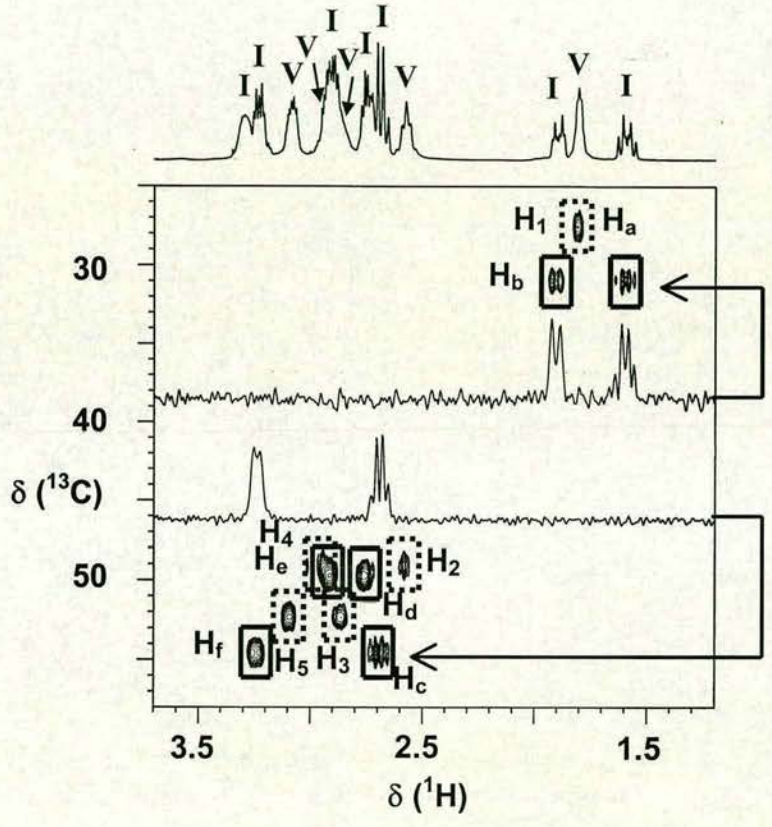

Figure 4.7 2D [^{1}H, ^{13}C] HSQC NMR spectrum of complex **1** in 10% D_2O / 90% H_2O. Resonances (H_a to H_f) for the *trans*-I configuration are designated by solid boxes and resonances (H_1 to H_5) for *cis*-V configuration are designated by dashed boxes. 1D slices are shown for the two ^{13}C shifts of the 6-membered rings (N***CH$_2$CH$_2$CH$_2$***N).

4. 3. 3 Titration of Cd(cyclam)$(ClO_4)_2$ (1) with $^{13}CO_3^{2-}$

In a separate series of NMR experiments, the perchlorate complex **1** was added to a solution of 40 mM $Na_2{}^{13}CO_3$ in 10% D_2O/ 90% H_2O at pH 11. This pH value was chosen because the complex exists predominantly as a single configuration at this pH (*trans*-I, see Discussion) and carbonate is fully deprotonated (pK_1, 10.29; pK_2, 6.35)[16]. Ten separate additions of **1** were made to the $Na_2{}^{13}CO_3$ solution to give $Na_2{}^{13}CO_3$:**1** molar ratios from 1:0.2 to 1:3.5. The solution was re-adjusted to pH 11 using 0.1 M NaOH after every addition of the complex.

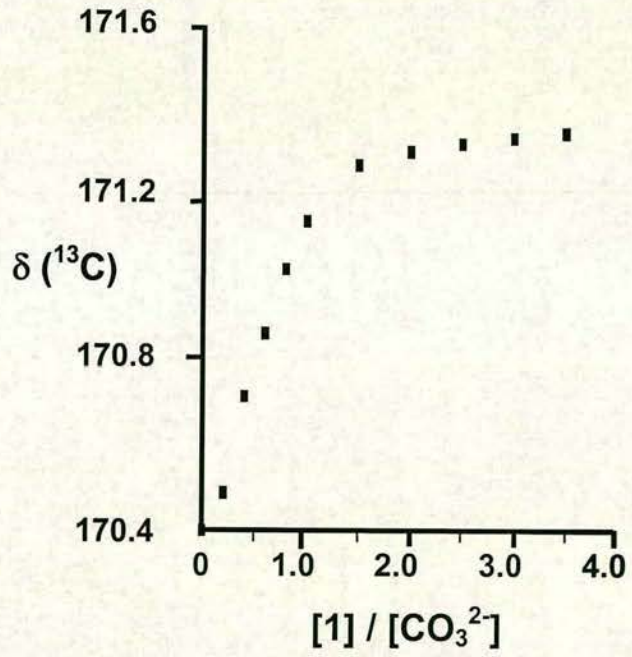

Figure 4.8 Plot of ^{13}C chemical shift of $^{13}CO_3^{2-}$ versus the molar ratio of **1** : $Na_2{}^{13}CO_3$ at pH 11.

Addition of aliquots of **1** to $^{13}CO_3^{2-}$ resulted in a gradual shift of the ^{13}C resonance of $^{13}CO_3^{2-}$ from 170.4 to 171.33 ppm with an apparent end point at a 1:1 mol ratio (Figure 4.8).

In a reverse titration, ^1H NMR spectra of **1** were acquired in the presence of increasing quantities of Na_2CO_3 at pH 9 to give **1**:Na_2CO_3 molar ratios of 1:0.5, 1:1, 1:2, 1:4. The **NH** resonance for **1** in the absence of Na_2CO_3 appeared at 3.31 ppm. With increasing concentrations of CO_3^{2-}, the **NH** resonance gradually shifted to lower frequency, reaching an apparent end-point at a 1:1 molar ratio (Figures 4.9 and 4.10).

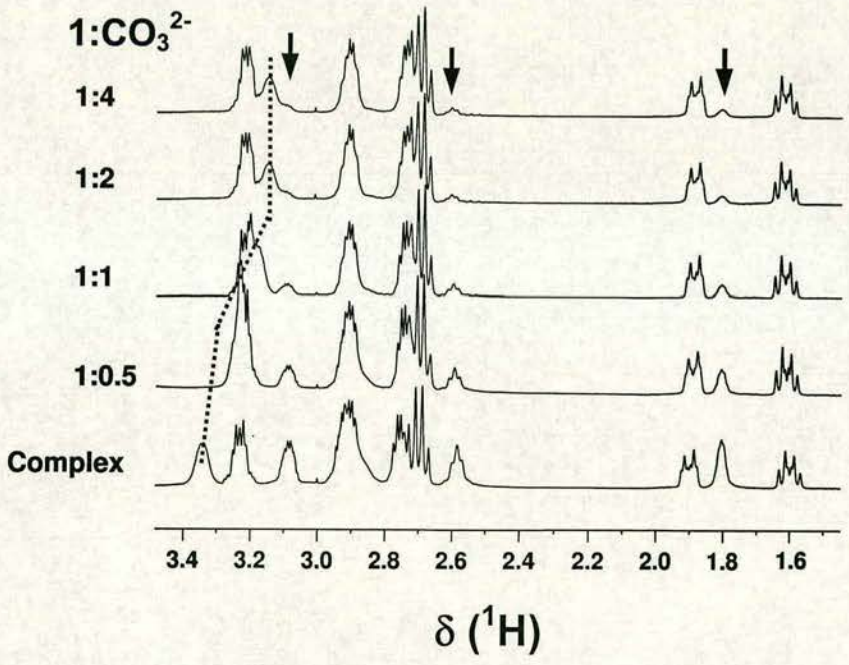

Figure 4.9 ^1H NMR spectrum of complex **1** and after addition of Na_2CO_3 in 10% D_2O / 90% H_2O, pH 9.

The reduction in the intensity of the ^1H NMR signals $\mathbf{H_1}$-$\mathbf{H_5}$ with simultaneous growth of signals $\mathbf{H_a}$-$\mathbf{H_f}$ showed that configuration **V** converts almost entirely to

configuration **I** under these conditions (Figure 4.9). Although the ratio of configurations is strongly pH dependent, this effect appears to be due to the presence of Na_2CO_3 given that the solution was re-adjusted to pH 9.

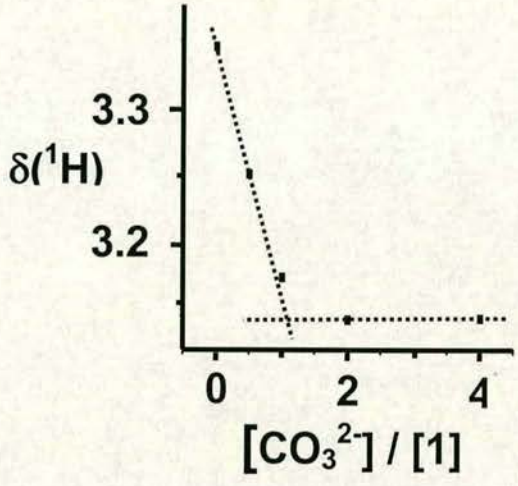

Figure 4.10 Plot of NH ^{1}H NMR chemical shift versus the molar ratio of Na_2CO_3 **: 1**.

4. 3. 4 Effect of pH on Cd(cyclam)$(ClO_4)_2$ (1) studied by ^{1}H NMR

The ^{1}H NMR spectrum of the perchlorate complex **1** in 10% D_2O / 90% H_2O was strongly pH-dependent (Figure 4.11). Only three sharp ^{1}H NMR peaks (3.11, 3.02 and 1.90 ppm) were observed at pH 5.3, corresponding to the free ligand at this pH. No free ligand was observed at pH > 8.2, and at pH 12.1, integration showed that 94% of complex **1** existed in configuration **I** and 6% as configuration **V**. As the pH was lowered from 12.1, free ligand peaks appeared at pH 8.2, and at this pH

accounted for 6% of the total cyclam, with the proportion of configuration **V** increasing to 39%. The process was reversible with lowering or raising pH.

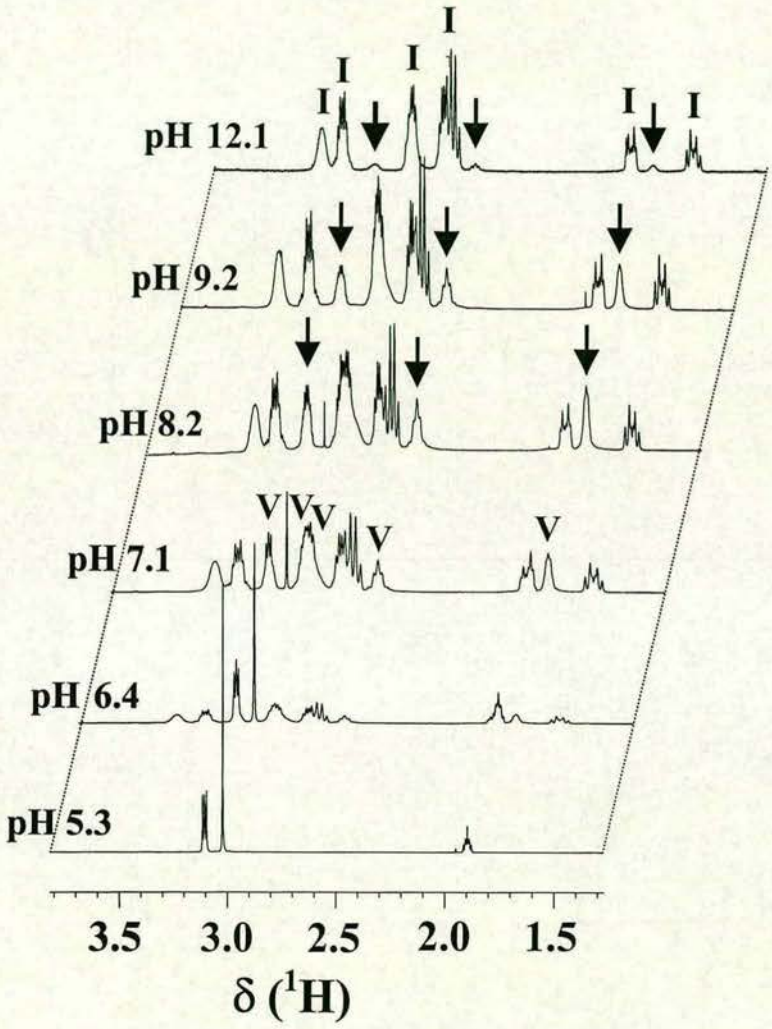

Figure 4.11 pH dependence of the ^{1}H NMR spectrum of **1** in 10% D_2O / 10% H_2O. At pH 5.3 only free cyclam is present. Peaks for configuration **V** diminish as the pH increases and configuration **I** is predominant.

4. 3. 5 NMR analysis of $[Cd_3(cyclam)_3(CO_3)](ClO_4)_4 \cdot 3H_2O$ (3) in solution

The solution configuration of **3** was studied in CD_3CN as solvent. Some organic solvents have been successfully used previously in circumstances where it was desirable to retain CO_3^{2-} bound to a complex in solution.[17] The ^1H NMR spectrum of **3** was acquired immediately after dissolving crystals in acetonitrile (Figure 4.12). The 1D ^1H NMR spectrum is similar to that of **1** in H_2O but consists of

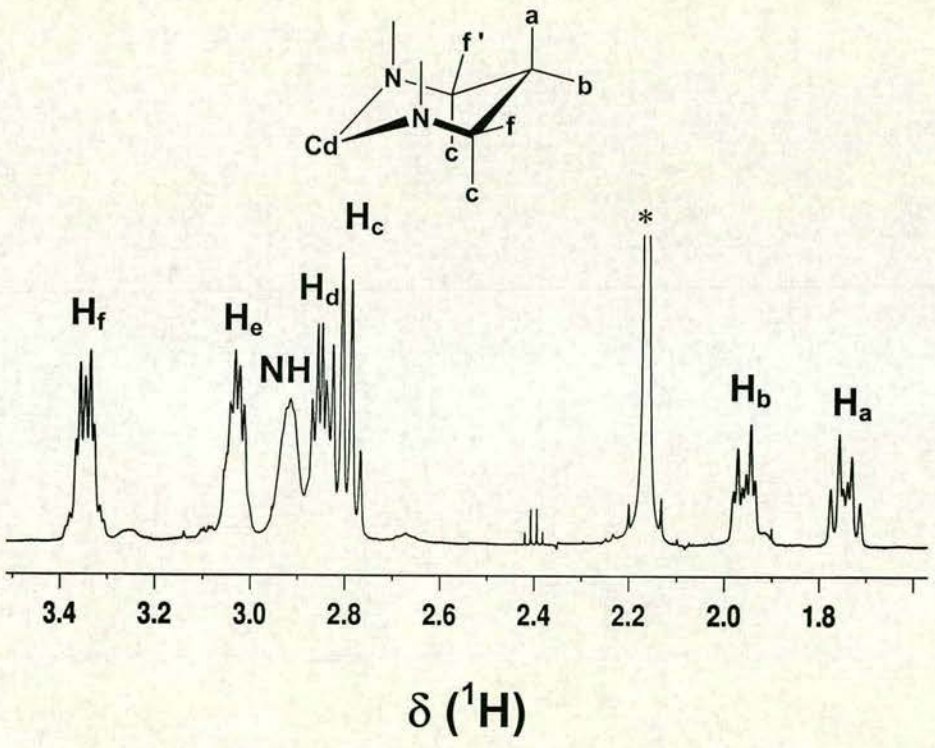

Figure 4.12 ^1H NMR spectrum of complex **3** in CD_3CN and the labelling scheme for protons in the 6-membered ring (chair conformation). * = CHD_2CN.

only a single set of resonances. 2D [^{1}H, ^{1}H] COSY NMR data revealed the presence of three spin-systems (Figure 4.13). Within the first spin-system, resonance **a** (1.74 ppm) couples to **b** (1.96 ppm) and to **c** (2.79 ppm) and weakly to **f** (3.34 ppm). Resonance **b** couples strongly to **f** and weakly to **c**. In the second spin-system, **d** (2.84 ppm) couples to **e** (3.02 ppm). The last spin-system is composed of three minor peaks corresponding to the free cyclam ligand (**m**, **n** and **o**: 3.20, 3.13, 1.99 ppm, respectively). Subsequent ^{1}H NMR spectra acquired on the same sample at later times showed that the signals **m** to **o** had increased in intensity, indicating the release of free ligand with time. Minor cross-peaks were also observed, and may arise from a second species.

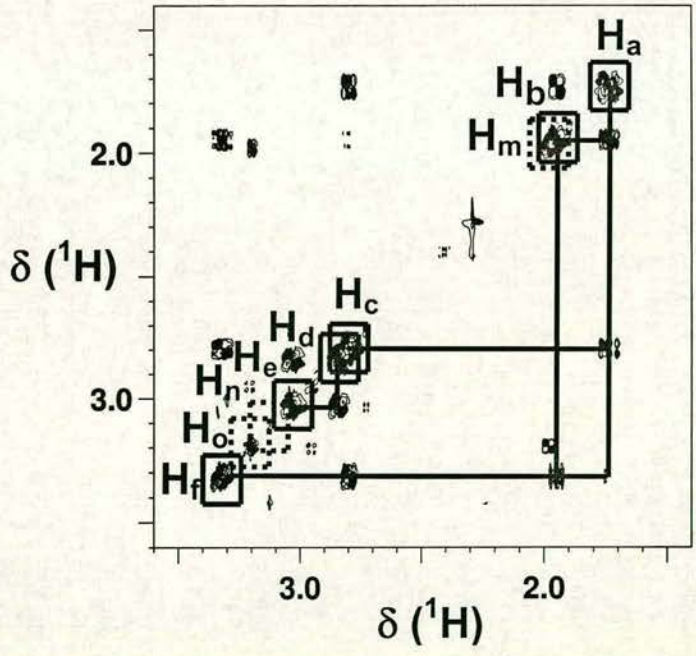

Figure 4.13 2D [^{1}H, ^{1}H] COSY NMR spectrum of **3** in CD_3CN. Resonances for the *trans*-I configuration are designated by solid boxes and resonances for the free ligand are designated by dashed boxes. For peak labels and assignments see Figure 4.12.

High resolution, first-order resonances for H_a and H_b allowed direct measurement of coupling constants and the spectrum was also simulated. The ^1H NMR resonance for H_a consists of a doublet of triplet of triplets (Figure 4.14d), the result of coupling to H_b, H_c, and H_d with coupling constants of 16.3, 11.1, and 1.6 Hz,

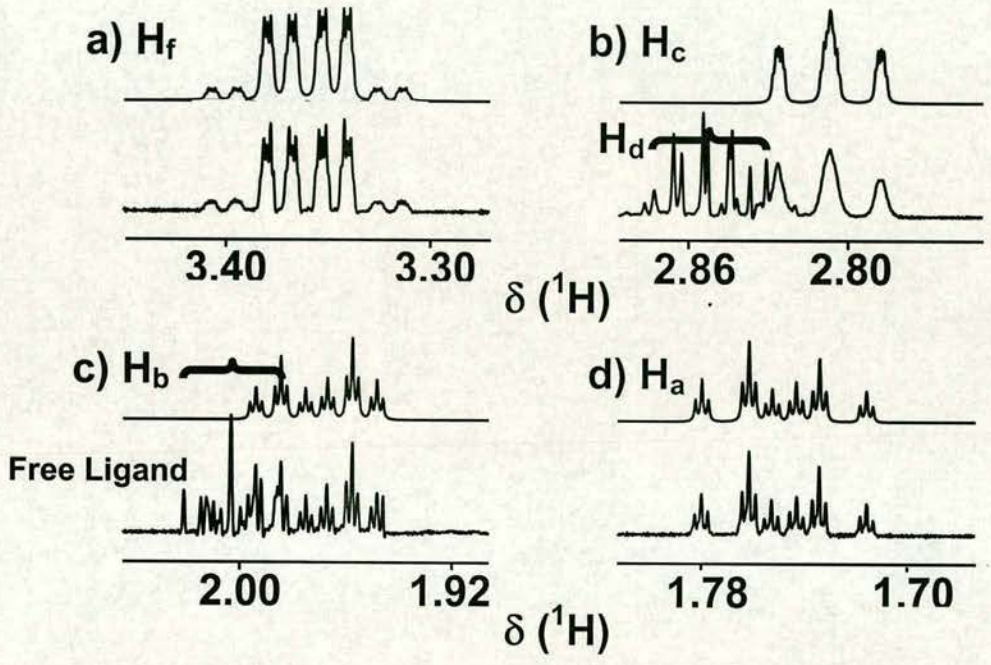

Figure 4.14 Experimental (bottom) and simulated ^1H NMR for the 6-membered ring of complex **3**. a) H_f in the presence of ^{111}Cd at natural abundance; b) H_c (resonance H_d is included in the experimental data, but was not included in the simulation); c) H_b – the resonance for $CH_2\underline{\boldsymbol{CH_2}}CH_2$ of the free ligand is overlapped with H_b in this region; d) H_a. Coupling constants derived from the simulation are shown in Tables 4.3 and 4.4. The value of $^3J(^{111}Cd\text{-}H_f)$ = 25 Hz is comparable with the experimental value of 29 Hz measured from a 2D [^1H, ^{13}C] HSQC NMR spectrum with natural abundance ^{13}C but with 95.29% ^{111}Cd.

respectively. The H_b ^1H NMR resonance is also a doublet of triplet of triplets (Figure 4.14c), the result of coupling to H_a, H_c, and H_d with coupling constants of 16.3, 5.7, and 1.4 Hz, respectively.

4. 3. 6 Solution NMR studies of Cd(cyclam)Cl_2 (2)

^1H, ^{13}C and ^{15}N NMR data were also acquired for the chloride complex **2** in 10% D_2O / 90% H_2O (Figures 4.15 and 4.4a). The NMR data are summarised in Table 4.2.

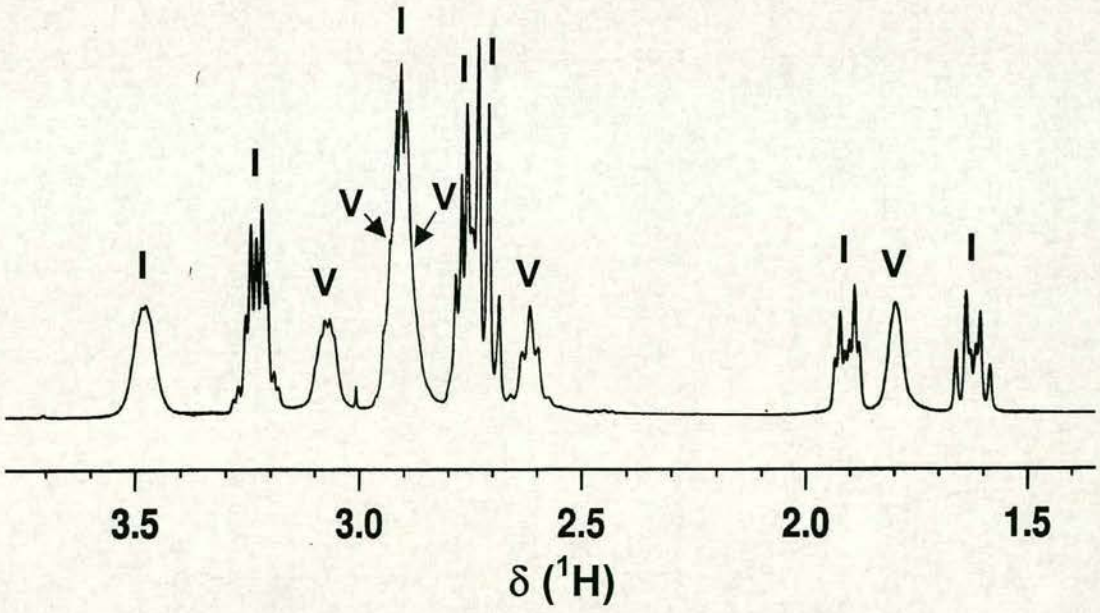

Figure 4.15 ^1H NMR spectrum of complex **2** in 10% D_2O/90% H_2O. Resonances assigned to the *trans*-I configuration are designated **I** and resonances for *cis*-V configuration are designated **V**. For assignments see Table 4.2.

4. 3. 7 Conformational analysis of $Cd(cyclam)(ClO_4)_2$ (1) and $[Cd_3(cyclam)_3(CO_3)](ClO_4)_4 \cdot 3H_2O$ (3)

For **3**, ^3J (^{1}H, ^{1}H) coupling constants were derived from spin system simulations for signals **a**, **b**, **c** and **f** (Figure 4.14; Table 4.3). For ^{111}Cd-**1**, a fully ^{111}Cd-coupled [^{1}H, ^{1}H]-2D TOCSY NMR spectrum was used to measure ^3J(^{1}H, ^{111}Cd) coupling constants (Table 4.4).

Extension of the standard Karplus equation[18] by Haasnoot[19] has permitted broader applications. The H-C-C-H fragment in the rings under study carries two non-hydrogen substituents. In this case, the generalised Karplus equation takes the form shown in eq 1,

$$^3J(^1H, ^1H) = 13.89\cos^2\phi_{HH} - 0.98\cos\phi_{HH} + \sum\Delta\chi_i\{1.02 - 3.4\cos^2(\zeta_i\phi + 14.9|\Delta\chi_i|)\} \quad (1)$$

in which ϕ_{HH} is the Klyne-Prelog defined[20] proton-proton torsion angle and $\Delta\chi_i$ denotes the differences in electronegativity between the substituent S_i and hydrogen on the Huggin's scale[21] corrected for the influence of β substituents[19]; ζ_i takes on a value of +1 or –1 according to the orientation of the substituent S_i with respect to the coupling proton on the same carbon atom.[19]

The only reported Karplus–type correlation for ^3J(^{1}H,^{113}Cd) coupling constants appears to be that established for cysteine C^β protons and H^β- C^β- S^γ- Cd dihedral angles.[5] This takes the form shown in eq 2.

$$^3J(^{113}Cd, ^1H) = 36\cos^2\phi - 13\cos\phi + 1 \quad (2)$$

Table 4.3 ^3J and ^2J (^1H, ^1H) coupling constants (Hz) and corresponding torsion angles (°) for the six-membered rings of complex **3**

	$^3J(H_a, H_c)$	$^3J(H_a, H_f)$	$^3J(H_b, H_c)$	$^3J(H_b, H_f)$	$^2J(H_a, H_b)$	$^2J(H_c, H_f)$
simulated	11.0	1.5	1.3	5.7	16.3	12.6
measured	11.1	1.6	1.4	5.7	16.3	
Torsion angles (NMR)[a]	164	69	81	39		
Torsion angles (X-ray)[b]	164	78	81	37		

[a] Torsion angles were calculated using the expression $^3J(^1H, ^1H) = 13.89\cos^2\phi_{HH} - 0.98\cos\phi_{HH} + \sum\Delta\chi_i\{1.02 - 3.4\cos^2(\zeta_i\phi + 14.9|\Delta\chi_i|)\}$; $\Delta\chi_i$ takes the values 0.97 and 0.196 for C_1 and C_2 respectively; $\zeta_i = \pm 1$ according to the definition of position and negative substituents.[20]

[b] Torsion angles in the X-ray crystal structure of **3**.

Table 4.4 ^3J (^{111}Cd, ^1H) coupling constants (Hz) and corresponding torsion angles (°) for **3**

	Six-membered ring		Five-membered ring	
	$^3J(H_c, ^{111}Cd)$	$^3J(H_f, ^{111}Cd)$	$^3J(H_d, ^{111}Cd)$	$^3J(H_e, ^{111}Cd)$
Coupling constant (measured)	1.6	27.4	14.0	15.3
Torsion angle (NMR)[a]	66	134	115	118
Torsion angle (measured)[b]	65	177	121	123

[a] Calculated using the expression $^3J(^{111}Cd, ^1H) = 36\cos^2\phi - 13\cos\phi + 1$.[5]

[b] Torsion angles measured from a model for *trans*-I based on *cis*-V in the crystal structure of **3**.

The coupling constants $^3J(^{111}Cd, ^1H)$ for ^{111}Cd labelled **1** and $^3J(^1H, ^1H)$ for **3** were used to calculate torsion angles based on eqs 1 and 2. Calculated torsion angles and experimentally-measured coupling constants are listed in Tables 4.3 and 4.4.

4. 3. 8 X-ray crystal structure of Cd cyclam complex with carbonate, $[Cd_3(cyclam)_3(CO_3)](ClO_4)_4 \cdot 3H_2O$ (3)

Complex of **3** contains carbonate fixed from atmospheric CO_2. The crystal structure of the cation is shown in Figure 4.16 together with the atomic numbering scheme, and is illustrated schematically in Figure 4.17a. Selected bond lengths and angles are listed in Table 4.5. The complex contains three independent $[Cd(cyclam)]^{2+}$ units. Each unit has a distorted octahedral geometry of the *cis*-CdO_2N_4 type. Each Cd ion is bound to four nitrogens of cyclam with bond lengths for Cd(1)-N(1), Cd(1)-N(4), Cd(1)-N(8), Cd(1)-N(11) of 2.323(12) Å, 2.270(12) Å, 2.289(12) Å and 2.311(12) Å, respectively. Two oxygens of the carbonate anion occupy axial positions with Cd-O bond lengths of 2.373 and 2.412 Å. Pairwise bidentate combinations of the three carbonate oxygens join the three Cd(cyclam) units to form a C_3 symmetric arrangement. In each unit, due to the *cis* coordination of carbonate, cyclam is folded. The configuration of each cyclam unit is *cis*-I (*R,S,R,S*; Figure 1.3).

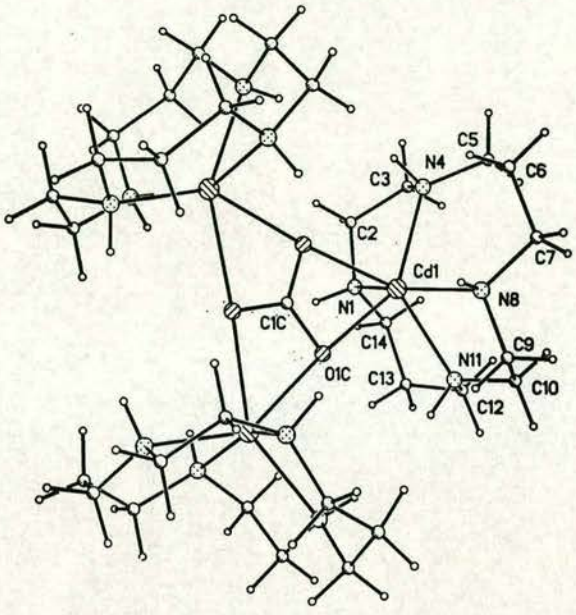

Figure 4.16 X-ray crystal structure of the cation of complex **3** together with the atom numbering scheme.

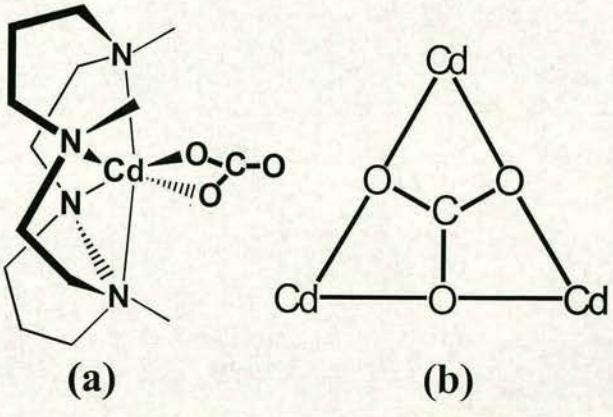

Figure 4.17 Schematic illustrations of (a) the *cis*-I configuration, and (b) the mode of carbonate coordination, in the crystal structure of **3**.

Table 4.5 Selected bond distances (Å) and angles (°) for **3**

Cd(1) – N(4)	2.270(12)
Cd(1) – N(11)	2.311(12)
Cd(1) – O(1C)	2.373(7)
Cd(1) – N(8)	2.289(12)
Cd(1) – N(1)	2.323(12)
Cd(1) – O(1C)#1	2.412(7)
N(4) – Cd(1) – N(11)	124.5(4)
N(4) – Cd(1) – N(1)	79.9(5)
N(11) – Cd(1) – N(1)	89.7(5)
N(8) – Cd(1) – N(11)	77.3(5)
N(8) – Cd(1) – N(1)	156.7(4)

(#1 –x+y, -x, z)

4. 4 Discussion

4. 4. 1 IR spectroscopy

The ν_3 vibration appears strongly at 1415 cm^{-1} for free CO_3^{2-} with D_{3h} symmetry.[22] In most carbonato complexes, it splits into two bands due to loss of the symmetry.[22,23] However, in the present case, the coordinated CO_3^{2-} in $[Cd_3(cyclam)_3(CO_3)](ClO_4)_4 \cdot 3H_2O$ has high symmetry and therefore, only a single ν_3 band appears at 1451 cm^{-1} without split. This confirms the bridging bidentate CO_3^{2-} coordination mode.

4. 4. 2 Solution NMR analysis of Cd(cyclam)$(ClO_4)_2$ (1)

Analysis of the proton connectivities in the 2D [^{1}H, ^{1}H] COSY (Figure 4.2) and TOCSY (Figure 4.3) NMR spectra and the $^1H/^{13}C$ connectivities in the 2D [^{1}H, ^{13}C] HSQC NMR spectrum of the perchlorate complex **1** show that the ^{13}C NMR resonances at 31.12, 49.73 and 54.53 ppm are due to form **I** of the cyclam ligand and

those at 27.68, 49.08 and 52.29 ppm are due to ligand form **V**. The former three ^{13}C NMR resonances from **I** correlate with six ^{1}H NMR signals. The ^{13}C NMR resonance at 31.12 ppm correlates with two ^{1}H NMR peaks at 1.59 and 1.90 ppm, which are assignable on the basis of chemical shifts to the central methylene protons in the six-membered Cd-cyclam rings. The latter three ^{13}C NMR signals from **V** correlate with five ^{1}H NMR resonances and the ^{13}C NMR signal at 27.68 ppm correlates with only one ^{1}H NMR resonance at 1.81 ppm. This is also assigned to the central methylene of the six-membered ring on the basis of chemical shift. Only the *trans*-I and *trans*-III configurations can give rise to six non-equivalent proton resonances, two of which correspond to the central methylene of the six-membered rings. Both six-membered rings adopt chair conformations in the *trans*-I and *trans*-III configurations in which H_a and H_b are nonequivalent and give rise to two ^{1}H NMR resonances, respectively (see **A** in Figure 4.18). Since the *trans*-I configuration is considered to be the best fit for larger metal ions (see below Discussion), species **I** is likely to correspond to the *trans*-I configuration. The *trans*-IV and *trans*-V configurations have five non-equivalent protons and give rise to five proton resonances, one of which corresponds to the central methylene protons

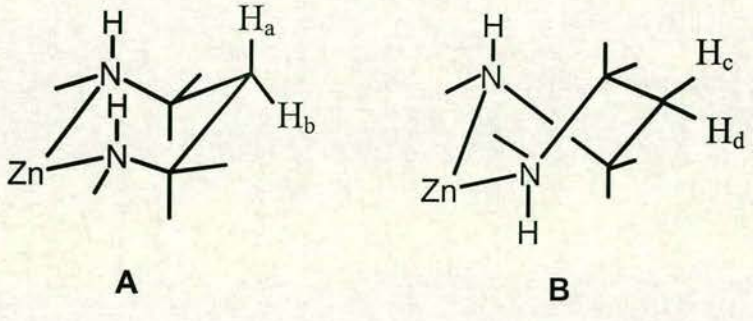

Figure 4.18 A chair and **B** twist-boat conformations for the six-membered rings

of the six-membered rings. Both six-membered rings adopt twist-boat conformations in the *trans*-IV and *trans*-V configurations in which H_c and H_d are equivalent and give rise to only one ^1H NMR resonance (see **B** in Figure 4.18). The *cis*-V configuration is strain-free and can exist as two equivalent states in fast exchange on the NMR timescale with averaging of the ^1H chemical shifts for the central methylene group. Therefore, the species **V** can be assigned as the *cis*-V configuration.

Further information about the configurations of the five- and six-membered rings of complex **1** in solution was obtained from the $^3J(^1H, ^{111}Cd)$ couplings. For the six-membered rings, the large difference between two $^3J(^1H, ^{111}Cd)$ couplings (27.4 Hz, torsion angle $^{111}Cd\text{-}N\text{-}C\text{-}H_f$, and 1.6 Hz, torsion angle $^{111}Cd\text{-}N\text{-}C\text{-}H_c$) results from H_c being axial and H_f being equatorial in a 6-membered ring with a chair conformation. Based on eq 2, the torsion angles $^{111}Cd\text{-}N\text{-}C\text{-}^1H_f$ and $^{111}Cd\text{-}N\text{-}C\text{-}^1H_c$ were calculated to be 134° and 66°, respectively (Table 4.4). The latter value is similar to that determined from both the crystal structure (*cis*-I configuration) and from a model (*trans*-I configuration), but the former value deviates from the expected value of 180° by *ca.* 45°. This is probably because eq 2 was established on the basis of Cd-S-C-H spin systems in proteins[5] and requires modification for our Cd-N-C-H system in the region 120° to 180°. Unfortunately, too few data are available to establish a new equation for Cd-N-C-H systems. The $^3J(H_d, ^{111}Cd)$ and $^3J(H_e, ^{111}Cd)$ couplings are very similar (14.0 and 15.3 Hz, respectively) indicating that the 5-membered ring is either in rapid equilibrium between two gauche configurations or adopts the eclipsed conformation. In either case the solution conformation of **3** differs significantly from that in the crystal.

The best-fit M-N bond length for metal coordination to cyclam is 2.06 Å.[10] Such a distance corresponds to a metal with an ionic radius of *ca.* 0.65-0.7 Å.[10] Due to the flexibility of the cyclam ring, smaller metal ions (ionic radius < 0.75 Å - mainly those of the first row transition metal series) ensure that the cyclam ring adopts the most stable configuration, *trans*-III.[24] With increasing ionic radius, metal ions no longer fit the cyclam cavity well. For example, the Hg(II) (1.10 Å) cyclam exists in the *trans*-I configuration in which the metal lies above the cyclam plane,[10] and Pb(II) (1.21 Å) cyclam adopts a *cis*-V configuration.[25] On this basis it is likely that Cd(II) (0.97 Å) cyclam adopts the *trans*-I rather than *trans*-III configuration. The crystal structure of **3** shows that cadmium cyclam can also adopt the *cis*-I configuration when an additional chelating ligand is bound.

In the *trans*-IV and *trans*-V configurations, due to conformational constraints of the macrocycle, both six-membered rings adopt skew-boat conformations in which the central methylene has two equivalent hydrogens (see Figures 1.3 and Figure 4.18). Possessing higher energy, the skew-boat conformation is not stable. The *trans*-V configuration can fold about the diagonals a or b (Chart 4.1) to form the more common *cis*-V configuration in which case the 6-membered-rings exist in chair conformation and 5-membered-rings in gauche conformation. The two forms represented in Figure 1.3 can inter-convert. The rapid inter-conversion gives rise to the averaging of these conformation. Such rapid inter-conversion on the NMR timescale have been observed for a number of nickel (II) complexes.[26] We did not observe an N<u>H</u> NMR signal for the *cis*-V configuration, which may be related either to the inter-conversion process or to fast exchange with the solvent.

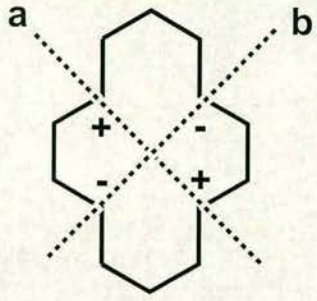

Chart 4.1 The folding of the *trans*-V configuration along axes a or b to give the c*is*-V configuration is shown (+ indicates NH proton above the cyclam plane, – below).

From ^{13}C NMR titrations of $^{13}CO_3^{2-}$ with **1** (Figure 4.8) and ^{1}H NMR in the reverse titration (Figures 4.9 and 4.10), it can be concluded that carbonate coordinates to Cd(II) cyclam in aqueous solution. It appears that a 1:1 pyramidal complex [Cd(cyclam)CO_3] is formed with an axially coordinated carbonate anion and cyclam in the *trans*-I configuration.

4.4.3 Effect of pH on Cd(cyclam)$(ClO_4)_2$ (1)

Complex **1** is stable only at high pH. At pH < 8.2 dissociation of Cd(II) from cyclam was observed. Free ligand began to appear at pH 8.2 and the complex had dissociated completely by pH 5.3. The *cis*-V configuration converts to *trans*-I with increasing pH and *trans*-I dominates at highly basic pH. This process is reversible. A number of Cu(II), Zn(II), and Cd(II) macrocyclic complexes can readily form the CO_3^{2-} complexes from fixing the atmospheric CO_2.[9,27,28] The mechanism for the formation of the carbonate complexes is as follows: the complexes can form L-M-OH^- species at alkaline pH and the hydroxo complexes have a great affinity for

atmospheric CO_2 to produce a hydrogen carbonate complex which can further react to form a trinuclear complex.[28] The isomerisation from *cis*-V to *trans*-I needs to convert the nitrogen configurations twice via *trans*-II. The intermediate hydroxo complex, cyclam-Cd-OH^- in this case probably adopts *trans*-II configuration. The formation of *trans*-II from *cis*-V configuration are base-catalysed.[29] The *trans*-II configuration for cyclam-Cd-OH^- continues to convert to *trans*-I and may be base-catalysed as well. Therefore, the configurational inversion from *cis*-V to *trans*-I is very fast and no distribution change for each configuration was observed at any pH.

4. 4. 4 NMR analysis of $[Cd_3(cyclam)_3(CO_3)](ClO_4)_4 \cdot 3H_2O$ (3) in solution

The exchange behaviour of the NH resonance at 2.92 ppm and the appearance of three resonances from the free ligand indicates that this cadmium complex is unstable in CD_3CN. Two ^1H NMR spin-systems exist for this complex in solution and can be assigned as follows: the first with resonances centred at 1.74, 1.96, 2.79 and 3.34 ppm, corresponds to the six-membered rings, and the second with resonances centred at 2.84 and 3.02 ppm, corresponds to the five-membered rings (Figure 4.13). The multiplets at 1.74 and 1.96 ppm are assigned, on the basis of splitting patterns and chemical shifts, to the central methylene protons in the six-membered rings, namely H_a and H_b (Figure 4.14c/d). For H_a, the largest coupling constant 16.3 Hz can be deduced to result from a geminal coupling, while 11.1 and 1.6 Hz can be deduced to be vicinal couplings. The large coupling of 11.1 Hz ($^3J_{HaHc}$) indicates a trans-diaxial relationship between H_a and H_c. The H_b ^1H NMR resonance is also a doublet

of triplet of triplets (Figure 4.14c), the result of coupling to H_a, H_c, and H_d with coupling constants of 16.3, 5.7, and 1.4 Hz, respectively. The largest splitting also results from a geminal coupling and the absence of other large splittings indicates that H_b and H_d bear an equatorial relationship to one another. These observations are consistent with a six-membered ring in the chair conformation. However, in the crystal structure the ligand is folded into a *cis*-I geometry. It therefore seems likely that the weaker Cd-O bond between carbonate and each monocyclam unit breaks and carbonate becomes a μ_3-CO_3^{2-} bridged unit binding to three Cd(II) ions through each of three O atoms, as is typical of Zn(II) complexes with macrocyclic polyamines (e.g cyclen).[30] Each monocyclam unit of **3** adopts the *trans*-I configuration in CD_3CN.

The torsion angles for the six-membered rings of **3** in CD_3CN determined from ^1H NMR data are close to those found in the crystal structure (Table 4.3). The six-membered rings therefore adopt a chair-conformation. In the crystal structure, the five-membered rings adopt the gauche-conformation, but the NMR data for **3** in solution indicate an eclipsed conformation for these rings. This can be explained in one of two ways. Either the five-membered rings exercise pseudo-rotational mobility and average their couplings, giving the appearance of an eclipsed conformation, or the five-membered rings are locked in an eclipsed conformation in the same way as the six-membered rings.

4. 4. 5 Crystal structure of $[Cd_3(cyclam)_3(CO_3)](ClO_4)_4 \cdot 3H_2O$ (3)

Carbonate can adopt a variety of different coordination modes, as summarised by Einstein and Willis.[31] Complex **3** and the trinuclear Gd(III) complex, $Na_2[\{Gd(DO3A)\}_3CO_3]$ (DO3A = 1, 4, 7-tri(carboxymethyl)-1, 4, 7, 10-

tetraazacyclododecane), contain carbonate bound in a bidentate mode to each of three metal ions which form an equilateral triangle as shown in Figure 4.17b.[32]

The very sharp bite angle O(1)-Cd-O(2) of 55.5(4)° for complex **3** is similar to that for $[Cd(O_2COH)(Me_4[14]aneN_4)](ClO_4)$ (54.2°).[9] The angle N(4)-Cd-N(11) (124.5(4)°) is closer to the 120° value expected for a trigonal bipyramidal structure than that for the hydrogencarbonate complex (128.9°).[9] The other N - Cd - N angles are normal and lie in the range 77-90°, because the rigidity of the macrocycle causes narrow bite angles for the five-membered chelate rings. Complex **3** may be considered as trigonal bipyramidal with the two donor oxygen atoms occupying an apex of the in-plane triangle.

$Na_2[\{Gd(DO3A)\}_3CO_3]$ differs from complex **3** in that Gd(III) is coordinated to each oxygen of the three carboxylate arms in the N-substituted cyclen in addition to four nitrogens and two carbonate oxygens. A recent survey of the Cambridge Structural Database indicated that complex **3** is the only known crystal structure of a cadmium complex containing unsubstituted cyclam, and the only known crystal structure of an unsubstituted cyclam complex with a *cis*-I configuration.

4.5 Conclusions

I have synthesised cadmium cyclam complexes with perchlorate (**1**), chloride (**2**) or carbonate (**3**) and have made the first detailed analysis of the solution configurations of Cd(II) cyclam in solution using NMR spectroscopy. Assignments of ^{1}H, ^{13}C, ^{15}N and ^{111}Cd NMR signals were made for aqueous or CD_3CN solutions using 1D and 2D methods. Complexes **1** and **2** both exist as equilibrium mixtures of *cis*-V and *trans*-I configurations in aqueous solution which were stable only at high

pH. As the pH was decreased below 8.2, dissociation of free ligand was observed, and the complexes were dissociated completely at pH 5.3. $^{111/113}$Cd-^{1}H coupling constants were used to derive Karplus-type conformational information about the chelate rings. The only previous application of this procedure appears to be that for Cd thiolate proteins.[5] In the *trans*-I configuration, the $^{3}J(^{111}\text{Cd}, ^{1}\text{H})$ coupling constants for the two different five-membered rings in ^{111}Cd-labelled **1** in aqueous solution were similar (14.0 and 15.3 Hz) consistent with eclipsed conformations. This contrasts with the diverse $^{3}J(^{111}\text{Cd}, ^{1}\text{H})$ coupling constants (1.6 and 27.4 Hz) associated with the six-membered rings of the *trans*-I configuration which adopt chair conformations. Exposure of complex **1** to the atmosphere led to formation of the novel carbonate-bridged tri-cadmium complex **3** in which cyclam adopts the unusual *cis*-I configuration with all the N-H bonds oriented in the same direction. NMR data show that complex **3** in CD_3CN exists as only one species, the *trans*-I configuration, with eclipsed conformations for the five-membered rings. The torsion angles calculated using an extension of the standard Karplus relation indicate that the six-membered rings adopt conformations in solution close to those in the crystal structure (chair conformations).

These studies of Cd cyclam complexes have allowed the characterisation of the *trans*-I and *cis*-V configurations by NMR spectroscopy. This has enabled similar NMR studies to be carried for Zn cyclam complexes in Chapter 5. For Zn cyclam in aqueous solution, in addition to the *trans*-I and *cis*-V configurations, the *trans*-III configuration has also been detected, which becomes dominant since Zn(II) is a smaller metal ion than Cd(II) and is a better fit for the cyclam ring cavity.

4.6 References

(1) Cotton, F. A.; Wilkinson, G. In *Advanced Inorganic Chemistry*, 4th ed.; John Wiley & Sons: New York, 1980, Chap. 19, p 590.

(2) Luchinat, C.; Sola, M. In *Encyclopedia of Inorganic Chemistry*; King, R. B., Edt; John Wiley & Sons: Chichester, 1994; Vol. 1, p 455.

(3) Summers, F. M. *Coord. Chem. Rev.* **1988**, *86*, 43.

(4) McAteer, K.; Lipton, A. S.; Ellis, P. D. In *Encyclopaedia of Nuclear Magnetic Resonance*; Grant, D. M, Harris, R. K., Edts; John Wiley & Sons: Chichester, 1996; Vol. 2, p 1085.

(5) (a) Zerbe, O.; Pountney, D. L.; von Philipsborn, W.; Vašák, M. *J. Am. Chem. Soc.*, **1994**, *116*, 377. (b) Zerbe, O.; Pountney, D. L.; von Philipsborn, W.; Vašák, M. *J. Am. Chem. Soc.*, **1994**, *116*, 7957.

(6) (a) De Clercq, E. *Metal-Based Drugs* **1997**, *4*, 173. (b) Inouye, Y.; Kanamori, T.; Yoshida, T.; Bu, X.; Shionoya, M.; Koike, T.; Kimura, E. *Biol. Pharm. Bull.* **1994**, *17*, 243.

(7) Kimura, E. *Prog. Inorg. Chem.* **1994**, *41*, 443.

(8) Kodama, M.; Kimura, E. *J. Chem. Soc., Dalton Trans.*, **1978**, 1081.

(9) Ito, H.; Ito, T. *Acta Crystallogr.* **1985**, *C41*, 1598.

(10) Alcock, N. W.; Curson, E. H.; Herron, N.; Moore, P. *J. Chem. Soc., Dalton Trans.* **1979**, 1987.

(11) Piotto, M.; Saudek, V.; Sklenar, V. *J. Biomol. NMR* **1992**, *2*, 661.

(12) Smallcombe, S. H., Patt, S. L., Keifer, P. A. *J. Magn. Reson., Ser. A* **1995**, *117*, 295.

(13) X-shape: Stoë and Cie, X-shape, Darmstadt, Germany, 1998.

(14) Altomare, A.; Burla, M. C.; Camalli, M.; Cascarano, G. L.; Giacovazzo, C.; Guagliardi, A.; Moliterni, A. G. G.; Polidori, G.; Spagna, R. *J. Appl. Cryst.* **1999**, *32*, 115.

(15) Sheldrick, G. M., *Shelxl97*; University of Göttingen: Göttingen, Germany, 1997.

(16) Dasgupta, P.; Nara, O. *Anal. Chem.* **1990**, 1117.

(17) Schrodt, A.; Neubrand, A.; van Eldik, R. *Inorg. Chem.* **1997**, *36*, 4579.

(18) Karplus, M. J. *J. Chem. Phys.* **1959**, *30*, 11. (b) Looney, A.; Han, R.; McNeill, K.; Parkin, G. *J. Am. Chem. Soc.* **1993**, *115*, 4690.

(19) Haasnoot, C. A. G.; de Leeuw, F. A. A. M.; Altona, C. *Tetrahedron* **1980**, *36*, 2783.

(20) Klyne, W.; Prelog, V. *Experientia* **1960**, *16*, 521.

(21) Huggins, M. L. *J. Am. Chem. Soc.* **1953**, *75*, 4123.

(22) Nakamoto, J.; Fujita, S.; Tanaka; Kobayashi, M. *J. Am. Chem. Soc.* **1957**, *79*, 4904.

(23) Nakamoto, K. In *Infrared and Raman Spectra of Inorganic and Coordination Compounds*, 4th ed.; John Wiley & Sons: New York, 1978; part III, p 253.

(24) (a) Tyson, T. A.; Hodgson, K. O.; Hedman, B.; Clark, G. R. *Acta Crystallogr.* **1990**, *C46*, 1638. (b) Tasker, P. A.; Sklar L. *J. Cryst. Mol. Struct.* **1975**, *5*, 329. (c) Endicott, J. F.; Lilie, J.; Kuszaj, J. M.; Ramaswamy, B. S.; Schmonsees, W. G.; Simic, M. G.; Glick, M. D.; Rillema, D. P. *J. Am. Chem. Soc.* **1977**, *99*, 429.

(25) Alcock, N. W.; Herron, N.; Moore, P. *J. Chem. Soc., Dalton Trans.* **1979**, 1486.

(26) Billo, E. J.; Connolly P. J.; Sardella, D. J.; Jasinski, J. P.; Butcher, R. J. *Inorg. Chim. Acta* **1995,** *230*, 19.

(27) (a) Kato, M.; Ito, T. *Inong. Chem.* **1985**, *24*, 504-508. (b) Kajiwara, T.; Yamaguchi, T.; Kawabata, H. S.; Kuroda, R.; Ito, T. *Inorg. Chem.* **1993**, *32*, 4990.

(28) Bazzicalupi, C.; Bencini, A.; Bianchi, A.; Fusi, V.; Paoletti, P.; Valtancoli, B. *J. Chem. Soc., Chem. Commun.,* **1995**, 1555-1556.

(29) Hay, R. W.; Pujari, M. P. *J. Chem. Soc., Dalton Trans.* **1986**, 1485.

(30) (a) Bazzicalupi, C.; Bencini, A.; Bianchi, A.; Fusi, V.; Paoletti, P.; Valtancoli, B. *J. Chem. Soc., Chem. Commun.* **1995**, 1555 and references therein. (b) Murthy, N. N.; Karlin, K. D. *J. Chem. Soc., Chem. Commun*. **1993**, 1236 and references therein.

(31) Einstein, F. W. B.; Willis, A. C. *Inorg. Chem*. **1981**, *20*, 609.

(32) Chang, C. A.; Francesconi, L. C.; Malley, M. F.; Kumar, K.; Gougoutas, J. Z.; Tweedle, M. F. *Inorg. Chem*. **1993**, *32*, 3501.

Chapter 5

Zn Cyclam Complexes

5.1 Introduction

The bicyclam AMD3100 (see Figure 6.1) has highly potent and selective anti-HIV activity.[1] It consists of 2 monocyclam units linked by an aromatic linker. Therefore, studies on the properties of monocyclam and its complexes will assist understanding of the behaviour of bicyclam. There are five possible configurations for cyclam complexes depending on the alignment of NH protons (Figure 1.3).[2] Nine Zn cyclam complexes were found in the Cambridge Structural Database (CSD) (see Table 5.1). All these Zn(II) cyclam complexes adopt the most stable *trans*-III configuration, in which the 6-membered chelate rings take the chair conformation and the 5-membered rings are gauche.

Table 5.1 Zn(II) cyclam complexes with *trans*-III configuration in CSD

Complex	Reference
$[Zn(cyclam)(O_2COCH_3)]_n(ClO_4)_n$	3
$[Zn(cyclam)(I_3)]I$	4
$[Zn(cyclam)(NCS)_2]$	5
$[Zn(cyclam)Br_2]$	6
$[Zn(cyclam)I_2]$	6
$[Zn(cyclam)(ClO_4)_2]$	7
$[Zn(cyclam)Cl]_2(ZnCl_4)$	8
$[Zn(cyclam)Cl]_{2n}(ZnCl_4)_n$	9
$[Zn(cyclam)Cl_2]$	6

Three configurations, *trans*-I, *trans*-II and *trans*-III have been detected in solution for a Ni(II) cyclam complex.[10,11] The *trans*-I and *trans*-III configurations equilibrate readily in donor solvents, presumably via the intermediate *trans*-II (*RSRR*) configuration.[10] The ^{13}C NMR spectra for $[Zn(cyclam)Cl]_{2n}(ZnCl_4)_n$ show that there are two isomers with *trans*-I and *trans*-III configurations in aqueous solution. The *trans*-III form is most probably six coordinate with two axially bonded water molecules. A minor isomer with the *trans*-I configuration forms after 24 hours. It is likely that in the *trans*-I form the Zn(II) is five coordinate, with the axial position occupied by a water molecule or chloride ion.

In order to obtain structural information on Zn cyclam complexes in the solid state and in solution, and to investigate the interaction of Zn cyclam complexes with carboxylates which are present in the side-chains of the co-receptor CXCR4, $[Zn(cyclam)(H_2O)_2](OAc)_2$, $Zn(cyclam)(ClO_4)_2$, $Zn(cyclam)Cl_2$ and $[Zn(cyclam)(phthalate)]_n(CH_3OH)_{2n}$ were synthesised and their conformation studied in the solid state by X-ray crystallography and in solution by 1D and 2D ^1H, ^{13}C, ^{15}N NMR spectroscopy. Kinetic studies and pH titrations on them and studies of the interactions between $Zn(cyclam)Cl_2$ and acetate were also performed.

5.2 Experimental

5.2.1 Synthesis and crystallisation of Zn cyclam complexes

$[Zn(cyclam)(H_2O)_2](OAc)_2$ (4). Cyclam (100.2 mg, 0.5 mmol) and $Zn(OAc)_2{\cdot}2H_2O$ (109.6 mg, 0.5 mmol) were heated under reflux in 15 ml of methanol for 2 hours. The solution was reduced in volume to *ca.* 4 ml by rotary evaporation. Crystals were grown by diffusion of Et_2O into the solution at 20 °C. The crystals were filtered off to give the product. Yield 133.3 mg (63.5%). Found for

$C_{14}H_{34}N_4ZnO_6$: C, 40.21; H, 8.30; N, 13.51%. Calc.: C, 40.05; H, 8.16; N, 13.35%. Selected IR (KBr, cm^{-1}): 3225 s, (NH), 3213 s (NH), 3156 s, (NH), 2928 m (CH), 2862 m (CH), 1577 s (CO).

$[Zn(cyclam)(phthalate)]_n(CH_3OH)_{2n}$ (5). Cyclam (150.3 mg, 0.75 mmol), ZnO (60.9 mg, 0.75 mmol), and phthalic acid (124.4 mg, 0.75 mmol) were stirred in 15 ml of water for 6 hours. The water was removed by rotary evaporation. The residue was dissolved in about 4 ml of methanol. Then the crystals were grown by diffusion of Et_2O into the solution at 20 °C. The crystals were filtered off to give the product. Yield 258.2 mg (70%). Found for $C_{20}H_{36}N_4ZnO_6$: C, 49.03; H, 7.50; N, 11.52%. Calc.: C, 48.64; H, 7.35; N, 11.34%. Selected IR (KBr, cm^{-1}): 3418 m, br (OH), 3254 s (NH), 3211 s, (NH), 2906 s (CH), 2838 s (CH), 1594 s (CO), 1577 s (CO), 1377 s (CO), 1364 s (CO).

$Zn(cyclam)(ClO_4)_2$ (6). Cyclam (100.2 mg, 0.5 mmol) and $Zn(ClO_4)_2 \cdot 6H_2O$ (185.9 mg, 0.5 mmol) were heated under reflux in 15 ml of methanol for 2 hours. The solution was kept in a refrigerator for overnight. Then the precipitate was filtered off to give the product. Yield 162.2 mg (70%). Found for $C_{10}H_{24}N_4ZnCl_2O_8$: C, 25.60; H, 5.47; N, 12.20%. Calc.: C, 25.85; H, 5.21; N, 12.06%. Selected IR (KBr, cm^{-1}): 3271 s, (NH), 3214 w (NH), 2935 m (CH), 2876 m (CH).

$Zn(cyclam)Cl_2$ (7). Cyclam (240 mg, 1.2 mmol) and $ZnCl_2$ (163.3 mg, 1.2 mmol) were heated under reflux in 15 ml of methanol for 2 hours. The solution was kept in a refrigerator for overnight. Then the crystals were filtered off to give the product. The solution was reduced to about 5 ml by rotary evaporation, and kept at 4 °C in the refrigerator to collect more product after a period of 2 days. Yield 257.4 mg (64%). Found for $C_{10}H_{24}N_4ZnCl_2$: C, 35.64; H, 6.56; N, 16.16%. Calc.: C, 35.68; H,

7.19; N, 16.64%. Selected IR (KBr, cm^{-1}): 3223 s, (NH), 3161 m (NH), 2927 s (CH), 2862 s (CH), 1647 w (NH).

5.2.2 NMR spectroscopy

All data were acquired at a probe temperature of 298 K. ^1H chemical shifts were internally referenced to the methyl singlet of TSP (3-trimethylsilyl- propionate-d_6) at 0 ppm; ^{13}C chemical shifts were referenced externally also using TSP. All NMR experiments were performed in 10% D_2O / 90% H_2O with **4**, **5**, **6** and **7** at a concentrations of 120 mM, pH 6.8, 7.4, 7.2, and 6.7, respectively, unless otherwise stated.

^1H NMR data were acquired over a ^1H frequency width of 6 kHz into 32 k data points (acquisition time = 2.73 s). The water resonance was suppressed by presaturation or *via* the WATERGATE pulsed-field-gradient sequence.[12]

2D [^1H, ^{13}C] HSQC NMR data were typically acquired over a ^1H frequency width of 5 kHz and a ^{13}C frequency width of 5 kHz (40 ppm) centred at 43 ppm. Data were acquired with 64 transients into 2 k complex data points (acquisition time 205 ms) for each of 128 t_1 increments (acquisition time 12.7 ms).

2D [^1H, ^{15}N] HSQC NMR data were acquired over a ^1H frequency width of 3.5 kHz and a ^{15}N frequency width of 2.5 kHz (50 ppm) centred at 10 ppm. Data were acquired with 240 transients into 2 k complex data points for each of 128 t_1 increments.

All NMR data were processed using Xwin-nmr (version 2.0, Bruker).

5.2.3 Kinetic studies

Kinetic studies were carried out using ^1H NMR spectroscopy. Complex **4** (40 mM, pH 6.8) was dissolved in 10% D_2O / 90% H_2O. After an initial period of mixing, sample insertion into the NMR probe, temperature equilibration (25 °C) and

shimming, 1D ^{1}H NMR spectra were repeatedly acquired on the sample over a 24 h period in order to monitor its behaviour with time.

The rate equations were set up assuming that the conformational changes to complex **4** occur by two parallel first-order reactions in which species III undergoes independent, concurrent isomerisation to yield two other different species I and V (see below). Rate constants were further obtained by fitting the rate equations using the program Scientist (MicroMath, Inc, version 2.0).

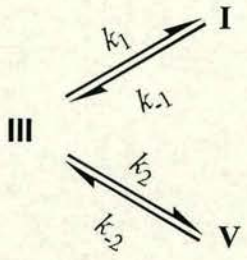

The rate equation for the loss of III:

$$-\frac{dC_{III}}{dt} = k_1 C_{III} + k_2 C_{III} - k_{-1} C_I - k_{-2} C_V \qquad (1)$$

The rate equations for the formation of I and V:

$$\frac{dC_I}{dt} = k_1 C_{III} - k_{-1} C_I \qquad (2)$$

$$\frac{dC_V}{dt} = k_2 C_{III} - k_{-2} C_V \qquad (3)$$

5.2.4 pH dependence

^{1}H NMR spectroscopy was employed to study the effects of pH on complexes **4** and **6** in the pH range of about 6.8 to 12.8 and 7.2 to 12.2, respectively, with TSP as internal reference. Values of pH were measured with a pH-meter (Corning 145) equipped with a microcombination electrode (Aldrich) calibrated with Aldrich standard buffers (pH 4, 7, and 10). pH values were adjusted with 0.1 M NaOH in the NMR tube. No attempt was made to correct for deuterium isotope effects. ^{1}H NMR spectra were acquired for the sample at each pH.

5.2.5 Effect of acetate on the configuration distribution of Zn(cyclam)Cl_2

Complex **7** (27 mM) was dissolved in 90% H_2O / 10% D_2O in the presence of TSP. Addition of CH_3COONa was made to this solution in nine separate NMR tubes to give **7**:CH_3COO^- ratios of 1:0.5 to 1:9. Each solution was readjusted to pH 7.4 using 0.1 M NaOH or 0.1 M HCl after addition of 1 M NaOAc in aqueous solution. ^{1}H NMR spectra were acquired overnight on these samples as well as for **7** itself in 10 % D_2O / 90% H_2O.

5.2.6 X-ray crystal structures of [Zn(cyclam)$(H_2O)_2$]$(OAc)_2$ and [Zn(cyclam)(phthalate)]$_n(CH_3OH)_{2n}$

Crystal data and details of data collection for complexes **4** and **5** are provided in Table 5.2. Data were collected and the structures were solved by Dr. Simon Parsons and Pamela A. McGregor An absorption correction was performed by Gaussian integration following refinement of the crystal face-indices and dimensions against a set of Ψ-scans (Stoë X-shape[13]). Data were collected to $2\theta_{max}$ = 140° and

the structure solved by direct methods (Shelx-97)[14] and refined by full matrix least squares against F^2. Methyl groups were treated as rotating rigid groups. H-atoms attached to coordinated water in complex **4** were located in a difference map and refined freely; other H-atoms were placed in calculated positions and allowed to ride on their parent atoms. Hydroxyl groups in complex **5** refined freely, and H-atoms were placed in calculated positions and allowed to ride on their parent atoms. All non-H atoms were refined with anisotropic displacement parameters, to give convergence $R1$ and w$R2$ values as indicated in Table 5.2. The final difference map extremes are also provided in Table 5.2.

Table 5.2 Crystal data and data collection for complexes **4** and **5**

	4	**5**
formula	$C_{14}H_{34}ZnN_4O_6$	$C_{20}H_{36}ZnN_4O_6$
FW	412.82	493.90
crystal system	monoclinic	triclinic
space group	$P2_1/c$	P-1
V, Å^3	963.68 (19)	1182.6(3)
Z	2	2
a, Å	9.1377(10)	8.6255(11)
b, Å	12.1643(16)	10.2268(17)
c, Å	8.7265(8)	15.110(2)
α, deg	90	94.596(9)
β, deg	96.537(10)	100.913(8)
γ, deg	90	113.450(7)
T, K	220(2)	150(2)
d_{calcd}, g/cm^{-3}	1.447	1.387
absorp coeff, mm^{-1}	2.093	1.797
unique reflections	1720	4188
observed reflections	2643	4219
$R1$ (obs/all refl)	0.0336	0.0508
w$R2$ (obs/all refl)	0.0933	0.1408

5.3 Results

5.3.1 ^{1}H, ^{13}C and ^{15}N NMR studies of $[Zn(cyclam)(H_2O)_2](OAc)_2$ in aqueous solution

As can be seen in Figure 5.1, the ^{1}H NMR spectrum of the crystalline Zn acetate complex, $[Zn(cyclam)(H_2O)_2](OAc)_2$ (**4**) dissolved in 10% D_2O / 90% H_2O at pH 6.8, consists of two distinct regions. A set of multiplets and a very strong singlet appear between 1.5 and 2.1 ppm. The second region of signals lies between 2.4 and 3.6 ppm. The 1D ^{1}H NMR spectrum is very complicated. In order to fully assign the ^{1}H NMR spectrum, 2D homonuclear [^{1}H, ^{1}H] TOCSY and DQF-COSY NMR data sets and natural abundance 2D heteronuclear [^{1}H, ^{13}C] and [^{1}H, ^{15}N] HSQC NMR data were acquired.

Three spin-systems were found in the 2D [^{1}H, ^{1}H] TCOSY spectrum (Figure 5.2). 2D [^{1}H, ^{1}H] COSY NMR data (Figure 5.3) showed that the couplings in the first spin-system (designated III) appeared as follows: $\mathbf{H_a}$ (1.64 ppm) couples to $\mathbf{H_b}$ (1.90 ppm), to $\mathbf{H_d}$ (2.70ppm) and to $\mathbf{H_g}$ (3.20 ppm) and $\mathbf{H_b}$ couples to $\mathbf{H_f}$ (3.18 ppm); $\mathbf{H_c}$ (2.48 ppm) and $\mathbf{H_e}$ (3.03 ppm) couple to one another and they both also couple to $\mathbf{H_g}$. The second spin-system (designated V) is composed of 5 signals: $\mathbf{H_1}$ (1.74 ppm) is coupled to $\mathbf{H_3}$ (2.79 ppm), $\mathbf{H_5}$ (3.08 ppm), and weakly to a broad signal $\mathbf{H_6}$ (3.35 ppm); $\mathbf{H_2}$ (2.56 ppm) and $\mathbf{H_4}$ (2.91 ppm) couple to each other. Both $\mathbf{H_2}$ and $\mathbf{H_4}$ also couple to the broad signal $\mathbf{H_6}$. The third spin-system (designated I) consists of seven signals: $\mathbf{H_A}$ (1.69 ppm), $\mathbf{H_B}$ (1.92 ppm), $\mathbf{H_C}$ (2.73 ppm), $\mathbf{H_D}$ (2.76 ppm), $\mathbf{H_E}$ (2.91 ppm), $\mathbf{H_F}$ (3.16 ppm) and a broad signal $\mathbf{H_G}$ (3.50 ppm) in the TCOSY NMR spectrum. The last spin-system can not easily be observed in the COSY NMR data due to extensive overlap and low intensity. The strong singlet (1.93 ppm) can be assigned to OAc^- since it does not couple to any other resonances.

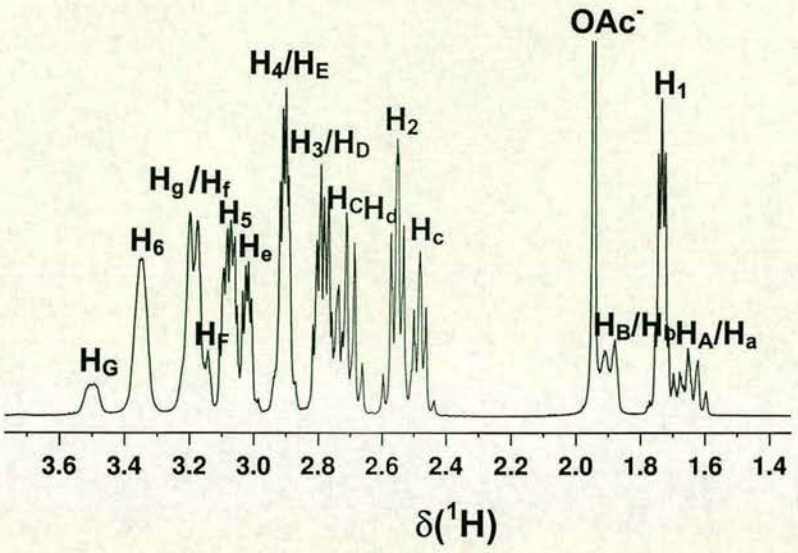

Figure 5.1 ^{1}H NMR spectrum of complex **4** in 10% D_2O / 90% H_2O. Resonances for *trans*-I, *trans*-III and *cis*-V are designated H_A-H_G, H_a-H_g and H_1-H_6, respectively.

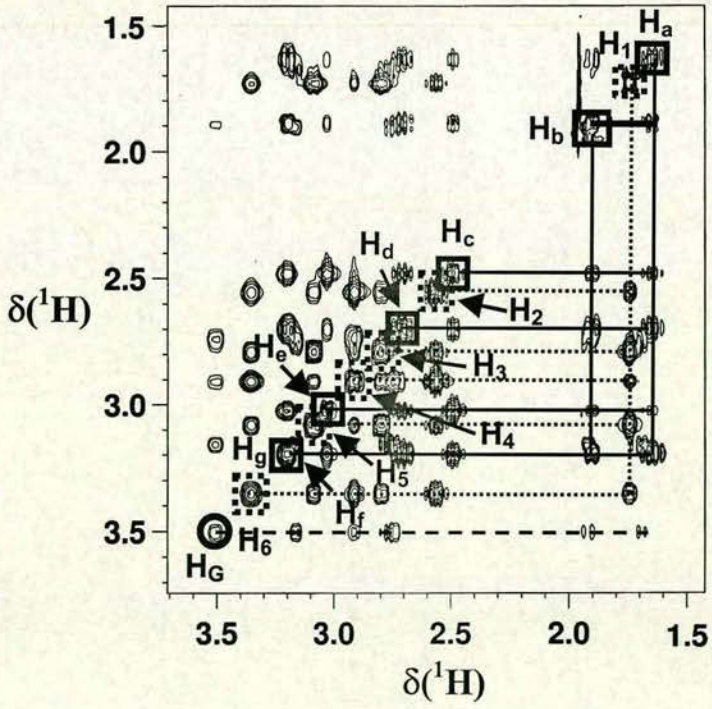

Figure 5.2 2D [^{1}H, ^{1}H] TOCSY NMR spectrum of **4** in 10% D_2O / 90% H_2O. Resonances for *trans*-I (H_G), *trans*-III (H_a to H_g) and *cis*-V (H_1 to H_6) are designated by circles, solid and dashed boxes, respectively.

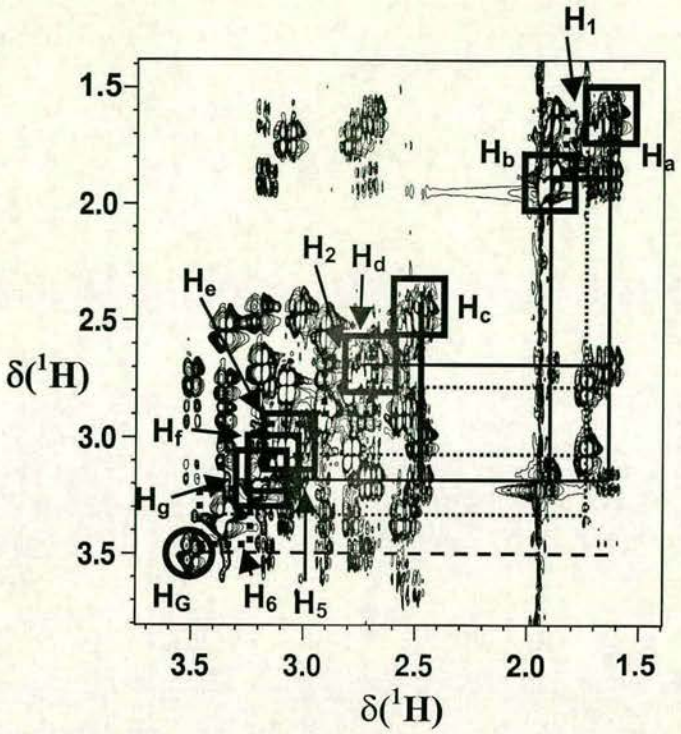

Figure 5.3 2D [^{1}H, ^{1}H] COSY NMR spectrum of **4** in 10% D_2O / 90% H_2O. Resonances for *trans*-I (H_G), *trans*-III (H_a to H_g) and *cis*-V (H_1 to H_6) are designated by circles, solid and dashed boxes, respectively.

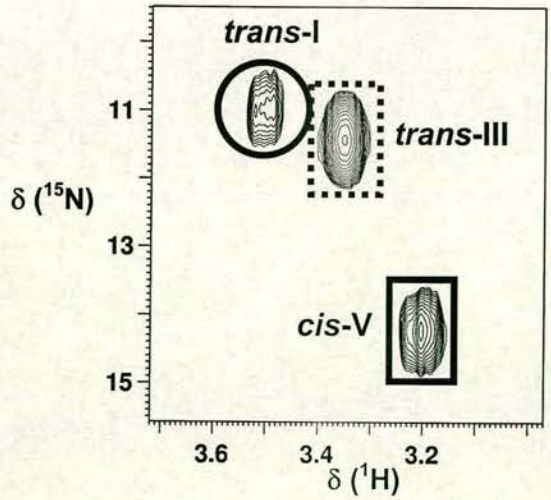

Figure 5.4 2D [^{1}H, ^{15}N] HSQC NMR spectrum of complex **4** in 10% D_2O / 90% H_2O. NH resonances for the *trans*-I (H_G), *trans*-III (H_g) and *cis*-V (H_6) configurations are designated by circles, solid and dashed boxes, respectively.

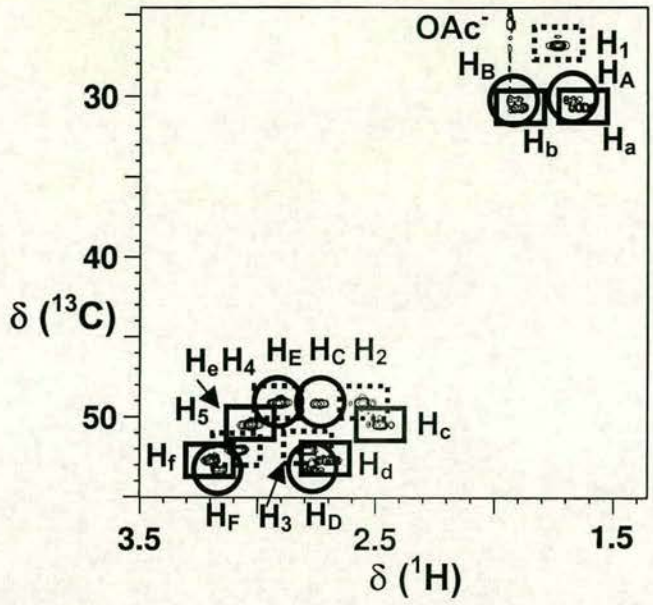

Figure 5.5 2D [^{1}H, ^{13}C] HSQC NMR spectrum of complex **4** in 10% D_2O / 90% H_2O. Resonances for the *trans*-I (H_A to H_G), *trans*-III (H_a to H_g) and *cis*-V (H_1 to H_6) configurations are designated by circles, solid and dashed boxes, respectively.

Three NH signals can be found in the 2D [^{1}H, ^{15}N] HSQC NMR spectrum (Figure 5.4). The spin-system $\mathbf{H_a}$-$\mathbf{H_f}$ showed correlations to the NH signal $\mathbf{H_g}$; the spin-system $\mathbf{H_1}$-$\mathbf{H_5}$ relates to the broad NH signal $\mathbf{H_6}$; the third spin-system $\mathbf{H_A}$-$\mathbf{H_B}$ relates to the broad NH signal $\mathbf{H_G}$. Three identified spin-systems arise from three different configurations (I, III and V) of complex **4**. Time and pH dependent experiments also support this conclusion.

The 2D [^{1}H, ^{13}C] HSQC NMR spectrum (Figure 5.5) revealed the presence of 17 proton signals corresponding to those described above, which were correlated to a total of nine ^{13}C NMR signals (Table 5.3). Geminal pairs of protons were identified as follows: $\mathbf{H_a/H_b}$ (δ ^{13}C: 30.77 ppm); $\mathbf{H_c/H_e}$ (δ ^{13}C: 50.59 ppm); $\mathbf{H_d/H_f}$ (δ ^{13}C: 52.82

Table 5.3 Total assignment of ^{1}H, ^{13}C and ^{15}N NMR resonances of complexes **4**, **5**, **6** and **7**

Complex	solvent	config.		δ (^{1}H), (^{13}C) and (^{15}N) and assignment						
				NCH_2CH_2N		$NCH_2CH_2CH_2N$		$NCH_2CH_2CH_2N$		NH
4	D_2O/H_2O (pH 6.8)	*trans*-I	^{1}H	2.91	2.73	3.16	2.76	1.92	1.69	3.50
			^{13}C	49.22		53.34		30.32		
			^{15}N							11.0
		trans-III	^{1}H	3.03	2.48	3.18	2.70	1.90	1.64	3.20
			^{13}C	50.59		52.82		30.77		
			^{15}N							14.2
		cis-V	^{1}H	2.91	2.56	3.08	2.79	1.74		3.35
			^{13}C	49.28		52.19		27.68		
			^{15}N							11.5
5	D_2O/H_2O (pH 7.4)	*trans*-I	^{1}H	2.99	2.74	3.20	2.78	1.93	1.78	3.59
			^{13}C	49.29		53.39		30.34		
			^{15}N							10.8
		trans-III	^{1}H	3.02	2.55	3.18	2.74	1.88	1.66	3.28
			^{13}C	50.58		52.95		30.70		
			^{15}N							14.0
		cis-V	^{1}H	2.97	2.63	3.14	2.86		1.76	3.48
			^{13}C	49.27		52.20		27.08		
			^{15}N							11.0
6	D_2O/H_2O (pH 7.2)	*trans*-I	^{1}H	2.92	2.76	3.16	2.81	1.96	1.71	3.59
			^{13}C	49.17		53.24		30.17		
			^{15}N							10.2
		trans-III	^{1}H	3.04	2.48	3.20	2.70	1.90	1.64	3.12
			^{13}C	50.52		52.75		30.71		
			^{15}N							14.3
		cis-V	^{1}H	2.92	2.61	3.12	2.84	1.76		3.29
			^{13}C	48.77		51.85		26.39		
			^{15}N							11.2
7	D_2O/H_2O (pH 6.7)	*trans*-I	^{1}H	2.93	2.76	3.16	2.80	1.95	1.72	3.58
			^{13}C	49.10		53.34		30.20		
			^{15}N							11.4
		trans-III	^{1}H	3.03	2.50	3.19	2.73	1.90	1.65	3.15
			^{13}C	50.53		52.76		30.75		
			^{15}N							14.9
		cis-V	^{1}H	2.93	2.63	3.13	2.84	1.77		3.39
			^{13}C	48.81		51.81		26.47		
			^{15}N							11.6

Note: 1.93 ppm for OAc^- in **4**; 7.52 and 7.46 ppm for Ph in **5**.

ppm); $\mathbf{H_A/H_B}$ (δ ^{13}C: 30.32 ppm); $\mathbf{H_C/H_E}$ (δ ^{13}C: 49.22 ppm), $\mathbf{H_D/H_F}$ (δ ^{13}C: 53.34 ppm); $\mathbf{H_2/H_4}$ (δ ^{13}C: 49.28 ppm); $\mathbf{H_3/H_5}$ (δ ^{13}C: 52.19 ppm). Since all protons except for three **NH** signals belong to geminal pairs in this complex, the remaining signal, $\mathbf{H_1}$ (δ ^{13}C: 27.68 ppm) corresponds to two equivalent protons.

5.3.2 Solution NMR studies of three Zn cyclam complexes, $[Zn(cyclam)(phthalate)]_n(CH_3OH)_{2n}$, $Zn(cyclam)(ClO_4)_2$ and $Zn(cyclam)Cl_2$

^{1}H, ^{13}C and ^{15}N NMR data were also acquired for complexes **5**, **6** and **7** in 10% D_2O / 90% H_2O (Figures 5.6, 5.7 and 5.8). The NMR data are summarised in Table 5.3.

5.3.3 Kinetic studies

The time dependence of the Zn cyclam complex with acetate (**4**) in water was observed by 1D ^{1}H NMR spectroscopy. During the initial period, only one major form (III) was observed by 1D ^{1}H NMR spectroscopy (Figure 5.9). Two other forms (I and V) appeared and increased with time. Form V increased strongly and form I increased slightly as form III decreased over time. Form I approached equilibrium faster than form V.

5.3.4 Effect of pH on Zn complexes, $[Zn(cyclam)(H_2O)_2](OAc)_2$ and $Zn(cyclam)(ClO_4)_2$

The NMR spectra of complexes **4** and **6** were highly pH dependent. As the pH was increased, form V decreased and form I increased whereas form III was almost constant for **4** (Figure 5.10). As the pH increased, form III decreased and form I increased whereas form V was almost constant for **6** (Figure 5.11).

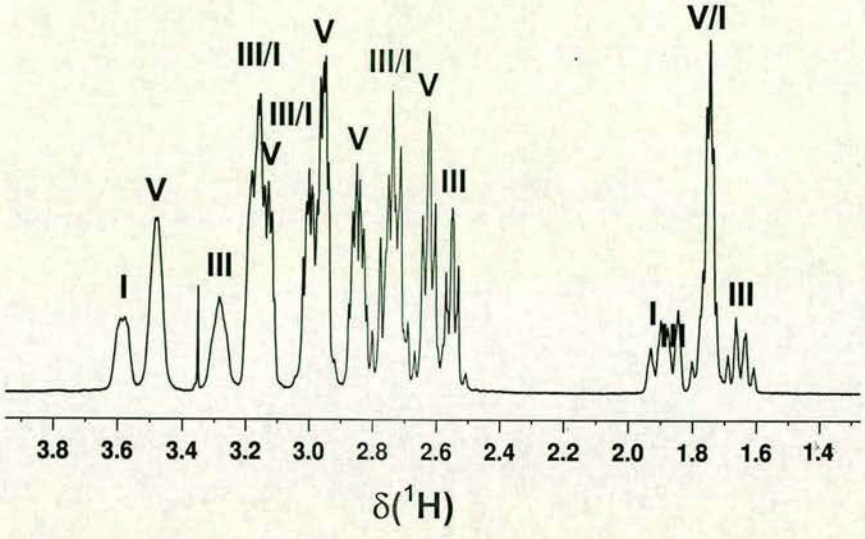

Figure 5.6 ^{1}H NMR spectrum of $[Zn(cyclam)(phthalate)]_n(CH_3OH)_{2n}$ **(5)** in 10% D_2O and 90% H_2O. Resonances for *trans*-I, *trans*-III and *cis*-V are designated I, III and V, respectively.

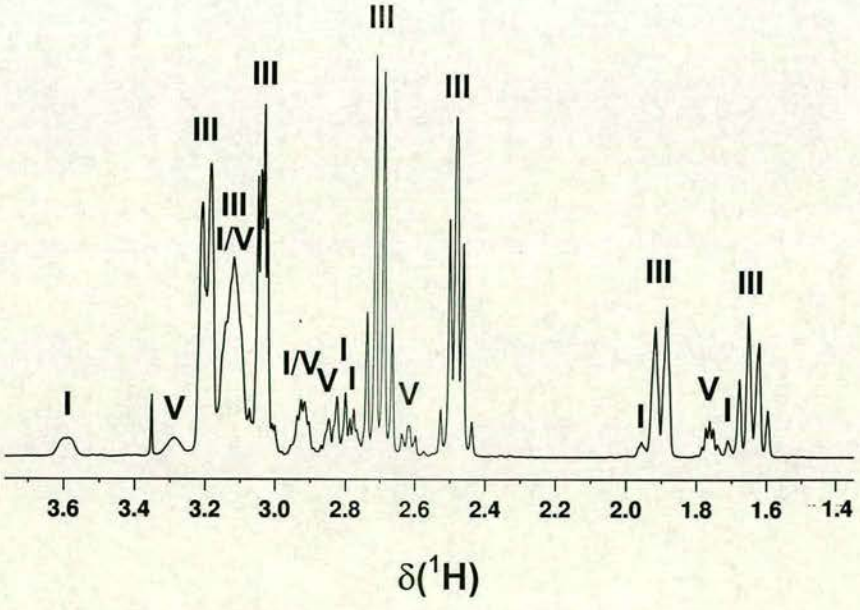

Figure 5.7 ^{1}H NMR spectrum of $Zn(cyclam)(ClO_4)_2$ **(6)** in 10% D_2O and 90% H_2O. Resonances for *trans*-I, *trans*-III and *cis*-V are designated I, III and V, respectively.

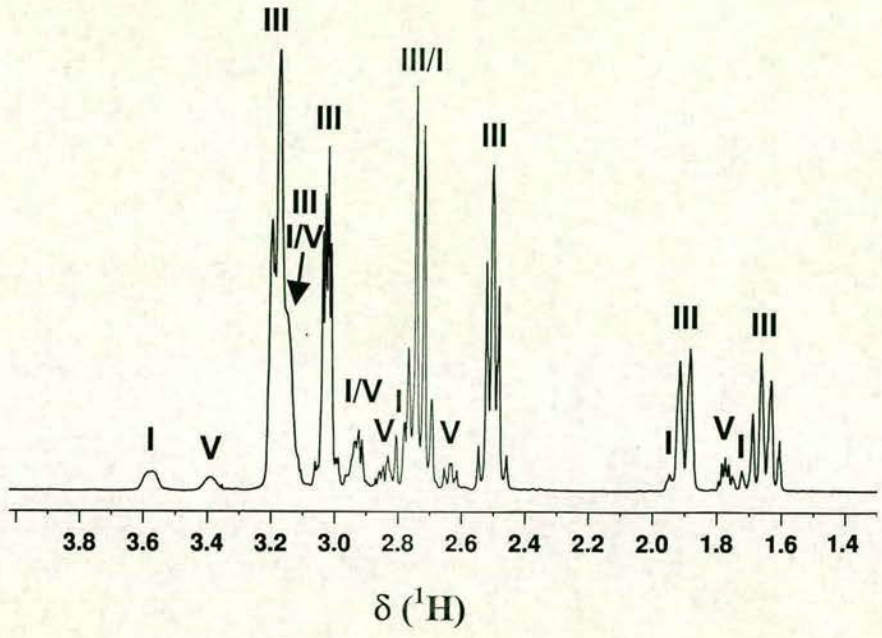

Figure 5.8 ^{1}H NMR spectrum of Zn(cyclam)Cl_2 **(7)** in 10% D_2O and 90% H_2O. Resonances for *trans*-I, *trans*-III and *cis*-V are designated I, III and V, respectively.

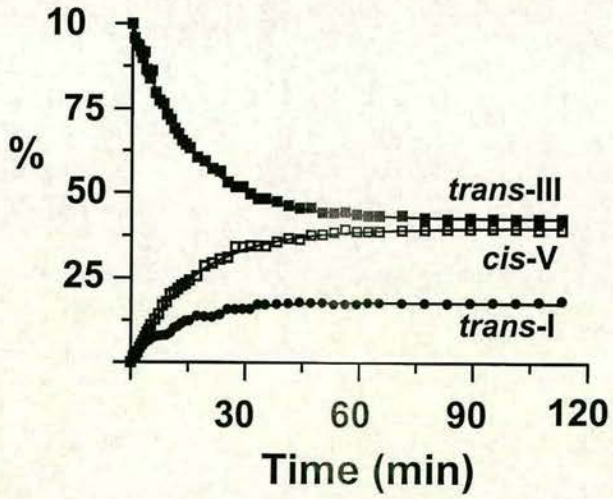

Figure 5.9 Time dependent configurational changes of resonances for complex **4** in water as determined from integration of the ^{1}H NMR peaks (see Figure 5.1). The solid lines represent best fits to the data and the following rate constants: k_1, 2.54 × 10^{-3} min^{-1}; k_{-1}, 2.70×10^{-3} min^{-1} for *cis*-V and k_2, 1.33×10^{-3} min^{-1}; k_{-2}, 3.24×10^{-3} min^{-1} for *trans*-I.

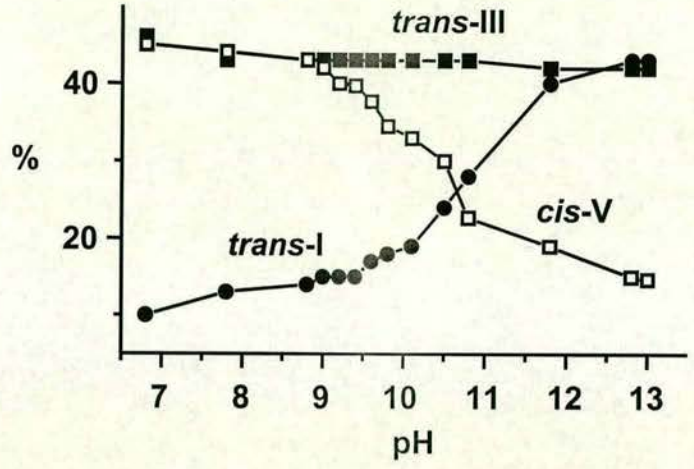

Figure 5.10 pH dependent configurational changes for complex **4** in water. *Trans*-I, *trans*-III and *cis*-V configurations are designated by black circles, black squares and white squares, respectively.

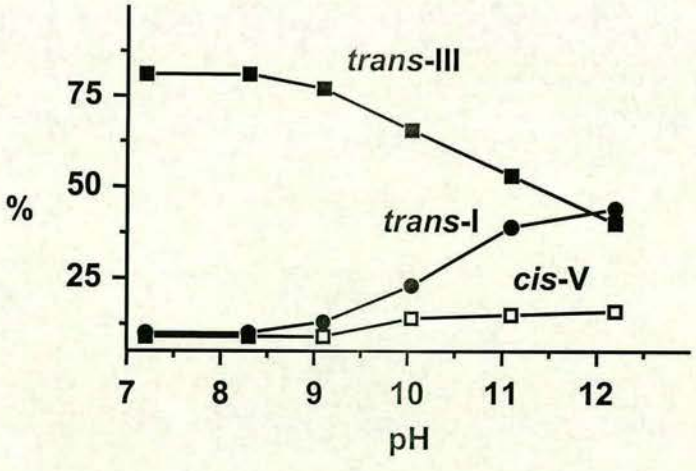

Figure 5.11 pH dependent configurational changes for complex **6** in water. *Trans*-I, *trans*-III and *cis*-V configurations are designated black circles, black squares and white squares, respectively.

5.3.5 Effect of carboxylates on $Zn(cyclam)Cl_2$

All four Zn cyclam complexes can be categorised into two groups according to the distribution of three different configurations in aqueous solution at equilibrium (Table 5.4). Form V is predominant for Zn cyclam complexes with acetate (**4**) and phthalate (**5**). Form III is predominant whereas form V is minor for Zn cyclam complexes with perchlorate (**6**) and chloride (**7**). These results show that anions can affect the distribution of three configurations of Zn cyclam complexes and carboxylate can increase form V.

Table 5.4 Distribution of configurations of complexes **4-7** (40 mM) in 10% D_2O / 90% H_2O at equilibrium

complex	*trans*-I	*trans*-III	*cis*-V
$Zn(cyclam)(OAc)_2$ (**4**)	11.9%	45.3%	42.8%
$[Zn(cyclam)(phthalate)]_n$ (**5**)	22.7%	31.9%	45.3%
$Zn(cyclam)(ClO_4)_2$ (**6**)	8.2%	83.2%	8.6%
$Zn(cyclam)Cl_2$ (**7**)	11.2%	79.6%	9.2%

Subsequently, ^1H NMR spectra of **7** were acquired in the presence of increasing quantities of NaOAc to thirteen separate NMR tubes to give **7**:NaOAc molar ratios of 1:0.5 to 1:9. ^1H NMR observations showed that form III decreases and form V increases whereas form I is almost constant with increasing NaOAc concentration in the aqueous solution of **7** (Figure 5.12).

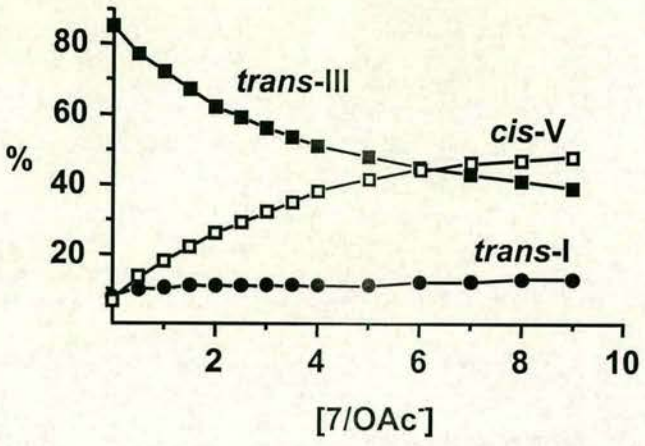

Figure 5.12 Effect of acetate on the distribution of complex **7** in water as determined by integration of the ^{1}H NMR resonances. *Trans*-I, *trans*-III and *cis*-V configurations are designated by black circles, black squares and white squares, respectively.

5.3.6 X-ray crystal structures of $[Zn(cyclam)(H_2O)_2](OAc)_2$ and $[Zn(cyclam)(phthalate)]_n(CH_3OH)_{2n}$

$[Zn(cyclam)(H_2O)_2](OAc)_2$ (**4**) and $[Zn(cyclam)(phthalate)]_n(CH_3OH)_{2n}$ (**5**) were characterised by X-ray crystallography. The crystal structure of complex **4** consists of $[Zn(cyclam)(H_2O)_2]^{2+}$ cations, and uncoordinated OAc^- anions, which are linked by a network of hydrogen bonds. The Zn(II) ion sits at a centre of symmetry and is surrounded octahedrally by four nitrogen atoms of the macrocyclic ligand in a plane with the distances of 2.08 and 2.12 Å and by two water molecules occupying the axial positions with the same distance of 2.27 Å (Figure 5.13). The overall structure of the cation is the *trans*-III conformation with two adjacent N-H hydrogen atoms directed toward one side of the cyclam plane and the other two directed toward the opposite side of the plane. The *trans*-III configuration is the most stable one for cyclam complexes in which the two six-membered chelate rings are in chair conformations and the two five-membered rings are in gauche conformations and is

found in a number of cyclam complexes.[3,15,16] All bond lengths and angles are listed in Table 5.5.

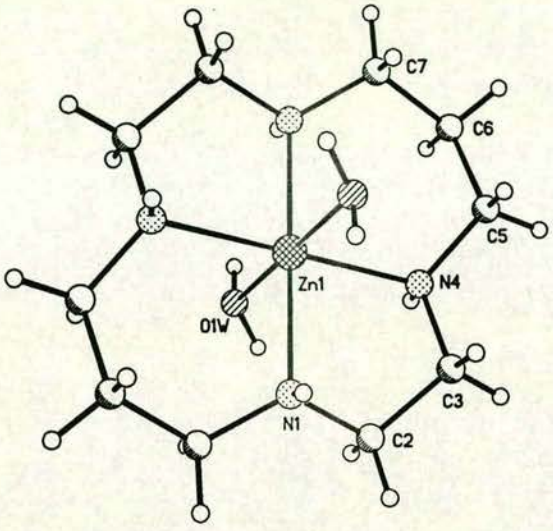

Figure 5.13 X-ray crystal structure of the cation of $[Zn(cyclam)(H_2O)_2](OAc)_2$ (**4**) together with the atom numbering scheme.

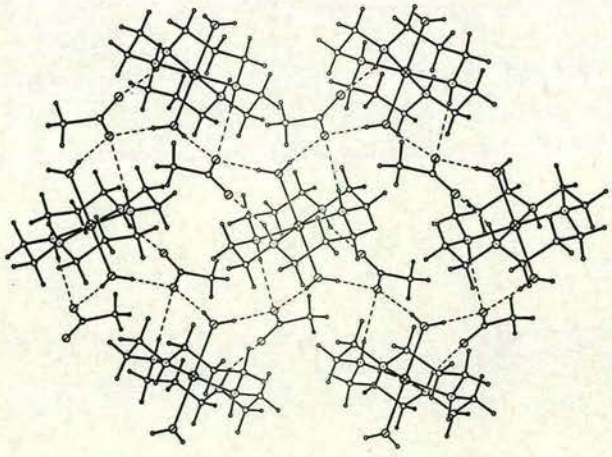

Figure 5.14 Packing of $[Zn(cyclam)(H_2O)_2](OAc)_2$ (**4**). Hydrogen bonds are shown by dotted lines.

Table 5.5 Selected bond distances (Å) and angles (deg) for complexes **4** and **5**

Complex **4**	
Zn(1) – N(1)	2.1198 (15)
Zn(1) – N(4)	2.0809 (15)
Zn(1) – O(1W)	2.2719 (14)
N(1) – Zn(1) – N(1)	180.00 (8)
N(4) – Zn(1) – N(1)	84.94 (6)
N(4) – Zn(1) – N(1)	95.06 (6)
Complex **5**	
Zn(1) – N(3)	2.097(2)
Zn(1) – N(6)	2.100(2)
Zn(2) – N(21)	2.100(2)
Zn(2) – N(17)	2.108(3)
Zn(1) – O(2)	2.220(2)
Zn(2) – O(3)	2.190(2)
N(3) – Zn(1) – N(3)	180.0(2)
N(3) – Zn(1) – N(6)	95.75(9)
#1[b]	
N(3) – Zn(1) – N(6)	84.25(9)

[a] #1 -x, -y, -z; [b] #1 -x,-y+1,-z+1

The crystal packing and hydrogen-bonding scheme for $[Zn(cyclam)(H_2O)_2](OAc)_2$ (**4**) are shown in Figure 5.14. In this structure, eight intermolecular interactions link a complex cation to eight neighbouring complex cations via six acetate anions to form a 3-dimensional network of hydrogen bonds. There are two types of hydrogen bonds: O – H ··· O with H ··· O distances ranging from 1.84 to 1.95 Å and O – H ··· O angles ranging from 169 to 176° and N – H ··· O with H ··· O distances ranging from 1.99 to 2.24 Å and O – H ··· O angles ranging from 158 to 164°. Both carboxyl oxygen atoms act as acceptors, with one of them participating in three intermolecular hydrogen bonds. All four H atoms of the secondary amine groups for each complex cation and all four H atoms of two water

molecules coordinated to the Zn(II) atom act as donors. The details of hydrogen bonds are shown in Table 5.6.

The crystal structure of complex **5** consists of an infinite chain of [Zn(cyclam)(phthalate)] with methanol molecules from the solvent which are linked by hydrogen bonds (Figure 5.15). The phthalate anion plays the role of a bridging ligand, forming a linear chain structure. Each Zn(II) ion sits at a centre of symmetry and is surrounded octahedrally by four nitrogen atoms of the macrocyclic ligand in a plane with a Zn-N distance of 2.10 Å and by two oxygen atoms of phthalate molecules occupying the axial positions with an N-O distance of 2.22 Å. All bond lengths and angles are listed in Table 5.5.

Table 5.6 Hydrogen bonds in complexes 4 and **5** (bond length Å and angle °)

complex	D – H ··· D	d (H ··· A)	∠DHA	D (D ··· A)
4	O1W – H1W ··· O1A[a]	1.953	169.36	2.736
	O1W – H2W ··· O1A[b]	1.843	176.10	2.727
	N1 – H1 ··· O1A[c]	2.242	163.51	3.136
	N4 – H4 ··· O2A[d]	1.994	158.36	2.869
5	N3 – H3 ··· O2M	2.079	161.77	2.976
	N6 – H6 ··· O1	2.012	152.63	2.870
	N17 – H17 ··· O4	2.314	146.56	3.132
	N21 – H21 ··· O1	1.963	169.43	2.882
	O1M – H1M ··· O4	1.939	168.45	2.770
	O2M – H2M ··· O4	1.885	173.47	2.715

[a] **O1A [-x+1, -y, -z]**; [b] **O1A [-x+1, y-1/2, -z+1/2]**; [c] **O1A [x-1, y, z]**; [d] **O2A [-x+1, y-1/2, -z+1/2]**

There are three different intramolecular hydrogen bonds between two free oxygen atoms (O1 and O4) of each carboxylate and two H atoms (H21 and H17) of the secondary amine groups from one cyclam ligand and one H atom (H6) of the secondary amine group from the other cyclam ligand. O1 is shared by H6 and H21. The methanol solvent molecules form two hydrogen bonds to O4: H1M ··· O4, 1.94 Å; H1M ··· O4, 1.89 Å. The other intermolecular hydrogen bond involves O2M as an acceptor and H3 as a donor. The details of hydrogen bonds are shown in Table 5.6.

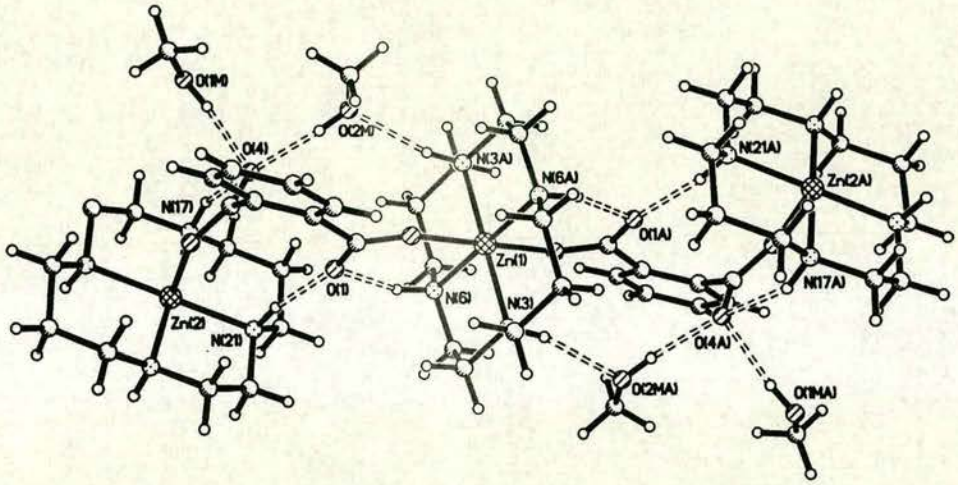

Figure 5.15 X-ray crystal structure of $[Zn(cyclam)(phthalate)]_n(CH_3OH)_{2n}$ **(5)** together with the atom numbering scheme. Hydrogen bonds are shown by dotted lines.

5.4 Discussion

5.4.1 Solution NMR studies of $[Zn(cyclam)(H_2O)_2](OAc)_2$

The three cross-peaks from separate spin-systems of complex **4** in the 2D [^{1}H, ^{15}N] HSQC spectrum revealed that there are three configurations I, III, V in aqueous

solution. The signals between 2.4 and 3.6 ppm can be easily assigned to the central methylene in the six membered-rings by their chemical shifts. In the first spin-system (form III), therefore, $\mathbf{H_a}$ and $\mathbf{H_b}$ are assigned to $NCH_2C\boldsymbol{H_2}CH_2N$ in the six membered-rings. 2D [^{1}H, ^{1}H] COSY showed that $\mathbf{H_d}$ and $\mathbf{H_f}$ correlate to $\mathbf{H_a}$ and $\mathbf{H_b}$. Hence, it can be concluded that H_d and H_f are from $NC\boldsymbol{H_2}CH_2C\boldsymbol{H_2}N$ in the six membered-rings. The remaining two signals $\mathbf{H_c}$ and $\mathbf{H_e}$, therefore, are assigned to $NC\boldsymbol{H_2}C\boldsymbol{H_2}N$ in the five membered-rings. H_g can be clearly distinguished as a NH signal in the 2D [^{1}H, ^{15}N] HSQC spectrum whereas it overlaps with $\mathbf{H_f}$ in the 1D ^{1}H NMR spectrum. For the second spin-system (form V), it can similarly be concluded that $\mathbf{H_1}$ is from $NCH_2C\boldsymbol{H_2}CH_2N$ and H_3 and H_5 are from the $NC\boldsymbol{H_2}CH_2C\boldsymbol{H_2}N$ in the six membered-rings. $\mathbf{H_2}$ and $\mathbf{H_4}$ are from the $NC\boldsymbol{H_2}C\boldsymbol{H_2}N$ in the five membered-rings. In the third spin-system (form I), two weak signals $\mathbf{H_A}$ and $\mathbf{H_B}$ of seven signals including one broad NH signal can be assigned to $NCH_2C\boldsymbol{H_2}CH_2N$ in the six membered-rings.

Cyclam complexes can adopt five different configurations depending on the spatial alignment of the NH protons (Figure 1.3). After analysis of the structure of these possible configurations, it can be seen that only *trans*-I and *trans*-III can produce six $-CH_2-$ proton signals, and two of them for the central methylene of the six membered-rings. Both six-membered rings in *trans*-I and *trans*-III configurations adopt a chair conformation and H_a and H_b are nonequivalent and give rise to two ^{1}H NMR resonances (see Figure 1.3 and **A** in Figure 5.16). From the time-dependent experiment, form III can be easily assigned to *trans*-III since complex **4** adopts the most stable configuration *trans*-III in the crystals. Therefore, form I is assigned to *trans*-I.

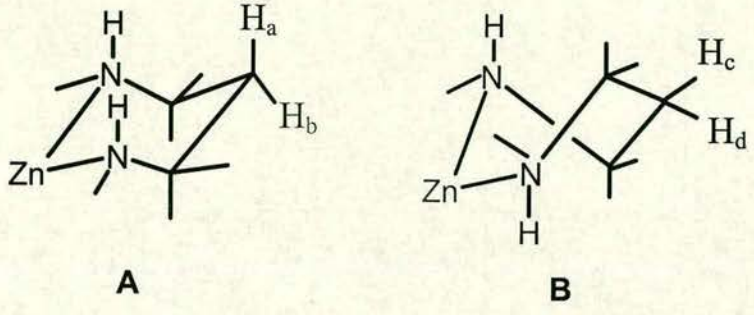

Figure 5.16 Chair and twist-boat conformations for six-membered rings

Configuration analysis also indicates that only *trans*-IV and *trans*-V have five non-equivalent $-CH_2-$ protons which can produce five $-CH_2-$ proton signals and only one of them for the central methylene of the six membered-rings. Both six-membered rings in *trans*-IV and *trans*-V adopt twist-boat conformation and H_c and H_d are equivalent and give rise to only one ^1H NMR resonance (see Figure 1.3 and **B** in Figure 5.16). However, both *trans*-IV and *trans*-V do not appear to be stable because of two six membered-rings with high energy in the twist-boat conformation for each of them. *Cis*-V is the strain free option and only *trans*-V can easily fold along diagonal a or b (Chart 4.1) to form the more common *cis*-V configuration with two six membered-rings in the chair conformation. These two enantiomeric forms can exchange rapidly to give the appearance of a *trans*-V configuration. Therefore, it is proposed that form V could be the *cis*-V configuration.

5.4.2 Kinetic studies

Isomerisation from *trans*-III to *cis*-V and *trans*-I for $[Zn(cyclam)(H_2O)_2](OAc)_2$ in aqueous solution requires the successive inversion of two amine nitrogens via an intermediate *trans*-II configuration (see Figure 1.3). It is

slow for configurations to reach the equilibrium in this process (at neutral pH). However, the configuration *trans*-II can not be detected in aqueous solution. It seems that the formation of the *trans*-II configuration is the slow step and determines the isomerisation speed. *Trans*-II is not stable and rapidly converts to the other configurations (Scheme 5.1).

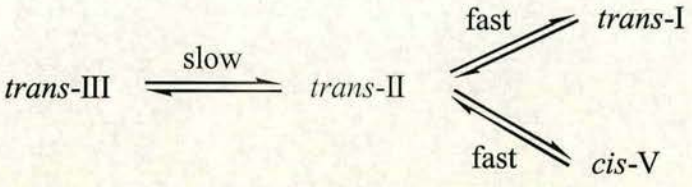

Scheme 5.1 Isomerisation from *trans*-III to *cis*-V and *trans*-I at neutral pH

5.4.3 Effect of acetate on Zn(cyclam)Cl_2

In aqueous solution, the distribution of the three configurations for Zn cyclam complexes is strongly dependent on the counter-ion present (Table 5.4). Aqueous solutions of **6** and **7** consist mainly of *trans*-III whereas for the carboxylato complexes **4** and **5**, the *cis*-V form is predominant. Titration of complex **7** with a carboxylate also gives rise to an increase of *cis*-V at the expense of *trans*-III (Figure 5.12). It seems that carboxylate can act as a bidentate ligand, with hydrogen bonds between carboxylate and the secondary amine NH stabilising *cis*-V in aqueous solution. Hence, the *cis*-V configuration becomes more stable than *trans*-III in aqueous solution in the presence of carboxylates, and *trans*-III isomerizes to *cis*-V.

5.4.4 Effect of pH on $[Zn(cyclam)(H_2O)_2](OAc)_2$ and $Zn(cyclam)(ClO_4)_2$

As the pH increases, the *cis*-V form decreases and *trans*-I increases, whereas *trans*-III is almost constant for **4**, whilst *trans*-III decreases and *trans*-I increases, whereas *cis*-V is almost constant, for **6** (Figures 5.10 and 5.11). As Cd(II) cyclam complexes discussed in 4.4.3, Zn(II) complexes can also form cyclam-Zn-OH^- species in *trans*-II configuration. The inversion from *cis*-V to *trans*-I for complex **4 is** identical to that for Cd cyclam complexes (see Section 4.4.3). The inversion from *trans*-III to *trans*-I for **6** as shown in Scheme 5.1 also needs to convert the nitrogen configurations twice via *trans*-II. The formation of *trans*-II for cyclam-Zn-OH^- from *trans*-III is base-catalysed as well.[17] The *trans*-II configuration for cyclam-Zn-OH^- continues to convert to *trans*-I and is base-catalysed. Therefore, the isomerisation from *trans*-III to *trans*-I for complex **6** is very fast at high pH since no proportion change for each configuration observed at each pH. The base-catalysed mechanism can be confirmed by the slow inversion from *trans*-III to *trans*-I for **4** at neutral pH (see Section 5.4.2). The *trans*-I configuration may also involve a carbonate complex after fixing the atmospheric CO_2.

5.4.5 X-ray crystal structures of $[Zn(cyclam)(H_2O)_2](OAc)_2$ (4) and $[Zn(cyclam)(phthalate)]_n(CH_3OH)_{2n}$ (5)

Compared with the Zn-O bond distances for bound water in the other Zn(II) complexes in the Cambridge Structural Database, complex **4** has one of the longest axial Zn-O distances (2.27 Å). The elongation of the Zn-O bond distance in the complex may be attributed to the competition of two acetate anions for hydrogen

bonds with water. The Zn-N bond lengths of 2.08 Å and 2.12 Å are comparable with those in the complex Zn(cyclam)$(ClO_4)_2$.[16] The average value for Zn-N bond length of 2.10 Å is very close to the "ideal" metal-nitrogen bond length (2.07 Å)[18] in *trans*-cyclam complexes and to the bond lengths in a number of complexes containing 1,2-ethanediamine and 1,3-propanediamine.[19]

The Zn-O distance of 2.22 Å in complex **5** is slightly longer than the normal value for Zn(II) binds to the oxygen atom of CO_3^{2-}.[3] Two cyclam ZnN_4 planes associated with a phthalate ion are not parallel, therefore, steric constraints may exist between the neighboring cyclam ligands. Each complex cation in complex **5** is quite similar to that in complex **4**. It also takes the most stable conformation *trans*-III and has the same value of average Zn-N bond length as in complex **4**. Bond distances and angles within the chelate rings correspond closely to the same measurements in complex **4** as well.

Among the hydrogen-bonds for both **4** and **5**, the secondary amine NH of cyclam and OH in water molecules, or methanol molecules act as proton donor groups, and the hydrogen-bonding acceptors are the C=O groups of carboxyl residues and the OH group from methanol. The OH group in methanol molecules displays dual hydrogen bond functionality and therefore can give rise to hydrogen-bond cooperativity and form multi-centre hydrogen bonds. As we expected, both **4** and **5** form an infinite supra-molecular network structure and an infinite supra-molecular chain, respectively, through hydrogen bonds. There are two strong hydrogen bonds O1W - H2W ··· O1A (H ·· O, 1.84 Å) in complex **4** and O2M - H2M ··· O4 (H ·· O, 1.89 Å) in complex **5** with near linear geometry (176 and 168°, respectively).

5.5 Conclusions

The crystal structures of $[Zn(cyclam)(H_2O)_2](OAc)_2$ (**4**) and $[Zn(cyclam)(phthalate)]_n(CH_3OH)_{2n}$ (**5**) indicate that cyclam complexes adopt the most stable conformation *trans*-III in which six membered-rings are in the chair conformation and five membered-rings are in the gauche conformation. Three isomers *trans*-I, *trans*-III, and *cis*-V were found in aqueous solution by NMR for complexes **4**, **5**, **6** and **7**. ^{1}H NMR spectra were fully assigned by combining 2D NMR data. Both time dependence experiments and titration of the chloride cyclam complex with carboxylates indicate that the interaction with carboxylates gives rise to a large increase in the proportion of *cis*-V and a slight increase in *trans*-I. This result shows that carboxylates have high conformationally recognition abilities. A large number of hydrogen bonds exist in both aqueous solution and solid state, and may also play an important role in the anti-HIV activity of cyclams. This result implies that carboxylates in the side-chains of the target protein CXCR4 may also have high conformational recognition ability. This conclusion is further confirmed by the similar studies on the bicyclam complexes in Chapter 6.

5.6 References

(1) De Clercq, E., Yamamoto, N., Pauwels, R., Baba, M., Schols, D., Nakashima, H., Balzarini, J., Debyser, Z., Murrer, B. A., Schwartz, D., Thornton, D., Bridger, G., Fricker, S., Henson, G., Abrams, M.; Picker, D. *Proc. Natl. Acad. Sci. USA* **1992**, *89*, 5286.

(2) Bosnich, B.; Poon, C. K.; Tobe, M. L. *Inorg. Chem.* **1965**, *4*, 1102.

(3) Kato, M.; Ito, T. *Inorg. Chem.* **1985**, *24*, 509-514.

(4) Heinlein, T.; Tebbe, K.-F *Z. Kristallogr.* **1985**, 170, 70.

(5) Ito, T.; Kato, M.; Ito, H. *Bull. Chem. Soc. Jpn.* **1984**, *57*, 2634.

(6) Porai, M. A.; Antsyshkina, A. S.; Shevchenko, Yu. N.; Yashina, N. I.; Varava, F. B. *Zh. Neorg. Khim.* **1994,** *39, 435.*

(7) Tyson, T. A.; Hodgson, K. O. *Acta Cryst.* **1990**, *C46*, 1638.

(8) Pickardt, J.; Staub, B.; Gong, G.-T *Z. Kristallogr.* **1994**, *209*, 554.

(9) Alcock, N. W.; Berry, A.; Moore, P. *Acta Cryst.* **1992**, *C48*, 16.

(10) Moore, P.; Sachinidis, J.; Willey, G. R. *J. Chem. Soc., Chem. Commun.* **1983**, 522.

(11) Lincoln, S. F.; Pisaniello, D. L.; Coates, J. H.; Hadi, D. A. *Inorg. Chim. Acta Lett.* **1984**, *81*, 9.

(12) Piotto, M.; Saudek, V.; Sklenar, V. *J. Biomol. NMR* **1992**, *2*, 661-665.

(13) X-Shape, Stoë and Cie, Darmstadt, Germany, **1995**.

(14) Sheldrick, G. M., *SHELX-97, Program for Crystal Structure Refinement*; University of Göttingen: Göttingen, Germany, **1997**.

(15) (a) Ito, T.; Kato, M.; Ito, H. *Bull. Chem. Soc. Jpn.* **1984**, *57*, 2634-2640. (b) Alcock, N. W.; Berry, A.; Moore, P. *Acta Cryst.* **1992**, *C48*, 16-19.

(16) Tyson, T. A.; Hodgson, K. O. *Acta Cryst.* **1990**, *C46*, 1638-1640.

(17) Hay, R. W.; Pujari, M. P. *J. Chem. Soc., Dalton Trans.* **1986**, 1485.

(18) Martin, L. Y.; Dehayes, L. J.; Zompa, L. J.; Busch, D. H. *J. Am. Chem. Soc.* **1974**, *96*, 4046-4048.

(19) (a) Neill, D.; Riley, M. J.; Kennard, C. H. L. *Acta Cryst.* **1997**, *C53*, 701-703. (b) Muralikrishna, C.; Mahadevan, C.; Sastry, S.; Seshasayee, M.; Subramanian, S. *Acta Cryst.* **1983**, *C39*, 1630-1632. (c) Welch, J. H.; Bereman, R. D.; Singh, P.; Moreland, C. *Inorg. Chim. Acta* **1989**, *158*, 9-16.

Chapter 6

Zn Bicyclam Complexes

6.1 Introduction

There is current medical interest in the drug AMD3100, a bicyclam containing two cyclam units connected by a *p*-phenylenebis(methylene) linker (AMD3100, bicyclam·8HCl, Figure 6.1). AMD3100 is in phase I clinical trials for stem cell transplantation used in the treatment of patients who have cancers involving the blood and immune system. It is also one of the most potent anti-HIV agents known,[1] blocking entry of T-lymphotropic HIV-1 and HIV-2 strains by specific binding to the CXCR4 co-receptor.[2] CXCR4 is a member of the classical G-protein-coupled receptor family of membrane proteins, which contain 7 transmembrane helices.

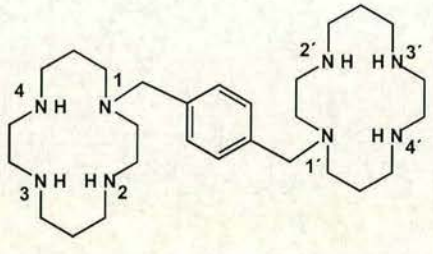

Figure 6.1 Bicyclam, 1-1'-[1,4-phenylenebis(methylene)]-bis(1,4,8,11-tetraazacyclotetradecane). The octa-HCl salt is the anti-HIV drug AMD3100.

Cyclams are strong metal chelating agents. The concentration of Zn(II) in blood plasma is *ca.* 20 μM,[3] and Zn(II) binds strongly to cyclam (log K 20.12)[4]. Taking account of cyclam pK_a values, this gives a conditional dissociation constant (K_d) at blood plasma pH (7.4) of *ca.* 0.1 pM. Since the level of free Zn(II) in plasma

is *ca.* 1 nM,[3] and the affinity of alkyl-substituted cyclams is likely to be even higher than for cyclam itself, it is reasonable to expect that bicyclam can exist as a Zn(II) complex in *vivo*.

The Zn(II) complex of bicyclam is 10x more active than AMD3100 in its interaction with the CXCR4 receptor,[5] and there is a close correlation between anti-HIV activity and CXCR4 interaction, decreasing in the order:

$Zn(II)_2$ > AMD3100 > $Ni(II)_2$ > $Cu(II)_2$ >>$Pd(II)_2$ (as perchlorate salts).

This has led to the suggestion that the Zn(II) complex is an important antagonist in *vivo*.[5]

Configurations with H atoms pointing in the same direction at the end of a diagonal can fold to generate a trigonal bipyramid or a *cis* structure. Thus the *R,R,S,S* configuration can form only a *trans*-III complex, whereas *trans*-V can fold to *cis*-V. Energy calculations on Ni(II) complexes[6] show that *trans*-III has the lowest energy, but *trans*-I becomes more stable relative to *trans*-III on decreasing the metal coordination number from 6 (octahedral) to 5 to 4 (square-planar), in agreement with a recent survey of X-ray structures.[7]

Studies on bicyclam complexes have mostly focused on compounds as shown in Chapter 1 which two monocyclam units are linked together by bridging the carbon atoms of the cyclam backbone by crystallography.[8] In their complexes, each monocyclam ring adopts the *trans*-III configuration. Bicyclam complexes in which two monocyclam units are linked together by bridging the amine nitrogen atoms of the cyclam backbone are the other type of bicyclam. The redox chemistry of some of these dinickel(II) and dicopper(II) complexes has been investigated with regard to the M(II) to M(III) oxidation process.[9] No crystals or NMR studies of such bicyclam complexes have been reported.

The aim of the work described in this thesis was to elucidate the nature of potential first and second coordination sphere interactions of metal (bi)cyclam complexes with the CXCR4 receptor. The investigations include solid state and dynamic solution studies as well as modelling. Interactions of metal bicyclams with acetate were studied since there is strong evidence[10] from receptor mutagenesis studies that bicyclam blocking of CXCR4 is dependent on the carboxylate side-chains of Asp171 and Asp262 in trans-membrane helices IV and VI. The findings in this study provide a new basis for the improved design of receptor-targeted macrocycles. I prepared the bicyclam AMD3100 by the route in Scheme 6.1 which constitutes a simple extension of the previously published mono N-alkylation procedure using phosphoryl-protected cyclam.[11]

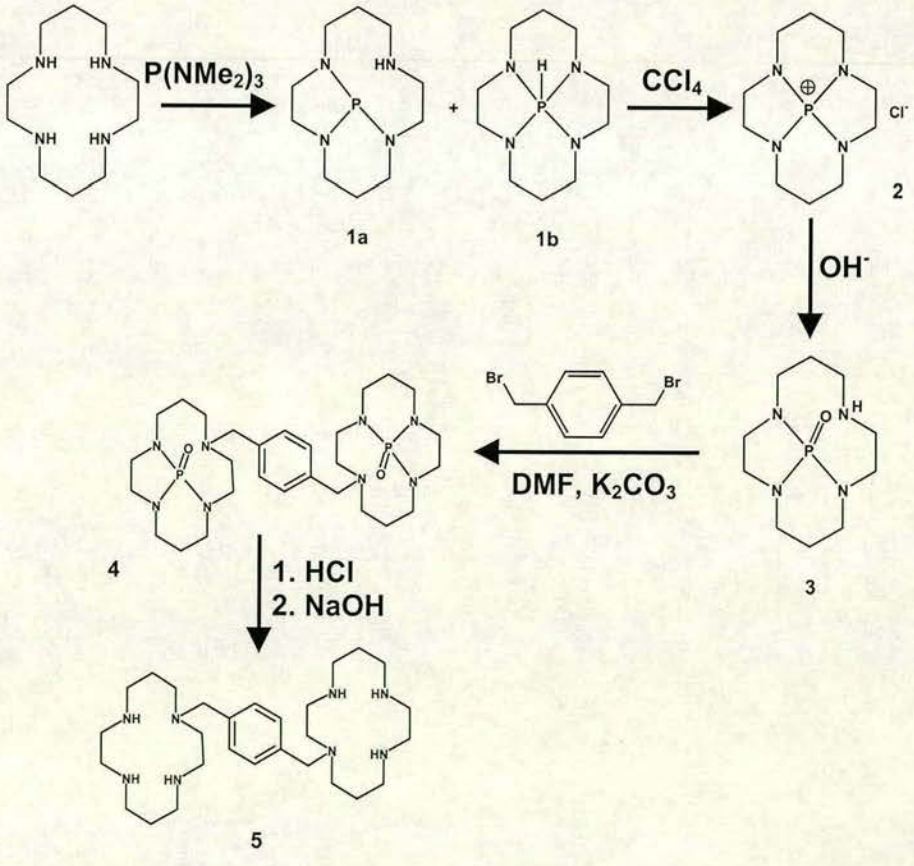

Scheme 6.1 The synthetic route for bicyclam

6.2 Experimental

6.2.1 Synthesis and crystallisation of Zn bicyclam complexes

Synthesis of bicyclam Following the reported method,[11] cyclam (0.5 g, 2.5 mmol) in 100 ml of dry toluene was heated under reflux with hexamethylphosphoric triamide (454 µl, 2.5 mmol) overnight. After cooling to 0 °C, dry CCl_4 (375 µl, 3.9 mmol) was added whereupon a white precipitate separated. The solvent was evaporated under high vacuum and the residue **2** treated with 25 ml of 10% sodium hydroxide. The aqueous phase was extracted with chloroform (4×100 ml). The combined organic phases were dried over $MgSO_4$, and then evaporated and dried under vacuum to give a white powder **3** (580 mg, 94.8%).

The protected cyclam **3** (580 mg, 2.4 mmol), 1, 4-bis-bromomethyl-benzene (313 mg, 1.2 mmol) and potassium carbonate (520 mg, 3.8 mmol) were heated at 120 °C in 70 ml of dry DMF for 20 hours. After removing the solvent, 40 ml of 10% hydrochloric acid was added into the residue of **4** and refluxed for 2 days. The solution was washed with 20 ml of toluene and the volume reduced to about 15 ml. Then pH was adjusted to >13 with sodium hydroxide pellets and extracted with chloroform (3×100 ml). The organic phase was dried over anhydrous sodium sulfate. The solvent was evaporated to give a pale yellow powder **5** (0.62 g, 52%). ^{1}H NMR ($CDCl_3$): 7.23 (m, 4H, C_6H_4); 3.53 (s, 4H, $CH_2C_6H_4CH_2$); 2.98 - 2.39 (m, 32H, NCH_2); 1.85 (m, 4H, $NCH_2CH_2CH_2N$); 1.68 (m, 4H, $NCH_2CH_2CH_2N$). EI MS 503 *m/e* (M^+).

Zn_2(bicyclam)$(ClO_4)_4$ (**8**) Bicyclam (387.15 mg, 0.77 mmol) and $Zn(ClO_4)_2{\cdot}6H_2O$ (571 mg, 1.53 mmol) were stirred in 10 ml of methanol at 60°C (oil bath) for one hour. The precipitate was filtered off and washed with a small amount

of methanol to give Zn_2(bicyclam)$(ClO)_4$ (707.6 mg, 89.1%). Selected IR (KBr, cm^{-1}): ν= 3435 (NH), 3246 (NH), 2930 (CH_2), 2875 (CH_2), 1653 (NH); elemental analysis calcd for $C_{28}H_{54}Cl_4N_8O_{16}Zn_2$ (%): C 32.61, H 5.28, N 10.86; found: C 32.19, H 5.35, N 10.22.

$[Zn_2$(bicyclam)$(OAc)_2](OAc)_2 \cdot 2CH_3OH$ (**9**) Bicyclam (49.6 mg, 0.1 mmol) and $Zn(OAc)_2$ (43.34 mg, 0.2 mmol) in methanol (3 ml) were heated under reflux for one hour. The solvent was evaporated on a rotary evaporator and the residue was dissolved in methanol, then recrystallised by diffusion of Et_2O into the solution to give the crystals of $Zn_2[$(bicyclam)$(OAc)_2](OAc)_2$ (66.67 mg, 57.8%). Selected IR (KBr, cm^{-1}): ν= 3486 (NH), 3436 (NH), 3147 (NH), 2920 (CH_2), 2867 (CH_2), 1576 (CO), 1410 (CO); elemental analysis calcd for $C_{38}H_{74}N_8O_{10}Zn_2$ (%): C 48.88, H 7.99, N 12.00; found: C 48.99, H 7.68, 11.86.

6.2.2 NMR spectroscopy

All data were acquired at a temperature of 298 K unless otherwise stated. ^1H chemical shifts were internally referenced to the methyl singlet of TSP (3-trimethylsilyl- propionate-d_6) at 0 ppm; ^{13}C chemical shifts were referenced externally for 2D [^1H, ^{13}C] and internally for 1D ^{13}C NMR spectra also using TSP. ^{15}N chemical shifts were referenced externally for 2D [^1H, ^{15}N] using NH_4Cl at 0 ppm. All NMR experiments were performed in 10% D_2O / 90% H_2O with complex **8** at a concentration of 5 mM, pH 6.6, and complex **9** at a concentration of 16 mM, pH 7.1, unless otherwise stated.

1D ^1H NMR data were acquired over a ^1H frequency width of 4.4 kHz into 64 k data points (acquisition time = 2.34 s). The water resonance was suppressed by presaturation or *via* WET.[12]

^{13}C-{^{1}H}NMR data were acquired over a ^{13}C frequency width of 31.44 kHz into 25154 data points (acquisition time = 0.4 s).

2D [^{1}H, ^{13}C] HSQC NMR data were typically acquired with gradient coherence selection over a ^{1}H frequency width of 4.4 kHz, and a ^{13}C frequency width of 25 kHz (167 ppm) centred at 72 ppm. Data were acquired with 32 transients into 2048 complex data points (acquisition time 232 ms) for each of 2×256 t_1 increments (acquisition time = 10.2 ms). Solvent suppression was achieved using WET. A relaxation delay of 1.6 s was applied between transients.

2D [^{1}H, ^{15}N] HSQC NMR data were acquired over a ^{1}H frequency width of 4.4 kHz and a ^{15}N frequency width of 1000 Hz (17 ppm) centred at 0 ppm. Data were acquired with 256 transients into 2 k complex data points for each of 2×64 t_1 increments. Relaxation delay and solvent suppression were the same as for the equivalent ^{13}C experiment.

Homonuclear 2D [^{1}H, ^{1}H] (z-filtered)-TOCSY, NOESY and DQF-COSY NMR data were acquired at 600 MHz over a ^{1}H frequency width of 4.4 kHz into 2048 complex data points (acquisition time = 232 ms); 8, 8 and 16 transients per FID were acquired for each experiment respectively. Data were acquired with 2×512 t_1 increments in F1 (frequency width = 4.4 kHz). A relaxation delay of 1.6 s was allowed between transients, and solvent suppression was achieved using WET. For the TOCSY experiment, a spin-lock time of 70 ms was used. For the NOESY experiment, a mixing time of 750 ms was used. All data were converted to Xwinnmr (Version 2.0, Bruker U.K. Ltd.) format prior to Fourier transformation.

6.2.3 X-ray crystal structure of $[Zn_2(bicyclam)(OAc)_2](OAc)_2 \cdot 2CH_3OH$ (9)

Crystals suitable for X-ray diffraction were grown by slow diffusion of ether into a methanol solution of **9**. A colourless block 0.17 x 0.12 x 0.10 mm was selected for X-ray crystallographic studies. Unit cell parameters were as follows: $C_{38}H_{74}N_8O_{10}Zn_2$, triclinic, space group P $\bar{1}$, a = 9.652(2), b = 10.089(2), c = 14.429(2) Å, α = 105.741(3), β = 101.629(3), γ = 94.304(4)°, V = 1311.9(4) Å^3, Z = 2, ρ_{calcd} = 1.111 mg m^{-3}, $Mo_{K\alpha}$ radiation (λ = 0.71073 Å), $2\theta_{max}$ = 52.8°. A total of 8482 data points were collected on a Bruker SMART diffractometer at 150(2) K. Absorption and *Lp* corrections were applied using the program SADABS[13] T_{min} = 0.80. Merging gave 5226 independent data points. The structure was solved by Dr. Robert O. Gould using DIRDIF[14], which gave an automatic solution and expansion to show all 27 atoms in the asymmetric unit. Refinement of 292 parameters by full-matrix least squares on F^2 using SHELX97[15] gave wR_2 = 0.116 based on all data and R_1 = 0.047, based on 3995 data with $I \geq 2\sigma(I)$, GOF = 0.929, max Δ/σ on last cycle 0.08, max residual electron density = 1.5 e Å^{-3}. All non-hydrogen atoms refined anisotropically; hydrogen atoms were placed in calculated positions and allowed to ride on atoms of the complex. Other hydrogen atoms were located, idealised and also allowed to ride.

6.2.4 Kinetic studies

Kinetic studies were carried out using ^{1}H NMR spectroscopy. Complexes **8** and **9** were dissolved in 10% D_2O / 90% H_2O separately. After an initial period of mixing, sample insertion into the NMR probe, temperature equilibration (298 K) and shimming, 1D ^{1}H NMR spectra were repeatedly acquired over a 24 h period for both

complexes in order to monitor their behaviour with time. However, the process was much more rapid for complex **9**, and could be followed by ^{1}H NMR spectroscopy only for complex **8**.

The rate equations were set up assuming that the conformational changes to complex **8** occur by two parallel first-order reactions in which species **III** undergoes independent, concurrent isomerisation to yield two other different species **I** and **V** (see below). Rate constants were further obtained by fitting the rate equations using the program Scientist (MicroMath, Inc, version 2.0).

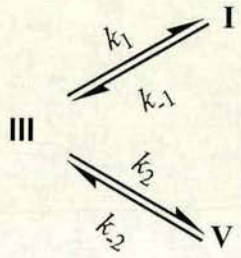

The rate equation for the loss of **III**:

$$-\frac{dC_{III}}{dt} = k_1 C_{III} + k_2 C_{III} - k_{-1} C_I - k_{-2} C_V \qquad (6\text{-}1)$$

The rate equations for the formation of **I** and **V**:

$$\frac{dC_I}{dt} = k_1 C_{III} - k_{-1} C_I \qquad (6\text{-}2)$$

$$\frac{dC_V}{dt} = k_2 C_{III} - k_{-2} C_V \qquad (6\text{-}3)$$

6.2.5 Effect of acetate on Zn_2(bicyclam)$(ClO_4)_4$

$CH_3{}^{13}COONa$ (2 mM) was dissolved in 90% H_2O / 10% D_2O in the presence of dioxane. Stepwise addition of **8** was made to this solution to give ^{13}C-acetate: **8** molar ratios of 1:1, 1:2, 1:3 and 1:4. Further reverse addition of $CH_3{}^{13}COONa$ to this solution was made to give ^{13}C-acetate: **8** ratios of 2:4, 3:4, 4:4, 6:4, 8:4 and 12:4. ^{13}C-{^{1}H} NMR spectra were acquired after each addition. In a similar experiment, NaOAc was added stepwise to a 5 mM solution of Zn_2(bicyclam)$(ClO_4)_4$ in 10% D_2O / 90% H_2O at 298 K to give molar ratios Zn_2(bicyclam)$(ClO_4)_4$:acetate of 1:1, 1:2 and 1:4, and ^{1}H NMR spectra were acquired at each molar ratio. The pH of the solutions was within the range 6.6 to 7.4 and in each case equilibrium was reached within an hour. The proportions of species present at the 1:4 mol ratio are similar to those for a solution of crystalline **9**.

6.2.6 Molecular modelling

An homology model of human CXCR4 (sequence SWISS_PROT: CCR4_HUMAN, P30991) based on the X-ray structure of bovine rhodopsin (PBD accession code 1F88)[16] was built using the Homology module of Insight II (Version 2000, Biosym Technologies) by Drs. Claudia Blindauer, Hye-seo Park, and Stephen J. Paisey. The sequence alignment is shown in Table 6.1. The loops were generated *de novo* and selected so as to avoid clashes with Zn_2-bicyclam which had been incorporated into the rhodopsin template. The Discover simulation package (Biosym Technologies) with the consistent valence force-field was employed for energy

minimisation. The final step employed 500 cycles of the steepest descent method until the r.m.s. derivative of the energy was <0.001.

Since the NMR studies indicated that the major solution configuration of Zn bicyclam acetate is *cis*-V/*trans*-I, this was built by Dr. John Parkinson from the X-ray coordinates of **9** with modification of the second ring to *trans*-I (based on the published X-ray structure[17] of [Zn(1,4,8,11-tetramethyl-tetraazacyclotetradecane (CH_3COCO_2)]ClO_4 followed by energy minimisation using Sybyl (Version 6.7, Tripos Inc.). Zn_2-bicyclam was manually docked with the receptor so as to bring the *cis*-V ring near to Asp262 and *trans*-I ring close to Asp171. Following docking, the ligand was fixed relative to the receptor, and distance restraints of 2.2 Å with an average force constant of 500 kcal mol^{-1} $Å^{-2}$ were applied to the Zn-O bonds to Asp 171 and Asp 262. Bad contacts between the protein and metal bicyclam were then relieved by energy-minimising the protein whilst maintaining the original structure for the metal bicyclam. During the minimisation, the side-chains of Asp171 and Asp262 moved into more favourable positions for binding to Zn without additional restraints. A similar procedure was used to optimise the H-bonds between the carboxylate oxygens of Glu288 and the diagonal NH protons on the *cis*-V ring using distance restraints of 2.0 Å and an average force constant of 200 kcal mol^{-1} $Å^{-2}$. WebLab ViewerPro 4 (Molecular Simulations Inc.) and MOLMOL (Version 2K.1)[18] were also used for modelling and graphics.

Table 6.1 Sequence alignment of human CXCR4 and bovine rhodopsin obtained using the homology module of insight II.

```
1F88  :     MNGTEGPNFYVP--FSNKTGVVRSPFEAPQYYL--AEPWQFSMLAAY (1-43)
CXCR4 :       MEGISIYTSDNYTEEMGSGDYDSMKEPCFREENANFNKIFLPTI (1-44)

1F88  : MFLLIMLGFPINFLTLYVTVQHKKLRTPLNYILLNLAVADLFMVFGGFTT (44-93)
CXCR4 : YSIIFLTGIVGNGLVILVMGYQKKLRSMTDKYRLHLSVADLLFVITLPFW (45-94)

1F88  : TLYTSLHGYFVFGPTGCNLEGFFATLGGEIALWSLVVLAIERYVVVCKPM (94-143)
CXCR4 : AVDAVANWYF--GNFLCKAVHVIYTVNLYSSVLILAFISLDRYLAIVHAT (95-142)

1F88  : SNFRF-GENHAIMGVAFTWVMALACAAPPLVGWSRYIPEGMQCSCGIDYY (144-192)
CXCR4 : NSQRPRKLLAEKVVYVGVWIPALLLTIPDFI-FANVSEADDRYICDRFY- (143-190)

1F88  : TPHEETNNESFVIYMFVVHFIIPLIVIFFCYGQLVFTVKEAAA|SATTQK (193-245)
CXCR4 : -P-NDLWVVVFQFQHIMVGLILPGIVILSCYCIIISKLSHSKG--HQ--- (191-233)

1F88  : AEKEVTRMVIIMVIAFLICWLPYAGVAFYIFTHQGSDFGP---------I (246-286)
CXCR4 : -KRKALKTTVILILAFFACWLPYYIGISIDSFILLEIIKQGCEFENTVHK (234-282)

1F88  : FMTIPAFFAKTSAVYNPVIYIMMNKQFRNCMVTTLCCGKNP|STTVSKTE (287-341)
CXCR4 : WISITEALAFFHCCLNPILYAFLGAKFKTSAQHALTSVSRGSSLKILSKG (283-332)

1F88  : TSQVAPA                                           (342-348)
CXCR4 : KRGGHSSVSTESESSSFHSS                               (333-352)
```

6.3 Results

6.3.1 ^{1}H, ^{13}C and ^{15}N NMR of $Zn_2(bicyclam)(ClO_4)_4$ (8) in aqueous solution

^{1}H NMR spectrum of Zn bicyclam perchlorate in 10% D_2O / 90% H_2O acquired on a 600 MHz NMR instrument is very complicated (Figure 6.2). The resonances in the spectrum can be categorised into four types: resonances from the NH protons, resonances from the protons in the bridging aromatic ring, resonances from the bridging CH_2 groups, and resonances from the protons in the cyclam rings. In order to fully assign the ^{1}H NMR spectrum, 2D [^{1}H, ^{1}H] TOCSY and DQF-

COSY, and [^{1}H, ^{13}C] and [^{1}H, ^{15}N] HSQC data were further acquired on a 600 MHz NMR instrument by Dr. John Parkinson. Data for Zn-Bz-cyclam chloride, [Zn(Bz-cyclam)Cl]Cl·2.5$CDCl_3$ are also included for comparison. This complex was prepared by Dr. Stephen Paisey who also acquired the NMR data on it.

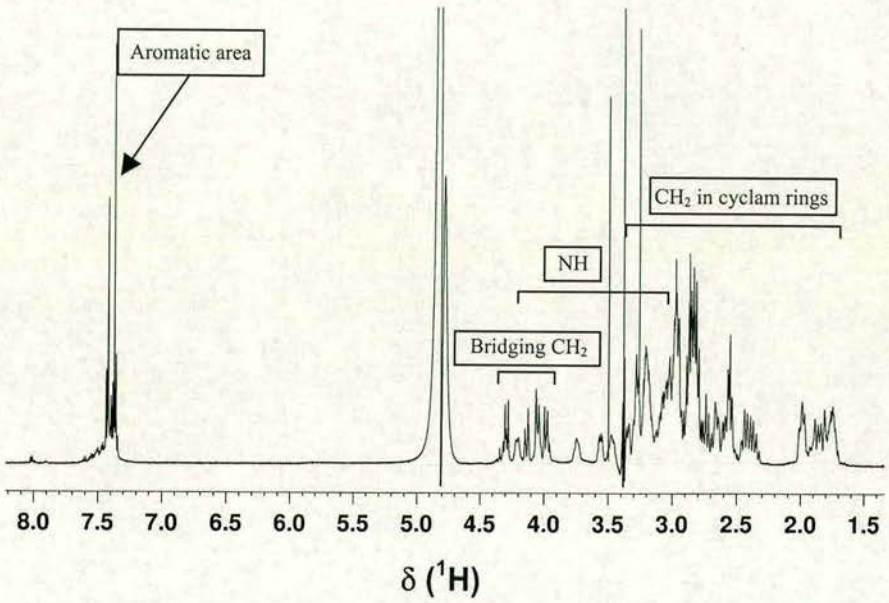

Figure 6.2 ^{1}H NMR spectrum of Zn_2(bicyclam)$(ClO_4)_4$ in 10% D_2O and 90% H_2O

1. NH proton resonances

The 2D [^{1}H, ^{15}N] HSQC NMR data for an equilibrium solution of Zn bicyclam perchlorate in 10% D_2O / 90% H_2O show the presence of 9 ^{1}H/^{15}N correlations (Figure 6.3a and Table 6.2). NH_F, NH_G and NH_H (designated by triangles) have very low intensity and therefore belong to the same group. [^{1}H,^{1}H] COSY and TOCSY data show that the other NH protons fall into the following two groups: NH_A, NH_B and NH_D (designated by squares); NH_C, NH_E and NH_I (designated by circles) (Figures 6.4 and 6.5).

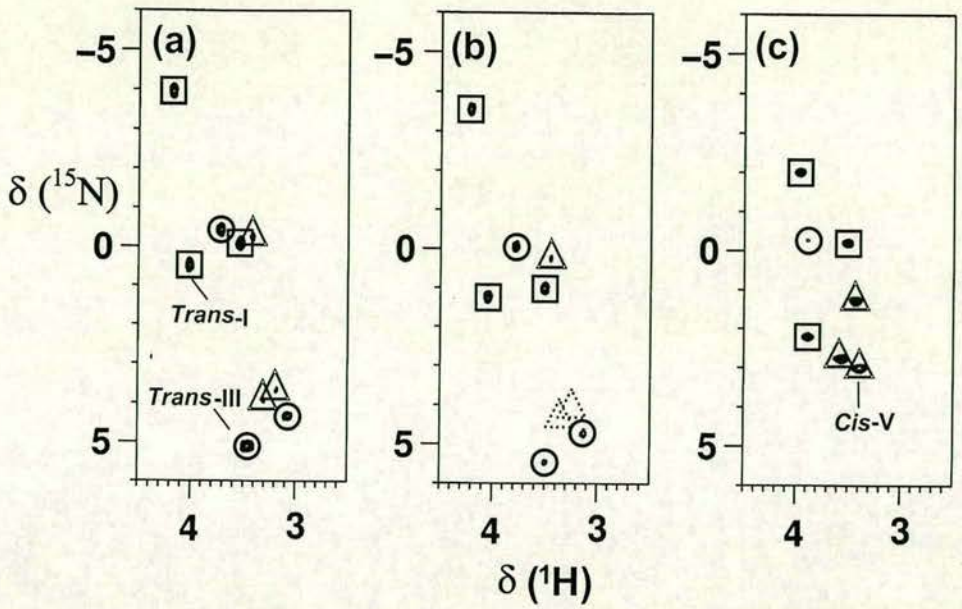

Figure 6.3 Comparison of [^{1}H, ^{15}N] HSQC spectra of (a) Zn bicyclam perchlorate (**8**), (b) Zn-Bz-cyclam chloride, and (c) Zn bicyclam acetate (**9**) in 10% D_2O / 90% H_2O. In each case, 3 sets of NH peaks can be identified (due to their connectivities in COSY and TOCSY spectra, and by integration) corresponding to 3 major cyclam configurations, *trans*-I, *trans*-III and *cis*-V. Peaks for the latter are strong only for complex **9**.

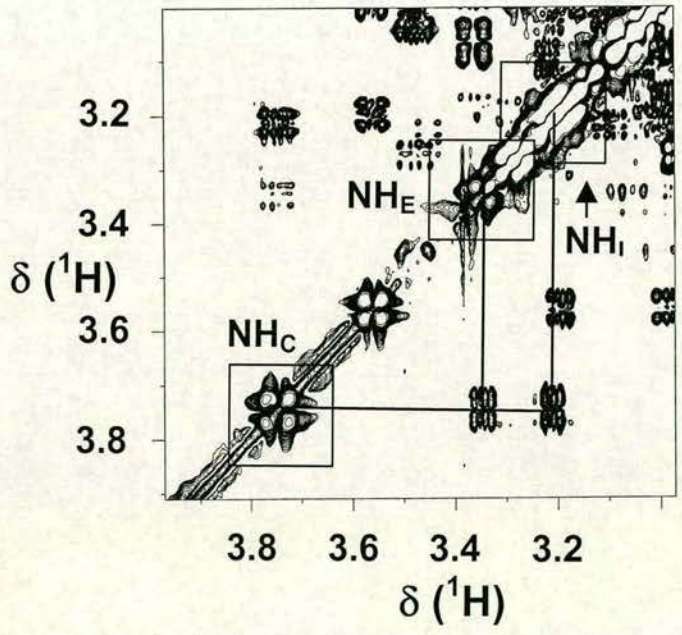

Figure 6.4 2D [^{1}H,^{1}H] TOCSY NMR spectrum of NH region for Zn_2(bicyclam)$(ClO_4)_4$ in 10% D_2O/90% H_2O

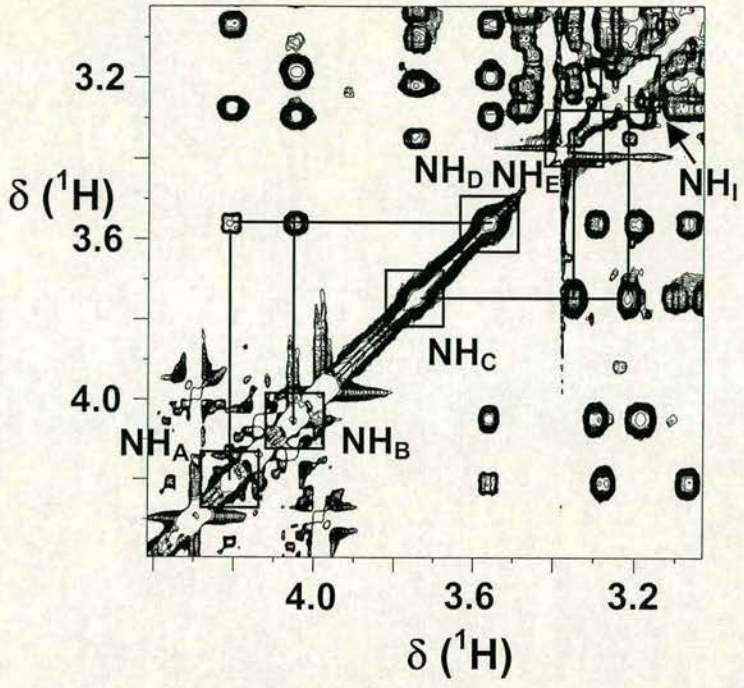

Figure 6.5 2D [^{1}H,^{1}H] TOCSY NMR spectrum of NH region for Zn_2(bicyclam)$(ClO_4)_4$ in 10% D_2O and 90% H_2O

Table 6.2 ^{1}H and ^{15}N NMR data for Zn bicyclam perchlorate in 10% D_2O / 90% H_2O, at equilibrium.

	Chemical Shift (ppm)	
Peak Label	**^{1}H**	**^{15}N**
NH_A	4.20	-4.00
NH_B	4.04	0.04
NH_C	3.74	-0.04
NH_D	3.55	-0.01
NH_E	3.46	4.80
NH_F	3.42	-0.24
NH_G	3.30	3.93
NH_H	3.18	3.67
NH_I	3.08	4.20

2. Bridging methylene proton resonances

Six resonances for bridging methylene protons are clearly visible in the 2D [^{1}H,^{13}C] HSQC NMR spectrum (Figure 6.6a): **M1** and **M6** are a geminal pair (δ ^{1}H/^{13}C: 4.29/58.8 and 3.97/58.8, respectively); **M2** and **M5** are a geminal pair(δ ^{1}H/^{13}C: 4.28/56.2 and 3.97/56.2 respectively); **M3** and **M4** are a geminal pair (δ ^{1}H/^{13}C: 4.12/52.0 and 4.04/52.0 respectively). In this data set, **M1** and **M6** are of lower intensity compared with the other methylene CH_2 resonances.

M3 and **M4** show nOes to **Ar(1)** from one cyclam ring (δ ^{1}H: 7.37) and **M2/M5** show nOes to another cyclam ring **Ar(2)** (Figure 6.7). Hence it is apparent that the two main configurations of bicyclam involve **M2/M5** and **M3/M4**, respectively and the minor configuration involve **M1/M6** which can not be observed in the [^{1}H,^{1}H] NOESY NMR spectrum (Figure 6.7).

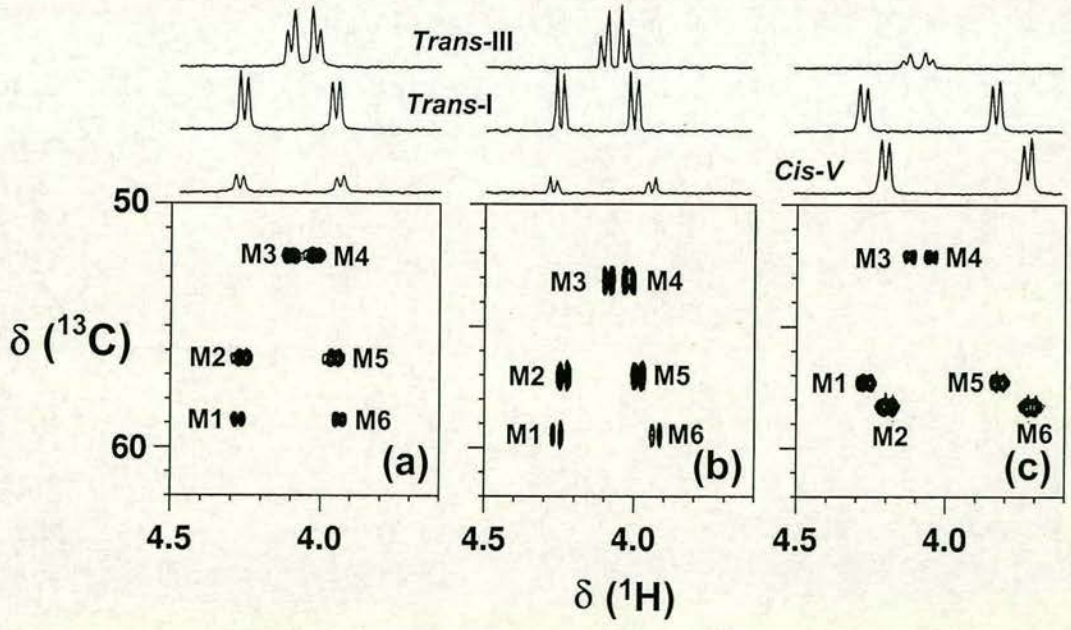

Figure 6.6 2D [^{1}H, ^{13}C] HSQC NMR spectra of the aromatic ring linker CH_2 region for (a) Zn bicyclam perchlorate (**8**), (b) Zn-Bz-cyclam chloride, and (c) Zn bicyclam acetate (**9**). Top: slices taken at each of the 3 ^{13}C chemical shifts showing the 2 non-equivalent geminal protons.

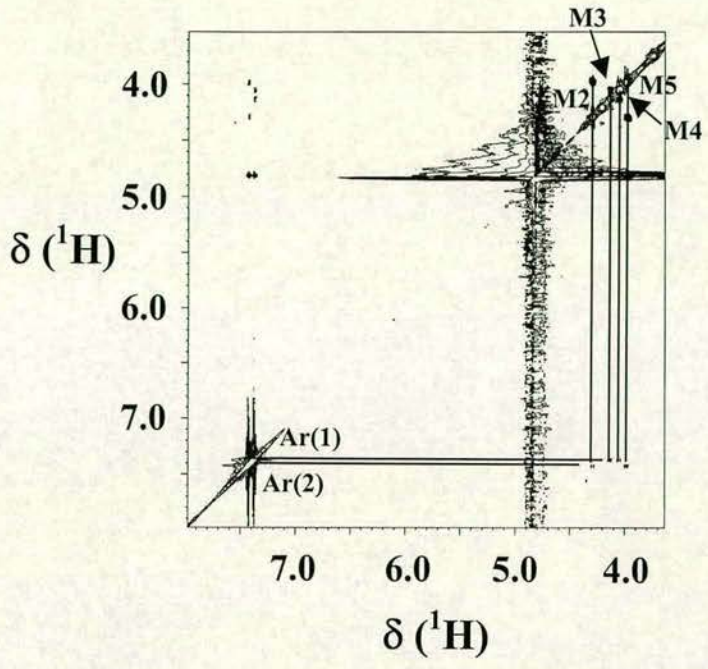

Figure 6.7 2D [^{1}H,^{1}H] NOESY NMR spectrum of aromatic and linker CH_2 regions for Zn_2(bicyclam)$(ClO_4)_4$ in 10% D_2O and 90% H_2O.

3. Proton resonances from the cyclam rings

Three sets of NH peaks and three sets of linking CH_2 groups show that there are three types of cyclam rings, which are designated here as **I**, **III** and **V**, present in the solution of Zn_2(bicyclam)$(ClO_4)_4$ in 10% D_2O / 90% H_2O. It is therefore possible for a mixture of **I-I**, **I-III**, **I-V**, **III-III**, **III-V** and **V-V** bicyclam molecules to coexist in solution. Two types of cyclam rings, **III** and **I** predominate, which relate to **M3/M4;** and **M2/M5,** respectively. The third type of cyclam ring, which relates to **M1/M6**, is minor. Of particular interest are **M3/M4** from configuration **III**. These appear in the data for Zn bicyclam acetate in aqueous solution at equilibrium at a much lower concentration but at identical $^1H/^{13}C$ chemical shifts. It was not possible to elucidate the nature of the configuration to which **M3** and **M4** belonged in the Zn

bicyclam acetate case. From the 2D [^{1}H,^{1}H] TOCSY and COSY, and [^{1}H,^{13}C] HSQC spectra, the detailed conformational information was required for configuration **III** for Zn_2(bicyclam)$(ClO_4)_4$ in solution (see Appendix I). A model for the *trans*-III configuration was set up based on the NMR data (Figure 6.8).

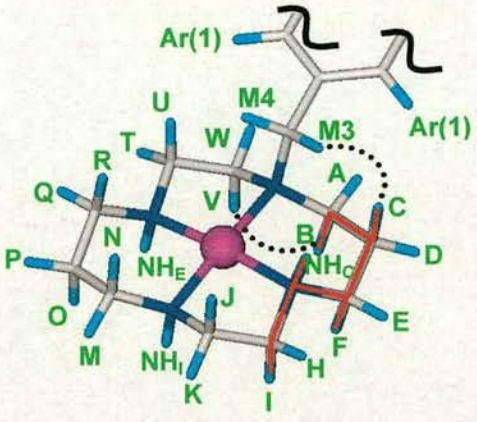

Figure 6.8 Model of *trans*-III configuration for Zn_2(bicyclam)$(ClO_4)_4$ in aqueous solution. Dotted black lines denote selected observed NOESY interactions and solid red lines refer to strong ^{1}H, ^{1}H COSY NMR interactions.

6.3.2 Solution ^{1}H, ^{13}C and ^{15}N NMR of $[Zn_2(bicyclam)(OAc)_2](OAc)_2 \cdot 2CH_3OH$ (9)

The ^{1}H NMR spectrum of crystalline complex **9**, $[Zn_2(bicyclam)(OAc)_2](OAc)_2 \cdot 2CH_3OH$ was acquired in 10% D_2O / 90% H_2O at equilibrium (Figure 6.9). The resonances in the spectrum can be categorised into four types: resonances from the NH protons, resonances from the protons in the bridging aromatic ring, resonances from the bridging CH_2 groups, and resonances from the protons in the cyclam rings. The resonances in the whole spectrum overlap severely. In order to fully assign the ^{1}H NMR spectrum, 2D [^{1}H, ^{1}H] TOCSY and DQF-

COSY, and [^{1}H, ^{13}C] and [^{1}H, ^{15}N] HSQC data were further acquired on the 600 MHz instrument by Dr. John Parkinson.

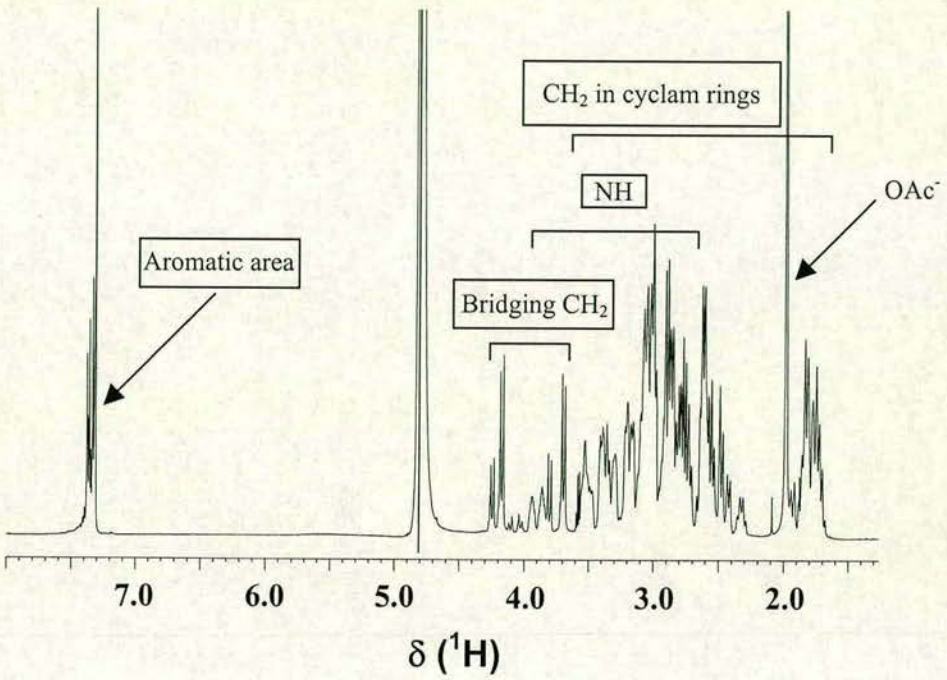

Figure 6.9 ^{1}H NMR spectrum of $[Zn_2(bicyclam)(OAc)_2](OAc)_2$ in 10% D_2O and 90% H_2O

1. NH proton resonances

The 2D [^{1}H, ^{15}N] HSQC NMR data show the presence of 9 ^{1}H/^{15}N correlations (Figure 6.3c and Table 6.3). From the volume integral values shown in Table 6.3, the NH signals can be grouped as follows: **ABD**, **CEF**, and **GHI**. Analysis of these data in their most basic form leads to the conclusion that there are 3 types of cyclam ring, which are designated here as **I**, **III** and **V**, present in the solution of Zn bicyclam acetate dissolved in 10% D_2O / 90% H_2O. Two types of cyclam rings, **I** and **V** predominate.

Table 6.3 ^{1}H and ^{15}N NMR data for Zn bicyclam acetate crystals in 10% D_2O / 90% H_2O, at equilibrium

	Chemical Shift (ppm)		**Relative Volume**
Peak Label	**^{1}H**	**^{15}N**	**Integral**
NH_A	3.95	-2.00	1.00
NH_B	3.87	2.30	0.9
NH_C	3.54	2.80	1.37
NH_D	3.48	-0.20	1.06
NH_E	3.40	1.40	1.38
NH_F	3.36	3.00	1.53
NH_G	3.87	-0.30	0.24
NH_H	3.51	4.80	0.20
NH_I	3.15	4.50	0.18

2. Resonances for bridging methylene protons

Three sets of bridging methylene CH_2 signals appeared clearly in both 2D homonuclear [^{1}H, ^{1}H] 2D NMR TOCSY and DQF-COSY data, and 2D [^{1}H, ^{13}C] HSQC NMR data (Figure 6.3c): **M1** and **M5** (δ $^{1}H/^{13}C$: 4.26/57.4 and 3.81/57.4 respectively); **M3** and **M4** (δ $^{1}H/^{13}C$: 4.12/52.1 and 4.04/52.1 respectively); **M2** and **M6** (δ ^{1}H/δ ^{13}C: 4.19/58.3 and 3.70/58.3 respectively). The integrals of these sets of peaks follow the order **M2**/**M6** > **M1**/**M5** >> **M3**/**M4**. Hence the $^{1}H/^{13}C$ NMR data

for the bridging methylene groups matches that of the $^{1}H/^{15}N$ data in relative intensities and supports the assertion that two main types of cyclam ring configuration co-exist in solution with a third configuration present to a lesser extent.

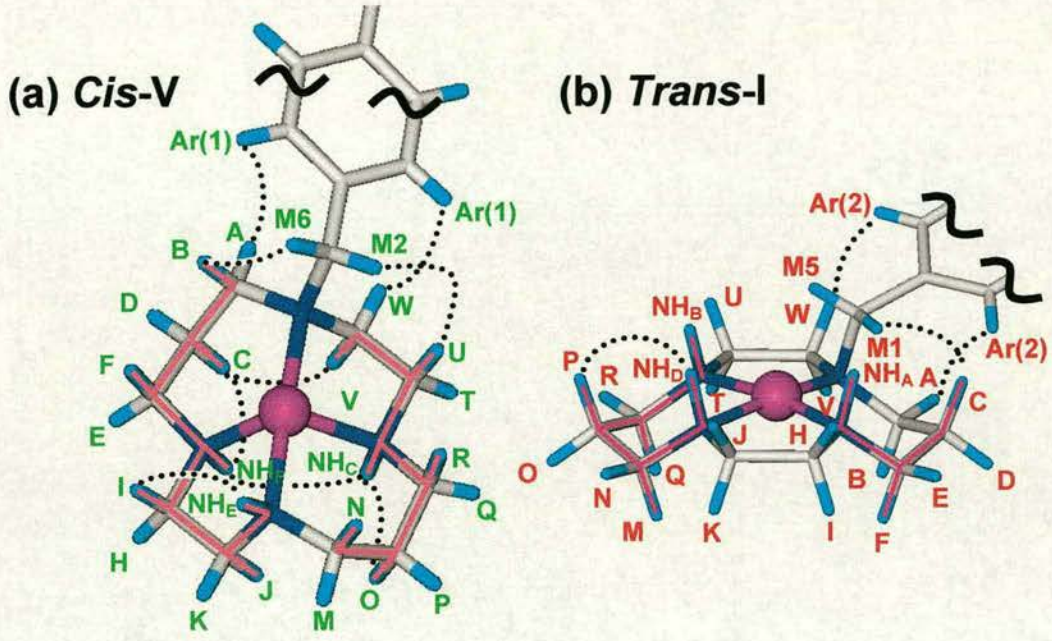

Figure 6.10 Models of *cis*-V and *trans*-I configurations for $[Zn_2(bicyclam)(OAc)_2](OAc)_2$ in aqueous solution. Dotted black lines denote selected observed NOESY interactions and solid red lines refer to strong ^{1}H, ^{1}H COSY NMR interactions.

3. Proton resonances in the cyclam rings

Three sets of NH peaks and three sets of linking CH_2 groups show that there are three types of cyclam rings, which are also from three configurations **I**, **III** and **V**, present in the solution of $[Zn_2(bicyclam)(OAc)_2](OAc)_2$ in 10% D_2O / 90% H_2O. Two types of cyclam rings, **V** and **I** predominate, which relate to **M2/M6;** and **M1/M5,** respectively. The third type of cyclam ring, which relates to **M3/M4** from

configuration **III**, is minor. From the 2D [^{1}H,^{1}H] TOCSY and COSY, and [^{1}H,^{13}C] HSQC spectra, the detailed conformation information was acquired for configurations **V** and **I** for $[Zn_2(bicyclam)(OAc)_2](OAc)_2$ in solution (see Appendix II).

4. Proton resonances for the aromatic ring

The assignment of the aromatic ^{1}H NMR resonances is completely dependent on a knowledge of the assignment of the rest of the ^{1}H NMR data. The relationship between the cyclam ring and the aromatic ring is given only by nOes.

Two large nOes exist between the aromatic protons and proton resonances assigned to configuration **V**. An aromatic resonance **Ar(1)** (δ ^{1}H: 7.33) shows strong nOes to both **A** and **W** in green colour for configuration **V** in Figure 6.10a.

Another aromatic resonance **Ar(2)** (δ ^{1}H: 7.37) also shows nOes to **T** and **W** in red colour for configuration **I** shown in Figure 6.10b.

6.3.3 Crystallography

The crystal structure of $[Zn_2(bicyclam)(OAc)_2](OAc)_2{\cdot}2CH_3OH$ (**9**) was determined by single crystal X-ray crystallography. The crystal structure of the complex cation along with the atom-labelling scheme is shown in Figure 6.11a. Selected bond lengths and angles are listed in Table 6.4. The crystal structure of complex **9** comprises $[Zn_2(bicyclam)(OAc)_2]^{2+}$ cations, acetate anions and MeOH molecules as solvent of crystallisation. The aromatic linker symmetrically bridges the cyclam rings. Each monocyclam ring resides on a centre of inversion, is folded diagonally about N (4)/N (11) and adopts a *cis*-V configuration with chelation by acetate on one cyclam face and double H-bonding on the other. Five- and six-

membered rings are in gauche and chair conformations, respectively. Zn(II) has a distorted octahedral geometry.

Table 6.4 Selected bond distances (Å) and angles (°) for complex **9**

Zn(1)–N(1)	2.252(2)	N(4)–Zn(1)–N(11)	105.32(10)
Zn(1)–N(4)	2.087(3)	N(4)–Zn(1)–N(1)	83.37(9)
Zn(1)–N(8)	2.161(3)	N(11)–Zn(1)–N(1)	93.94(9)
Zn(1)–N(11)	2.071(2)	N(8)–Zn(1)–N(11)	83.49(10)
Zn(1)–O(11A)	2.089(2)	N(8)–Zn(1)–N(1)	174.67(4)
Zn(1)–O(12A)	2.407(2)	O(11A)–Zn(1)–O(12A)	58.34(8)

Table 6.5 Distances (Å) and angles (°) for possible hydrogen bonds in complex **9**

D–H···A	H···A (Å)	D···A (Å)	∠ D–H···A
N(4)–H(4) ··· O(11B)[a]	2.06	2.953(3)	162
N(8)–H(8B) ··· O(1C)[b]	2.06	2.972(4)	168
N (11)–H(11B) ··· O(12B)[a]	1.90	2.831(4)	174
O (1C)–H(1C) ··· O(11B)[c]	1.81(2)	2.697(4)	168(4)

Symmetry transformations used to generate equivalent atoms:

a = -x+1, -y+1, -z; b = x, y+1, z-1; c = -x, -y, z+1

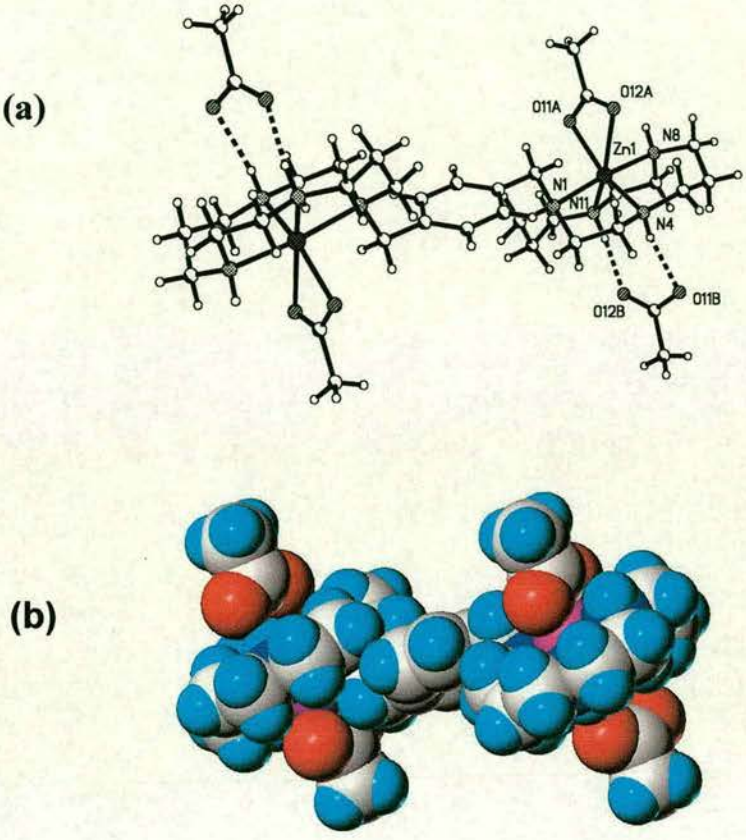

Figure 6.11 (a) X-ray crystal structure of $[Zn_2(bicyclam)(OAc)_2](OAc)_2 \cdot 2CH_3OH$ (**9**) (CH_3OH not shown). (b) Space-filling model.

A notable feature of the structure is the pair of relatively strong H-bonds N(4)H(4) ···O(11B) (2.06 Å, 162° and N(11)H(11) ···O(12B) (1.90 Å, 174°) between acetate oxygens of a non-coordinated acetate anion and cyclam NH protons on the cyclam face opposite to coordinated acetate (Figure 6.11). On the coordination side, N(8)H(8B) forms an H-bond to solvent MeOH (2.06 Å, 168°). The H-bond interactions of methanol molecules and acetate anions with NH protons of cyclam units link the bicyclam complex molecules into a supramolecule (Figure 6.12). All

these H-bonds also stabilise the supramolecular polymer. Hydrogen bond data are also listed in Table 6.5.

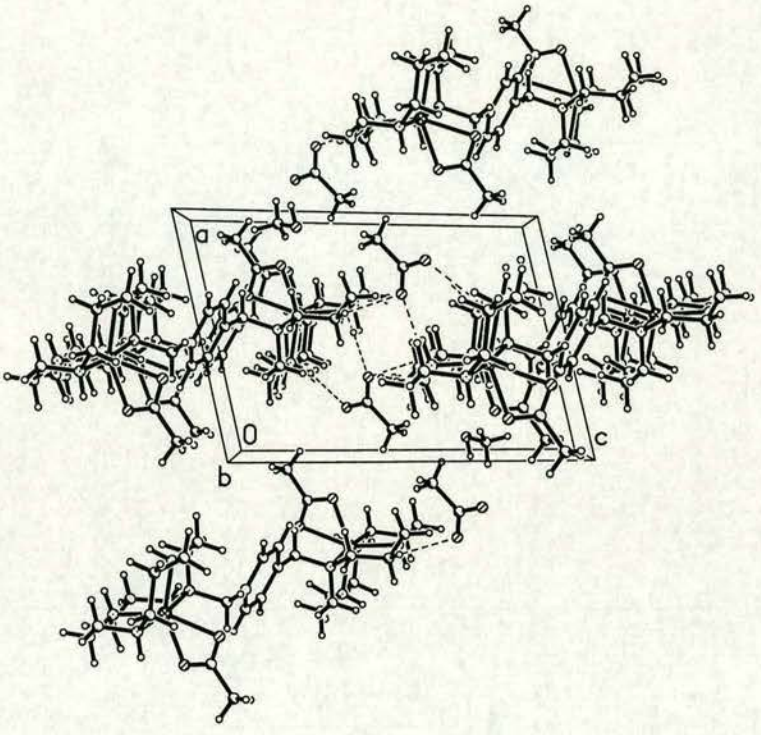

Figure 6.12 Crystal packing of $[Zn_2(bicyclam)(OAc)_2](OAc)_2 \cdot 2CH_3OH$ (**9**).

6.3.4 Kinetic studies

Aqueous solutions of **8** attained equilibrium in ca. 6 h, and consisted of ca. 45 % *trans*-I, 34 % *trans*-III and 21 % *cis*-V, determined from integration of the ^1H NMR peaks for the linker CH_2 protons (see Figure 6.6a). These configurational changes had half-lives of 14-87 min at 298 K (Figure 6.13). The solid lines in Figure 6.13 represent best fits to the data and the following rate constants: k_1, 3.58×10^{-3} min^{-1}; k_{-1}, 6.01×10^{-3} min^{-1} for forward and reverse rate constants of the *trans*-III/*cis*-

V equilibrium, and k_2, 8.07×10^{-3} min^{-1}; k_{-2}, 6.35×10^{-3} min^{-1} for the *trans*-III/*trans*-I equilibrium (assuming each end of bicyclam behaves independently).

Complex **9** adopts the *cis*-V/*cis*-V conformation in the crystal. After dissolution of the crystalline in 90% H_2O / 10% D_2O, equilibrium was reached rapidly within 20 minutes (Figure 6.14). The distribution of three configurations *cis*-V (58%), *trans*-I (35%) and *trans*-III (7%) was acquired by integration of the corresponding resonance of the linker methyl protons in ^1H NMR spectrum at equilibrium (Figure 6.6c). At the same time, the percentages of the predominating *cis*-V/*trans*-I configuration (44%) and *cis*-V/*cis*-V, the crystal configuration, accounting for ca. 29% of the total bicyclam configurations were also obtained by integration of the resonances of the aromatic region in the ^1H NMR spectrum. The curves in Figure 6.14 represent fits but the rates are ca. 10x faster and there are too few data points in the early stages to provide reliable rate constants.

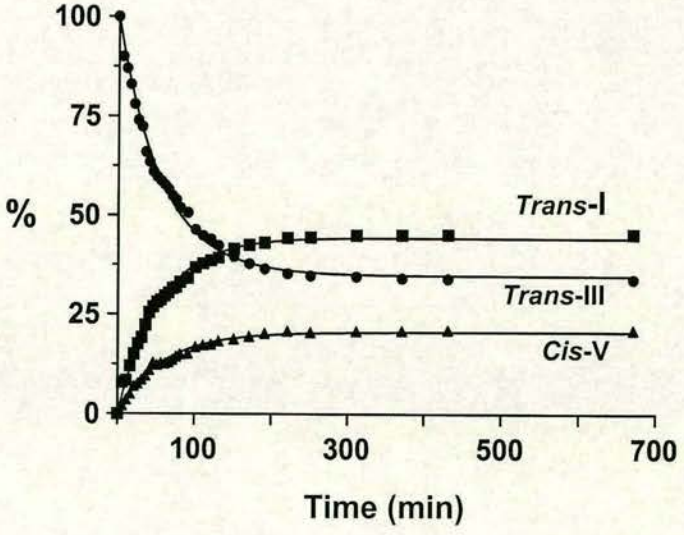

Figure 6.13 Dependence of the distribution of configurations of **8** (perchlorate complex) on time after dissolving in 10% D_2O/90% H_2O.

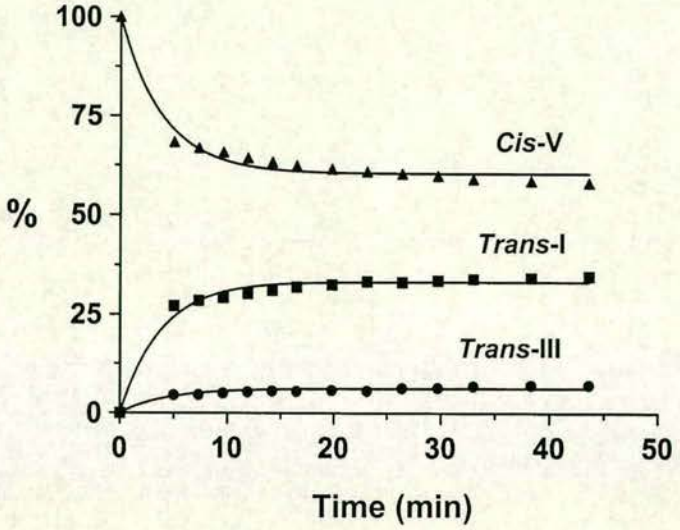

Figure 6.14 Dependence of the distribution of configurations of crystalline **9** (acetate complex) on time after dissolving in 10% D_2O / 90% H_2O.

6.3.5 Effect of acetate on Zn_2(bicyclam)$(ClO_4)_4$

Addition of acetate to aqueous solutions of **8**, Zn_2(Xyl-bicyclam)$(ClO_4)_4$ produced dramatic changes in the ^{1}H NMR spectrum, as illustrated in Figure 6.15 for the aromatic linker resonances. Equilibria were reached within 1 h (at 298 K). The proportion of the *cis*-V/*cis*-V configuration increased from 0 % to ca. 19% on addition of 4 mol equivalents of acetate, and that of the *cis*-V/*trans*-I configuration from 26% to 38% (Figure 6.16). The aromatic resonances are sensitive to both of the attached cyclam units, being singlets when the two units are the same, but AB quartets when they are different. Acetate induces a marked increase in the proportion of *cis*-V/*cis*-V and *cis*-V/*trans*-I species (see Figure 6.16).

Acetate binding to Zn_2-bicyclam was shown by ^{13}C. The ^{13}C NMR resonance for ^{13}C-labelled $CH_3{}^{13}\underline{C}OONa$ in the absence of **8** appears at 183.49 ppm relative to internal dioxane (69.3 ppm). Gradual addition of $CH_3{}^{13}\underline{C}OO^-$ to **8** until 1:4 molar

ratio of $CH_3{}^{13}\underline{C}OO^-$ to **8** resulted in the gradual shift of the $CH_3{}^{13}\underline{C}OO^-$ resonance to high frequency (184.13 ppm) (Figure 6.17). However, further reverse addition of **8** to this solution resulted in a gradual reverse shift of the signal to 183.73 ppm at a 12:4 molar ratio of $CH_3{}^{13}\underline{C}OO^-$ to **8**. Only one ^{13}C peak was observed, indicative of fast exchange on the NMR timescale between acetate bound in the first and second coordination spheres and free acetate.

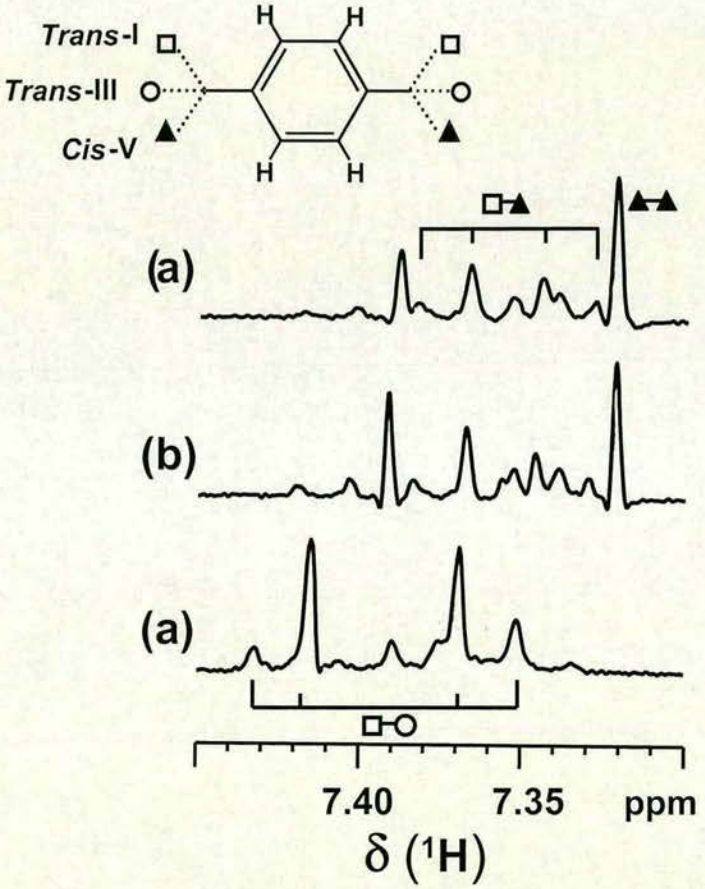

Figure 6.15 Effect of acetate on the configurations of the cyclam rings of Zn_2-bicyclam. The aromatic linker region of resolution-enhanced ^1H NMR spectra of aqueous solutions of (a) Zn bicyclam perchlorate (**8**), (b) as (a) but after addition of 4 mol equiv of acetate, and (c) crystalline Zn bicyclam acetate (**9**). The solvent was 10% D_2O / 90% H_2O and all samples were at equilibrium. Labels: □ *trans*-I, ○ *trans*-III, ▲ *cis*-V.

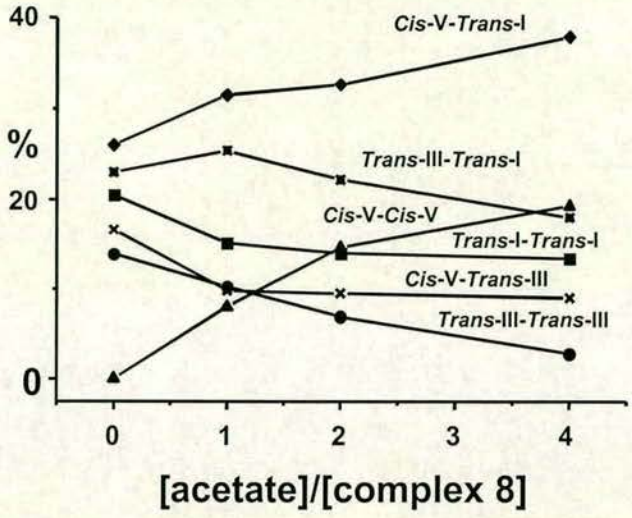

Figure 6.16 Effect of acetate on the distribution of cyclam configurations of Zn_2-bicyclam as determined by integration of the ^1H NMR resonances for the aromatic linker (see Figure 6.15).

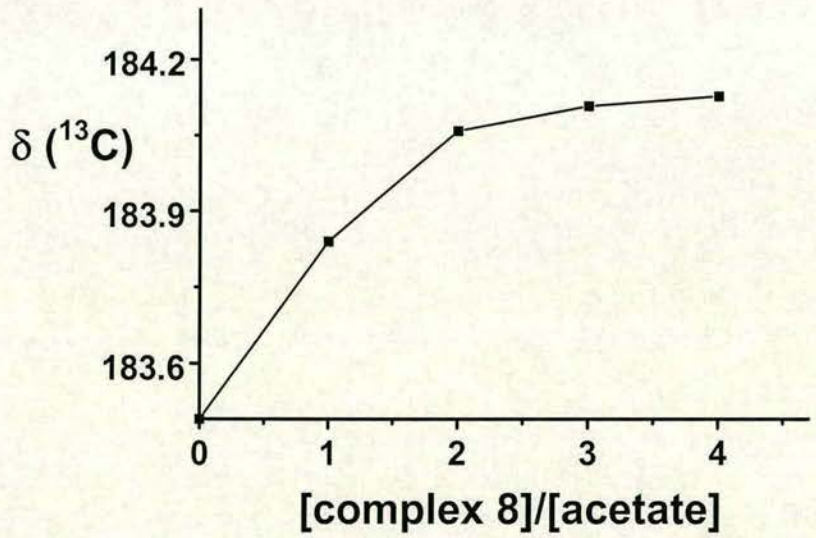

Figure 6.17 Plot of ^{13}C chemical shift versus the molar ratio of **8** : $CH_3{}^{13}COONa$. $CH_3{}^{13}COONa$ (2 mM) was dissolved in 10% D_2O / 90% H_2O (pH 6.6) in the presence of dioxane.

6.3.6 Recognition of zinc bicyclam by the viral coreceptor CXCR4

The *cis*-V/*trans*-I Zn_2-bicyclam model was docked onto an homology model of CXCR4 based on the 7-helical trans-membrane structure of bovine rhodopsin.[10,16] In the energy-minimised model (Figure 6.18 and 6.19), one of the Zn(II) cyclams is in the *cis*-V configuration and has axial coordination to the oxygens of Asp262 with Zn(II)-carboxylate bonds of similar length (2.27 Å) to the average for **9** and double H-bonds between two of its NH groups and the oxygens of Glu288 (COO···H-N, 2.01 Å) on the opposite cyclam face, resembling that in the crystal structure of **9** (Figure 6.11). The second Zn(II) cyclam is *trans*-I with axial coordination to Asp171 (Zn-O 2.28 Å). The *cis*-V cyclam is visible through a channel on one side of the protein (Figure 6.19).

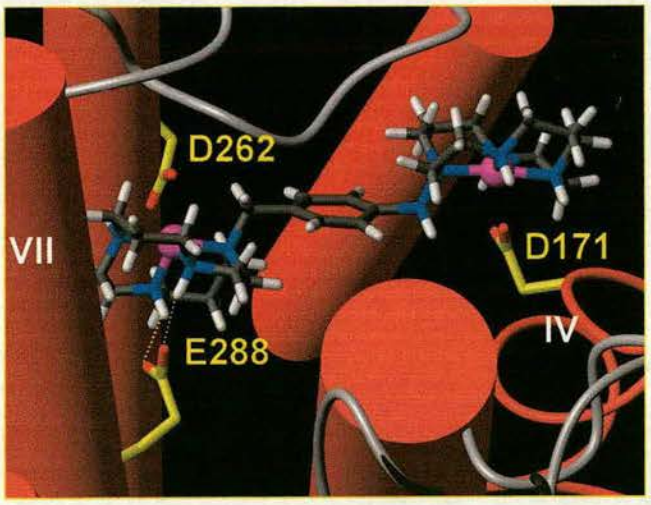

Figure 6.18 Model of Zn_2-bicyclam bound to the CXCR4 coreceptor. Transmembrane helices are red cylinders except helix IV which is depicted as a ribbon for clarity.

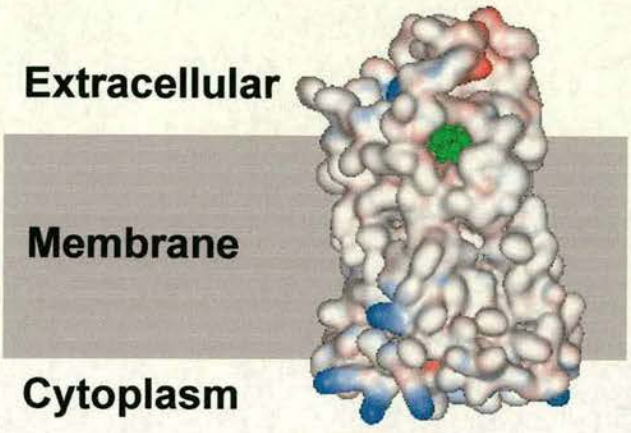

Figure 6.19 View of the model of CXCR4 showing the location of the proposed Zn_2-bicyclam binding site. The likely position of the membrane is indicated in grey, Zn_2-bicyclam is green, electrostatic potentials are coloured blue-positive, red-negative and white-neutral. The unstructured N-terminus (residues 1-38) and C-terminus (residues 320-352) have been omitted.

6.4 Discussion

6.4.1 Conformation of Zn_2(bicyclam)$(ClO_4)_4$ (8) in aqueous solution

Analysis of the NMR spectra of **8** was aided by the assignment of the NMR peaks for a monocyclam complex, Zn(II)-Bz-cyclam chloride, effectively complex **8** with one methylene-Zn(II)-cyclam removed. The X-ray crystal structure of the Zn(II)-Bz-cyclam chloride, [Zn(Bz-cyclam)Cl]Cl·2.5$CDCl_3$ showed it to be 5-coordinate with an axial Cl ligand and NMR data for a $CDCl_3$ solution were consistent with the presence of a single configuration, *trans*-III, as in the crystal. Over a period of 3 h after dissolution of Zn(II)-Bz-cyclam chloride in water at 298 K,

the initially-intense set of peaks assignable to *trans*-III gave rise to 3 sets of peaks (Figures 6.3b and 6.6b) assignable to *trans*-III (43%), *trans*-I (42%; planar 5-membered rings, Figure 1.3) and a minor configuration (15%, possibly *cis*-V). The 2D [^{1}H,^{15}N] (Figures 6.3) and aliphatic region of the 2D [^{1}H,^{13}C] NMR (Figure 6.6) spectra for equilibrium aqueous solutions of Zn-Bz-cyclam chloride and Zn bicyclam perchlorate were almost identical. This suggests that the cyclam units in the bicyclam complex **8** have little influence on each other in aqueous solution. Therefore, the configuration for Zn bicyclam perchlorate in the solid state involving **M3/M4** was assumed to be *trans*-III as in most cyclam complexes.[19,20] The resonances for the other main configuration involving the bridging CH_2 resonances, **M2/M5** was assumed to be *trans*-I, but cannot be well observed due to severe overlap of the NMR signals. The minor configuration involving **M1/M6** was assumed to be *cis*-V. Both *cis*-V and *trans*-I configurations are predominant and well-observed in the acetate Zn bicyclam complex in aqueous solution.

6.4.2 Conformation of $[Zn_2(bicyclam)(OAc)_2](OAc)_2$ (9) in aqueous solution

Three sets of NH peaks and three sets of linking CH_2 groups show that there are also three configurations, *trans*-I, *trans*-III and *cis*-V, present in the solution of $[Zn_2(bicyclam)(OAc)_2](OAc)_2$ in 10% D_2O / 90% H_2O. Over a period of 20 minutes after dissolution of crystalline $[Zn_2(bicyclam)(OAc)_2](OAc)_2$ in water at 298 K, the initially-intense set of peaks from *cis*-V in the solid state gave rise to 3 sets of peaks (Figures 6.3c and 6.6c) assignable to *cis*-V (62%), *trans*-I (32%) and a minor configuration, *trans*-III (6%). It is therefore possible for a mixture of *trans*-I/*trans*-I,

trans-I/*trans*-III, *trans*-I/*cis*-V, *trans*-III/*trans*-III, *trans*-III/*cis*-V and *cis*-V/*cis*-V bicyclam molecules to coexist in solution. When the sample is first dissolved, it quickly changes from pure *cis*-V/*cis*-V to a mixture of *cis*-V/*cis*-V, *cis*-V/*trans*-I and *trans*-I/*trans*-I, with a smaller contribution from *trans*-III/*trans*-III, *trans*-III/*trans*-I and *trans*-III/*cis*-V, all of which exist at equilibrium (based on integration) in the following approximate ratios: *cis*-V/*cis*-V(29%), *cis*-V/*trans*-I (44%), and *trans*-III/*trans*-I(12%) (Figure 6.20).

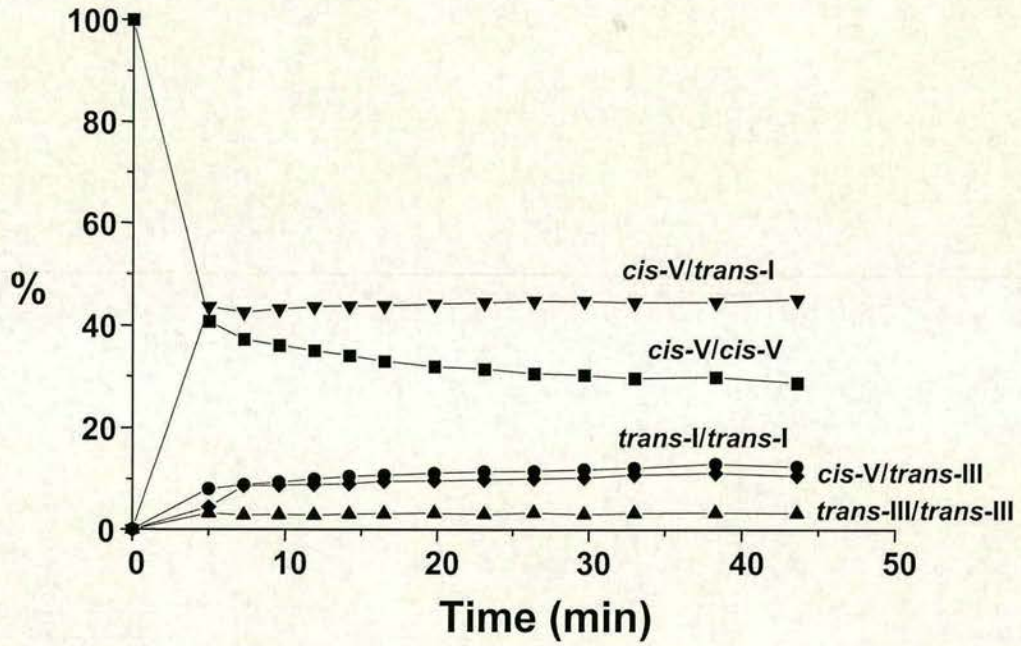

Figure 6.20 Dependence of the distribution of cyclam configurations of crystalline $[Zn_2(bicyclam)(OAc)_2](OAc)_2$ on time after dissolving in 10% D_2O/90% H_2O.

6.4.3 Kinetic studies

As discussed for Zn cyclam complexes in Section 5.4.2, isomerisation from *trans*-III to *cis*-V and *trans*-I (Scheme 6.2) for complex **8** in aqueous solution requires the successive inversion of two amine nitrogens via an intermediate *trans*-II configuration (see Figure 1.3). The formation of *trans*-II configuration is the slow step and determines the rate of isomerisation. *Trans*-II is not stable and converts rapidly to the other configurations. The isomerisation from *cis*-V to *trans*-III and *trans*-I (Scheme 6.2) for complex **9** in aqueous solution also requires the successive inversion of two amine nitrogens via an intermediate *trans*-II configuration (see Figure 1.3). Both steps, from *cis*-V to *trans*-I via *trans*-II, are fast, therefore, the *trans*-I configuration predominates at equilibrium and *trans*-III is minor in aqueous solution at equilibrium due to slow reaction from *trans*-II to *trans*-III.

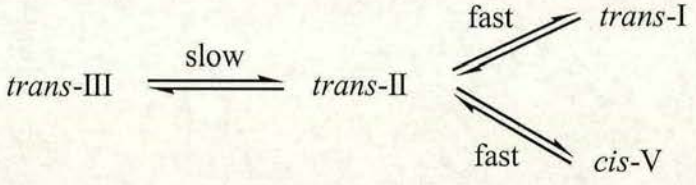

Scheme 6.2 Isomerisation of *trans*-III to *cis*-V and *trans*-I at neutral pH

6.4.4 Acetate triggered rapid configurational change of zinc bicyclam perchlorate

This distribution is very similar to that obtained after addition of 4 mol equivalents of acetate to complex **8** (Figure 6.16). It is evident that acetate stabilises the folded *cis*-V configuration in solution and increases its distribution.

Binding of acetate was confirmed by both ^{13}C NMR studies in the titration of $CH_3{}^{13}COO^-$ with **8** (Figure 6.17), and by ^1H NMR studies in the reverse titration. The increasing proportion of the *cis*-V configuration with addition of sodium acetate to the solution of complex **8** can be explained by strong binding of the carboxylate to Zn^{2+} by chelation. Also, extensive hydrogen bonds can stabilise the *cis*-V configuration. Thus, the *trans*-III configuration in solutions of complex **8** can readily change to the *cis*-V configuration.

6.4.5 $[Zn_2(bicyclam)(OAc)_2](OAc)_2 \cdot 2CH_3OH$ (9) adopts the unusual *cis*-V configuration in the solid state

There are five possible configurations for cyclam complexes (Figure 1.3). Normally, *trans*-III is the most stable configuration and very common. However, only *cis*-V configuration in which the six-membered rings adopts gauche conformation and the six-membered rings adopts the chair conformation was found for each cyclam unit in $[Zn_2(bicyclam)(OAc)_2](OAc)_2 \cdot 2CH_3OH$. Cyclam nitrogens N(1) and N(8) can be considered to occupy axial Zn(II) coordination sites, and N(4) and N(11) and two acetate oxygens the equatorial positions. The equatorial Zn-N bond lengths (2.07, 2.09 Å, Table 1) are normal for Zn cyclam complexes, but the axial bonds are long (Zn-N(1) 2.25 Å, Zn-N(8) 2.16 Å). One of the Zn-O bonds is also long (2.41 Å) compared to the other (2.09 Å) which is normal in length.[17]

The *cis*-V configuration is unusual for Zn cyclam complexes. In a search of the Cambridge Structural Database, I found 46 structures for Zn(II) cyclam complexes: 4 *trans*-I, 33 *trans*-III, 1 *cis*-IV, 1 *trans*-V and 7 *cis*-V, but of the latter, 6 contain highly-constrained cyclams (e.g. N,N linker across macrocycle) and the 7th is

highly substituted on the periphery. No *cis*-V Zn cyclams with carboxylates as ligands appear to have been reported previously. The reported studies on bicyclam complexes have mostly focused on which two monocyclam units are linked together by bridging the carbon atoms of the cyclam backbone by crystallography. It seems that a C-substituent affects the properties of the cyclam units in this type of bicyclam complexes only slightly. Each cyclam unit just like monocyclam still adopts the *trans*-III configuration for such bicyclam complexes as reported in the solid state.[21] Bicyclam complexes in which two monocyclam units are linked together by bridging the amine nitrogen atoms of the cyclam backbone are the other type of bicyclam. No crystals or NMR studies of such bicyclam complexes have been reported.

As shown in Table 6.5, there are four pairs of strong hydrogen-bonding interactions between the secondary amine protons and the two free acetate anions. Such extensive hydrogen bonds may also play an important role in the target protein recognition for anti-HIV bicyclam.

6.4.6 Recognition of zinc bicyclam by the viral coreceptor CXCR4

The high anti-HIV potency of Zn_2-bicyclam can be accounted for by its ability to block the CXCR4 co-receptor via interactions with 3 specific sites, Asp171, Asp262, and Glu288. Asp171 and Asp262 in trans-membrane helices IV and VI, respectively, have already been identified by receptor mutagenesis studies as key sites for bicyclam blocking.[10]

Mutation of Glu288 in helix VII, which may be involved in interactions with the V3 loop of the HIV envelope protein gp120,[22] is relatively close to the cell

surface, impairs coreceptor activity. The hydrophobic para-substituted *p*-phenylenebis(methylene) linker is known to be important for the high anti-HIV activity of cyclams[23] and it is notable that there is a high population of aromatic amino acid side-chains in the extracellular loop regions of our homology model of CXCR4. Aromatic π-π stacking interactions may be important for stabilizing intermediate binding steps along the pathway through the extracellular loops. Lack of loop flexibility prevented docking of Zn_2-bicyclam into a similar site in a CXCR4 model with a C109-C186 disulfide bond analogous to that found in rhodopsin. This might suggest that in *vivo* docking will be enhanced under reducing conditions, a postulate which could be explored in cell systems, and which might have implications for combination therapy.

6.5 References

(1) De Clercq, E., Yamamoto, N., Pauwels, R., Baba, M., Schols, D., Nakashima, H., Balzarini, J., Debyser, Z., Murrer, B. A., Schwartz, D., Thornton, D., Bridger, G., Fricker, S., Henson, G., Abrams, M.; Picker, D. *Proc. Natl. Acad. Sci. USA* **1992**, *89*, 5286.

(2) De Clercq, E. *Mol. Pharmacol.* **2000**, *57*, 833.

(3) May P. M. in *Handbook of Metal-Ligand Interactions in Biological Fluids*; Berthon, G., Ed.; Marcel Dekker Inc.: New York, 1995; vol 2, pp1184.

(4) Moriguchi, Y., Hashimoto, M.; Sakata, K. *Bull. Fukuoka Univ. Education* **1990**, *39*, 43.

(5) Esté, J. A., Cabrera, C., De Clercq, E., Struyf, S., Van Damme, J., Bridger, G., Skerlj, R. T., Abrams, M. J., Henson, G., Gutierrez, A., Clotet, B.; Schols, D. *Mol. Pharmacol.* **1999**, *55*, 67.

(6) Connolly, P. J.; Billo, E. J. *Inorg. Chem.* **1987**, *26*, 3224.

(7) Donnelly, M. A.; Zimmer, M. *Inorg. Chem.* **1999**, *38*, 1650.

(8) (a) Barefield, E. K.; Chueng, D.; Van Derveer, D. G.; Wagner, F. *Chem. Commun.* **1981**, 302. (b) Mochizuki, K. *Chem. Lett.*, **2000**, 26. (c) Kajiwara, T.; Yamaguchi, T.; Kawabata, H. S.; Kuroda, R.; Ito, T. *Inorg. Chem.* **1993**, *32*, 4990.

(9) Ciampolini, M.; Fabbrizzi, L.; Perotti, A.; Poggi, A.; Seghi, B.; Zanobini, F. *Inorg. Chem.*, **1987**, *26*, 3527.

(10) Gerlach, L. O., Skerlj, R. T., Bridger, G. J.; Schwartz, T. W. *J. Biol. Chem.* **2001**, *276*, 14153.

(11) Filali, A.; Yaouanc, J. J.; Handel, H. *Angew. Chem. Int. Ed. Engl.* **1991**, *30,* 560.

(12) Smallcombe, S. H.; Patt, S. L.; Keifer, P. A. *J. Magnetic Resonance, Series A*, **1995**, *117*, 295.

(13) SADABS: Area-Detector Absorption Correction; Siemens Industrial Automation, Inc.: Madison, WI, **1996**.

(14) DIRDIF96 program system. P. T. Beurskens, G. Beurskens, W. P. Bosman, R. de Gelder, S. Garcia-Granda, R. O. Gould, R. Israel and J. M. M. Smits, Crystallography Laboratory, University of Nijmegen, The Netherlands. **1996**.

(15) SHELX97 Programs for Crystal Structure Analysis (Release 97-2). G. M. Sheldrick, Institüt für Anorganische Chemie der Universität, Tammanstrasse 4, D-3400 Göttingen, Germany, **1998**.

(16) Palczewski, K.; Kumasaka, T.; Hori, T.; Behnke, C. A.; Motoshima, H.; Fox, B. A.; Le Trong, I.; Teller, D. C.; Okada, T.; Stenkamp, R. E.; Yamamoto, M.; Miyano, M. *Science* **2000**, *289*, 739.

(17) Kato, M.; Ito, T. *Inorg. Chem.* **1985**, *24*, 509.

(18) Koradi, R.; Billeter, M.; Wüthrich, K. *J. Mol. Graphics* **1996**, *14*, 51.

(19) (a) Ito, T.; Kato, M.; Ito, H. *Bull. Chem. Soc. Jpn.* **1984**, *57*, 2634-2640. (b) Alcock, N. W.; Berry, A.; Moore, P. *Acta Cryst.* **1992**, *C48*, 16-19.

(20) Tyson, T. A.; Hodgson, K. O. *Acta Cryst.* **1990**, *C46*, 1638-1640.

(21) (a) Barefield, E. K.; Chueng, D.; Van Derveer, D. G.; Wagner, F. *Chem. Commun.* **1981**, 302. (b) Mochizuki, K. *Chem. Lett.*, **2000**, 26. (c) Kajiwara, T.; Yamaguchi, T.; Kawabata, H. S.; Kuroda, R.; Ito, T. *Inorg. Chem.* **1993**, *32*, 4990.

(22) Brelot, A.; Heveker, N.; Montes, M.; Alizon, M. *J. Biol. Chem.* **2000**, *275*, 23736.

(23) Bridger, G. J.; Skerlj, R. T.; Padmanbhan, S.; Martellucci, S. A.; Henson, G. W.; Struyf, S.; Witvrouw, M.; Schols, D.; De Clercq, E. *J. Med. Chem.* **1999**, *42*, 3971.

Chapter 7. Interaction of Zn Bicyclam Complexes with a Model Protein Target

7.1 Introduction

It was demonstrated recently that AMD3100 inhibits HIV entry through the coreceptor CXCR4.[1] CXCR4 is a G-protein-coupled, 7-transmembrane domain receptor with a disulfide bridge (-S-S-) between positions (109 and 178). Recent experiments have revealed that the affinity of the bicyclam AMD3100 to the target protein CXCR4 is dependent on both Asp171 and Asp262 residues of CXCR4.[2] Cyclam has a strong propensity to interact with carboxylate groups which suggests that each of the cyclam moieties of the bicyclam binds to each of these two Asp residues located in TM-IV and TM-VI of CXCR4, respectively.[2]

Lysozyme is a relatively small secretory enzyme (129 residues, 14 KD) that catalyses the hydrolysis of specific kinds of polysaccharides comprising the cell walls of bacteria and exceptionally abundant in egg whites. Hen egg white lysozyme (HEWL) was the first enzyme to have its three-dimensional structure determined by X-ray diffraction techniques.[3] The primary structure of HEWL is a single polypeptide chain of 129 amino acids. It has an alpha+beta fold, consisting of five to seven alpha helices and a three-stranded antiparallel beta sheet (Figure 7.1). The enzyme is approximately ellipsoidal in shape, with a large cleft on one side forming the active site. There are four pairs of cysteines that form disulfide bridges (-S-S-) between amino acid residue

positions 6 and 127, 30 and 115, 64 and 80, and 76 and 94. HEWL forms globular and compact particles rigidified by four disulfide bonds.[4,5] The most reactive groups of lysozyme are the carboxyl groups of glutamic acid at position 35 (Glu35) and aspartic acid at position 52 (Asp52).[6] Parsons and Raftery determined experimentally that Asp52 and Glu35 are the important carboxyls by determining the enzymatic activity of hen egg white lysozyme.[7] HEWL binding to various anions,[8] e.g. Cl^- was recently described for high-resolution crystal forms eight chlorides were identified as binding to the residues of lysozyme.[9]

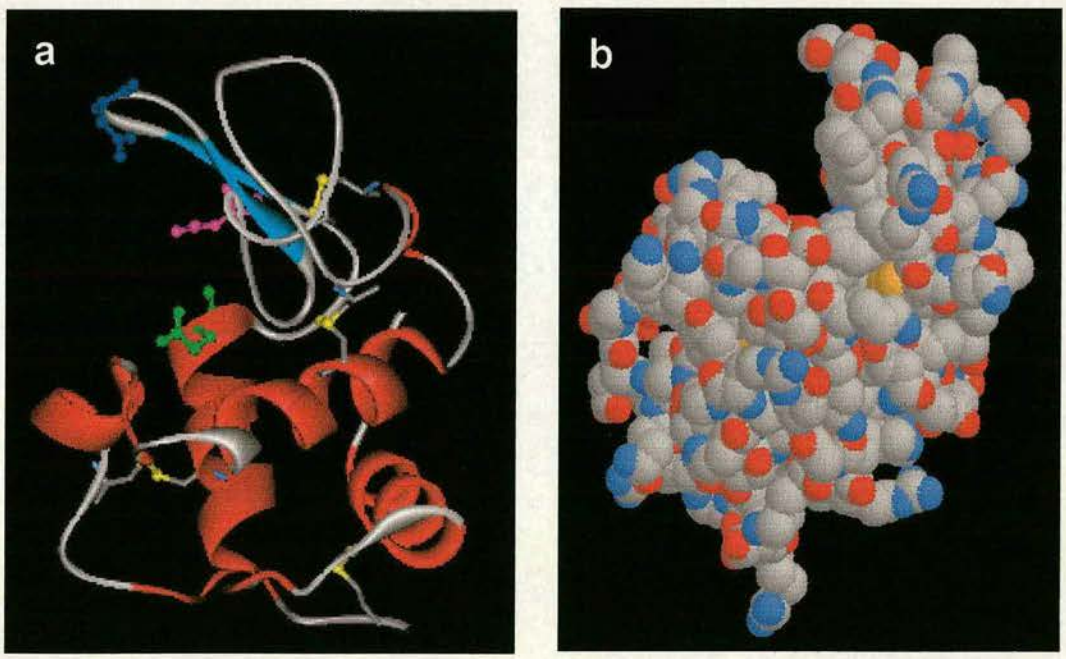

Figure 7.1 (a) Ribbon drawing showing -S-S- disulfide bridges (in yellow), Glu35 (in green), Asp48 (in blue) and Asp52 (in magenta), and (b) showing the cleft which forms the active site of HEWL. The X-ray data were downloaded from the PDB (Code: 193L).

Negatively charged free carboxylate groups of Asp171 and Asp262 act as binding sites in CXCR4. Similarly, Asp52 and Glu35 with free carboxylates form the active site in the large cleft of HEWL and they are close to each other. The cleft allows other molecules to approach these active site residues. In addition, both proteins have disulfide bridges (-S-S-) whose presence in certain secondary structural conformation may result in the interaction of the carboxylate groups of amino acid residues with other molecules. Therefore, HEWL was used as a model protein target in this study of zinc bicyclam interaction.

7.2 Experimental

7.2.1 Crystallisation of lysozyme in the presence of $[Zn_2(bicyclam)(OAc)_2](OAc)_2$

1. Method: The most common method to grow protein crystals is by the hanging drop technique. A few microliters of protein solution are mixed with an about equal amount of reservoir solution containing the precipitants. A drop of this mixture is put on a glass slide which covers the reservoir (Figure 7.2). As the protein / precipitant mixture in the drop is less concentrated than the reservoir solution, water evaporates from the drop into the reservoir. As a result the concentration of both protein and precipitant in the drop slowly increases, and crystals may form.

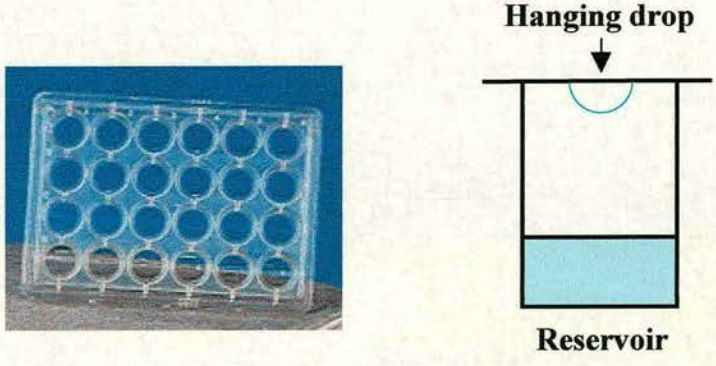

Figure 7.2 A Linbro crystallisation plate (left) and a well with hanging drop (right).

2. Preparation of crystals

The crystals were grown using the hanging drop vapour diffusion method at 277 K in the refrigerator by mixing 2.5 μl of 50 mg/ml HEWL, 2.5 μl of 60.9 mg/ml $[Zn_2(bicyclam)(OAc)_2](OAc)_2$, and 5 μl of reservoir solution containing 100 μl of 0.5 M NaH_2PO_4/Na_2HPO_4 buffer (pH 8.3), 200 μl of saturated NaCl, and 700 μl of distilled water. A further 3 different complex concentrations were prepared and used for the crystal growth by the same method as used for the above samples. The final molar ratios of $[Zn_2(bicyclam)(OAc)_2](OAc)_2$ to HEWL in the hanging drops were 20, 17.5, 15 and 10. The control sample was prepared using the same amount distilled water instead of the complex solution in the drops. A large number of crystals were observed after two days in almost all wells including the controls. All of them have the same shape as shown in Figure 7.3. The crystals were big enough for diffraction after 2 weeks' growth.

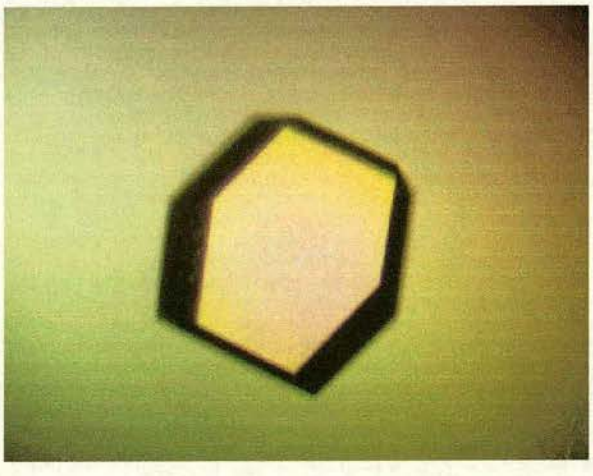

Figure 7.3 The crystal of HEWL grown by hanging up vapour diffusion method in the presence of $[Zn_2(bicyclam)(OAc)_2](OAc)_2$

7.2.2 Microanalysis of the crystals by SEM/EDX spectroscopy

The determination was performed by Dr. Paula McDade in the Department of Geology. Samples of hen egg white lysozyme crystallised in the presence of $[Zn_2(bicyclam)(OAc)_2](OAc)_2$ and a control sample of lysozyme were washed with distilled water. Then a crystal was mounted firmly and coated so they are electrically conductive. The crystal was examined with a scanning electron microscope (SEM, Philips XL30CP) equipped with an energy dispersive X-ray microanalyser (EDX, Oxford Instruments Isis 300). The elemental analysis by EDX was carried out with an acceleration voltage of 20 keV, probe current of 0.3 nA and dead time of 20 - 30%. The take-off angle for the EDX detector was fixed at 35°. These conditions were found to be suitable for good X-ray analysis and allowed reasonable secondary electron imaging. The electron beam was usually directed at the central part of an individual particle to obtain the average composition, and the data were accumulated for 100 s. For the qualitative analysis, an element in the particle was determined when the characteristic X-ray intensity was three times the standard deviation (σ) of the background intensity near the peak. For the quantitative analysis, X-ray analysis data were processed by a standardless $\phi(\rho z)$ routine supplied by Horiba, and the results were normalised to 100% on the basis of oxide composition.[10]

7.2.3 ESI-MS

ESI-MS spectra were acquired on a Platform II mass spectrometer (Micromass, Manchester, U.K). A collision energy of 4 eV, a source temperature of 353 K, a

capillary voltage of 1.5 kV, and a cone voltage of 90 V were applied to produce the spectrum. The protein sample was dissolved in water at a concentration of 0.35 mM and pH was adjusted to 6.4 using dilute of NaOH. One molar equivalent of lysozyme in the stock solution was added in Zn_2(bicyclam)$(ClO_4)_2$ aqueous solution (0.5 mM) to achieve a concentration of 0.21 mM. The mixture was further diluted by a mixed solvent (1:1 (v/v) acetonitrile/water) and then 10-20 μl sample was injected using a syringe pump.

7.3 Results and Discussion

7.3.1 Microanalysis of the crystals by SEM/EDX spectroscopy

Figure 7.4 shows EDX spectra for crystals of hen egg white lysozyme grown in the presence of Zn_2(bicyclam)$(ClO_4)_2$, and for hen egg white lysozyme itself. Four elements, C, O, S and Cl were detected with high intensity.

Trace amounts of Si was also detected in both spectra. Both Na and Zn have very low intensity in spectrum (a) in Figure 7.4. However, elements, Na and Zn have higher intensity in spectrum (b) in Figure 7.4.

It can be seen in Figure 7.4 (a), that the elements, S and Cl, are predominant in the crystals of lysozyme itself, while elements Zn and Na are minor. These results are consistent with the elemental composition of lysozyme. There are four cysteine amino acid residues (8 S atoms) and eight Cl^- anions found in the X-ray crystal structure of HEWL. In Figure 7.4 (b), both elements, S and Cl are still predominant, while the overlapping peaks from Na and Zn increased in intensity. A reasonable explanation for this is that Zn_2(bicyclam)$^{4+}$ is bound to lysozyme and therefore, Zn, not Na, has very high distribution in the crystals of lysozyme with Zn_2(bicyclam)$^{4+}$.

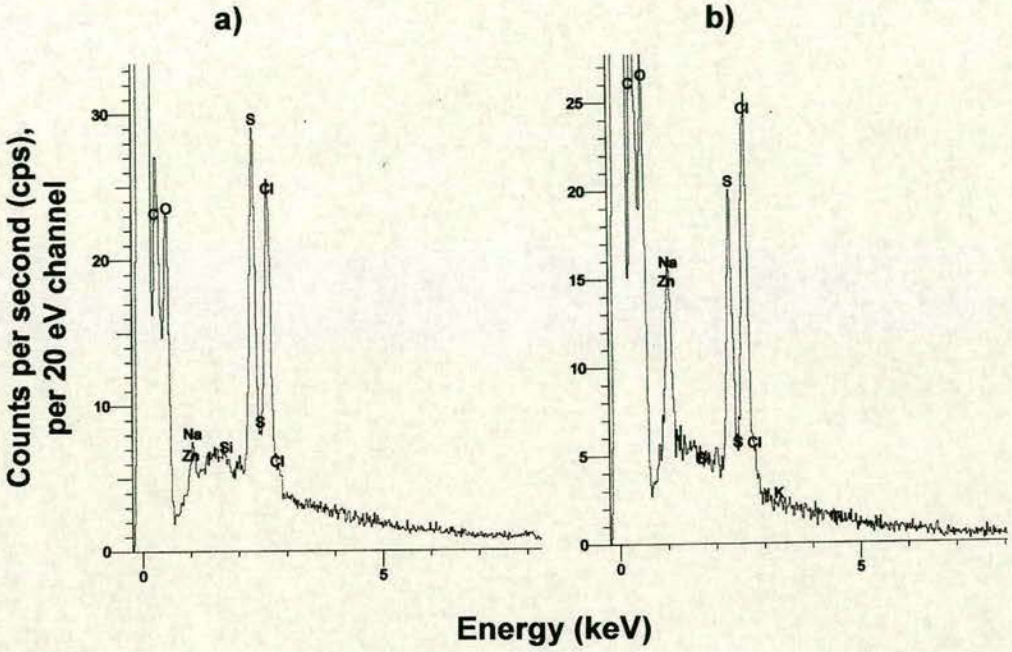

Figure 7.4 EDX spectra of (a) a crystal of hen egg white lysozyme, and (b) a crystal of HEWL grown in the presence of Zn_2(bicyclam)$(ClO_4)_2$

7.3.2 ESI-MS

ESI-MS produces multiply charged gas-phase ions from protein molecules in solution. The mass spectrum of a 1:1 mixture of lysozyme and Zn_2(bicyclam)$(ClO_4)_2$ is shown in Figure 7.5. The spectrum gives two well-resolved series of charged states and two peaks appear with m/z: 14307.73 ± 0.68 and 14943.24 ± 9.04.

The detected ion at *m/z* 14307.73 ± 0.68 (calculated: 14300) is from HEWL, while the ion detected at *m/z* 14943.24 ± 9.04 is from an adduct of the complex $Zn_2(bicyclam)^{4+}$ with the protein. The mass difference between two peaks is 635.51

(calculated for $Zn_2(bicyclam)^{4+}$: 633.4). Therefore, it is likely that Zn^{2+} in cyclam rings binds to three free carboxylate groups of three separate amino acid residues of lysozyme due to the high affinity of $Zn_2(bicyclam)^{4+}$ for carboxylate, most probably Asp52, Glu35, and Asp48. These three amino acid residues are close to one another and in the large cleft of HEWL which allows $Zn_2(bicyclam)^{4+}$ to approach these three amino acid residues. Two of them may bind to one cyclam unit in *trans*-I (or *trans*-III) configuration and the other amino acid residue may bind to the other cyclam unit in *cis*-V configuration. This result confirms that $Zn_2(bicyclam)^{4+}$ does bind to the model target protein lysozyme in solution.

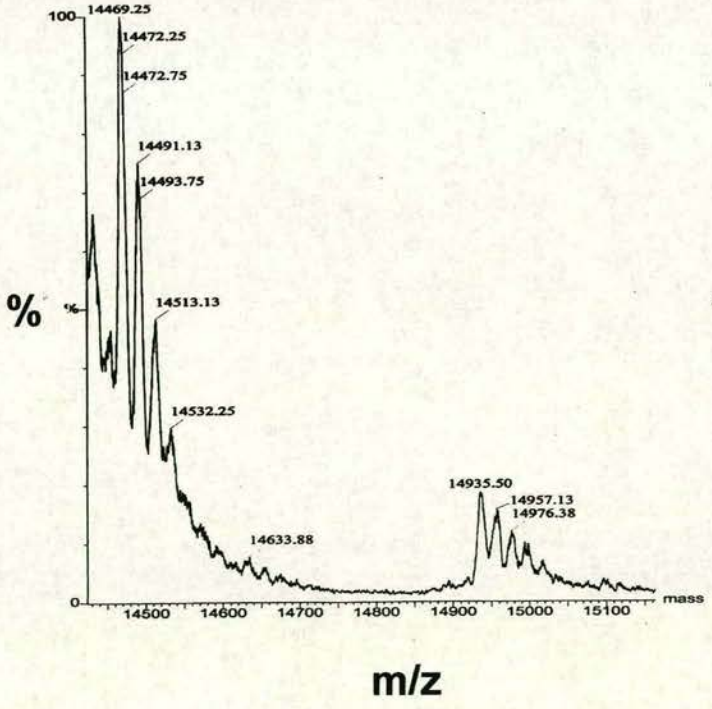

Figure 7.5 ES-MS spectrum of a 1:1 mixture of lysozyme with $Zn_2(bicyclam)(ClO_4)_2$.

7.3.3 X-ray crystallography

X-ray data were collected and a Fourier map calculated. However, no binding bicyclam molecules were observed in the crystal. A reason for this could be that acetate binds Zn(II) in $[Zn_2(bicyclam)(OAc)_2](OAc)_2$ strongly and therefore, carboxylates on the side-chain of the model target protein can not replace the bounded acetates. More work still needs to be done.

7.4 References

(1) (a) Labrosse, B., Brelot, A., Heveker, N., Sol, N., Schols, D., Declercq, E., Alizon, M., *J. Virol.* **1998**, *72*, 6381. (b) Donzella, G. A., Schols, D., Lin, S. W., Este, J. A., Nagashima, K. A., Maddon, P. J., Allaway, G. P., Sakmar, T. P., Henson, G., De Clercq, E. & Moore, J. P. *Nature Medicine*, **1998**, *4*, 72.

(2) Gerlach, L. O., Skerlj, R., Bridgers, G. J. & Schwartz, T. W. *J. Biol. Chem.*, **2001**, *276*, 14153.

(3) Blake, C. C.; Koenig, D. F.; Mair, G. A.; North, A. C.; Phillips, D. C.; Sarma, V. R. *Nature* **1965**, *206*, 757.

(4) Sauter, C.; Otálora, F.; Gavira, J.-A.; Vidal, O.; Giegé, R.; García-Ruiz, J. M. *Acta Cryst.* **2001**, *D57*, 1119.

(5) Vaney, M. C.; Maignan, S.; Riès-Kautt, M.; Ducruix, A. *Acta Cryst.* **1996**, *D52*, 505.

(6) Chipman, D. M.; Sharon, N. *Science* **1969**, *165*, 454.

(7) Parsons, S. M.; Raftery, M. A. *Biochemistry* **1969**, *8*, 4199.

(8)Vaney, M. C.; Broutin, I.; Retailleau, P.; Douangamath, A.; Lafont, S.; Hamiaux, C.; Prangé, T.; Ducruix, A.; Riès-Kautt, M. *Acta Cryst.* **2001**, *D57*, 929.

(9) Dauter, Z.; Dauter, M.; de La Fortelle, E.; Bricogne, G.; Sheldrick, G. M. *J. Mol. Biol.* **1999**, *289*, 83.

(10) Kyotani, T.; Koshimizu, S. *Bull. Chem. Soc. Jpn.* **2001**, *74*, 723.

Chapter 8 Conclusions

8.1 Synthesis of ^{15}N-cyclam and bicyclam

A very convenient and efficient synthesis of (^{15}N)cyclam has been described in Chapter 3. The synthetic route is outlined in the Scheme 1 in Chapter 3. (^{15}N)1,3-Diaminopropane (**2**) was synthesised by the well-known Gabriel method[1] in a modified literature procedure from 1,3-dibromopropane and (^{15}N)phthalimide with subsequent alkaline degradation of the ^{15}N-diphthalimidopropane (**1**). Another ^{15}N source, ^{15}N labelled glycine is commercially available. The amino group of (^{15}N)glycine was protected by a trityl group throughout the reactions where necessary. The formation reaction of (^{15}N)tritylglycine (**3**) was very slow due to the low solubility of trityl chloride in the isopropanol-water solvent system. Therefore, the reaction time was further prolonged and was reduced. As a result, the yield was improved from 61.6% to 77%. The coupling reagent TBTU was employed in the coupling reaction of (^{15}N)1,3-diaminopropane (**2**) and (^{15}N)tritylglycine (**3**), affording (^{15}N)bistritylglycyl)-(^{15}N)diaminopropane (**4**). Reduction of (^{15}N)bistritylglycyl)-(^{15}N)diaminopropane (**4**) with BH_3·THF in refluxing anhydrous THF led (^{15}N)1,11-dityrityl-1,4,8,11-tetraazaundecane **(5)** and subsequent deprotection of (^{15}N)1,11-dityrityl-1,4,8,11-tetraazaundecane **(5)** was achieved by heating (^{15}N)1,11-dityrityl-1,4,8,11-tetraazaundecane **(5)** in the diluted aqueous solution of HCl to give (^{15}N)1,4,8,11-tetraazaundecane·4HCl **(6)**. Purification of (^{15}N)1,4,8,11-tetraazaundecane·4HCl **(6)** was achieved by addition of ethanol to the aqueous solution of (^{15}N)1,4,8,11-tetraazaundecane·4HCl **(6)** to produce a white

precipitate. The aqueous solution of (^{15}N)1,4,8,11-tetraazaundecane·4HCl (**6**) was adjusted by solid NaOH to a pH exceeding 13, and extracted by $CHCl_3$. The following bis-aminal (^{15}N)diacetyl protected 1,4,8,11-tetraazaundecane (**7**) was easily obtained through a simple condensation of butanedione with (^{15}N)1,4,8,11-tetraazaundecane·4HCl (**6**) in CH_3CN. The reaction of 1,3-dibromopropane with (^{15}N)diacetyl protected 1,4,8,11-tetraazaundecane (**7**) in CH_3CN gave (^{15}N)diacetyl protected cyclam (**8**) in good yield. An acid hydrolysis under mild conditions, i.e. diluted HCl solution, released (^{15}N)cyclam tetrahydrochloride. The aqueous solution of (^{15}N)cyclam tetrahydrochloride was washed by benzol, adjusted by solid NaOH to a pH exceeding 13, and extracted by $CHCl_3$. The solution was evaporated to give the final product (^{15}N)cyclam (**9**).

8.2 Conformation of (bi)cyclam complexes

There are five possible configurations for cyclam complexes (Figure 1.3),[2] only three of them are detected for Zn cyclam complexes in aqueous solution (*trans*-I, *trans*-III and *cis*-V). Energy calculations reveal that these three configurations have the lower energy[3] and supports our conclusion. A Ni complex with the tetramethyl substituted cyclam was reported to adopt three configurations *trans*-I, *trans*-III and *trans*-II in aqueous solution.[4] The behaviour of this Ni complex may be affected by the methyl groups and *trans*-II configuration becomes stable instead of *cis*-V which was detected in Zn unsubstituted cyclam complexes. Therefore, it adopts a *trans*-II configuration rather than a *cis*-V configuration in aqueous solution. Alcock and co-workers have detected *trans*-I and *trans*-III configurations for

$[Zn(cyclam)Cl]_n$ by ^{13}C NMR spectroscopy.[5] The reason for the difference from the results in this work could be that *trans*-III can convert to *trans*-I and *cis*-V after dissolving in water, however, *trans*-III still predominates in solution and the amounts of *cis*-V and *trans*-I are very low at equilibrium. Only *trans*-III and *cis*-V are detectable by ^{13}C NMR rather than *trans*-III and *trans*-I since the distribution of *cis*-V is higher than that of *trans*-I and the latter is too low to be detectable. $[Zn(cyclam)(H_2O)_2](OAc)_2$ and $[Zn(cyclam)(phthalate)]_n(CH_3OH)_{2n}$ in the crystals, like the reported Zn cyclam complexes[6], adopt the most stable conformation, *trans*-III in which six membered-rings are in the chair conformation and five membered-rings are in the gauche conformation. However, the *trans*-III configuration which is the most stable conformation for small metal ions is no longer stable for large metals, e.g., Cd(II). $[Pb(cyclam)](NO_3)_2$ with *cis*-V configuration[7] and [Hg(cyclam)Cl]Cl with *trans*-I configuration[8] support our conclusion. Therefore, only other two configurations exist for Cd cyclam complexes. The six-membered rings still adopt the chair conformation as in the solid state and the five-membered rings adopt an eclipsed conformation in solution for the *trans*-I configuration. Cd cyclam adopts the *cis*-I configuration in the solid state after fixing atmospheric CO_2.

The xylylbicyclam AMD3100 has two cyclam rings and three configurations of the cyclam ring, *trans*-I, *trans*-III and *cis*-V are detected in aqueous solution. Bicyclam is therefore a mixture of *trans*-I/*trans*-I, *trans*-I/*trans*-III, *trans*-I/*cis*-V, *trans*-III/*trans*-III, *trans*-III/*cis*-V and *cis*-V/*cis*-V which coexist in aqueous solution. Only two types of cyclam ring (*trans*-I and *cis*-V) predominate for the acetate complex, while *trans*-I and *trans*-III predominate for the perchlorate complex. Two cyclam rings in the bicyclam acetate complex adopt *cis*-V configurations in the solid

state. As far as I am aware, previous studies on bicyclam complexes mostly focused on derivatives in which two monocyclam units are linked together by bridging the carbon atoms of the cyclam backbone as shown by crystallography.[9] In the later case, each monocyclam ring adopts the *trans*-III configuration in the crystals. Bicyclam complexes in which two monocyclam units are linked together by bridging the amine nitrogen atoms of the cyclam backbone is the other type. The redox chemistry of some of these dinickel(II) and dicopper(II) complexes has been investigated with regard to the M(II) to M(III) oxidation process.[10] No X-ray crystal structural or NMR studies have been reported.

Isomerisation from *trans*-III to *cis*-V and *trans*-I or from *cis*-V to *trans*-I and trans-III for (bi)cyclam complexes is slow at neutral pH. The conversion from *cis*-V to *trans*-I or from *trans*-III to *trans*-I can be base-catalysed at high pH and is fast.

The configurations for both cyclam and bicyclam complexes have been successfully characterised using 1D and 2D NMR spectroscopy. However, the axial ligands of each configuration can not be distinguished. It is hard to determine which and how many ligands bind axially to each Zn cyclam complex by NMR spectroscopy. Some other methods may be needed to investigate.

8.3 Structure-activity relationships

The structure-function relationship with respect to the antiviral effect of the bicyclams has been generalised[11]. However, there is a lack of deep insight into structural information of cyclams and their complexes. Based on our structural

studies, we propose a possible mechanism to explain the effect of the aromatic linker on the anti-HIV activity of bicyclam.

Cyclams could be viewed as prodrugs for Zn complexes since Zn complexes with cyclams are stable, having higher anti-HIV activity than cyclams on their own[12] and Zn is available in the human body.

Anions can affect the distribution of the three configurations, and the *cis*-V configuration predominates for Zn (bi)cyclam complexes with carboxylates in aqueous solution. The titration of acetate with Zn (bi)cyclam complexes also confirms that carboxylates really can increase the proportion of the *cis*-V configuration. Two aspartic acid residues asp171 and asp262 of the target protein CXCR4 are the binding sites for (bi)cyclam[13] and this could be related to binding to the free carboxylate group of the aspartates. Therefore, we assume that the *cis*-V configuration is very important for the anti-HIV activity of (bi)cyclam complexes.

After coordination to Zn(II), monocyclam adopts the most stable configuration *trans*-III in the solid state. In Zn xylylbicyclam complexes, the aromatic ring is too close to the two flat monocyclam rings if they are in *trans* configurations, which forces each monocyclam to fold to be *cis*-V configuration. Acetate can further stabilise the *cis*-V configuration by bidentate coordination and formation of hydrogen bonds. Therefore, the Zn bicyclam complex with acetate in contrast to the Zn cyclam complex with acetate adopts the *cis*-V configuration in the solid state. Hence, two cyclam rings connected via a 1,4-phenylenebis(methylene) linker have their anti-HIV activity increased by about 70-fold. Thus the aromatic ring plays an important role in the anti-HIV activity for bicyclam complexes.

It should be possible to modify the design of (bi)cyclam drugs to increase their selectivity even further. In particular it is important to optimise inhibition of HIV recognition without affecting chemokine receptor activity. For example, consideration could be given to the use of pre-formed metal (bi)cyclam complexes since bicyclam may be able to bind to a range of metal ions in vivo (e.g. Cu(II), and Ni(II) as well as Zn(II)), and also to configurational locking of one cyclam unit in the potentially active *cis*-V configuration since we detected at least 6 configurations for Zn(II) bicyclam in aqueous solution. These new insights into the general principles governing the configurational control of cyclams are also likely to be of use in the design of macrocycles for many other specific purposes.

8.4 Future work

1. Analysis of the coordination number of zinc in the observed configurations by EXAFS.
2. Studies of the dynamic processes between the different isomers and their thermodynamic parameters by NMR via quantitative two-dimensional exchange spectroscopy (EXSY).

8.5 References

(1) Gabriel, S.; Weiner, J. *Chem. Ber.* **1888**, *21*, 2669.

(2) Bosnich, B.; Poon, C. K.; Tobe, M. L. *Inorg. Chem.* **1965**, *4*, 1102.

(3) (a) Thöm, V. J.; Fox, C. C.; Boeyens, J. C. A.; Hancock, R. D. *J. Am. Chem. Soc.* **1984**, *106*, 5947. (b) Adam, K. R.; Atkinson, I. A.; Lindoy, L. F. *J. Mol. Struct.*

1996, *384*, 183. (c) Adam, K. R.; Atkinson, I. A.; Lindoy, L. F. *Inorg. Chem.* **1997**, *36*, 480. (d) Hancock, R. D. *Prog. Inorg. Chem.* **1989**, *37*, 187.

(4) Moore, P.; Sachinidis, J.; Willey, G. R. *J. Chem. Soc., Chem. Commun.* **1983**, 522.

(5) Alcock, N. W.; Berry, A.; Moore, P. *Acta Cryst.* **1992**, *C48*, 16.

(6) (a) Tyson, T. A.; Hodgson, K. O. *Acta Cryst.* **1990**, *C46*, 1638. (b) Ito, T.; Kato, M.; Ito, H. *Bull. Chem. Soc. Jpn.* **1984**, *57*, 2634.

(7) Alcock, N. W.; Herron, N.; Moore, P. *J. Chem. Soc., Dalton Tran.* **1979**, 1486.

(8) Alcock, N. W.; Curson, E. H.; Herron, N.; Moore, P. *J. Chem. Soc., Dalton Trans.* **1979**, 1987.

(9) (a) Barefield, E. K.; Chueng, D.; Van Derveer, D. G.; Wagner, F. *Chem. Commun.* **1981**, 302. (b) Mochizuki, K. *Chem. Lett.*, **2000**, 26. (c) Kajiwara, T.; Yamaguchi, T.; Kawabata, H. S.; Kuroda, R.; Ito, T. *Inorg. Chem.* **1993**, *32*, 4990.

(10) Ciampolini, M.; Fabbrizzi, L.; Perotti, A.; Poggi, A.; Seghi, B.; Zanobini, F. *Inorg. Chem.*, **1987**, *26*, 3527.

(11) (a) De Clercq, E.; Yamamoto, N.; Pauwels, R.; Baba, M.; Schols, D.; Nakashima, H.; Balzarini, J.; Debyser, Z.; Murrer, B. A.; Schwartz, D. *Proc. Natl. Acad. Sci. U. S. A.* **1992**, *89*, 5286. (b) Bridger, G. J.; Skerlj, R. T. *Adv. Antiviral Drug Des.* **1999**, *3*, 161. (c) Bridger, G. J.; Skerlj, R. T.; Thornton, D.; Padmanabhan, S.; Martellucci, S. A.; Henson, G. W.; Abrams, M. J.; Yamamoto, N.; De Vreese, K.; Pauwels, R. *J. Med. Chem.* **1995**, *38*, 366. (d) Joao, H. C.; De Vreese, K.; Pauwels, R.; De Clercq, E.; Henson, G. W.; Bridger, G. J. *J. Med. Chem.* **1995**, *38*, 3865. (e) Bridger, G. J.; Skerlj, R. T.; Padmanabhan, S.; Martellucci, S. A.; Henson, G. W.;

Abrams, M. J.; Joao, H. C.; Witvrouw, M.; De Vreese, K.; Pauwels, R.; De Clercq, E. *J. Med. Chem.* **1996**, *39*, 109.

(12) (a) Este, J. A.; Cabrera, C.; De Clercq, E.; Struyf, S.; Van Damme, J.; Bridger, G.; Skerlj, R. T.; Abrams, M. J.; Henson, G.; Gutierrez, A.; Clotet, B.; Schols, D. *Mol. Pharmacol.* **1999**, *55*, 67. (b) Inouye, Y.; Kanamori, T.; Yoshida, T.; Bu, X.; Shionoya, M.; Koike, T.; Kimura, E. *Antiviral Chem. Chemother.* **1995**, *6*, 337.

(13) Gerlach, L. O.; Skerlj, R.; Bridgers, G. J.; Schwartz, T. W. *J. Biol. Chem.* **2001**, *276*, 14153.

Appendix I. Configuration *Trans*-III for Zn_2(bicyclam)$(ClO_4)_4$ in Aqueous Solution

The conformational analysis of *trans*-III for Zn_2(bicyclam)$(ClO_4)_4$ was carried out based on 2D [^{1}H,^{1}H] COSY, TOCSY, and NOESY and [^{1}H,^{13}C] HSQC (Figures I-1 to I-4).

M3 shows a strong nOe to **C** (δ ^{1}H: 2.34). The geminal partner for **C** is **D** (δ ^{1}H: 1.82, δ ^{13}C: 26.1). Based on chemical shifts and nOe correlation between **M3** and **C**, it can be concluded that **C** and **D** belong to a central methylene unit in a propyl group (6-membered ring) adjacent to the benzyl bridge. The large difference in chemical shift between **C** and **D** indicates that **C** is almost certainly axial and belongs to a chair conformation. The chemical shift of **C** is strongly affected by the presence of a benzene ring nearby and shifted to low field. **C** shows a large axial-axial coupling to **B** (δ ^{1}H: 2.73) and **F** (δ ^{1}H: 2.84). **D**, on the other hand, shows very weak coupling to both **B** and **F**. **B** has a geminal partner **A** (δ ^{1}H: 2.96). **F** has a geminal partner **E** (δ ^{1}H: 3.34). **F** shows a large coupling to $\mathbf{NH_C}$ (δ ^{1}H: 3.74). **E** shows a small coupling to $\mathbf{NH_C}$. **B** is not coupled to via DQF-COSY to an NH signal, consistent with **B**/**A** being adjacent to N-benzyl.

An interesteing twist in the NMR data is the following. **B** shows a very strong nOe to **V** (δ ^{1}H: 2.43), which shows a TOCSY correlation to $\mathbf{NH_E}$. $\mathbf{NH_E}$ is clearly associated with another 6-membered ring. **V** has a geminal partner **W** (δ ^{1}H: 2.95, δ ^{13}C: 55.0). **U** (δ ^{1}H: 2.99, axial) is directly overlapped with another resonance, but shows a large coupling to $\mathbf{NH_E}$. **U** shows a nOe to **M4**, placing **U** axially in a 5-membered ring adjacent to the benzyl group. The geminal partner of **U** cannot be distinguished due to resonance overlap.

$\mathbf{NH_E}$ shows a large coupling to **R** (δ ^{1}H: 2.81). **R** shows a large coupling to **O** (δ ^{1}H: 1.73, axial), which has a geminal partener **P** (δ ^{1}H: 1.99, δ ^{13}C: 30.3). **P** and **O** are the central methylene pair in a 6-membered ring. **O** couples to **N** (δ ^{1}H: 2.87, axial). **N** is coincident with a resonance, which couples to $\mathbf{NH_B}$ (which is associated with the other cyclam ring). Geminal partners of **R** and **N** are not assigned due to resonance overlap in both ^{1}H-^{1}H correlations and in 2D [^{1}H, ^{13}C] HSQC correlations.

$\mathbf{NH_C}$ and $\mathbf{NH_I}$ correlate to one another via TOCSY. $\mathbf{NH_I}$ shows a strong coupling to **J** (δ ^{1}H: 2.56, axial), which has a geminal partner **K** (δ ^{1}H: 3.01, δ ^{13}C: 49.6). $\mathbf{NH_C}$ shows a large coupling to **I** (δ ^{1}H: 2.54), which has geminal partner **H** (δ ^{1}H: 3.66, δ ^{13}C: 51.1). **H** shows small coupling to $\mathbf{NH_C}$. **I** and **H** show TOCSY coorelations to $\mathbf{NH_I}$.

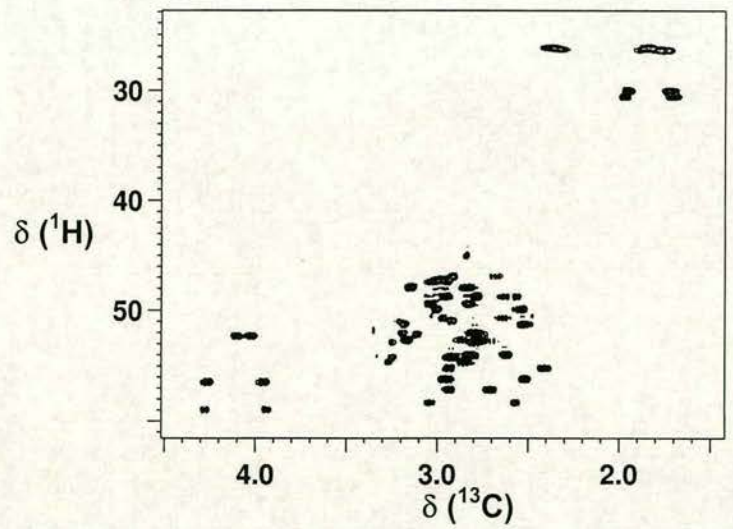

Figure I-1. 2D [^{1}H,^{13}C] HSQC NMR spectrum of Zn_2(bicyclam)$(ClO_4)_4$ (**8**) in 10% D_2O / 90% H_2O at equilibrium (aromatic region not shown).

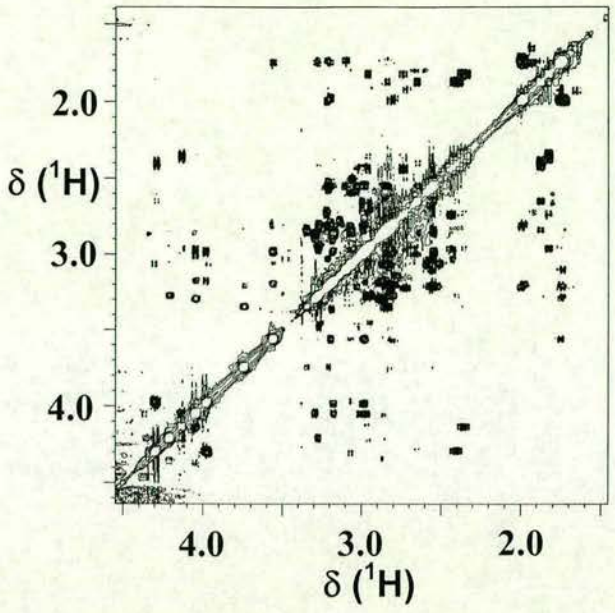

Figure I-2. 2D [^{1}H,^{1}H] NOESY NMR spectrum of Zn_2(bicyclam)$(ClO_4)_4$ (**8**) in 10% D_2O/90% H_2O at equilibrium (aromatic region not shown).

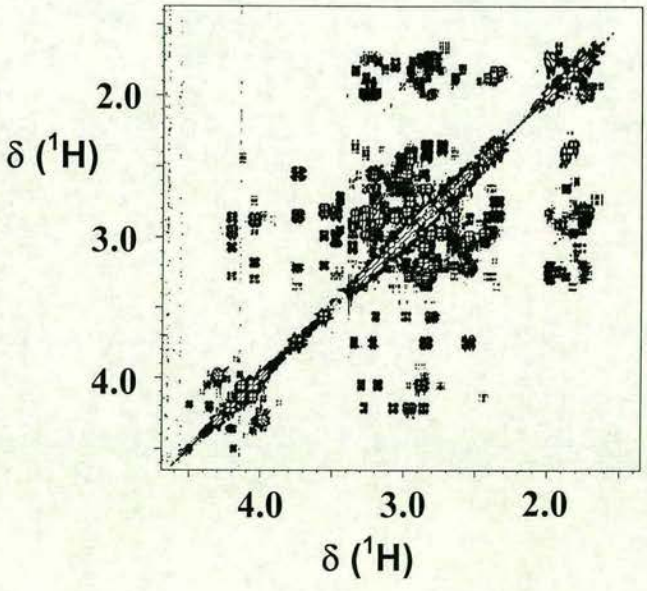

Figure I-3. 2D [^{1}H,^{1}H] COSY NMR spectrum of Zn_2(bicyclam)$(ClO_4)_4$ (**8**) in 10% D_2O/90% H_2O at equilibrium (aromatic region not shown).

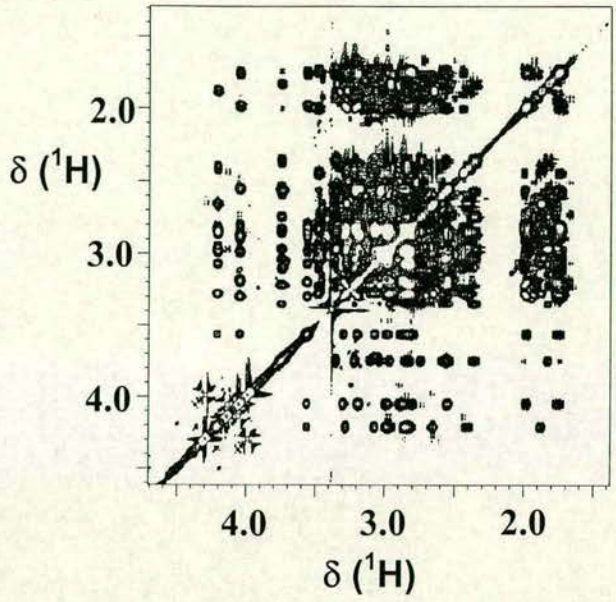

Figure I-4. 2D [^{1}H,^{1}H] TOCSY NMR spectrum of Zn_2(bicyclam)$(ClO_4)_4$ (**8**) in 10% D_2O/90% H_2O at equilibrium (aromatic region not shown).

Appendix II. Configurations *Cis*-V and *Trans*-I for $[Zn_2(bicyclam)(OAc)_2](OAc)_2$ in Aqueous Solution

The conformational analysis of configurations *cis*-V and *trans*-III for $[Zn_2(bicyclam)(OAc)_2](OAc)_2$ was carried out based on 2D [^{1}H,^{1}H] COSY, TOCSY, and NOESY and [^{1}H,^{13}C] HSQC (Figures II-1 to II-4).

(A) Configuration *trans*-I

Six-membered ring A: M1 shows a large nOe to **C** (δ ^{1}H: 2.34). **C** shows a large coupling to **D** (δ ^{1}H: 1.83). The 2D [^{1}H, ^{13}C] HSQC NMR data show that **C/D** are a geminal pair (δ ^{13}C: 26.0). Their chemical shifts enable assignment of these cross-peakss to a CH_2-***CH_2***-CH_2 methylene group (6-membered ring). Due to the nOe **M1-C**, this 6-membered ring is located adjacent to a benzyl methylene group. **C** shows a large coupling (DQF-COSY) to **F** (δ ^{1}H: 2.86) whereas **D**, the geminal partner of **C**, shows no DQF-COSY cross-peak to **F** (although **D** and **F** do show a TOCSY correlations to **C**). **E** (δ ^{1}H: 3.32) is strongly coupled to **F**; **F** and **E** are a geminal pair (δ ^{13}C: 55.9). The ^{13}C chemical shift places the **F/E** methylene group adjacent to a nitrogen atom. Together with the large coupling **F** to **C**, this enables assignment of **F/E** to N-***CH_2***-CH_2-CH_2-N. **F** shows a large coupling to $\mathbf{NH_A}$ to which **E** only shows a small coupling. **M5** shows a long range DQF-COSY correlation (W-coupling) to resonance **B** (δ ^{1}H: 2.82) which is heavily overlapped with 2 other resonances. A resonance at this chemical shift couples to **C** consistent with a **B-C** coupling. It is not possible to assign the geminal partner of **B** due to resonance overlap.

5-membered ring B (adjacent to A)**:** $\mathbf{NH_A}$ couples to **H** (δ ^{1}H: 3.07) and **I** (δ ^{1}H: 2.83). **H** and **I** form a geminal pair (δ ^{13}C: 49.4). It is not possible to assign the

relative positions of **H** or **I** due to resonance overlap. It is also difficult to assign resonances to the methylene group adjacent to **H/I**.

6-membered ring C: That $\mathbf{NH_B}$ and $\mathbf{NH_D}$ belong together is provided by the presence of a TOCSY correlation between their two proton resonances. $\mathbf{NH_D}$ notably shows a direct nOe correlation to **P** (δ ^{1}H: 1.73). From its chemical shift, **P** is clearly part of a propyl unit (CH_2-$\boldsymbol{CH_2}$-CH_2). The nOe places $\mathbf{NH_D}$ and **P** on the same face of the cyclam ring as one another. The geminal partner of **P** is **O** (δ ^{1}H: 1.94, δ ^{13}C: 30.14). Both **P** and **O** couple to four other protons with different sized couplings. **P** couples weakly and **O** couples strongly to **R** (δ ^{1}H: 3.30). **P** couples weakly and **O** couples strongly to **N** (δ ^{1}H: 3.13). **P** couples strongly and **O** couples weakly to **Q** (δ ^{1}H: 2.82). **P** couples strongly and **O** couples weakly to **M** (δ ^{1}H: 2.75). **N** and **M** are geminal partners (δ ^{13}C: 52.22), and **Q** and **R** are geminal partners (δ ^{13}C: 54.92). $\mathbf{NH_B}$ shows a large coupling to **Q**, which in turn shows a large coupling to **P**. In contrast, **R** shows a small coupling to $\mathbf{NH_B}$ and **P**. In a similar way, $\mathbf{NH_D}$ shows a large coupling to **M**, which in turn shows a large coupling to **P**. **N** shows a small coupling to both $\mathbf{NH_D}$ and **P**.

5-membered ring D: Assignment of resonances for protons in ring D is hampered by resonance overlap. It is clear that $\mathbf{NH_B}$ shows TOCSY correlations to **W** (δ ^{1}H: 3.02) and **V** (δ ^{1}H: 2.44), which are also a geminal pair of protons (δ ^{13}C: 56.9). No DQF-COSY correlations appear between $\mathbf{NH_B}$ and **W/V** implying that protons **W/V** are remote from $\mathbf{NH_B}$ i.e. adjacent to the nitrogen bearing the benzyl linker. **V** shows an nOe to **B**. The relationship between **B** and **M5** has already been demonstrated in which **B** is axial on the 6-membered ring A. Hence the nOe **V** to **B** should result

from **V** and **B** being in axial positions on rings D and A respectively. The strong nOe **W** to **M5** places proton **W** close to the methylene proton **M5**.

(B) Configuration *cis*-V

5-membered ring A: The benzyl methylene **M2** shows a strong nOe to **U** (δ ^{1}H: 3.08). **U** is strongly coupled to $\mathbf{NH_c}$, to **V** (δ ^{1}H: 2.62) and to **T** (δ ^{1}H: 3.01), which also couples to $\mathbf{NH_c}$ with a small coupling. **U** and **T** are geminal partners (δ ^{13}C: 47.65). **V** shows a W-coupling to **M6** and a strong coupling to **W** (δ ^{1}H: 2.49). **W** also shows a weak nOe to **M2**, which is reasonable given that **V** and **W** are geminal partners (δ ^{13}C: 48.7).

6-membered ring B: $\mathbf{NH_C}$ shows an nOe to $\mathbf{NH_F}$ but no nOe or TOCSY correlation to $\mathbf{NH_E}$. $\mathbf{NH_C}$ is strongly coupled to **R** (δ ^{1}H: 2.90) and weakly coupled to **Q** (δ ^{1}H: 3.21). **Q** and **R** are geminal partners (δ ^{13}C: 53.0); **R** is axial and **Q** is equatorial relative to $\mathbf{NH_C}$. **R** shows a large coupling to **O** (δ ^{1}H: 1.86, axial) and a small coupling to **P** (δ ^{1}H: 1.79, equatorial), which are at chemical shifts characteristic of N-CH_2-***CH_2***-CH_2-N. **P** and **O** are geminal partners (δ ^{13}C: 27.06). $\mathbf{NH_E}$ shows TOCSY correlations to **P** and **O** placing $\mathbf{NH_E}$ in the 6-membered ring B. **N** (δ ^{1}H: 3.09, axial) shows a large coupling to **O** but a medium sized coupling to $\mathbf{NH_E}$. **M** (δ ^{1}H: 2.91) is the geminal partner of **N** (δ ^{13}C: 51.19). **M** shows only very small couplings to $\mathbf{NH_E}$.

5-membered ring C: $\mathbf{NH_E}$ shows a large coupling to **J** (δ ^{1}H: 2.65, axial) and a small coupling to **K** (δ ^{1}H: 2.86, equatorial). **J** and **K** form a geminal pair (δ ^{13}C: 47.0). **J** shows a large coupling to **I** (δ ^{1}H: 2.57), which also shows a large coupling to $\mathbf{NH_F}$. **J** is therefore axial to both $\mathbf{NH_E}$ and **I**, and **I** is axial to $\mathbf{NH_F}$. **H** (δ ^{1}H: 3.05)

is the geminal partner of **I** (δ ^{13}C: 51.32). **I** shows an nOe to $\mathbf{NH_E}$, firmly placing **I** and $\mathbf{NH_E}$ on the same side of 5-membered ring C.

6-membered ring D: $\mathbf{NH_F}$ shows a large coupling to **F** (δ ^{1}H: 2.77, axial) and a small coupling to **E** (δ ^{1}H: 3.18, equatorial). **F** and **E** form a geminal pair (δ ^{13}C: 52.56). **F** shows a large coupling to **C** (δ ^{1}H: 1.75, axial) and a small coupling to **D** (δ ^{1}H: 1.84). **C** and **D** are geminal partners (δ ^{13}C: 26.8). **C** shows an nOe to $\mathbf{NH_F}$ placing **C** and $\mathbf{NH_F}$ on the same side of the cyclam ring. **C** shows an nOe to **V** confirming the fold of the molecule along the linear N-Zn-N axis. **C** shows a large coupling to **B** (δ ^{1}H: 3.02), which also shows a strong nOe to **M6**, thereby confirming that **M6** and **B** are close in space to one another. **B** shows a large coupling to **A** (δ ^{1}H: 2.63). **B** and **A** are geminal partners (δ ^{13}C: 58.8).

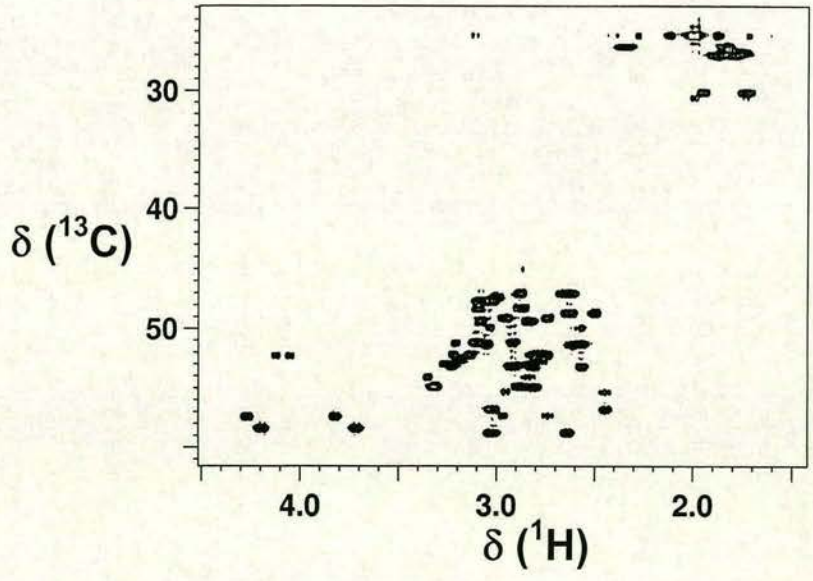

Figure II-1. 2D [^{1}H,^{13}C] HSQC NMR spectrum of $[Zn_2(bicyclam)(OAc)_2](OAc)_2$ (**9**) in 10% D_2O / 90% H_2O at equilibrium (aromatic region not shown).

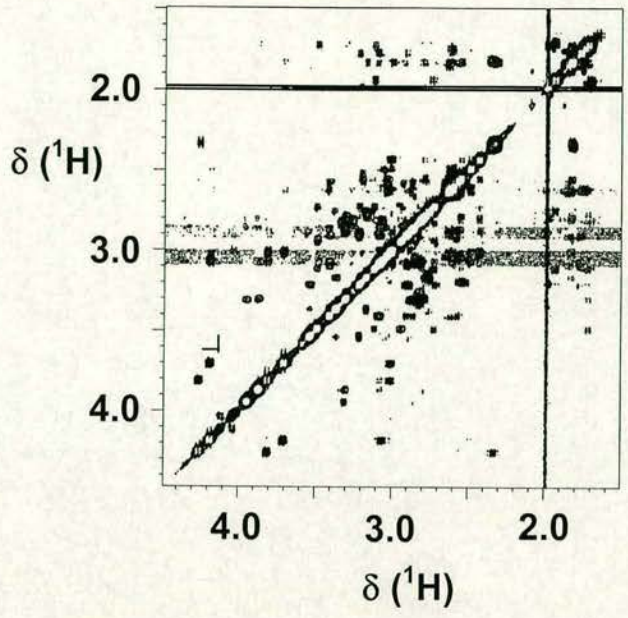

Figure II-2. 2D [^{1}H,^{1}H] NOSEY NMR spectrum of $[Zn_2(bicyclam)(OAc)_2](OAc)_2$ (**9**) in 10% D_2O/90% H_2O at equilibrium (aromatic region not shown).

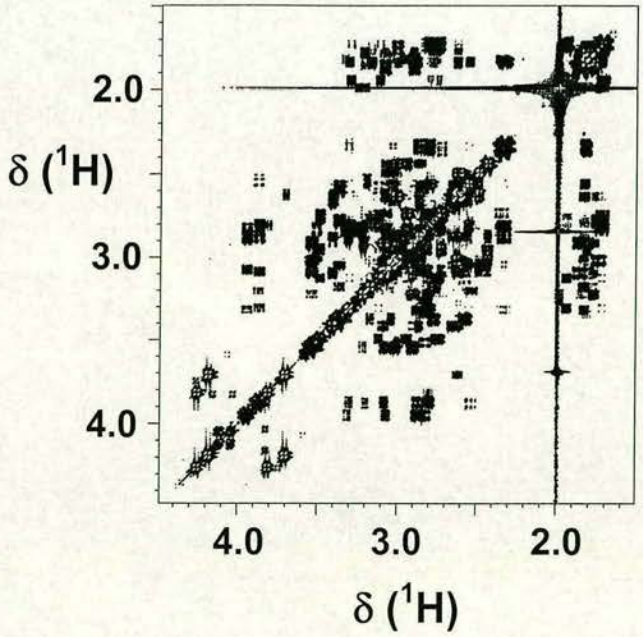

Figure II-3. 2D [^{1}H,^{1}H] COSY NMR spectrum of $[Zn_2(bicyclam)(OAc)_2](OAc)_2$ (**9**) in 10% D_2O/90% H_2O at equilibrium (aromatic region not shown).

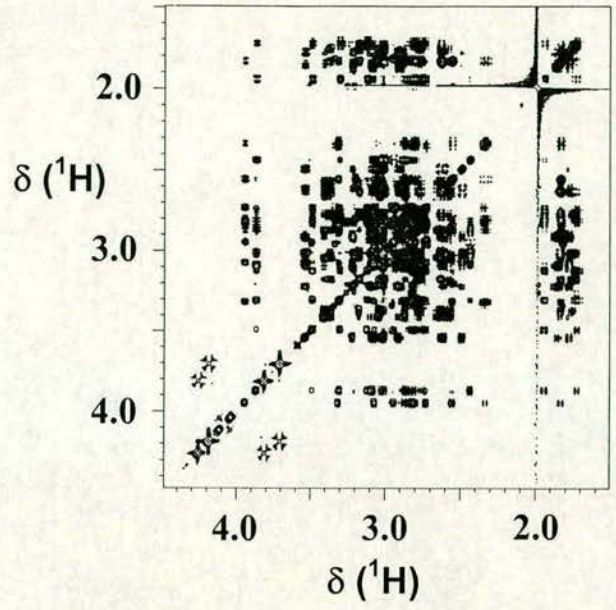

Figure II-4. 2D [^{1}H,^{1}H] TOCSY NMR spectrum of $[Zn_2(bicyclam)(OAc)_2](OAc)_2$ (**9**) in 10% D_2O/90% H_2O at equilibrium (aromatic region not shown).

Appendix III. Publications

1. Cadmium Cyclam Complexes: Interconversion of *Cis* and *Trans* Configurations and Fixation of CO_2

Inorg. Chem. (accepted)

Xiangyang Liang, John A. Parkinson, Simon Parsons, Michael Weishäupl and Peter J. Sadler

2. Structure and Dynamics of Metallo-Macrocycles: Recognition of a Viral Co-Receptor by Zinc Bicyclam

J. Am. Chem. Soc. (accepted)

Xiangyang Liang, John A. Parkinson, Michael Weishäupl, Robert O. Gould, Stephen J. Paisey, Hye-seo Park, Tina M. Hunter, Claudia A. Blindauer, Simon Parsons, and Peter J. Sadler